Analysis of Exogenous Over-Expression of 14-3-3σ/Stratifin in Transgenic Mouse Skin Carcinogenesis

Carol Marie McMenemy

MSci, MSc

Submitted in fulfilment of the requirements for the Degree of Doctor of Philosophy

School of Medicine

College of Medical, Veterinary and Life Sciences

University of Glasgow

2021

Abstract

Cutaneous squamous cell carcinoma is the second most common skin cancer and the most commonly diagnosed cancer capable of metastasis diagnosed in Caucasians. While many are surgically curable, survival rates for those which metastasise to regional lymph nodes and beyond are dismal in comparison, with 5-year-survival estimates averaging around 30%. There is a clear need, therefore, to establish better prognostic markers and systemic therapeutics to avoid or treat metastatic disease.

While chemical carcinogenesis of mouse skin has been the mainstay of cSCC research for decades, this process introduces a raft of mutations which are not integral to cancer development and the papillomas generated have a low rate of conversion; therefore, transgenic models mimicking the initiation and promotion steps have been developed to study specific pathways. Using a modified human Keratin 1 (HK1) promoter, oncogenes H-Ras and Fos have been targeted to the epidermis to study their involvement in initiation and promotion and, together, generated aggressive yet benign papillomas. Further work found that induced ablation of the Pten tumour suppressor, which results in deregulation of the PI3K/Akt pathway, reliably caused conversion to well-differentiated SCC in this *HK1.ras/fos-Δ5Pten* model, marked by loss of the major TSG, p53, due to upregulating of its main inhibitor, Mdm2. Thus, the first area of study investigated the p53-Mdm2 interaction, which identified the chaperone protein 14-3-3σ, known as Stratifin, as a positive regulator of p53. Stratifin was found to persist after loss of p53 in *HK1.ras/fos-Δ5Pten* wdSCCs, alongside cell cycle regulator p21, but was lost as tumours converted to poorly-differentiated SCC. This apparent tumour suppressor role fit with much of the literature which described its functions in differentiation and cell cycle arrest, as well as its role in protecting p53.

In light of this, a transgenic mouse model was obtained which overexpressed Stratifin in the skin and hair follicles using a Keratin 14 promoter (*K14.stratifin*), with the intention of suppressing tumour conversion in the *HK1.ras/fos-Δ5Pten* model of carcinogenesis, in part via p53 protection. The first step introduced the *K14.stratifin* transgene into this multistage model and, unexpectedly, initial *HK1.fos/K14.stratifin* mice developed rapidly growing

keratotic tumours on the ears which were found to convert to malignancy at an early stage. Detailed analysis found that these tumours seem to recapitulate an under-recognised subtype of cutaneous SCC arising from the hair follicle (HF) cells; fSCC. Further investigating discovered that mice harbouring the *K14.stratifin* transgene aberrantly express murine K1 in the HF, indicating that these fSCCs were possible due to spurious *HK1.fos* expression in these cells alongside elevated Stratifin, becoming the first model to directly link Stratifin and Fos deregulation in malignancy. Moreover, despite strong expression of p53 in these tumours, ablation of the p53 gene did not have any observable effect on this model indicating a p53-independent Stratifin pathway is responsible for the fSCC tumour aetiology. This model may be the first to implicate Stratifin and Fos in the aetiology of fSCC and, once validated in humans, may provide greater information on this poorly understood SCC variant.

Further to this, *K14.stratifin* was then co-expressed with *HK1.ras*, which alone produces benign wound-dependent papillomas. Here, two very distinct tumour types were observed: Type 1 tumours were wound-dependent and slow growing, though eventually developed areas of carcinoma and invasion, while Type 2 tumours did not require ongoing wound-promotion and grew rapidly, converting to SCC in under 2 weeks from inception. Analysis of p53 again showed strong expression even in clearly malignant tumours of both types, while its downstream effector, p21, appeared to be strongly active in the nuclei of Type 1 tumours, yet confined to the cytoplasm in Type 2s. Ablation of p53 reconfirmed an odd "p53 paradox" previously reported in *HK1.ras* mice, in which tumours fail to form if p53 is ablated prior to growth of the papilloma. Here, however, *K14.ras.p53*$^{flx/flx}$*.stratifin* mice developed inflamed hyperplasia with clear signs of localised invasion, while *K14.ras.p53*$^{flx/flx}$ controls appeared grossly and histologically normal, indicating the cancer-promotion function of Stratifin overexpression despite no overt tumour development.

To observe the apparent oncogenic effects of *K14.stratifin* expression on a p53-null background in the absence of other known oncogenic activation, *K14.p53*$^{flx/flx}$*.stratifin* mice were generated. Wound-promoted skin appeared grossly similar to control mice lacking Stratifin overexpression; however, histological analysis at >4 months found hyperchromatic nuclei and areas of invasion suggestive of early malignancy, again, without precursor benign tumour

development. Similarly, when *K14.stratifin* was subsequently expressed on a Pten-null background, its inclusion clearly exacerbated the Cowden Syndrome-like *K14.Pten$^{flx/flx}$* phenotype, with much more pronounced inflamed hyperplasia, hyperkeratosis, and hair defects present. Moreover, wound-promoted ear skin in these *K14.Pten$^{flx/flx}$.stratifin* mice showed clear evidence of carcinogenesis and cell invasion on histological examination. Again, this did not involve a benign tumour intermediary, further indicating that Stratifin acts as an oncogenic agent which is involved in producing aggressive, invasive carcinoma directly, not requiring development of an overt tumour prior to malignant conversion; hence the poor prognosis reported in internal tumours which overexpress Stratifin. On a dual p53-null/Pten-null background, Stratifin overexpression caused development of small wound-independent tumours requiring biopsy at an early stage, unlike the p53- and Pten-null backgrounds alone. These were found to have varied histology, though all appeared to involve HF aberration and possible involvement of HF stem cells in tumour generation, which requires confirmation. Wound-dependent tumours did not form at the ear tag of these mice in the relatively short time prior to sacrifice. Thus, the wound-independent tumours may have acquired further genetic lesions or have been linked to the cycling of the HFs, which occurs differently in ear skin.

Finally, keratinocytes were isolated from transgenic pups expressing *HK1.fos* and K14.stratifin, alone and together, to examine the phenotypes of primary cell cultures and assess their malignant potential. Here, it was found that primary *HK1.fos*, *K14.stratifin*, and *HK1.fos*/*K14.stratifin* cultures did not grow from clonal density and were susceptible to calcium-induced differentiation. Cell lines derived from these initial cultures were subjected to the same tests and while *HK1.fos* and *K14.stratifin* lines still responded to increased Ca^{2+} concentrations, several *HK1.fos*/*K14.stratifin* lines exhibited a much-reduced differentiation response. One such line, FS2, was also able to grow from clonal density in both low and high Ca^{2+} medium, though the other, FS3m, which exhibited an unusual morphology somewhat akin to spinous layer cells in low Ca^{2+}, was unable to form colonies at this low density even in low Ca^{2+} conditions. Western blot analysis found that these lines expressed approx. 50- and 12-fold more Stratifin than normal, respectively, thus, their different phenotypes and behaviours may be directly linked to the level of Stratifin

present, as its functions are highly context-dependent. Stratifin overexpression was also found to be linked to increased migratory potential, with monogenic *K14.stratifin* cells closing the gap in a scratch assay experiment almost twice as fast as the next line, FS2, while *HK1.fos* and normal ICR cells took far longer. These data reflect the observations *in vivo* and so the lines generated may be useful in helping to elucidate protein interactions and pathways underlying the fSCC phenotype.

In summary, this model not only clearly demonstrates the oncogenic activity of Stratifin overexpression—as opposed to a tumour suppressive role—but also appears to be the first to show direct co-operation between Fos or Ras activation and Stratifin overexpression in cutaneous carcinogenesis. In the case of Fos and Stratifin, their co-operation appears to specifically mimic the aetiology of rare human fSCC. Given the plethora of mutations observable in SCC aetiology, it may be that Stratifin overexpression in combination with other parameters could become a useful biomarker of tumour prognosis and final tumour outcome also applicable to diverse carcinoma types, not just cutaneous SCC.

Table of Contents

List of Tables

List of Figures

Acknowledgements

I'd very much like to thank my primary supervisor, Dr David Greenhalgh, for the huge amount of support and guidance he's provided throughout my PhD and in completing this thesis. I also want to thank my secondary supervisor, Dr Jean Quinn, for all the technical help she gave me in performing Western Blot analysis, in addition to giving helpful feedback on my writing and for thinking of me when job opportunities arose. I'd further like to give thanks to the various researchers who gave their time each year to assess my annual reviews and give guidance, including, Dr Torsten Stein, Dr Lorraine Work, Dr Tomoko Iwata, and especially Dr Katherine West, who did so for all 4 years of this project.

I am also extremely grateful to all the technical staff who have made this project possible, in particular: the staff at the Central Research Facility which provided animal husbandry and BrdU injections on my mice, especially Stuart Lannigan and Dennis Duggan; and to Lynn Stevenson and colleagues at Veterinary Diagnostic Services who processed all my biopsy samples to provide paraffin embedded and H&E stained sections.

I'd like to acknowledge and thank the generosity of the Scott family, whose endowment to the University of Glasgow Dermatology Department funded this research, without which I would not have been able to undertake this PhD. I also must thank both the British Association of Dermatologists and the British Society for Investigative Dermatology for providing travel bursaries to attend and present at the BSID annual meetings in 2018 and 2019, respectively, which were very much appreciated.

Finally, I need to thank all the friends and family who supported me through the past 4 years, especially Sean, who kept me going while writing through the lockdowns of 2020 and attempted to keep me sane.

Author's declaration

I declare that this thesis is my own work and has not been submitted for any other degree or professional qualification.

Carol Marie McMenemy

December 2020

Abbreviations

BM	Basement membrane
BSA	Bovine serum albumin
BrdU	5-Bromo-2-deoxyuridine
Ca^{2+}	Calcium ions
CGM	Clonal growth medium: calcium-adjusted DMEM with the addition of either 20% KGM or 10% FbCM/10% KGM
Cre	Cyclisation recombination gene of bacteriophage P1
cSCC	Cutaneous squamous cell carcinoma
DAB	3,3'-Diaminobenzidine
DMBA	7,12-Dimethylbenz[a]anthracene
DMEM	Dulbecco's modified eagle medium
DNA	Deoxyribonucleic acid
dNTPs	Deoxynucleotide Triphosphates
EDTA	Ethylenediaminetetraacetic acid
FBS	Foetal bovine serum
FCM	Fibroblast-conditioned medium
fSCC	Follicular squamous cell carcinoma
GAP	GTPase-Activating Protein
GDP	Guanine diphosphate
GEF	Guanine-nucleotide exchange factor
GSK3β	Glycogen synthase kinase beta
GTP	Guanine triphosphate
H&E	Haematoxylin and eosin
HK1.fos	Transgenic mice expressing viral Fos (v-Fos) from a modified human keratin K1 vector
HK1.ras	Transgenic mice expressing viral H-Ras ($v\text{-}ras^{Ha}$) from a modified human keratin K1 vector
IF	Immunofluorescence

IHC	Immunohistochemistry
K14.stratifin	Transgenic mice expressing full length human 14-3-3σ (stratifin) from a Keratin 14 expression cassette
KGM	Keratinocyte Growth Medium (PromoCell)
MAPK	Mitogen activated protein kinase
NTE	Non-tagged ear
PBS	Phosphate buffered saline
PCR	Polymerase chain reaction
pdSCC	Poorly differentiated squamous cell carcinoma
p53	Tumour Suppressor Protein 53
PI_3K	Phosphatidylinositol 3-kinases
PIP_3	Phosphatidylinositol 3,4,5-triphosphate
PTEN/Pten	Phosphatase and Tensin homologue (Human/Mouse)
SCC	Squamous cell carcinoma
SDS	Sodium dodecyl sulphate
SDS-PAGE	SDS polyacrylamide gel electrophoresis
TBST	Tris-buffered saline and Tween20
TGE	Tagged ear
TPA	12-O-tetradecanoylphorbol-13-acetate
TSG	Tumour suppressor gene
wdSCC	Well-differentiated squamous cell carcinoma

Chapter 1 Introduction

1.1. General Introduction

Carcinogenesis is driven by the acquisition of genetic mutations and epigenetic changes that affect gene expression, resulting in dysregulation of normal cellular processes, such as those involved in tissue homeostasis or differentiation (Hanahan and Weinberg, 2001, 2011). The characteristics of the tumour which develops are dependent on the mutations involved and the order in which they occur coupled with the stage of tumour development. Tumour aetiology is also influenced by the mechanisms which are intended to resist carcinogenesis, both intracellular tumour suppressors and effects of other cell types and immune system components in the tissue microenvironment (Giglia-Mari & Sarasin, 2003; Olumi et al., 1999; Hampton, 2005). The complex interplay of these various factors can determine whether a tumour will remain benign, convert to malignancy, and if it will be capable of invasion and metastasis.

In skin, these complex mechanisms govern the development of benign lesions (e.g., actinic keratoses and papillomas) from hyperplastic keratinocytes which harbour initiating mutations, their potential to either regress with time or convert into well-differentiated squamous cell carcinoma, and whether or not this can subsequently progress to a poorly-differentiated state with the capacity for distant metastasis (Berenblum, 1941; Cockerell, 2000; Salasche, 2000). Alternatively, similar mutations can result in development of benign Keratoacanthomas (KAs) which may be grossly similar to, and histologically nearly indistinguishable from, SCC but which regress over time (Watanabe et al., 2015).

Studies involving tumour-derived cell lines from clinical samples have been useful in garnering information about some of the important mutations involved in skin cancer. However, it is difficult to elucidate which are the main driver mutations and how these are involved in the stepwise progression of carcinogenesis by this type of analysis alone. To address this, early mouse models of skin carcinogenesis used chemical initiators and promoters to identify possible driver mutations (Berenblum, 1941; Berenblum and Shubik, 1947; Van Duuren, 1969). Subsequently, transgenic models have been developed which facilitate manipulation of putative driver genes to assess their impact on each

stage of carcinogenesis, from hyperplasia to malignancy. These can be controlled in both a spatial (cell type restricted expression) and temporal (induction of expression when desired) manner, allowing study of the tissue of interest with minimal off-target effects. Using these techniques, a multistage model was developed in which viral H-Ras (v-H-Ras) and the viral c-Fos homologue (v-Fos) are targeted to epidermal keratinocytes to produce benign papillomas, followed by Cre-loxP-mediated ablation of the Pten tumour suppressor to induce malignant conversion. In skin carcinogenesis, the most significant stage from the patient viewpoint is conversion of benign tumours to malignancy and their subsequent progression. This model identified tumour suppressor p53 loss as a major contributor to this progression to SCC (MacDonald et al., 2014), therefore regulation of the level of this protein was studied, identifying 14-3-3σ (Stratifin) as a useful target for further study.

1.2. Skin Structure and Function

Skin is comprised of the epidermis and the underlying dermis as well as nerves, blood vessels and all the adnexal features including hair follicles, sebaceous glands, apocrine/eccrine sweat glands (Sundberg et al., 2012), and associated immune cells, e.g., Langerhans cells (tissue-specific macrophages) (Perdiguero and Geissmann, 2016). Cutaneous stem cells (SCs) which give rise to epidermal keratinocytes are located several hair follicle stem cells niches, notably the Bulge region, as well as in the interfollicular epidermis, where they seldom divide to produce more actively cycling Transit Amplifying cells (*Figure 1-1*) (Simpson et al., 2011). The regions incorporating stem cells, transit amplifying cells, and the keratinocytes they produce are known as proliferating units (Potten, 1974; Blanpain and Fuchs, 2006).

To maintain the skin barrier and therefore cope with continuous mechanical, chemical, and irradiative damage, the tissue is continuously renewed, with undifferentiated *stratum basale* (basal layer) cells entering the terminal differentiation program, involving loss of the hemidesmosomes which anchored them to the basement membrane and movement through the upper layers (*stratum spinosum*, *stratum granulosum*, and *stratum corneum*) before

being sloughed off and replaced from beneath (Simpson et al., 2011). The layers can be identified through their different protein expression profiles and histological appearance; especially the changes in the dominant cytokeratin pair, presence of keratohyalin granules, and expression of proteins involved in preparing and effecting the cornification process. The specificity of these proteins to specific layers makes them useful markers of early (K1 and K10) and late (loricrin, involucrin and filaggrin) differentiation, while undifferentiated keratinocytes express the K5/K14 pair, predominantly (Fuchs, 1990).

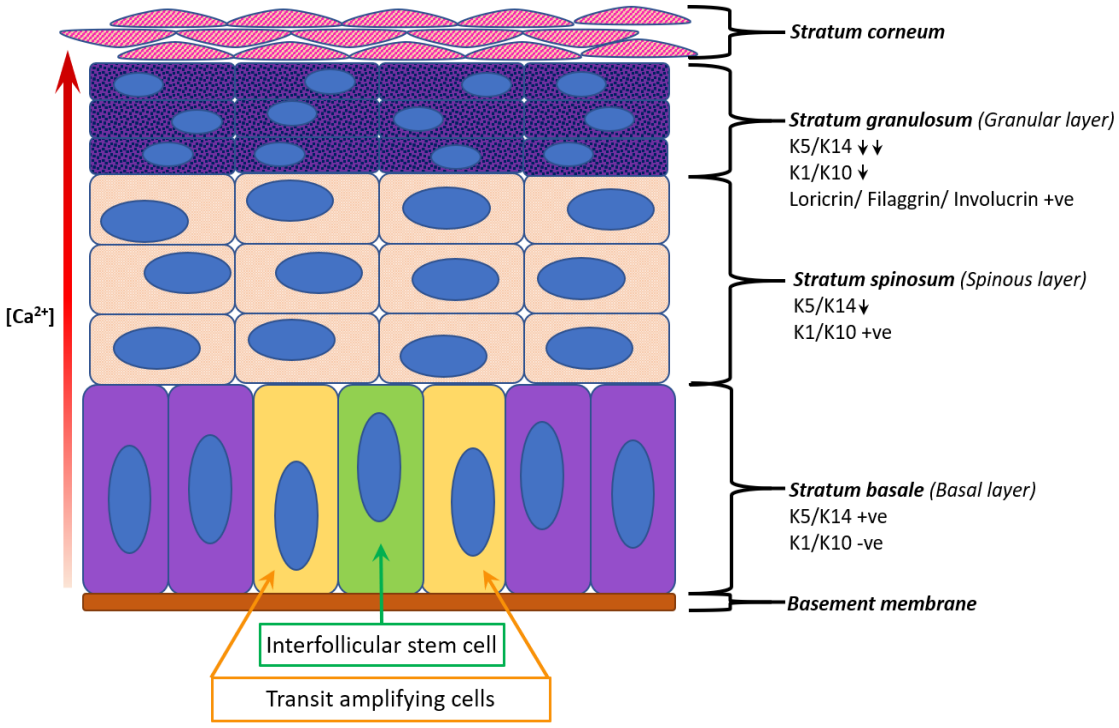

Figure 1-1: The epidermis.
Schematic depicting the general structure of the epidermis, including protein changes during differentiation, which is induced through an increasing Ca^{2+} gradient. Also note the presumed targets for carcinogenesis, the stem and transit amplifying cells in the basal layer.

Keratinocytes are so named for their abundance of the cytokeratin intermediate filaments which provide structural integrity to the cells as well as influencing many protein interactions in the cytoplasm. Currently, 54 keratin genes have been identified, with roughly half of the encoded keratins localised to the hair follicles. Keratins are either Type I (acidic) or Type II (basic/neutral); one member of each type come together to form heterodimers which then polymerise into long, unbranched filaments approximately 10 nm in diameter (Steinert et al., 1985; Moll et al., 2008).

The cytoplasmic keratin filament network links to the desmosomes (and, in the case of basal cells, hemidesmosomes) to provide both intercellular and intracellular stability. Additionally, these filaments form a dense network around the nucleus, which is thought to be important for nuclear positioning in epithelial cells as they are subject to frequent mechanical stresses. Each nucleus has an inner and outer membrane (INM; ONM), separated by an intermembrane space of approximately 30-50 nm (Cain and Starr, 2015). While Nesprins 1 and 2 are believed to be responsible for linkage of the actin cytoskeleton to the nuclear envelope (given their actin-binding domains; ABDs), the more recently described Nesprin-3 lacks this ABD and instead links the nucleus to intermediate filament networks (including keratins) indirectly, via the plakin family member, Plectin (Wilhelmsen et al., 2005). Plectin, like other plakins, is a very large protein (~500 kDa) with the domains which bind Nesprin-3 and IFs located at opposite ends of the protein; a feature which is thought to play an important role in spacing of the filaments (Wilhelmsen et al., 2005). Nesprins bind to SUN-1 and -2 in the intermembrane space, which in turn bind Lamin A/C which underlies the INM (Cain and Starr, 2015). This effectively links the nucleoskeleton to the cytoskeleton, providing mechanical stability but also allowing rapid signals regarding tension and other changes at the plasma membrane to be transmitted to the nucleus more rapidly than protein cascades could be capable of. Because of these findings, this linked network has been implicated in influencing rapid transcriptional changes following cell deformation, a process known as mechanotransduction (Reichelt, 2007).

In addition to the intracellular stability and signalling described, linkages of keratins at desmosomes and actin at adherens junctions provide powerful cell-cell adhesion. Given the network spans from the plasma membrane (PM) to the nucleus of each cell, this system essentially links cells in a continuous network to provide rapid cellular crosstalk as well as tensile strength at the tissue level, which is extremely important in skin since it is regularly subjected to mechanical stress. Desmosomes and hemidesmosomes, in particular, seem to be vital to the normal functioning of skin, with genetic mutations in either keratins (Jerábková et al., 2010) or other components (Pukkinen and Uitto, 1999; Charlesworth et al., 2003; Kiritsi et al., 2013) resulting in the epidermolysis bullosa (EB) group of blistering diseases and loss of tissue integrity

to varying degrees. In normal functioning, desmosomes are able to switch between high ("hyper-adhesive") and low affinity states, a process controlled by protein kinase C (PKC) (Kimura et al., 2007). This can reduce cell-cell adhesion in order to facilitate migration necessary in wound healing, and can contribute to skin cancer progression, as suggested by experiments showing low invasive potential of SCCs when desmosomal components are overexpressed (De Bruin et al., 1999). This switch in adhesive mode does not seem to involve a change in the proteins comprising desmosomal plaques, including desmogleins, plakophilins, and intercellular desmosomal cadherins, in addition to the keratin filament attachment (Kimura et al., 2007).

K5 (Type II) and K14 (Type I) are the predominant keratin pair expressed in the basal, undifferentiated cells of stratified, keratinising epithelia including the epidermis (Fuchs and Green, 1980). Individual polymers are bundled into "tonofilaments" which have been observed using transmission electron microscopy (TEM). They are also found in all outer root sheath (ORS) layers of the hair follicle (HF) but are absent from the companion layer (the layer immediately interior to the ORS). Their mRNA synthesis is halted as cells move into the suprabasal layers during terminal differentiation. However, K5/K14 protein filaments are detectable by immunostaining in the lower suprabasal layers as they remain part of the IF network early in differentiation before being degraded further through the programme (Moll et al., 2008).

1.3. Cancer

Mutations occur in DNA when exposed to some form of mutagenic agent(s), for example, UV light, x-rays, some aromatic hydrocarbons, among others (Parsa, 2012). The vast majority of these mutations are repaired by the cell during the DNA-damage response (DDR) (Zhou and Elledge, 2000). However, some are incorrectly or insufficiently repaired and persist in the cell, as well as in daughter cells if the original mutation occurred in a stem or transit amplifying cell (Rothkamm et al., 2002). Mutations can also be heritable, as in Li Fraumeni Syndrome, wherein *TP53*, encoding tumour suppressor protein p53, is mutated in the germline resulting in the development of multiple primary cancers, usually

at a young age (Malkin, 2011); or in Xeroderma Pigmentosum (XP), a rare autosomal recessive disorder (approximately 2.3 cases per million live births in Western Europe) which results in defective DNA repair mechanisms and thus greatly increases the incidence of skin cancer in affected individuals due to the failure to tolerate UV exposure (Lehmann et al., 2011).

The scope of the effects of persistent mutations varies greatly depending on the area of DNA affected; if the defect occurs in a non-coding region or where there is a level of redundancy built-in then the effects are likely to be minimal, whereas specific mutations in proto-oncogenes (e.g., *HRAS*) which lead to their constitutive activation (Su et al., 2014), or in major tumour suppressor genes (e.g., *TP53, PTEN, CDKN1A*) which result in loss of protective function and potentially gain of detrimental functions can have profound effects on cellular and tissue function (Pickering et al., 2015; Inman et al., 2018). These genotoxic insults can result in either apoptosis or senescence – or terminal differentiation in the case of skin – as protective mechanisms to inhibit carcinogenesis at each stage, but they may drive oncogenesis if such systems fail.

Usually, several mutations are required in the same cell to result in oncogenic transformation, with recent studies suggesting between two and eight are needed, varying between cancer types (Anandakrishnan et al., 2019). Rare exceptions can occur with a single mutation (identified in thyroid and testicular samples) or more than 10 (Martincorena et al., 2017), however, with greater numbers it becomes more difficult to ascertain which are true drivers of disease versus passenger mutations.

Often, transformed cells are detected through immunosurveillance and destroyed before tumorigenesis can occur (Swann and Smyth, 2007). This is supported by data showing that cancers are more common in immunocompromised individuals, with some types occurring almost exclusively in these patients, such as Kaposi's Sarcoma, a tumour type linked to Human Herpesvirus 8 (HHV8) which affects HIV patients and others on immunosuppressive drugs, e.g., following organ transplant (Schneider and Dittmer, 2018).

If immunosurveillance is compromised, the transformed cell may be able to freely undergo cell division and a tumour may form. Often, this uncontrolled proliferation can result in accumulation of further genetic mutations, creating a heterogeneous cell population which may develop different characteristics (Kent and Green, 2017), which are detailed in *Figure 1-2*. This figure also notes two so-called "enabling characteristics" (Hanahan and Weinberg, 2011), which are factors that make oncogenesis more likely, such as a pro-inflammatory phenotype which is known to favour malignancies (Birnie et al., 2008; Geng et al., 2013).

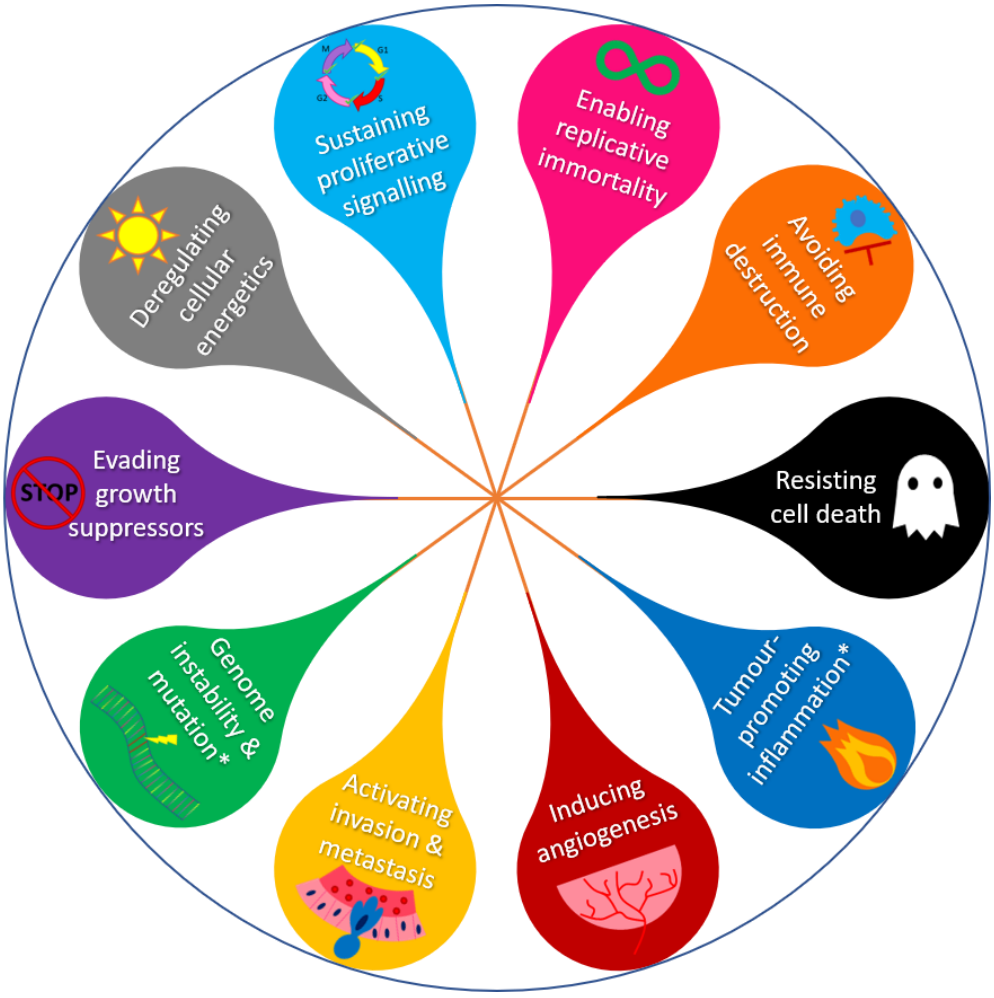

Figure 1-2: The Hallmarks of Cancer and Enabling Characteristics.
Asterisks denote Enabling Characteristics to distinguish them from the other Hallmarks. (Adapted from Hanahan and Weinberg, 2011)

Development of a pro-inflammatory phenotype is an example of how the tumour microenvironment is integral to tumour development and progression (Briso et al., 2013; Bottomly et al., 2019). While many effects of oncogene

activation or loss of tumour suppressors have actions within the mutated cells, much of the tumour aetiology is determined by the interactions between these cells and those in the surrounding tissues which do not harbour genetic mutations (Östman and Augsten, 2009). An example of this in tumours of the epidermis is the role of cancer-associated fibroblasts (CAFs) (Olumi et al. 1999; Kalluri & Zeisberg, 2006; Räsänen & Vaheri, 2010; Ni et al., 2017; Glentis et al., 2017). Under normal circumstances, there is cross-talk between the keratinocytes and fibroblasts in the skin to modulate skin structure, for example during wound-healing or remodelling of scar tissue, or to maintain homeostasis, which is mediated by paracrine signalling (Ghahary et al., 2007). In carcinogenesis, the signals sent out by mutated keratinocytes are akin to those released during wound-healing, causing activation of fibroblasts which are not themselves mutated and which are reacting correctly to the signals being received, but which are doing so in the wrong context, thereby increasing the likelihood of invasion and metastasis (Östman and Augsten, 2009; Karagiannis et al., 2012). For this reason, cancer has been described as “wounds that do not heal” (Dvorak, 1986).

1.4. Cutaneous Squamous Cell Carcinoma (cSCC)

Squamous cell carcinomas (SCCs) are malignancies of epithelial cells and, together with basal cell carcinomas (BCCs), their diagnoses outnumber all other cancer types. Cutaneous SCCs arise from keratinocytes which make up more than 90% of the cells in the epidermis. It is the second most common skin malignancy (after BCC), accounting for at least 20% of cutaneous cancers (Stratigos et al., 2015). Incidence is very difficult to accurately estimate due to underreporting, and while several studies have been conducted to improve estimates, they have suffered from small sample sizes and have therefore been inconclusive (Christianson et al., 2005).

Estimates of the increase in incidence have suggested a rise in cases of up to 200% in the past 30 years (Karia et al., 2013), with the greatest rise occurring in under 40s. Much of this increase has been attributed to rising popularity of artificial UV tanning beds and foreign holidays to high UV regions in people with Type I-III Fitzgerald phototype skin (Olsen and Green, 2012; Zhang et al., 2012),

as mutations caused by ultraviolet radiation (such as pyrimidine dimer formation) are implicated in the majority of cSCCs (Mullenders et al., 1993; Kim & He, 2014). A rise in the use of immunosuppressive drugs for patients with autoimmune (AI) conditions, HIV and organ transplants in this time has also contributed to the increase in cases. Incidence in immunosuppressed individuals is estimated to be 250-fold higher than the general population, with a greater risk of metastasis and mortality (Euvrard et al., 2003; Harwood et al., 2012). This is believed to be linked to a reduction in immunosurveillance—the process by which cells of the immune system remove damaged cells to counteract clonal expansion and carcinogenesis (Ribatti, 2017)—and greater UV sensitivity, particularly with the common AI drug azathioprine (Boukamp et al., 2005; Hampton et al., 2005).

The mutational landscape of cutaneous SCCs is extensive, with an average of 50 mutations per megabase pair of DNA identified by whole-exome sequencing (South et al., 2014), with in excess of 10,000 mutations often occurring in a single tumour (Pickering et al., 2014). These can be delineated into those with a so-called “UV-signature” and those without, the latter group tending to be associated with drug treatments like azathioprine or BRAF-inhibitors (Inman et al., 2018; Su et al., 2012).

As mentioned previously, SCCs of the skin generally arise from pre-existing benign lesions, commonly actinic keratosis (AK). Diagnosis based on gross appearance and histology can be difficult, as these lesions can have a very similar appearance to SCC *in situ* before having progressed to a malignant state (Cockerell, 2000). Additionally, while cutaneous SCC has a relatively low rate of metastasis (approximately 5%), the very high rate of incidence leads to a significant number of deaths per year in spite of this (Karia et al., 2013). Thus, being able to use markers to determine at which stage a lesion goes from a benign to malignant state is very useful. Identification of such markers has been aided greatly by the development and characterisation of mouse models of skin carcinogenesis.

1.5. Mouse Models of Cutaneous SCC

1.5.1. Advantages and Disadvantages of using mice to model cSCC

Mice are the most commonly utilised model organism in the research of human pathologies for numerous reasons, including their genetic and physiological similarities, relatively small size, ease of handling, and short generation time (Rosenthal & Brown, 2007). These features make them more useful in many ways than invertebrates like *Drosophila melanogaster* (fruit flies) or *Caenorhabditis elegans* (nematodes) which often lack human orthologous genes, and which do not exhibit much cell proliferation making them poor models for studying stem cell renewal, tissue repair, and cancer development (Murthy & Ram, 2015). In recent decades, genetic manipulation has become much more sophisticated and accessible, allowing researchers to knock-out, knock-in and otherwise mutate genes to alter their activity in precise ways (Rosenthal & Brown, 2007). The fully characterised mouse genome, together with their other desirable traits mentioned above, make them extremely useful genetic models in characterising protein functions, mutant phenotypes, and protein pathways and interactions which are involved in pathologies like cancer.

Mice are useful models for non-melanoma skin cancer research as their keratinocyte biology and differentiation programme is very similar to that in humans, with the same stem cell niches identified in the hair follicle and in the interfollicular epidermis (Levy et al., 2006; Blanpain & Fuchs, 2006; Watt & Jensen, 2009). Their use also allows for the study of the microenvironment as a whole, incorporating multiple cell types of the epidermis, dermis, immune system, vasculature and nervous system, which is far less feasible in *in vitro* modelling. This is important because research has shown comprehensively that cross-talk between cell types in the tumour microenvironment is integral to the aetiology of cancer development and progression (Lam et al., 2005; Goetz et al., 2011; Briso et al., 2013; Jolly et al., 2016). Given that a large proportion of human cutaneous SCCs are ultraviolet (UV) light-related (Mullenders et al., 1993; Soehnge et al., 1997; Narayanan et al., 2010; Kim & He, 2014), the ability to use an *in vivo* model to study the effects of UV radiation on cells in their native

environment is of particular use in skin cancer research (Strickland, 1986; Yang et al., 2014; Balupillai et al., 2018).

Despite these features, there are also drawbacks to relying on mice as models of human disease in general and, specifically, in modelling skin cancer. Numerous studies have highlighted the issue of strain-specificity in inbred laboratory mice; often very different phenotypes are produced in different mouse strains in response to genetic manipulation or responses to treatment with mutagens or drug therapies (Ashman et al., 1982; Slaga, 1986; Yoshiki & Moriwaki, 2006). This can be somewhat mitigated with the use of outbred mice which are not all genetically identical (as has been done in this project), though this may make phenotypic characterisation and statistical analyses more difficult as the mice do not necessarily develop a uniform phenotype. Some researchers have proposed the use of multiple inbred mouse strains or substrains as a way to account for strain-specific effects while still having all the genetic background information in place of outbred mice whose heterogeneous population introduces uncertainty (Festing, 2010).

Furthermore, recent data have indicated that grossly normal human skin contains a plethora of genetic mutations also found in skin cancers; their effects appear to be countered by differentiation and immunosurveillance mechanism, suppressing carcinogenesis (Martincorena et al., 2015; Martincorena et al., 2017; Hampton, 2005). Much of this is attributable to UV light exposure over a period of years, unlike in laboratory mice whose skin is only subject to UV irradiation if done as part of an experiment, which evidently does not accurately reflect the situation in human sun-exposed skin. This means that the background effects present in human skin on which SCC develops are not faithfully reproduced in the mouse, which could have important implications for skin research. There are also pertinent differences in the immunological features of mouse versus human skin, for example in the predominant T-cell receptors which are present; in mice, T-cells predominantly interact with keratinocytes, which in humans these cells associate largely with dendritic cells, like Langerhans cells (Naegu, 2016). The implications of such differences remains to be fully elucidated but may affect the weight of results based on mouse experiments in translational research.

Lastly, the tissue architecture of the mouse skin is not identical to that of human, generally being only one to three cells thick in non-pathologic skin and lacking the Rete ridges seen in human epidermis, which develop in response to mechanical stretching to resist shear forces (Topczewska et al., 2019); mouse skin is largely protected from such forces by the fur. Mice also have far more hair follicles in a given area than in human skin, which impacts the type of stem cells giving rise to new epidermis and somewhat influences the microenvironment (Zomer & Tentin, 2018). Ear skin is frequently used as this is mildly hyperplastic compared with back skin and the hair follicles are both sparser and do not cycle frequently in the adult mouse as in the rest of the body, making it more akin to human skin (Wang et al., 2017). These issues do not preclude mice from being good models for skin diseases such as SCC, as there are still many benefits to murine models, but the limitations must be understood when interpreting experimental results in translational research.

1.5.2. Chemical Carcinogenesis

The two-stage chemical carcinogenesis model was developed early in the 20th century following observations of the effects of tar and croton oil in tumour aetiology. The likely stages of tumorigenesis were described in detail in 1941 by Berenblum, termed: Precarcinogenesis, wherein cells are primed for carcinogenesis, but overt lesions do not form; Epicarcinogenesis, where further insult (genetic or epigenetic) induces tumorigenesis, and Metacarcinogenesis, where a benign tumour becomes malignant (Berenblum, 1941); these names were later changed to the now familiar Initiation, Promotion, and Progression (malignant conversion). This is typically part of a two-stage process involving application of a low dose of a carcinogenic compound, followed by a promoting agent which is non-mutagenic but significantly alters gene expression in the primed cells to elicit tumour formation (*Figure 1-3*).

Extensive study into this process identified Polycyclic Aromatic Hydrocarbons (PHAs) as useful compounds in inducing initiation events when topically applied to skin in subcarcinogenic doses. These initiation events occur when metabolites of PHAs – most commonly 7,12-dimethylbenz[a]anthracene

DMBA – bind to DNA and induce genetic (and, likely, epigenetic) changes, which are permanent. This initiation is thought to produce a heterogeneous population of keratinocytes harbouring changes which make them susceptible to tumour promotion. Early studies in the field deduced that promotion can be achieved by means which would not normally by themselves produce a malignant lesion (e.g., wounding). Work carried out in the 1940s (Berenblum, 1941; Berenblum and Shubik, 1947) found that croton oil (from seeds of the plant *Croton tiglium*) could potently promote initiated keratinocytes to form pre-malignant papillomas which could progress to SCC with repeated applications. Subsequently, it was discovered that phorbol diesters present in the oil were the promoting agents (Van Duuren, 1969), leading to the finding that 12-O-tetradecanoylphorbol-13-acetate (TPA) was the most potent of those which could be obtained from croton oil. In the widely used 2-step chemical carcinogenesis protocol (Abel et al., 2009), TPA is topically applied for up to a year following initiation with DMBA.

Application of early molecular biology cloning techniques discovered that an important proto-oncogene found to be a target of DMBA initiation; finding that the Harvey Ras gene (*HRAS*) was frequently mutated following treatment with DMBA, most notably at codon 61 (Balmain et al., 1984; Yuspa, 1994), usually resulting in constitutive activation of the gene. As outlined below in *Figure 1-3*, H-Ras (along with N- and K-Ras) is activated by mitogen-binding to the epithelial growth factor receptor (EGFR), initiating the canonical MAP-kinase pathway which can drive cell growth and proliferation, among other cell activities, hence the potency of Ras activation in human skin carcinogenesis.

Importantly, it has been noted that the length of time between initiation and promotion is not important to the ability of the process to produce papillomas; this indicates that the changes induced during initiation appear to be permanent. Since skin is continually differentiating and turnover allows most cells to be replaced in around 8 weeks, this suggests that the cellular population which is expanded via promotion to give rise to overt neoplasms are epidermal stem cells. Stem cell niches within the hair follicle (e.g., bulge region) are well known to provide new keratinocytes to the interfollicular epidermis (Watt and Jensen, 2009); however, interfollicular stem cells in the basal layer of the

epidermis are also thought to be likely targets for carcinogenesis (DiGiovanni, 1992; Morris et al., 2000; Abel et al., 2009).

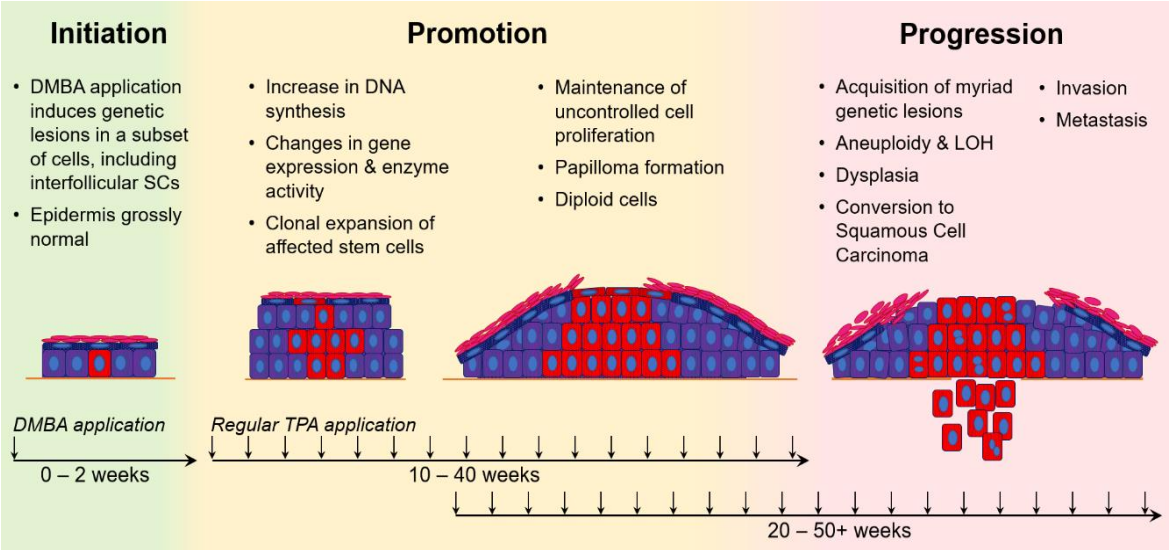

Figure 1-3: Multistage Chemical Carcinogenesis.
Initiating mutations (e.g., in *HRAS*) are induced using a single application of 7,12-Dimethylbenz[a]anthracene (DMBA), which does not generally cause a visible change in the skin. Promotion of tumorigenesis is achieved by repeated application of 12-*O*-tetradecanoylphorbol-13-acetate (TPA) for many weeks, up to around 1 year. This results in the changes detailed in the central (yellow) portion of the figure in roughly the first 2-20 weeks, wherein visible papillomas form but generally do not progress to carcinoma until much later (20-50+ weeks) if at all. In these later stages, a small proportion of the papillomas will undergo progression to invasive carcinoma, as further genetic mutations are obtained. (adapted from Abel et al., 2009)

While acquisition of activating mutations in H-Ras (by DMBA) and upregulation of AP-1 (by TPA) are sufficient to induce pre-malignant papilloma formation, it is believed that other genetic or epigenetic events are required for conversion, hence the long timescale of the chemical carcinogenesis model (Hennings et al., 1993; Segrelles et al., 2002). Evidence has shown that AKT activation is likely to contribute to this conversion, due to an increase in PI3K activity coupled with a decrease in PTEN inhibition of AKT activation (Segrelles, 2002).

1.5.3. Using Mutations Identified in Chemical Carcinogenesis as Transgenes to Target Driver Oncogenes to the Epidermis

Chemical carcinogenesis is useful in recapitulating the multistep nature of skin carcinogenesis which, as previously mentioned, often arises from benign lesions such as actinic keratosis, in contrast to the *de novo* development of basal cell carcinoma (BCC) (Feller et al., 2016). While several genes of interest have been identified through this technique, the stochastic nature of mutations following DMBA treatment means that many of those identified are so-called "passenger" mutations which do not contribute significantly to the disease aetiology. This, therefore, makes it difficult to assess those alterations which are driving, firstly, the appearance of papillomas and, later, the progression to SCC. Furthermore, TPA application is known to be a very potent promoter in the chemical model, however, it has many targets and thus wide-ranging effects which creates difficulties in identifying the key events underpinning tumour promotion.

To address these problems, transgenes can be utilised which drive overexpression of particular genes of interest. Exogenous activation of such genes allows us to target expression to the cells believed to be important for carcinogenesis and to reduce the level of confounding passenger mutations during of papillomatogenesis. Extensive study of the chemical model has identified H-Ras as a key target of DMBA, while TPA is known to upregulate the key transcription factor complex, AP1, comprised of Jun and Fos subunits. In order to determine the precise nature of the roles of these proteins in the development of papillomas, constructs were developed to allow their (independent) expression in early differentiating cells and, crucially, around 30% of basal keratinocytes, with the intention of targeting some of the interfollicular stem cells.

1.5.3.1. Ras Proteins

The Ras superfamily comprises more than 150 small guanine triphosphatase proteins (small GTPases). The superfamily is divided into five

main subgroups based on sequence homology and functional similarities, namely: Ras, Rho, Rab, Ran and Arf (Wennerberg et al., 2005).

Ras proteins have been described as binary molecular switches: they are inactive when GDP-bound and activated by binding to GTP. A GEF protein (Guanine Nucleotide Exchange Factor) catalyses the removal of GDP from Ras, which subsequently binds to GTP due to its greater abundance in the cytosol (ratio of 10 GTP: 1 GDP) (Prior and Hancock, 2011). The GTP-bound Ras undergoes conformational changes in the two Switch domains, revealing an effector binding site, resulting in activation. The low intrinsic GTPase activity (Wennerberg et al., 2005) means that hydrolysis of GTP to GDP is very slow, so rapid inactivation is achieved by interaction with GTPase-activating proteins (GAPs), which increase the rate of reaction by approximately 1000 times (Prior and Hancock, 2011).

The eponymous Ras subgroup –comprising H-Ras, N-Ras and the two splice variants of K-Ras (K-Ras4A and 4B) (Castellano and Santos, 2011)– are early effectors in the canonical MAPK (RAF-MEK-ERK) and PI3K-Akt transduction cascades, thereby positively regulating proliferation and cell survival (Zhang and Liu, 2002; Manning and Toker, 2017; Yu and Cui, 2016; Hossini et al., 2016). These isoforms are extremely similar, sharing ~80% sequence homology, with identical Switch and core G protein domains (Prior and Hancock, 2011). Most of the differences are clustered in the C-terminal hypervariable region (HVR) (Castellanos and Santos, 2011). Despite the high degree of similarity, the isoforms are not functionally redundant, which is believed to be attributable to differences in subcellular localisation, resulting in different pools of GEFs, GAPs, and effectors available for interaction (Laude and Prior, 2008; Prior and Hancock, 2011).

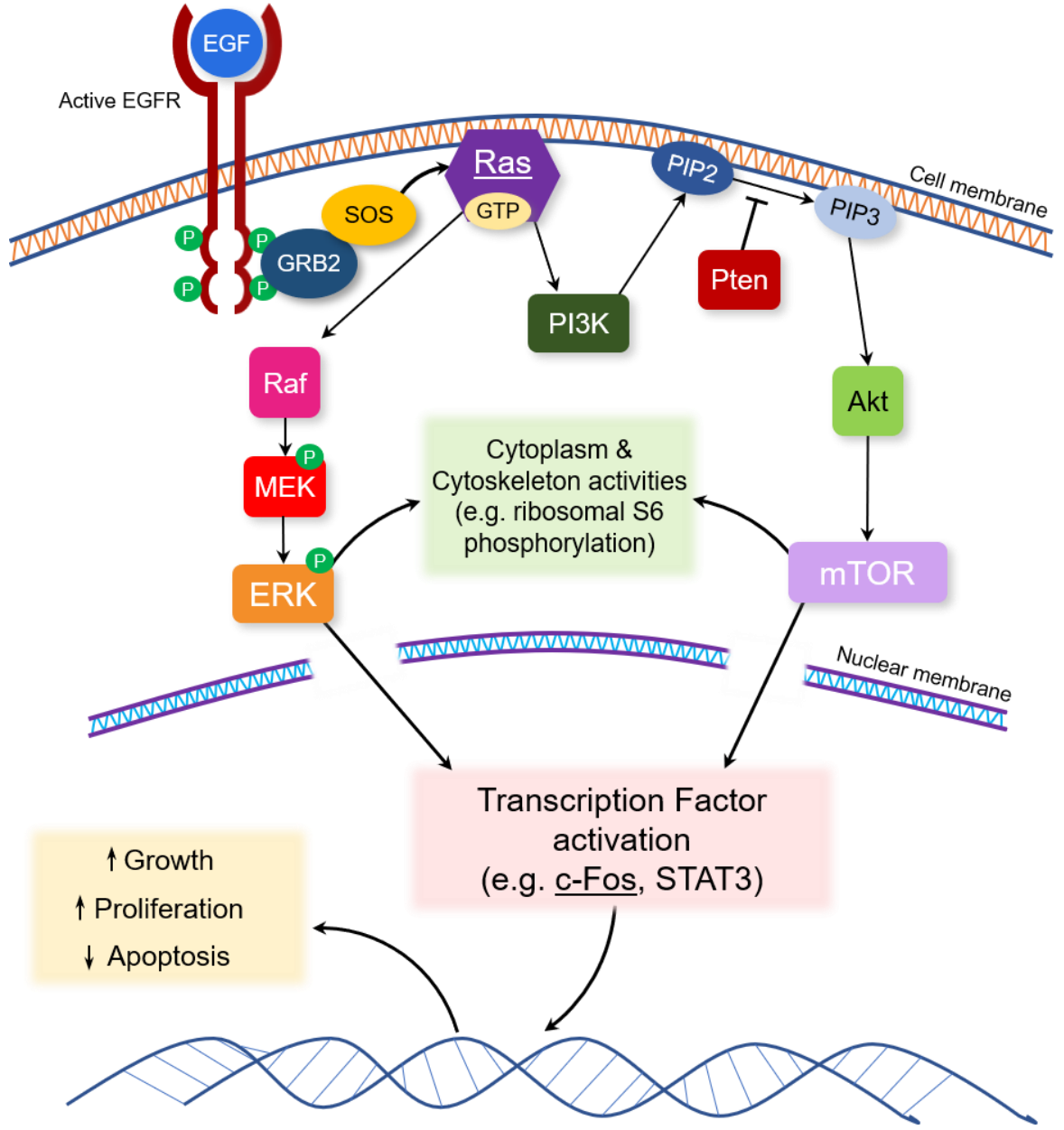

Figure 1-4: Ras activation and downstream effectors.
Activation of Receptor Tyrosine Kinases like EGFR (shown) trigger activation of downstream effectors in protein pathways including the canonical mitogen-activated protein kinase (MAPK) and PI3K-AKT-mTOR pathways, through activation of Ras protein family members (by inducing their switch from a GDP-bound to a GTP-bound state) at the cell membrane. MAPK activation generally enhances cell growth and proliferation, through transcription factors like AP-1 (involving c-Fos), while upregulation of Akt/mTOR have largely anti-apoptotic and thus pro-cell survival effects. Both p-ERK and mTOR also influence cytoplasmic proteins like ribosomes, and regulate components of the cytoskeleton, for example, to increase migratory potential. Additionally, p-ERK can not only induce c-Fos transcription but also enhance its activity through phosphorylation of its transactivation domain.

Membrane localisation of Ras proteins is required for signal transduction following tyrosine kinase receptor activation. Nascent proteins have a C-terminal CAAX motif (C= Cysteine; A= Aliphatic AA; X = any AA, but in Ras proteins this is either S or M) which undergoes post-translational modifications to result in targeting to the PM (Michaelson et al., 2005; Wennerberg et al., 2005).

All isoforms have a 15 Carbon farnesyl isoprenoid lipid attached to the Cysteine of the CAAX motif (farnesylation) by farnesyltransferase, which targets them to the endoplasmic reticulum for further processing. There, the AAX residues are cleaved by RCE-1 (Ras-converting CAAX endopeptidase-1), then a carboxymethyl group is added by ICMT (isoprenylcysteine carboxymethyltransferase) in a reversible process. This results in more hydrophobic tail, conferring greater membrane affinity. All isoforms except K-Ras4B are then palmitoylated by PAT (protein acyltransferase) in the Golgi apparatus—N-Ras and K-Ras4A at one further Cysteine residue, H-Ras at two—increasing hydrophobicity and therefore improving membrane affinity further. Both K-Ras isoforms also have 6 lysine residues (polybasic) attached to their tails to modify electrostatic interactions with the inner membrane, which is absent from N- and H-Ras processing. N-Ras has been found to require further processing in the HVR to stabilise membrane-association (Laude and Prior, 2008). If farnesyltransferase inhibitors are administered, K- and N-Ras can be alternately isoprenylated by geranylgeranyltransferase-I (GGT-1), however, this appears not to be the case for H-Ras (Prior and Hancock, 2011).

The plasma membrane was previously believed to be homogenous, but research has found that cholesterol- and sphingolipid-rich regions are present, referred to as “lipid rafts” (Brown and London, 2000; Simons and Ehehalt, 2002). These areas are more densely packed than the surrounding phospholipid membrane and are believed to improve signal transduction from receptors, in this case tyrosine kinase receptors like EGFR, to their effectors, such as the membrane-associated Ras proteins (Prior et al., 2001).

Additionally, Ras proteins were believed to only associate with, and therefore function at, the plasma membrane. This has also been challenged in recent years, with the discovery of Ras activation at endomembranes,

specifically on endosomes and in the Golgi and ER (Bivona and Philips, 2003), which have also been found to contain lipid rafts (Gkantiragas et al., 2001). This has further bolstered the hypothesis that the primary differences in functionality between H-, N- and K-Ras are mediated by differences in subcellular localisation (Hancock, 2003; Casar et al., 2009), since their regulatory and active domains are identical.

Overall, K-Ras (specifically the 4B splice variant) is the most abundant isoform across all tissues and is also the most commonly mutated of the three (H, N and K), with one study finding it to be altered in 22% of cancer specimens tested, while N-Ras mutants were found in 8% and H-Ras in only 3% . This ratio is quite different when only skin cancers are considered, where N-Ras was identified as the most commonly mutated at 18%, H-Ras next at 6% and K-Ras at only 3% (Prior et al., 2012). The majority of N-Ras mutations were detected in melanomas, where it has been frequently identified as a driver mutation (Muñoz-Couselo et al., 2017). Mutations related to cancer in these Ras genes are very often point mutations in codons 12, 13 or 61; codons 12 and 13 code for amino acid residues in the Switch I domain, while 61 normally encodes a Glutamine residue in the Switch II domain. These mutations generally confer poorer binding ability with the GAPs required to catalyse GTPase activity, therefore impairing the cell's ability to inactivate mutant Ras, causing constitutive activation.

H-Ras is the commonest Ras mutant in cutaneous SCC at 9%, vs 7% N-Ras and 5% K-Ras (Bamford et al., 2004). This incidence is greatly increased when the pool of SCCs is reduced to those aggressive cSCCs which are associated with previous vemurafenib for B-Raf^{V600E} melanomas. One study into these SCCs showed that 62% of those tested had some form of Ras mutation (13 of 21 samples), with all but one of those harbouring an H-Ras mutant (Su et al., 2012). The difference in incidence would be in part due to the fact that the majority of cutaneous SCCs (50-90%) harbour mutations in the *TP53* gene which codes for p53 (Giglia-Mari and Sarasin, 2003), and data shows that these vemurafenib-related tumours rarely have both *TP53* and *RAS* activating mutations concurrently (Pickering et al., 2014). This means that in general H-Ras mutant SCCs are a subset of the total, while in vemurafenib-related tumours they seem

to have a much higher frequency. This is possibly because *TP53* mutations are often UV-induced (Mullenders et al., 1993) therefore the mutational landscape is reflective of the difference in initiating factors. The majority of H-Ras mutations identified in the study were Glutamine to Leucine transition of reside 61 (Q61L) (Su et al., 2012) which has previously been determined to be caused by a SNP in the centre of the codon from A to T, thereby coding L (CTA) instead of Q (CAA) (Quintanilla et al., 1986).

1.5.3.2. Fos Transcription Factors

Transcription factors (TFs) are proteins which can initiate or regulate gene transcription, acting as effectors for signals from upstream signalling cascades, e.g., MAPK pathway. TFs bind to DNA at promoters or regulatory elements (e.g., enhancers or repressors) which may be close to the transcription start site of target genes (involved in forming the transcription initiation complex) or many kb away.

The Fos family of transcription factors is comprised of c-Fos (the cellular homologue of viral v-Fos), FosB (plus shorter splice variants, FosB2 and ΔFosB2), Fra-1 and Fra-2. These proteins dimerise with Jun isoforms (c-Jun, JunB and JunD) to form AP-1 (activating protein-1) transcription factor complexes which have wide-ranging roles in influencing proteins involved in nearly all cellular processes, including apoptosis, cell differentiation, proliferation and angiogenesis, among others.

The members differ in sequence primarily towards the C-terminal; all have a basic leucine zipper (bZIP) region which allows for binding to DNA and dimerization with an AP-1 partner, but only c-Fos and full-length FosB contain a C-terminal transactivation domain (TAD) (Wisdon and Verma, 1993) and as such are the only isoforms which have transforming properties in rat fibroblasts (NIH3T3 cells) (Miller et al., 1984).

In the epidermis, expression of different Fos isoforms is differentiation specific, as indicated in *Figure 1-5*, indicative of the different roles played by these isoforms in normal skin. Fra-1 is the most abundant Fos protein in the

undifferentiated basal layer, while Fra-1, FosB and c-Fos are all detected in the early-differentiated spinous cells, with only c-Fos and Fra-2 detected in the granular layer.

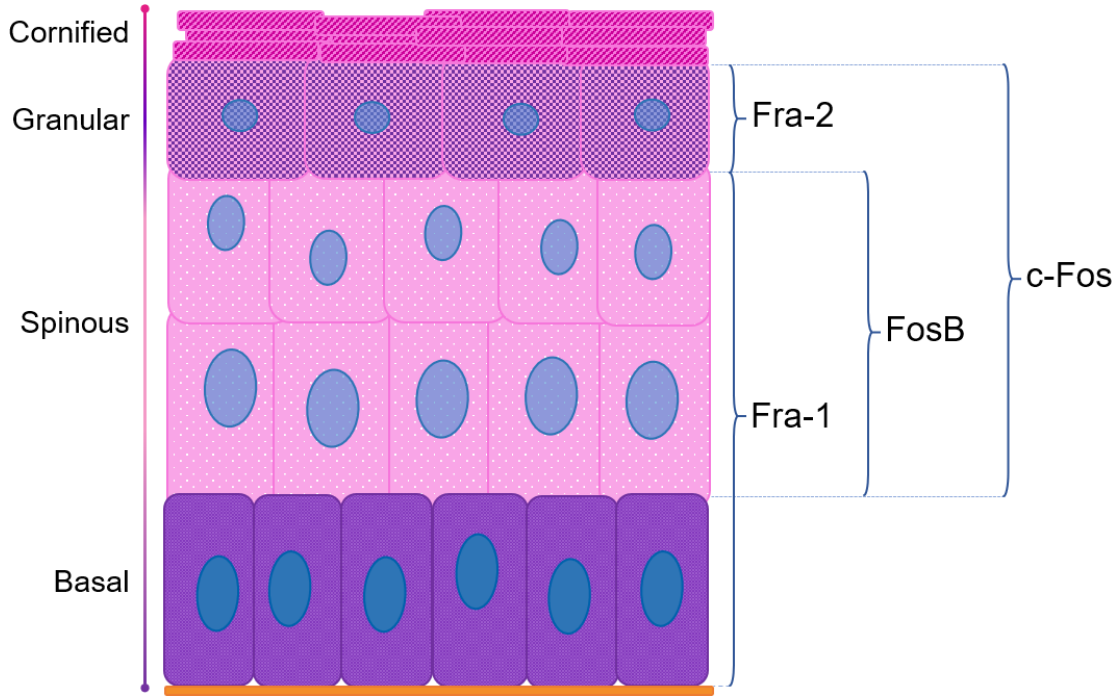

Figure 1-5. Fos protein isoforms in the epidermis.
Fos isoforms are expressed in specific layers of the epidermis, reflecting their different roles in cell cycle and differentiation at theses stages. Only c-Fos and the full-length variant of FosB have the transactivating domains (TADs) necessary to act as transcription factors, but those without (Fra-1, Fra-2, and FosB2/ΔFosB2) are believed to act as negative regulators of the transactivating isoforms. Their tight regulation is required for normal epidermal growth and differentiation, while deregulated forms of Fos have been implicated in promotion of numerous carcinomas.

As indicated in *Figure 1-4*, c-Fos mRNA transcription can be activated by ERK1/2 phosphorylation of transcription factor Elk1 following mitogen stimulation of the cell via Receptor Tyrosine Kinases, transduced by Ras proteins. Interestingly, it has been found that ERKs can subsequently enhance c-Fos (and therefore AP-1) activity by phosphorylation of pS/T-P residues in the C-terminal TAD (Monje et al., 2005), mediated by Pin1, which is also known to assist in enhancing c-Jun, NF-κB and p53 activities (Girardini et al., 2011; Kuboki et al., 2009; Wulf et al., 2001; Wulf et al., 2002; Zheng et al., 2002).

As may be expected given the differentiation-specific expression of the various Fos isoforms, *in vitro* experiments have identified differences in induction (by Ca^{2+} and TPA-treatment) and transcriptional regulation. Cultured keratinocytes maintained in low Ca^{2+} (0.05 mM) medium have basal-like expression profiles and morphology, while an increase to high Ca^{2+} (0.12 mM) will result in activation of the terminal differentiation program. The phorbol ester, TPA, mentioned earlier in relation to chemical carcinogenesis, can also induce differentiation, though the Fos isoforms induced in the process appear to be different; Ca^{2+} causes upregulation of Fra-1 and Fra-2, while TPA induces c-Fos and Fra-1. Exogenous expression of Fra-2 and c-Fos (either alone or concurrent with JunB expression) indicate that Fra-2 acts as a strong negative regulator of AP-1 transcriptional activity, whereas c-Fos increases AP-1 activity and is able to override endogenous Fra-2 negative regulation during Ca^{2+}-induced differentiation (Rutberg et al., 1997).

Fos family members must heterodimerise to function, primarily with Jun members, while Jun can form homodimers or heterodimers within the Jun family or with Fos or the lesser studied ATF and MAF families. Fos:Jun dimers are known to have higher DNA binding affinity than Jun:Jun complexes, though both bind to TPA-responsive elements(TREs)/AP-1 binding motifs and, to a lesser extent, cAMP-responsive elements (CREs), 5'-TGA(C/G)TCA-3' and 5'-TCACGTCA-3', respectively. Binding to other variant sequences has been detected in vitro and from tissue samples, for example, via ChIP-seq. Until recently, transcriptional activation by AP-1 was thought to mostly occur through binding to TREs close to the transcriptional start site (TSS) of target genes. However, advances in transcriptomics have discovered that the majority of gene regulation by AP-1 complexes actually occurs via binding to enhancer elements far from the target TSS, brought into close proximity by chromatin interactions (Bejjani et al., 2019).

Fos proteins, perhaps unsurprisingly given the ubiquity and wide-ranging effects of AP-1, is implicated in the aetiology of many cancers (Saez et al., 1995; Plaza-Menacho et al., 2007; Liu et al., 2018). However, unlike other oncogenes, its involvement in disease comes primarily from dysregulation of upstream signalling molecules, e.g., *H-Ras Q61L*, rather than mutations in its

own genetic sequence (Bejjani et al., 2019). This can involve any of the isoforms, with the TAD-containing c-Fos and FosB implicated in tumours of the bone (and possibly cartilage), endometrium, lung, and skin (Grigoriadis et al., 1993; Saez et al., 1995; Sunters et al., 1998 and 2004; Franchi et al., 1998; Bamberger et al., 2001; Volm et al., 2002; Silvers et al., 2003), while the negative regulating proteins Fra-1 and -2 are often increased in melanomas, ovarian, colorectal cancers (Yang et al., 2004; Tchernitsa et al., 2004; Wang et al., 2004). Interestingly, changes in regulation of c-Fos, FosB, Fra-1 and Fra-2 have been observed in various breast cancers and cancer-derived cell lines, though not all in the same tumour or cells (Kustikova et al., 1998; Bamberger et al., 1999; Andersen et al., 2002).

1.5.3.3. Phosphatase and Tensin Homologue (PTEN)

Aside from the MAP kinase pathway and activation of AP-1 responsive genes in the chemical carcinogenesis model, activation of Akt has been identified as an important even in development of SCC in the chemical carcinogenesis model. Therefore, in order to recapitulate these events using a transgenic system, its main inhibitor, PTEN, was targeted using an inducible Cre-loxP-mediated system, outlined below.

PTEN is a dual lipid and protein phosphatase located on chromosome 10 (10q23) at a site which frequently suffers loss of heterozygosity which can contribute to the formation and progression of many cancers. The N-terminal domain contains a CX5R catalytic motif, which is common to protein tyrosine phosphatases, forming the P-loop which, along with the WPD-loop, is required for phosphatase activities (Lee et al., 1999; Tautz et al. 2013). Specific protein tyrosine phosphatases have a binding cleft which is too deep for phospho-Serine/Threonine residues to reach the Cysteine residue of the P-loop, however, the cleft of PTEN has a wider opening which means that all 3 (Tyr/Ser/Thr) phospho-residues can be dephosphorylated (Myers et al., 1997).

It is best characterised in its inhibition of the PI_3K/Akt pathway by means of its lipid-phosphatase activity. PI_3Ks, in response to upstream signalling, e.g., by IGF-1, phosphorylates phosphatidylinositol-4, 5-bisphosphate (PIP_2) to

phosphatidylinositol-3, 4, 5-triphosphate (PIP_3). This lipid second messenger is then able to bind proteins such as PKC and PKB/Akt at their pleckstrin-homology (PH) domain which causes their translocation to the plasma membrane. Binding of this domain also serves to alter conformation of the bound substrate, leading to a conformational change which better facilitates subsequent phosphorylation (Chen et al., 2018).

Akt is phosphorylated at positions Thr308 and Ser473 by PDK and mTORC2, respectively. Phosphorylation of Thr308 must occur first and confers an increase in Akt activity, allowing it to phosphorylate SIN1 on mTORC2, which then phosphorylates Akt in turn at Ser473 to maximise Akt kinases activity (Yang et al., 2015). PTEN interferes in this activation by dephosphorylating PIP_3 at the 3' position of the inositol ring to revert it to PIP_2 (Chen et al., 2018). Akt activation plays numerous roles in cell survival and proliferation, for example inhibition of pro-apoptotic proteins FOXOs, BAD, Cas 3 and Cas 9 (Brunet et al., 1999; Datta et al., 2000; Kermer et al., 2000; Cardone et al.,1999), nuclear exclusion of cell cycle inhibitors p21 and p27 (Zhou et al., 2001; Shin et al., 2002), and activation of Mdm2 to reduce p53 levels thereby inhibiting cell cycle arrest and the intrinsic apoptotic pathway (Ogawara et al., 2002; Gottlieb et al., 2002). PTEN is therefore a major tumour suppressor in its role as important inhibitor of these downstream effects of Akt activation.

Subcellular localisation has also been shown to be very important to PTEN functioning (Planchon et al., 2008). It contains a cytoplasmic localisation signal at residues 19-25; mutation of any of these except 22 results in nuclear accumulation (Denning et al., 2007). Nuclear import of wild-type PTEN (wtPTEN) is also mediated through mono-ubiquitination, but poly-ubiquitination results in degradation, thereby providing a rapid mechanism for regulating the level of PTEN in the cell which does not require changes to transcription or translation, similarly to regulation of p53 (Wang et al., 2007). Stabilising/inactivating phosphorylation occurs primarily at S370 and S385 (Li et al., 2014), while destabilisation occurs at site T366, which it has been shown to auto-dephosphorylate (Maccario et al., 2007). Phospho-PTEN is more stable, however, it is more active when dephosphorylated as this is correlated with a more open conformation (Rahdar et al., 2009).

While the inhibition of Akt activation is primarily cytoplasmic, nuclear PTEN has important roles in maintaining genomic stability, mediation of cytokinesis, and cell cycle arrest (Bononi and Pinton, 2015). This latter role utilises both protein-phosphatase activity, by downregulation of cyclin D1, and lipid-phosphatase activity which was demonstrated to lead to an increase in CDK-inhibitor p27 in addition to the aforementioned downregulation of Akt (Weng et al., 2001). These activities were determined by comparison of wild-type PTEN with a phosphatase-dead mutant, C124G, and a mutant lacking only lipid-phosphatase activity, G129E. The latter mutation is often present in Cowden Syndrome, a heritable disease which results in benign neoplasia (hamartomas) of multiple organs (Hanssen and Fryns, 1995), including a hyperplastic and hyperkeratotic skin phenotype (Brownstein et al., 1979; Starink et al., 1985), which can lead to malignancies following further genetic insults (Ngeow et al., 2014). In vivo studies of heterozygous G129E mice suggested gain-of-function (GOF) activities which promoted tumorigenesis when compared with C124G mutants, though it was unclear whether this was solely due to specific activities of mutant PTEN or if antagonism of wtPTEN functions were involved, since both G129E and C124G/C124S are known to be dominant-negative mutations (Papa et al., 2014). It also appears to be an important regulator of mitosis by dephosphorylating Polo-like kinase 1 (PLK1) at residue T210; loss of this regulation by protein-phosphatase activity ablation causes failed cytokinesis and thus an increase in the presence of polyploid cells (Zhang et al., 2016).

Cytoplasmic activities have been linked to morphological changes, inhibition of cell spreading and migration, with some mutations causing enhancement of these activities, for example due to the reduced dephosphorylation of focal adhesion kinase (FAK) and PIP_3 (Tamura et al., 1998; Papa et al., 2014). Nuclear activities antagonise genomic aberrations and cycle progression, with the loss of protein phosphatase activity in mutants like those found in Cowden Syndrome resulting in greater genomic aberrations (Bononi and Pinton, 2015; Hubbard et al., 2016). This fits well with the observations that in normal, mostly quiescent tissues, PTEN is often much more localised to the nucleus, whereas in malignant samples it is more abundant in the cytoplasm (Perren et al., 2000).

In cancers, PTEN is frequently subject to deletion, mutation and epigenetic silencing, contributing to tumour development and progression (Perren et al., 2000; Mirmohammadsadegh et al., 2006). For example, loss of one or more alleles has been found in more than 20% of primary prostate cancers and 50% of castration-resistant prostate cancers (Jamaspishvili et al., 2018).

Loss of function in skin has been shown in human SCCs including those associated with Cowden syndrome (Li et al. 2015; Brownstein et al., 1979) and has been investigated in mice using the chemical carcinogenesis model and by direct genetic manipulation (Yang et al., 2014; Suzuki et al., 2003). UV light causes rapid induction of PTEN in skin as it plays an important role in global genomic nucleotide excision repair (GG-NER), as evidenced by the impairment of this process when PTEN is downregulated (Ming et al., 2011). This, as well as the observations that it is downregulated in chemical carcinogenesis as well as in human actinic keratoses and SCC, make it an ideal target for use in inducing malignant progression of *HK1.ras/fos* papillomas.

1.5.4. *HK1.ras/fos-Δ5Pten* Multistage Carcinogenesis

As outlined above, previous experiments established that H-Ras and c-Fos are implicated in the aetiology of skin carcinogenesis, through characterisation of the Chemical Carcinogenesis model as well as manipulation of cancer cell lines and clinical tumour samples (Balmain et al., 1984; DiGiovanni, 1997; Greenhalgh et al., 1988, 1989, 1990; Pickering et al., 2014; Silvers et al., 2003). Studies which grafted transfected cell lines onto nude mice eliciting tumours were the first to identify direct co-operation between H-Ras and Fos in the progression from Ras-induced papillomas to malignant SCCs (Strickland et al., 1988).

However, in these systems, elucidating the impact of these genes in early carcinogenesis and progression is made difficult by the passenger mutations present, which may not contribute significantly to the disease. Therefore, in order to assess the effects of H-Ras and c-Fos specifically, both alone and concurrently, a model was devised using sequences of the viral homologues of these proteins, v-Ha-ras and v-fos. These were inserted into a modified human

Keratin 1 (HK1) expression vector (Greenhalgh et al., 1993a; 1993b; 1993c), the schematic for which is shown in *Figure 1-6*.

This vector is expressed exclusively in mouse epidermis under the conditions which regulate the endogenous Keratin 1 gene expression. Importantly, however, this is a truncated form of the original clone from which the sequence was obtained in which some regulatory sequences are missing which allows its expression in some (~30%) of proliferative basal keratinocytes where endogenous K1 is normally not present (Rosenthal et al., 1991). Moreover, this also allows its expression to be maintained throughout tumorigenesis where endogenous K1 is lost as the well differentiated phenotype is lost. Furthermore, exclusive epidermal expression eliminates unnecessary pathologies which a constitutive vector would elicit, thereby complying with the UK's 3R (reduce, refine, replace) framework for animal experimentation.

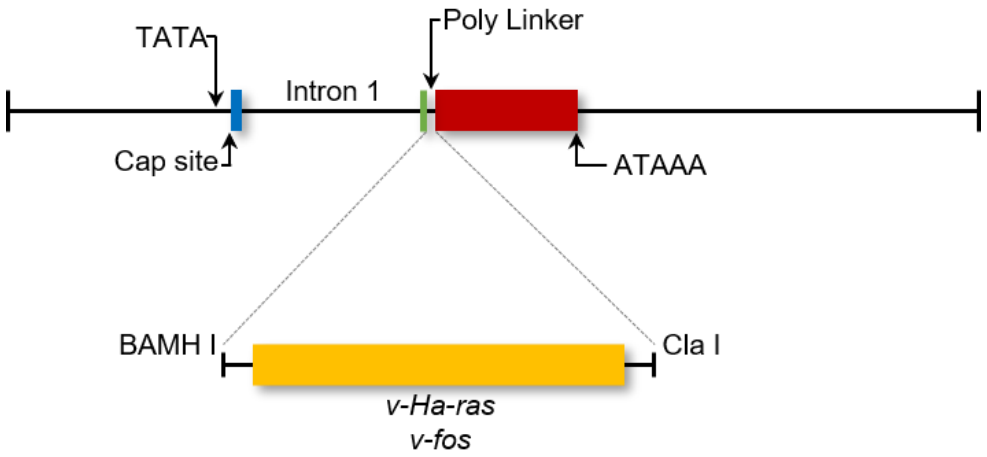

Figure 1-6: HK1 vector schematic for exogenous v-Ha-ras and v-fos expression in mouse keratinocytes.
The HK1 vector was originally derived from an EcorRI lambda clone of the full-length human Keratin 1 gene, from which the coding regions containing the 5' (blue) and 3' (red) flanking regions as well as the first intron (for efficient mRNA transcription and processing) were utilised. A polylinker sequence was inserted immediately downstream of the first intron, with the BamH I and Cla I restriction sites used to insert either the *v-Ha-ras* or FBJ/R chimeric form of *v-fos* genes were inserted. (adapted from Greenhalgh et al., 1993)

As shown in Figure 1-6, in addition to the 5' and 3' flanking sequences, intron 1 of HK1 was included in the transgene construct; this is an important feature to ensure normal processing of the nascent mRNA transcript, as their

removal by the spliceosome complex is able to influence processes such as correct polyadenylation and nuclear export, thereby impacting the desired and efficient expression of the gene (Le Hir et al., 2003).

Multiple founder lines of mice expressing either the *HK1.ras* or *HK1.fos* transgenes were established and characterised (Greenhalgh et al., 1993a, 1993b), with severity of symptoms varying, likely due to differences in copy numbers and insertion sites (Laboulaye et al., 2018). All *HK1.ras* mice exhibit hyperplasia and some hyperkeratosis at birth, appearing wrinkled when compared to their normal littermates, which subsides from about 10 days post-partum, leaving them indistinguishable from normal . Ear tagging for identification at 3-4 weeks of age also serves as a site of wound promotion. *HK1.ras*^{1205} mice develop papillomas at this site around 8 to 10 weeks after tagging which are prone to regression if the tag is lost or if given enough time, indicative of their benign nature. An alternate line, *HK1.ras*^{1276}, does not develop papillomas after tagging, just hyperplasia comparable with their untagged ear skin, without further genetic insult and was typically employed where the phenotype became too extensive to allow for reasonable animal welfare to be maintained within UK experimental guidelines (Greenhalgh et al., 1993a). *HK1.fos*^{488} (hereafter referred to as *HK1.fos*) mice are almost identical to their normal siblings, though by the time of tagging their ears tend to be mildly hyperplastic and smaller than their littermates. Their phenotype remains very mild until around 7 months of age, when the hyperplasia and hyperkeratosis tend to become pronounced on the tagged ear, while the untagged side remains almost normal.

When *HK1.ras*^{1205} mice were bred with *HK1.fos*, the resultant bi-genic pups developed severe hyperplasia and hyperkeratosis soon after birth which was not compatible with life as it considerably restricted their movement. Breeding of *HK1.fos* with the milder *HK1.ras*^{1276} line, however, generated pups with a phenotype only slightly more pronounced than mono-genic *HK1.ras* pups, thus allowing characterisation of the bi-genic phenotype. By the time these mice are tagged, they generally have pronounced hyperplasia and some hyperkeratosis on both ears. Despite the increased severity of the phenotype compared with *HK1.ras*, and in contrast to *in vitro* studies of bi-genic *v-Ha-*

ras/*v-fos* transfected keratinocytes, the papillomas which result from wound promotion of these mice still do not convert to malignancy (SCC), though they are not regression prone as observed in *HK1.ras*.

Thus, this autonomy coupled to a lack of malignant conversion made these mice ideal to study the requirements for malignant conversion. One of the first studies involved inducible, conditional ablation of the Pten ability to regulate the PI3K/Akt pathway (Lesche et al., 2001; Yao et al., 2008; MacDonald et al., 2014) in order to both model Cowden Syndrome and add Akt signalling analysis to that of MAPK effects.

Induction of a malignant phenotype requires further genetic aberrations, ideally tissue-specific and possessing a temporal component to control the stage of development at which new mutations are introduced. This was performed here by inducible Cre-mediated ablation of Pten exon 5, thereby preventing its inhibition of the PI3K/Akt pathway and other functions discussed earlier. This requires the presence of a keratinocyte-specific Cre recombinase which targets loxP sequences flanking the sequence to be knocked out, in this case, the entire exon 5 of *Pten*: *Δ5Pten*. Exon 5 encodes the core catalytic motif (Waite and Eng, 2002) which is required for its dual phosphatase functions. In this model, Cre expression is under a Keratin 14 promoter (*K14.CrePR1*) which targets it to the undifferentiated basal keratinocytes in the interfollicular epidermis as well as hair follicle cells (Berton et al., 2000), shown in *Figure 1-7A*. In order to temporarily control the ablation of Pten activity, that is, following *HK1.ras*/*fos* papilloma, the Cre transgene is conjugated to a modified progesterone ligand binding domain (PR1), which is insensitive to endogenous progesterone but can bind the synthetic steroid Mifepristone, also called RU486. Binding of RU486 to the PR1 domain causes translocation of Cre to the nucleus to allow it to excise sequences which are flanked by loxP sites ("floxed"), as depicted in *Figure 1-7B*.

Histology of the progression from normal skin through hyperplasia and benign papilloma to well-differentiated squamous cell carcinoma (wdSCC) is depicted in *Figure 1-8* alongside the expression of early differentiation marker, Keratin 1 (Yuspa et al., 1989), with Keratin 14 as a counterstain showing undifferentiated keratinocytes at each stage.

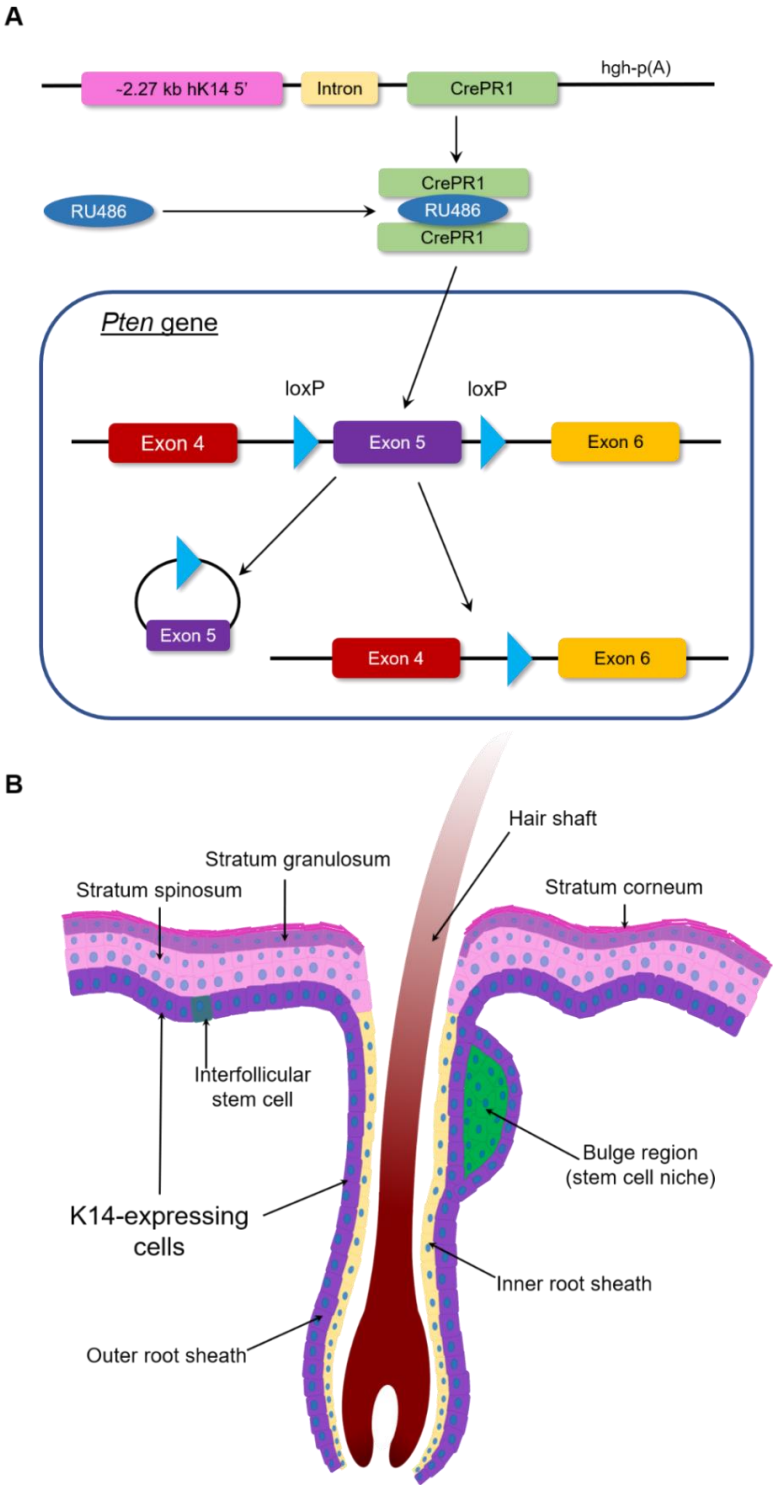

Figure 1-7: Pten ablation by *K14.CrePR1* in the epidermis and hair follicles.
(**A**) Schematic of Cre-loxP mediated excision of *Pten* exon 5. Cre recombinase bound to the modified progesterone ligand binding domain is translocated to the nucleus following binding to RU486 (topically applied). The enzyme mediates DNA excision after loxP sites, resulting in a loop of DNA including the excised exon 5 plus one loxP site, while the other remains in the genomic DNA (**B**) Depiction of the interfollicular epidermis and hair follicle (HF) showing the cells which express K14 in the interfollicular basal layer and the outer root sheath of the HF (purple), where *K14.CrePR1*-mediated excision will occur after RU486 treatment. The cells where ablation will occur include the stem cells in both the interfollicular epidermis and the bugle region of the HF (green). K14 is not expressed, thus *K14.CrePR1* is not active, in suprabasal spinous and granular layer cells (pink and hatched), not in the inner root sheath layers (yellow).

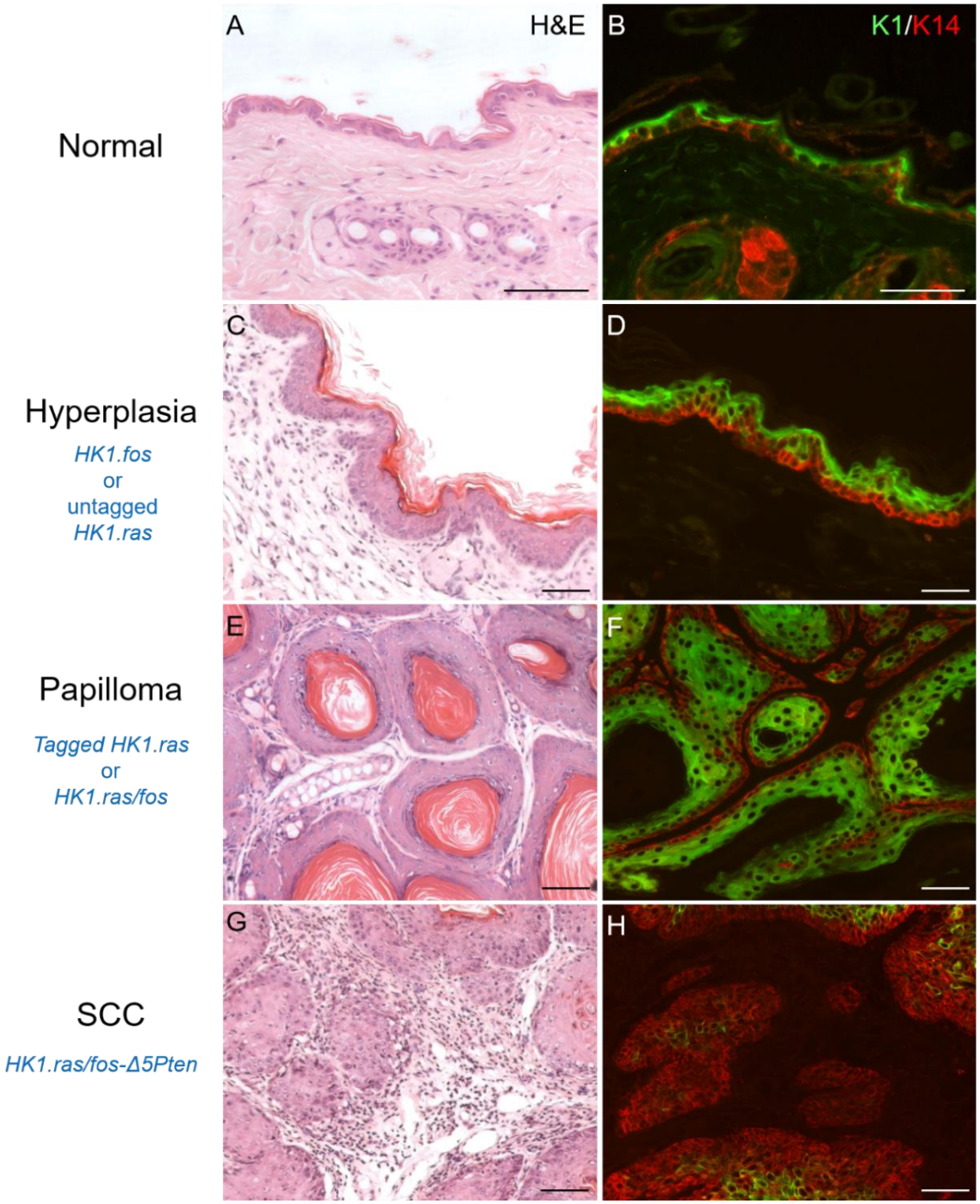

Figure 1-8: Spectrum of carcinogenesis in mouse skin histology and early differentiation marker (K1) expression.
Normal mouse skin is around 1-2 cells thick (**A** and **B**); exogenous Fos expression with wound promotion (tag) or H-Ras expression without tag results in hyperplastic skin which is more akin to normal human skin in appearance, with clearly defined basal, spinous, granular, and cornified layers (**C**) and strong suprabasal Keratin 1 expression in green (**D**); wound promotion of either *HK1.ras* mice or bi-genic *HK1.ras/fos* mice results in development of benign papillomas, characterised by keratin pearl formation (**E**) and strong K1 expression, indicating they are benign; induced ablation of Pten phosphatase activity in addition to *HK1.ras* and *HK1.fos* expression causes loss of differentiation and progression to a malignant histotype (**G**) and loss of K1 (**H**) indicating malignancy. Keratin 14 (red) stains undifferentiated cells. *Scale bars approx. 100 µm.*

Analysis of this multistage model found that p53 expression was strong in the basal layer of premalignant papillomas, while its inhibitor, Mdm2, was mostly suprabasal. As areas of the tumour progressed to well differentiated SCC, as determined by histology and K1 loss (*Figure 1-8*), p53 expression was greatly reduced, while Mdm2 expression became more basal. Interestingly, p53-independent p21 expression was found to persist for a time, limiting progression to a poorly differentiated state (Macdonald, et al., 2014), until an increase in Akt expression antagonises p21 activities allowing pdSCC to develop. This supports previous findings in *HK1.fos-Δ5Pten* mice which develop benign keratoacanthomas (KAs), rather than SCC, due to very strong induction of p53 and p21 expression to limit carcinogenesis (Yao et al., 2008). Therefore, it was hypothesised that if p53 levels could be maintained, conversion of *HK1.ras/fos-Δ5Pten* papillomas would be inhibited. This led to analysis of proteins involved in p53/Mdm2 regulation, with 14-3-3σ/stratifin identified as an ideal candidate to explore further.

1.6. 14-3-3σ/Stratifin

1.6.1. 14-3-3 proteins

The 14-3-3 family of adapter proteins comprises seven closely related, highly conserved isoforms: β, γ, ε, ζ, η, θ/τ and σ (α and δ were identified as further isoforms but are, in fact, just the phosphorylated forms of β and ζ) (Aitken et al., 1995; Aitken, 2006). They were named for the specifics of their discovery via 2D DEAE-cellulose chromatography and starch gel electrophoresis (14^{th} fraction of bovine brain homogenate in the DEAE-cellulose column and fraction 3.3. at a later step in the process); 14-3-3s make up approximately 1% of total protein in neurological tissue. These proteins have no intrinsic enzymatic activity but act to modulate the activity or subcellular localisation of their ligands (Sluchanko and Gusev, 2010).

They function as either homo or heterodimers, with each 28-33 kDa monomer comprising 9 alpha helices which are arranged such that the dimer is C-shaped, with the N-termini associated in the centre and two phosphobinding

grooves on the inner curve of each monomer. All isoforms have high affinity for two consensus binding motifs: RSXpSXP and RXXXpSXP; where pS represents a phospho-Serine, R is Arginine, P is Proline, and X is any amino acid except Cysteine. There have also been some cases identified involving different phosphorylation sites, or no phosphorylation at all (Nomura et al., 2015), though these are less common. A dimer is able to bind to 2 sites, most often on the same target protein, though a few instances in which a 14-3-3 isoform acts as an intermolecular bridge have been identified, most notably involving Raf-1 (Raf-1/Bcr and Raf-1/PKC, for example) (Braselmann and McCormick, 1995; Van Der Hoeven et al., 2000). The more common mode of binding to single targets has been described as a "gatekeeper" mechanism: whereby one site on the target protein must be bound first, which then increases the binding affinity of the second target site to the other side of the 14-3-3 dimer, which is believed to stabilise the interaction (Wilker et al., 2005).

14-3-3 proteins are highly conserved across eukaryotic species (phylogenetic analysis suggests that the isoforms evolved prior to the divergence of mammals) with orthologs of particular isoforms from different species having higher sequence similarity than different isoforms within a species (Wang and Shakes, 1996). 14-3-3 isoforms are present in all mammalian tissues and have been found (either by experiment or by motif homology) to interact with >300 proteins (MacKintosh, 2004). They are predicted to influence almost all cellular pathways in some manner and, as such, have functions in a wide variety of cellular processes including proliferation, autophagy, apoptosis, migration and wound healing, occasionally in contradictory roles. They are involved in cell signalling, cell cycle inhibition and progression, intracellular trafficking/targeting, cytoskeletal organisation and transcription (Fu et al., 2000; Sluchanko and Gusev, 2010). Due to the nature of many of these roles, 14-3-3 are primarily cytoplasmic proteins, though can also be found at the plasma membrane, in the nucleus and Golgi to a lesser degree (Fu et al., 2000). The high degree of conservation coupled with their ubiquitous presence in all cell types mediating a wide variety of processes is indicative of their importance in normal development and functioning.

While certain isoforms can perform specific functions in certain cell types, many of the effects exerted by 14-3-3s are not tissue-specific as they relate to global processes, for example, cell cycle regulation and apoptosis. These proteins have been implicated in both positive and negative regulation of these processes. For example, γ, ε and ζ isoforms can mediate activation of Raf and PI3K to promote cell growth and proliferation (Radhakrishnan and Martinez, 2010; Radhakrishnan et al., 2012), ζ is involved in BAD phosphorylation (deactivation) to inhibit apoptosis, while conversely, γ binds MDMX to prevent its ubiquitination of p21 to induce cell cycle arrest at the G1/S checkpoint (Aghazadeh and Papadopoulos, 2016), thereby counteracting its other growth-promoting effects.

1.6.2. Stratifin: the epithelial-specific 14-3-3

As mentioned earlier, most 14-3-3s can form either homo or heterodimers, with most isoforms preferentially forming heterodimers. 14-3-3σ, hereafter referred to as Stratifin, is unusual in that it almost exclusively functions as a homodimer. The reasons for this have been extensively researched, with five amino acid residues found to be important: mutations in Ser^{5}, Glu^{20} and Glu^{80} appear to encourage heterodimerisation, while mutations in Phe^{25} and Glu^{55} inhibit homodimerisation (though do not increase frequency of heterodimerisation); if all five are mutated, homodimerisation appears totally blocked but heterodimers are still able to form. Other unique features of this isoform include a salt bridge between Lys^{9} and Glu^{83} and a ring-ring interaction between Phe^{25} and Tyr^{84} (Wilker et al., 2005; Benzinger et al., 2005b). Stratifin is highly expressed in squamous epithelia and at a lower level in simple epithelia and is not usually expressed in brain unlike the other isoforms which are very abundant in neurological tissue (Cornell & Toyo-oka, 2017). The preference for homodimerisation coupled with the epithelial-specific nature of this isoform are indicative of the greater divergence of this isoform from the other 14-3-3 proteins and therefore of its tissue-specific functions.

Stratifin (gene: *SFN*) is so-called because of its identification as an important protein in epithelial differentiation, which gives rise to the different

epidermal layers, or stratifications, discussed in *Section 1.1*. The protein is ubiquitous in suprabasal epidermal cells, where its transcription is induced by the p53 gene family member, p63 (Trink et al. 2007), specifically the ΔNp63 isoform (Westfall et al., 2003) which lacks the transactivation domain of TAp63. In this role in epidermal differentiation, stratifin has been identified as an important mediator of keratinocyte spatial awareness, which is vital in development of a normally stratified epidermis. Work in *C. elegans* and in HEK 293 cells had shown that 14-3-3 proteins were able to bind to Par3 in the Par3/Par6/aPKC apical polarity complex, specifically around Ser144 of Par3 (Hurd et al., 2003). Subsequently, stratifin was identified as the binding partner of Par3 in mammary cells, with knockdown or knockout in those cells ablating normal cell polarization in 3D Matrigel cultures (Ling et al., 2010).

Stratifin has been found to limit cell cycle progression through several different protein interactions, the most well-known example being its effects in preventing p53 degradation following activation of the DNA-damage response (DDR), for which is has often been referred to as a DNA damage related protein (Hermeking et al., 1997). The level of p53 RNA is low in quiescent cells but increases quickly in response to mitogenic stimulation. However, while the cell cycle is progressing normally, p53 is bound to E3 ubiquitin-ligase MDM2 which tags it for degradation, thereby keeping the active level low (Reisman et al., 2012). This regulatory mechanism is presumably to allow rapid activation of p53 if DNA damage occurs during the growth phases of mitosis when the DNA is vulnerable, and at the G1/S checkpoint. When DNA damage occurs, e.g., double stranded breaks caused by UVB radiation, the DDR kinases ATM and ATR phosphorylate Chk1/2 which, in turn, phosphorylate p53 at several sites in the N- and C-termini (Shieh et al., 2000; Ou et al., 2005). This phosphorylation partially stabilising its levels to allow p53 to transcriptionally activate proteins involved in cell cycle arrest or apoptosis. Stratifin is an important transcriptional target during the DDR, though p53 binds a different DNA response element in the *SFN* promoter than p63 (Westfall et al., 2003). Stratifin binds MDM2 (and possibly MDMX) in the RING-finger domain (Lee and Lozano, 2006), which induces auto-ubiquitination and chaperones it out of the nucleus to allow p53 levels to increase as a result. This positive feedback loop is shown in *Figure 1-9*.

Aside from this, Stratifin has been found to limit cell cycle progression by several other interactions, such as inhibition of cyclin/cyclin-dependent kinase complexes: cyclin D/CDK4/6 at the G1/S checkpoint, and cyclin B/Cdc2 at the G2/M checkpoint (Hermeking et al., 1997; Laronga et al., 2000; Steiner et al., 2012). Conversely, it is able to exert positive influence on cell cycle progression by upregulating mTOR activity via a complex with cytokeratin 17 (K17) (Kim et al., 2006; Mikami et al., 2015). In a similar vein, it can promote cell survival through sequestration of the vital pro-apoptotic protein, BAX, as shown by *SFN* knockout which restores sensitivity to pro-apoptotic signalling (Samuel et al., 2001).

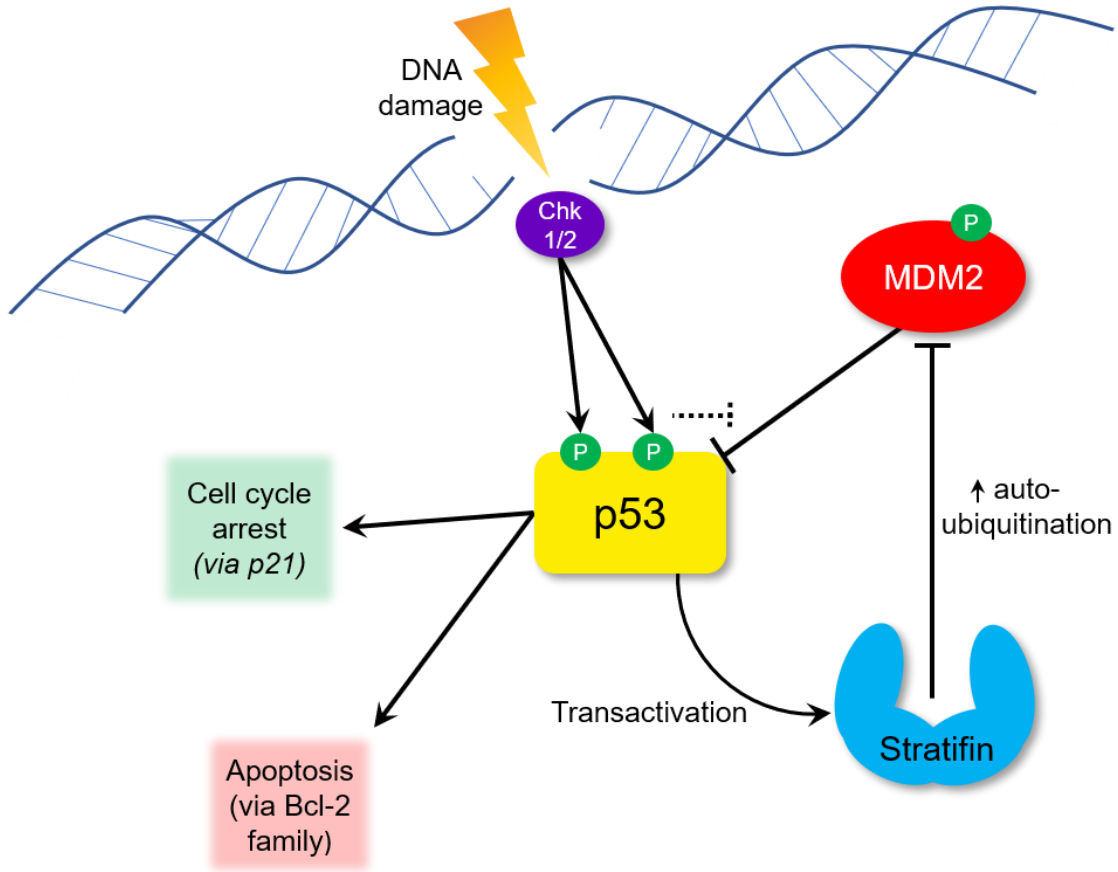

Figure 1-9: Schematic of p53 regulation following DNA damage.
DNA double-stranded DNA breaks, such as those caused by electromagnetic radiation, including UV light, induce the DNA damage response (DDR). Early in the process, ATM and ATR kinases (not shown) phosphorylate Chk1 & 2 kinases which, among other functions, stabilise p53 by phosphorylating the protein at multiple sites, somewhat inhibiting the E3 ubiquitin ligase, MDM2, from initiating p53 degradation, thereby allowing the quantity of p53 in the cell to rise. Subsequently, Stratifin is transactivated by p53 and can inhibit MDM2 by binding its RING finger domain and inducing auto-ubiquitination; thereby creating a positive feedback loop with p53, which can then induce cell cycle arrest via downstream effectors such as p21 and/or the intrinsic pathway apoptosis through interaction with proteins such as BAD, BAX and PUMA.

In addition, Stratifin has been shown to be required for normal development of hair follicles and production of hair shafts (Hammond et al., 2012), as demonstrated in Repeated Epilation (*Er*) mice, which have an insertion mutation in the SFN gene, producing a truncated protein (Herron et al., 2005). Homozygous (Er/Er) mice die shortly after birth due to defects in the airway and show defects in skin and limb development. Heterozygous (Er/+) mice are viable and have sparse fur, consistent with histology showing fewer hair follicles than normal and defects in those present. As the name suggests, the mutation causes repeated hair loss and, interestingly, aged Er/+ mice are also prone to spontaneously developing papillomas and squamous cell carcinomas (Lutzner et al., 1985).

Stratifin has also been shown to be released by keratinocytes to act on fibroblasts in the underlying dermis. It binds to receptor Aminopeptidase N/APN (also called CD13) on the surface of fibroblasts and causes the upregulating of AP-1 signalling in these cells (Lai et al., 2011). This induces expression of several matrix metalloproteinases, including: MMP-1/interstitial collagenase, MMP-3/stromelysin-1, MMP-8/neutrophil collagenase, MMP-10/stromelysin-2, and MMP-24/membrane-type5-MMP. Together, these can act to degrade many types of collagen (I, II, III, IV, IX, and X), as well as other matrix proteins like fibronectin, laminin, elastin, cadherins, and cartilage proteoglycans (Ghahary et al., 2005; Ghaffari et al., 2006). This allows extensive remodelling of the skin during wound healing, but has obvious implications in tumour invasion, also.

1.6.3. Stratifin in Cancer

Perhaps unsurprisingly, given the nature and variety of pathways the 14-3-3 family are known to modulate, several isoforms have now been implicated in various cancers. Of these, Stratifin is often cited as the isoform most closely linked with cancer (Aitken, 2006). However, its relationship with this group of diseases is not straightforward, as it has been described in both tumour suppressive and oncogenic roles in various carcinomas and adenocarcinomas.

Loss of function appears to rarely involve mutation or deletion of the *SFN* gene, rather suppression of expression is caused by hypermethylation of the

promoter in numerous cancer types including receptor-positive breast cancers (Ling et al., 2012), liver (Iwata et al., 2000), oesophagus (Ren et al., 2010), small cell and neuroendocrine lung cancers (Yatabi et al., 2002) and basal cell carcinoma (Lodygin et al., 2003). Downregulation via methylation of CpG islands downstream of the transcription start site has also been identified, though this appears to be less common than promoter methylation (Umbricht et al., 2001). Non-methylation dependent downregulation has also been reported, however, for example hypermethylation is uncommon in colorectal tumours (Ide et al., 2004; Shao et al, 2016). Reduction or loss of Stratifin expression is believed to be correlated with poorer survival outcomes in several of these carcinomas (Ren et al., 2010; Ling et al. 2012).

In contrast, Stratifin overexpression has been detected in many other carcinoma types, for example, in pancreatic ductal adenocarcinoma (PDAC) in which it is frequently overexpressed as a result of promoter hypomethylation (Tan et al., 2009). This can be quite dramatic, as in one case study wherein the mRNA level was 54-fold higher in PDAC tissue vs adjacent non-malignant tissue (Neupane and Korc, 2008). The same study went on to show that in pancreatic cell culture (PANC-1), Stratifin overexpression was demonstrated to confer a survival advantage following cisplatin treatment. Its overexpression also occurs commonly in lung adenocarcinoma (Shiba-Ishii et al., 2011; Kim et al., 2018). Interestingly, multiple studies have determined no correlation between the levels of Stratifin and p53, suggesting that in its oncogenic capacity, Stratifin often acts independent of the previously described Stratifin-p53-MDM2 regulatory axis.

Stratifin expression is also frequently upregulated (mostly via hypomethylation) in lung adenocarcinoma (Husni et al., 2019; Shiba-Ishii and Noguchi, 2012), non-small cell lung cancer (Radhakrishnan et al, 2011), late stage endometrial, as well as subsets of liver (Liu et al., 2014), gastric (Mühlmann et al., 2010) and colorectal cancers (Perathoner et al., 2005). Interestingly, one study showed that Stratifin positivity was more common in triple-negative breast cancers than any receptor-positive breast cancers tested, with Stratifin positivity conferring poorer prognosis (Ko et al., 2014). In these, positivity was also correlated with high histological grade, high nuclear grade

and p53 positivity; this is in contrast with other studies into pancreatic and gastrointestinal cancers where Stratifin and p53 levels were independent (Tanaka et al., 2004). Additionally, mouse models of basal-like breast cancer showed that Stratifin expression was associated with increased mammary cell invasiveness as it mediates a complex of G-actin/K5/K17 which allows rapid reorganisation of the actin cytoskeleton during invasion (Boudreau et al., 2013). In many cases where Stratifin overexpression is present it is well correlated with lymph node metastasis and overall worse prognosis (Li et al., 2009; Naidoo et al., 2012; Nakayama et al., 2005; Tanaka et al., 2004; Perathoner et al., 2005). Frequently, reports of overexpression in cancers specify cytoplasmic, rather than nuclear staining, highlighting the importance of subcellular localisation in its influence on the cell, especially considering that many of its tumour-suppressive functions are in the nucleus (Lodygin et al. 2003; Ko et al., 2014).

Given that p53 expression is lost upon malignant conversion in *HK1.ras/fos-Δ5Pten* multistage carcinogenesis, concurrent with greater activation of Mdm2 in the basal layers (Macdonald et al., 2014), it made sense to explore the expression of Stratifin in these tumours since it is integral to p53/Mdm2 balance. This will be explored in much greater detail in Chapter 3.

1.6.4. *K14.stratifin* Transgenic Mice

In the *HK1.ras/fos-Δ5Pten* multistage carcinogenesis model, p53 (and p21) status was significant to the inhibition of papilloma conversion to wdSCC, and to the further progression to poorly-differentiated SCC. Thus, it was hypothesised that exogenous overexpression of Stratifin could be employed to rescue the phenotype and prevent malignant conversion, or to explore the possibility of oncogenic effects, given the divergent activities described in the literature with regards to various carcinomas.

To explore this, a founder mouse was obtained which overexpressed full length human Stratifin under control of a K14 promoter (Cianfarani et al., 2011; Vassar et al., 1989). Thus, similar to the mechanism previously described to drive *K14.Cre* expression, the *K14.stratifin* transgene causes overexpression of Stratifin in undifferentiated basal layer and HF cells. In BDF-1 mice, the authors

described reduced epidermal thickness (tail skin), lower density of hair follicles, and reduced expression of keratins associated with an undifferentiated phenotype (K5, K14, and K15) on this genetic background. In cell culture, excess Stratifin impaired IGF-1 downstream effects (Cianfarani et al., 2011), consistent with observations in pancreatic cancers cells (PANC-1) where reduced IGF-mediated invasion was described (however, that study also showed an increase in EGF-mediated invasion) (Neupane and Korc, 2008).

These mice were crossed with the transgenes involved in the multistage model individually to assess the effects of bi-genic expression with the oncogenes: *HK1.fos*/*K14.stratifin* and *HK1.ras*^{1205}/*K14.stratifin*, or the loss of tumour suppressors: *K14.Pten*$^{flx/flx}$*.stratifin* and *K14.p53*$^{flx/flx}$*.stratifin*. Finally, ablation of p53 in both *HK1.fos*/*K14.stratifin* and *HK1.ras*^{1205}/*K14.stratifin* mice was also assessed to explore the roles Stratifin plays separate to p53. These will be described and discussed in detail in the following chapters.

1.7. Hypothesis

Does 14-3-3σ/Stratifin confer a protective (tumour suppressive) effects in transgenic mouse models of cutaneous squamous cell carcinoma or have oncogenic effects in line with findings in multiple human carcinomas?

1.8. Aims

To determine whether:

- endogenous Stratifin is a tumour suppressor in *HK1.ras*/*fos-Δ5Pten* multistage carcinogenesis

- Stratifin overexpression limits tumorigenesis when co-expressed with activated oncogenes *HK1.ras* (transgenic H-Ras) and *HK1.fos* (analogous to c-Fos)

- Stratifin is protective in the context of major tumour suppressor ablation (p53 and Pten)

Chapter 2 Materials and Methods

2.1. Materials

2.1.1. PCR Materials

Reagents/Kits	Manufacturer (Cat. Number)
Tail Lysis Buffer: 50 mM Tris-HCl pH 8.0, 100 mM EDTA pH 8.0, 100mM NaCl, 1% SDS, Proteinase K (20 mg/mL stock solution, added fresh)	
Taq DNA Polymerase • 10X PCR Buffer (200 mM Tris-HCl, pH 8.4, 500 mM KCl) • $MgCl_2$ (50 mM)	Invitrogen ™ 10342053
• AmpliTaq Gold® DNA Polymerase (1000 U) • 10X Buffer I (contains 15 mM $MgCl_2$)	Applied Biosystems ™
• Deoxynucleoside triphosphate set (100 mM each dATP, dTTP, dCTP, dGTP)	Roche DNTP-RO
6X DNA loading buffer: • 0.25% Bromophenol Blue • 0.25% Xylene Cyanol • 30% Glycerol	Sigma-Aldrich • B0126 • X4126 • G5516
UltraPure™ Agarose	Invitrogen ™ #16500500

Table 2-1: PCR materials and manufacturers/catalogue numbers.

2.1.2. Immunostaining Materials

Antibody	Dilution	Manufacturer (Cat. Number)
Rabbit polyclonal anti-Keratin 1	1:100	BioLegend® 905601 (previously Covance PRB-165P)
Rabbit polyclonal anti-Keratin 6A	1:100	BioLegend® 905701 (previously Covance PRB-169P)
Guinea pig polyclonal anti-Keratin 10	1:100	Fitzgerald 20R-2629
Guinea pig polyclonal anti-Keratin 14	1:400	Fitzgerald 70R-18180
Rabbit RabMAb® anti-Keratin 16	1:100	Abcam ab76416
Rabbit polyclonal anti-Keratin 17	1:100	Abcam ab53707
Rabbit polyclonal anti-14-3-3σ	IHC 1:200 IF 1:100	Invitrogen ™ PA5-23507
Rabbit polyclonal anti-E-Cadherin	1:200	Proteintech® 20874-1-AP
Rabbit polyclonal anti-β-Catenin	1:50	Abcam ab16051
	1:50	Sigma-Aldrich PLA0230
Rabbit polyclonal anti-p53	1:100	Abcam ab31333
	1:100	Abcam ab131442
	1:50	Santa Cruz (discontinued)
Rabbit polyclonal anti-p21	1:150	Proteintech® 10355-1-AP
	1:50	Santa Cruz (discontinued)
Rabbit RabMAb® anti-Akt1(phospho-Ser473)	1:100	Abcam ab81283
Rabbit RabMAb® anti-Tenascin-C	1:200	Abcam ab108930
Rat monoclonal Anti-BrdU	1:100	Abcam ab6326
HRP-conjugated goat anti-rabbit IgG	1:250	Vector® Laboratories PI-1000-1
Biotinylated goat anti-guinea pig IgG	1:100	Vector® Laboratories BA-7000-1.5
Texas Red® Streptavidin (non-Ab)	1:400	Vector® Laboratories SA-5006
Fluorescein (FITC) AffiniPure donkey anti-rabbit IgG (H&L)	1:100	Jackson ImmunoResearch Europe Ltd. 711-095-152
Goat anti-Rat IgG H&L (Alexa Fluor® 488)	1:200	Abcam ab15057

Table 2-2: Primary and secondary antibodies, their working dilutions, and manufacturers/catalogue numbers.

2.1.3. Cell Culture Materials

2.1.3.1. Reagents and Buffers

Material	Manufacturer (Cat. number)
L-glutamine (200 mM)	Gibco™ 25030081
Sodium pyruvate (100 mM)	Gibco™ 11360070
Penicillin/Streptomycin (10,000 U/mL)	Gibco™ 15140122
Foetal Bovine Serum	Gibco™
Chelex® 100 Sodium form	Sigma-Aldrich C7901
Dulbecco's Phosphate Buffered Saline (no Ca^{2+}, no Mg^{2+})	Gibco™ 14190169
2.5% Trypsin (+ 0.01% EDTA)	Sigma-Aldrich 59418C

Table 2-3: Cell culture materials and manufacturers/catalogue numbers.

2.1.3.2. Media

DMEM (Gibco 21068028): High glucose, no pyruvate, no glutamine, no calcium.

Keratinocyte Growth Medium Kit (PromoCell C-20111): 500 mL basal medium plus supplement pack including: Bovine Pituitary Extract, human Endothelial Growth Factor, Hydrocortisone, Insulin, Epinephrine, Transferrin-5 & $CaCl_2$)

Complete culture medium (low Ca^{2+}): 500 mL DMEM, 20% KGM (or 10% KGM/10% FCM), 10% FBS, 10 mM L-glutamine, 1 mM Sodium pyruvate, Penicillin/Streptomycin (50 U/mL and 50 µg/mL, respectively; approx. 85 µM each), 0.05 mM Ca^{2+}.

2.1.4. Western Blotting Materials

Material	Manufacturer (Cat. number)
Mini-PROTEAN® TGX™ Precast Gels (4-20%)	Bio-Rad 4561093
2x Laemmli Sample Buffer	Bio-Rad 1610737
Precision Plus Protein™ Dual Xtra Prestained Protein Standards	Bio-Rad 1610377
Transfer membrane Immobilon®-P PVDF	Merck-Millipore 10344661
10x Tris-Glycine (TG) Buffer	Bio-Rad 1610734
10x Tris-Glycine SDS (TGS) Buffer	Bio-Rad 1610732
Tween®-20 10% non-ionic, aqueous solution	Sigma-Aldrich 11332465001
TBS (50 mM Tris-HCl pH 7.5, 150 mM NaCl) (Prepared in-house)	Tris-HCl (Trizma®-HCl): Sigma-Aldrich T3253 NaCl: Sigma-Aldrich S7653

Table 2-4: Western blotting materials and manufacturers.

2.2. Methods

2.2.1. Mice

Mice were maintained under non-barrier conditions and fed a standard diet, with rotations including an ivermectin-containing diet as prophylaxis against ectoparasites, and water *ad libitum*. Husbandry was provided by staff at the University of Glasgow Central Research Facility (CRF), including weaning of pups and setting up matings if I was unable to do so. Animals were sacrificed by overexposure to isoflurane gas to the stage of non-recovery and confirmed by cervical dislocation. All experiments were carried out with the Personal Licence IAED844E7 and in accordance with the Project Licence P82170325 under the UK Home Office Guidelines.

2.2.2. Transgenic mouse lines

Transgenic mice expressing activated v-H-Ras and/or v-Fos from a human keratin K1-based vector, modified to express in basal- and suprabasal keratinocytes (*HK1.ras/fos*) have been described previously and produce autonomous papillomas without malignant conversion (Greenhalgh et al., 1990). These mice were crossed to mice expressing a keratin K14-driven Cre fusion protein (*K14.CrePR1*) (Berton et al., 2000) and breeding strategies maintained *HK1.ras/fos* and the RU486-inducible *K14.CrePR1* regulator as heterozygous transgenes in mice homozygous for the lox-P-flanked Pten exon 5 alleles (*Δ5PTEN*$^{flx/flx}$ (Lesche et al, 2001)). Bi-genic and tri-genic combinations of *HK1.ras/fos-5Pten*$^{flx/flx}$ progeny were genotyped by PCR as described (Yao et al., 2006, 2008; Macdonald et al., 2014) using primer pairs detailed in section 2.2.3. Pten phosphatase activity was ablated in epidermis following topical treatment of skin with 2 µg RU486 (Mifepristone; Sigma, Gillingham, UK) dissolved in 50 µL ethanol, with 15 µL applied to the dorsal surface of each ear and shaved back weekly for 3 weeks, and controls receiving ethanol alone.

Transgenic mice overexpressing human 14-3-3σ/Stratifin in undifferentiated epidermis (*K14.stratifin*) were generated as described on a BDF-1 genetic background at the Laboratory of Molecular and Cell Biology, IDI-IRCCS, Rome, Italy (Cianfarani et al., 2011). A homozygous male *K14.stratifin* mouse was obtained from this lab in 2015 and crossed into an outbred ICR genetic background for further crossbreeding with the transgenes involved in the multistage model, described above. The PCR primer pair detailed in the described method was found to produce a weak band, causing difficulty in genotyping. A new forward primer was designed which allowed the production of a larger DNA fragment (280 bp) which allowed for easier genotyping. The new pair is detailed in section 2.2.3. Similarly to Pten, p53 activity could be ablated by the same system after inclusion of the floxed p53 gene. All experiments adhered to UK Experimental Regulations (Licence: 60/4318 and P82170325 to DAG).

2.2.3. DNA isolation

DNA was extracted from approx. 5 mm pieces of tail tissue obtained from weaned pups at time of ear tagging (3-4 weeks old). Tissue samples were digested overnight at 55°C in 500-700 µL tail lysis buffer (50 mM Tris.HCl, 100 mM EDTA, 100 mM NaCl, 1% SDS) + 500-700 µL Proteinase K (20 mg/mL stock), depending on sample; 5 mm tail tips were digested in 500 µL, while biopsy samples were often larger or keratotic so 600/700 µL was used instead.

Digested samples were centrifuged at 13,000 rpm (approx. 19,000 x g) for 20 minutes to precipitate the undigested material, e.g., hair and bone fragments. An equal volume of ice-cold ethanol (EtOH) was then gently pipetted onto each sample to precipitate dissolved DNA from the buffer. Precipitated DNA was then wound onto a clean micropipette tip, excess buffer carefully blotted onto tissue paper, and the DNA resuspended in 300 µL dH_2O.

2.2.3. Polymerase Chain Reaction (PCR) Genotyping

1X Master Mix for all genotyping PCRs except *K14.stratifin* (total per reaction: 23 µL Master Mix + 2 µL DNA template):

Reagent	Volume (µL)
10X PCR buffer (200 mM Tris-HCl pH 8.4, 500 mM KCl; -$MgCl_2$)	2.50
$MgCl_2$ (25 mM stock)	2.00
Forward primer	0.50
Reverse primer	0.50
dNTP mix (20 mM)	0.25
Taq DNA Polymerase (5 U/µL) (Invitrogen)	0.25
dH_2O	17.0

Table 2-5: PCR reagents and volumes (µL) per reaction.

1X Stratifin PCR Master Mix (total per reaction: 27 µL MM + 3 µL DNA template):

Reagent	Volume (µL)
GeneAmp® 10X Buffer I (contains 15 mM $MgCl_2$)	3.20
Forward primer	0.76
Reverse primer	0.76
dNTP mix (Roche; made to 20 mM stock)	0.30
AmpliTaq Gold® DNA Polymerase (Applied Biosystems)	0.30
dH_2O	21.0

Table 2-6: PCR reagents and volumes for genotyping of *K14.stratifin*.

Transgene	Primer Pair
HK1.ras	5'-GGATCCGATGACAGAATACAAGC-3' 5'-ATCGATCAGGACAGCACACTTGC-3'
HK1.fos	5'-GGATCCATGATGTTCTCGGGTTT-3' 5'-CGATTATTGCCACCCTGCCATG-3'
*Pten**	5'-ACTCAAGGCAGGGATGAGC-3' 5'-GTCATCTTCACTTAGCCATTGG-3'
*Δ5Pten***	5'-ACTCAAGGCAGGGATGAGC-3' 5'-GGTTGATATCGAATTCCTGCAGC-3'
*p53**	5'-CACAAAAACAGGTTAAACCCAG-3' 5'-AGCACATAGGAGCAGAGAC-3'
*Δp53***	5'- CACAAAAACAGGTTAAACCCAG-3' 5'-GAAGACAGAAAAGGGGAGGG-3'
K14.CrePR1	5'-CGGTCGATGCAACGAGTGAT-3' 5'-CCACCGTCAGTACGTGAGAT-3'
K14.stratifin	5'-CATGGACATCAGCAAGAAGG-3' 5'-CTCCTAGGGACTCTAGAGG-3'

Table 2-7: Forward and Reverse primer sequences for detection of transgenes. *Distinguishes wild-type genes from those with loxP insertions (floxed genes). **Detects gene which has had sequence between loxP sites excised by Cre recombinase. All working primer concentrations = 20 µM.

(Trans)Gene	Initial denat.	Denaturation	Annealing	Extension	Cycles	Final exten.
K14.Stratifin	5 m/ 95˚C	30 s/ 95˚C	55 s/ 57˚C	60 s/ 72˚C	45	10 m/ 72˚C
HK1.Ras	5 m/ 95˚C	30 s/ 95˚C	60 s/ 56˚C	60 s/ 72˚C	35	10 m/ 72˚C
HK1.Fos	2 m/ 95˚C	30 s/ 95˚C	30 s/ 62˚C	60 s/ 72˚C	35	15 m/ 72˚C
K14.CrePR1/ K5.CrePR1	5 m/ 94˚C	30 s/ 94˚C	45 s/ 58˚C	60 s/ 72˚C	35	5 m/ 72˚C
Pten/ Δ5Pten	2 m/ 94˚C	30 s/ 94˚C	60 s/ 63˚C	90 s/ 72˚C	36	10 m/ 72˚C
p53/ Δp53	3 m/ 94˚C	30 s/ 94˚C	20 s/ 58˚C	60 s/ 72˚C	32	5 m/ 72˚C

Table 2-8: Thermocycler programme conditions for genotyping PCRs.

2.2.4. Immunostaining

All sections were heated to 60ºC for 40 min and then deparaffinised in xylene for a further 20 min before being re-polarised in 100% EtOH for 5 min. Sections were then washed twice in PBS between every subsequent step. Unmasking of proteins was achieved by heated-mediated epitope retrieval: sodium citrate (pH 6.0) was heated to between 95 and 100ºC in a microwave oven, and reheated subsequent to slides being added. Sections were allowed to cool in buffer for 40 min. For IHC, endogenous peroxidase activity was quenched by treatment with 3% H2O2 for 10 min at ambient temperature. Sections were blocked using the appropriate serum matching the secondary antibody, diluted in PBS (IHC: 10% normal goat serum; IF 10% normal goat/10% normal horse serum due to double labelling) for approximately 30 min. Primary antibodies were diluted in the blocking serum and incubated on sections overnight at 4ºC.

Immunohistochemistry: Sections were incubated for 1 hr with HRP-conjugated goat anti-rabbit in 10% BSA (1:200) at ambient temperature. After washing, sections were treated with DAB according to manufacturer's

instructions for optimised time periods/antibody to visualise antibody binding. Slides were washed with dH_2O and counterstained with haematoxylin, thoroughly washed with tap water then decolourised with acid-alcohol (1% HCl in EtOH). Sections were then treated with Scott's Tap Water for 1 min to induce blue colour in haematoxylin staining. Slides were then treated in EtOH for 3 min to displace water, followed by 3 min in Xylene. After drying, coverslips were attached using Pertex® mounting medium.

Immunofluorescence: Sections were first incubated with biotinylated goat anti-guinea pig IgG in 10% BSA for 1 hr (ambient temperature), then subsequently with a combination of FITC-conjugated donkey anti-rabbit IgG and Texas Red-Streptavidin (to bind biotin) for 1 hr. Coverslips were attached using PermaFluor™ Aqueous Mounting Medium.

Micrographs were captured using Zeiss Axio Cam with the Axioplan 2 Carl Zeiss Microscope along with imaging software AxioVision 3.0 for Windows. Composite images were subsequently assembled using Microsoft Image Composite Editor (ICE). Some light microscopy images were obtained using at the Queen Elizabeth University hospital.

2.2.5. BrdU labelling and analysis

Mice were injected intraperitoneally with 125 mg/kg bromodeoxyuridine (BrdU) suspended in saline (0.9% NaCl) approximately 2 hr prior to biopsy. BrdU labelling was visualised using IF analysis as describe previously, using rat anti-BrdU (abcam ab6326 1:100) primary antibody and Alexa Fluor® 488 anti-rat secondary antibody (abcam ab15057 1:200) with keratin 14 as a counterstain to identify basal layer keratinocytes. Enumeration of BrdU positive cells was done manually by counting number of positive cells first in 1 mm basal cells (attached to basement membrane) and separately in all suprabasal cells in the same distance. High suprabasal count was considered to be a marker for a less well-differentiated, more aggressive tumour. Boxplots to display count data were generated using SPSS software (IBM).

2.2.6. Primary Keratinocyte Culture and Generation of Cell Lines

Pups were obtained which had been euthanised at between 24 and 36 hr old prior to the development of follicles which would prevent epidermal-dermal separation. A small sample of tail tissue from each was taken to be digested in lysis buffer containing proteinase K for genotyping analysis (after a short 4-5 hr digestion DNA was isolated and analysed as described in Section 2.2.3) as the pups were separated into numbered 60 mm dishes. The limbs were removed at the elbow/hock joints and the skins were removed in a single piece to limit fibroblast contamination at a later stage. The skins were floated on 0.25% Trypsin at 4ºC o/n to facilitate separation of the layers the next morning. The epidermises were batched depending on the genotyping results into Wild Type (ICR), *K14.stratifin* only, *HK1.fos* only, and *HK1.fos/K14.stratifin* groups. The batches were placed in 50 mL corning tubes with DMEM-glutamax medium (high Ca^{2+}) and rocked by hand for 20 min to suspend as many keratinocytes as possible through the medium (indicated by the opacity of the liquid). The suspensions were filtered through sterile gauze to remove basement membrane components and other large cellular debris and centrifuged at 900 rpm for 3 min to pellet the cells. Pellets were resuspended in Low Ca^{2+} DMEM. Cells were plated out at a concentration of 5 x 106 cell/mL with the presumption of ~40-50% plating efficiency.

Primary cells were kept in clonal growth medium (Low Ca^{2+} DMEM + 10% FBS + 20% KGM) for 4 weeks without subculture. At this stage some were seen to be contaminated with fibroblasts which were growing more quickly than the keratinocytes, limiting colony growth. These were differentially trypsinised (as fibroblasts detach much more readily than keratinocytes) and left to continue growing to confluency. When confluent, 2 T25s + ½ of one more T25 were pooled and split into 3 T75s.

Photographs of cell cultures were captured using a Panasonic DMC-G5 camera mounted on an Olympus phase contrast microscope.

2.2.7. Clonal Growth Assay

Following trypsinisation and resuspension of cells in a confluent T75 flask a sample was taken to be counted using a haemocytometer: Four 4x4 grids were counted, ignoring non-viable cell debris and clumped cells which were not separated by trituration. The average count (N) was used to estimate the number of cells/mL in the suspension such that the concentration was N x 10^4. 100 µL had been taken from this suspension and added to 10 mL (10,000 µL) prior to counting to create a 1:100 dilution, therefore the original concentration is reduced to N x 10^2. The desired concentration to plate out "at clonal density" is 50 cell/mL therefore this 1:100 dilution was further diluted to achieve this concentration, e.g., 6500 cells/mL reduced to 50 cell/mL by diluting 184 µL with 24 mL clonal growth DMEM (low Ca^{2+}, 10% KGM/10% FbCM) which was then plated out in 6 x 60 mm dishes (4 mL per dish). 3 dishes for each line were treated with high calcium medium after 3 days.

2.2.8. Protein Isolation from Keratinocyte Cultures

RIPA (Radioimmunoprecipitation assay buffer): 150 mM NaCl, 50mM Tris.HCl (pH 7), 500 µL Triton-X 100, 1% (w/v) Deoxycholic acid (initially dissolved in 25 mL 1M NaOH solution to increase solubility). Adjusted to ~pH 7.0 by addition of HCl. ß-ME/SDS buffer: 50 mM Tris.HCl, 2% (v/v) ß-mercaptoethanol, 1% (v/v) SDS.

All primary cells and cell lines were lysed with both RIPA buffer (to obtain soluble proteins) and ß-ME/SDS buffer (to reduce and obtain insoluble components including the keratin intermediate filaments) in low, medium, and high (staggered) Ca^{2+} concentrations thus: low = 0.05 mM Ca^{2+}; medium = 0.125 mM Ca^{2+} for 24 hr; high = 0.125 mM for 24 hr, then 0.225 mM for a further 24 hr to encourage proper stratification. Cells were lysed with either 1.5 mL RIPA or 2 mL ß-ME/SDS buffer in the flasks and transferred to Eppendorf tubes where the samples were manually broken up by needle aspiration (19-22 gauge). RIPA lysates were then centrifuged at 13,000 rpm for 20 min to pellet the insoluble fraction (this pellet was subsequently treated with ß-ME/SDS buffer as for direct

lysates for back up). Centrifuged lysates were transferred to fresh Eppendorf tubes and stored at -70°C. ß-ME/SDS-lysed samples were heated to 90°C for approx. 20 min to facilitate proper dissolution prior to being centrifuged as for RIPA samples and subsequently stored at -70°C.

2.2.9. Western Blotting

Protein samples were quantitated using the Pierce BCA Protein Quantitation Assay on a 96 well plate, measured via a Thermo MultiSkan 1500 microplate reader detecting absorbance at 562 nm. The absorbance data were converted to concentrations using results of an albumin standard curve (duplicated) onto which a polynomial best fit line was applied. The resulting polynomial equation was then used to calculate unknown sample concentrations. These values were then used to calculate the volume of each required to run 10 µg total protein per well (could only run 5 µg each for primary cell lysates due to low concentration).

Prior to running samples, 100 µL of each was mixed in a fresh Eppendorf with an equal volume of 2x Laemmli buffer (prepared as 950 µL buffer + 50 µL ß-mercaptoethanol) and heated for 10 min at 95°C to facilitate denaturation. The running buffer was prepared according to instructions: 900 mL ddH2O + 100 mL 10X TGS buffer (Bio-Rad). The appropriate volume of each sample was loaded into the wells of Bio-Rad Mini-PROTEAN® TGM™ precast gels (4-20% gradient) for protein separation, with 5 µL undiluted Bio-Rad Precision Plus Protein™ Dual XTRA pre-stained protein standards loaded in the first and last wells as size markers. Gels were run at 100 V for approximately 90 min (or until the loading dye reached the bottom of the gel, denoted by a black line on the casing).

Buffer for wet transfer was prepared as per instructions: 700 mL ddH2O + 200 mL methanol + 100 mL 10X TG buffer (Bio-Rad). Proteins were transferred from the gel to a PVDF membrane which had been soaked in methanol for 5-10 min prior to use. The transfer was done at 300 mA for approx. 90 min (with an ice block to prevent overheating).

Blocking was performed in 5% BSA in TBS-T for 1 hr at room temperature (rocking). The membranes were briefly washed in TBS-T before addition of the primary antibody diluted in 0.3% BSA in TBS-T (Anti-Stratifin pAb Pierce®/ThermoFisher Scientific at 1:5,000; Anti-ß-Actin pAb Proteintech at 1:10,000). Primary antibody incubations were performed o/n at 4^{o}C (rocking). Membranes were washed 3 times for 10 min each in TBS-T prior to addition of the secondary antibodies: HRP-conjugated anti-Rabbit IgG (1:8,000) + HRP-conjugated anti-Ladder (1:50,000). Incubation was carried out for 1-1.5 hr at room temp (rocking). Visualisation of bands was performed via chemiluminescence using the Pierce ECL kit as instructed, followed by image capture using the SynGene system.

2.2.10. Wound closure assay

Cell lines developed from primary murine keratinocytes expressing either no transgenes, *HK1.fos* only, *K14.stratifin* only, or both *HK1.fos* and *K14.stratifin* were grown to confluence in 60 mm dishes (6 each). When confluent, the media was removed and each dish was scratched 3 times using a clean, sterile 200 µL pipette tip. The dishes were then washed 3 times with sterile PBS (-Ca^{2+}) to discard viable detached cells which may colonise the scratches and affect the assay results. The dishes were then refed with clonal growth medium (as described above). The centre point of each scratch was photographed immediately after being refed (T0) and every 12 hours subsequently until closed. For the normal ICR line, photographs were not taken past 120 hrs as the scratches did not appear to be closing due to a failure of the cells to migrate across the scratch border. These were kept for a further 5 days with little change thus further results have not been recorded.

Analysis was performed using ImageJ software to measure the area of the scratch (in pixels). Each photograph was analysed 3 times on different days to minimise bias, and the means and standard deviations were calculated to assess the viability of the technique. These data were then converted into a percentage closure of each scratch, represented as a graph, produced on MS Excel 2016.

2.2.11. Colocalisation Analysis on Dual-Colour Immunofluorescence Images

FIJI (ImageJ; National Institutes of Health and the Laboratory for Optical and Computational Instrumentation) was used in analysis of immunofluorescence images and western blots.

Keratin 1 and 10 Co-localisation Analysis: Used Plugin "Colocalization Threshold". Colour channels were split and the empty blue channel discarded. Zero-zero values, i.e., entirely black pixels in each channel (background and empty nuclei), were excluded from analysis since these would be perfectly correlated and skew results. This analysis provided scatter plots to visualise pixel colour correlation, the Pearson's correlation coefficient, and the Manders overlap coefficients, M1 and M2. M1 is the percentage of red pixels with a non-zero green value; M2 is the percentage of green pixels with a non-zero red value (Manders et al., 1993). The plugin also provided images showing all overlapping pixels in white and all non-overlapping pixels in either green or red as a clear visual representation of the coefficients calculated.

Chapter 3 Endogenous Stratifin expression in *HK1.ras/fos-Δ5Pten* carcinogenesis

3.1. Introduction

As described in Chapter 1, the HK1 transgenic multistage mouse model of carcinogenesis mimics the classic two-stage chemical carcinogenesis model in a more controlled way that allows for characterisation of each stage in the aetiology of skin carcinogenesis (Balmain et al., 1984; Sakai, 1990; Hennings et al., 1993; MacDonald et al., 2014). Using specific promoters targeting activated H-ras and Fos to the epidermis, it both allows for reduction in off-target effects of DMBA/TPA treatment and is able to control the specific cell types in which these oncogenes are activated. Being able to target to a desired cell type is important, as when H-ras is targeted to the hair follicle and all proliferative compartments, aggressive SCCs form very quickly (Brown et al., 1998), preventing stage-specific analysis and not recapitulating the course of human SCC development, which almost invariably involves a pre-malignant neoplasia (Dinehart et al., 1997; Cockerell, 2000).

In this model, a modified, truncated human keratin 1 promoter is used, which is expressed in all early differentiating epidermis, but also in approximately one third of basal layer cells, due to the truncated nature of the construct in which the 3' regulatory elements are missing (Rosenthal et al., 1993). Thus, *HK1.ras/fos* mice develop an aggressive papilloma some weeks after a wound-promotion stimulus (ear tag), but do not convert to well-differentiated SCC (wdSCC). That requires a further genetic insult, which is provided here by ablation of exon 5 of the tumour suppressor gene (TSG), Pten (Lesche et al., 2001); a major inhibitor of the PI_3K/Akt pathway (Chaloub & Baker, 2009; Manning & Toker, 2017). Expression of the mutant Pten allele lacking phosphatase activity is targeted to the proliferative cells of the epidermis using a Cre-mediated loxP system under the control of a K14 promoter and is linked to a progesterone ligand-binding domain to allow inducible activation in the skin by topical Mifepristone/RU486 treatment (Berton et al., 2000). This further allows for temporal control of carcinogenesis in that Pten ablation can be induced subsequent to papilloma formation, so that proteins of interest can we studied at well-defined stages in progression to SCC, and further to poorly-differentiated SCC (pdSCC).

Previous studies found that the cell cycle regulator and major tumour suppressor p53 was lost during the process of malignant conversion from papilloma to well-differentiated carcinoma (MacDonald et al., 2014). p53-independent p21 expression, however, was found to persist until its eventual loss which coincided with progression to pdSCC. Loss of p53 was accompanied by basal layer activation of its inhibitor, Mdm2, therefore control of this interaction warranted further analysis in this model to identify possible targets which may prevent malignant conversion. Through this, 14-3-3σ/Stratifin was identified as a key regulator of the Mdm2/p53 interaction, as detailed in Chapter 1 *Figure 1-9*, where it protects p53 by chaperoning Mdm2 into the cytoplasm and inducing its autoubiquitination.

The initial part of this project, therefore, sought to characterise the expression pattern of endogenous Stratifin at each stage in the progression of *HK1.ras/fos-Δ5Pten* model of carcinogenesis and to elucidate its possible function as a tumour suppressor gene in the model by maintaining strong basal layer p53 expression subsequent to induced Pten ablation.

3.2. Confirmation of genotype by PCR

Mouse genotypes were first confirmed at 3-4 weeks old using tail tip tissue obtained when the mice were tagged. This allowed for confirmation of the presence of *HK1.ras*, *HK1.fos* and *K14.CrePR1* transgenes (*Figure 3-1*). This DNA can also be used to determine Pten status: presence of a floxed Pten allele results in a larger band on the gel than the wild-type allele, with heterozygosity therefore resulting in a doublet pair of bands. Primers in this instance span a region containing the first loxP site, hence the larger PCR product. Cre-recombinase activity must be induced by treatment with Mifepristone/RU486, as detailed in Chapter 1 (*Figure 1-7*). It was therefore not active in mice at the time of tagging, thus Pten exon 5 could not be detected in these samples (not shown).

All mouse genotypes determined from tail tissue were reconfirmed with biopsy tissue, including presence of the Δ5Pten band (*Figure 7-1*, bottom row) in

heterozygous and floxed mice from tissue which had been treated with RU486. Treated controls lacking the *K14.CrePR1* gene were also tested to ensure PCR specificity and confirm the requirement of Cre-recombinase to excise the floxed region.

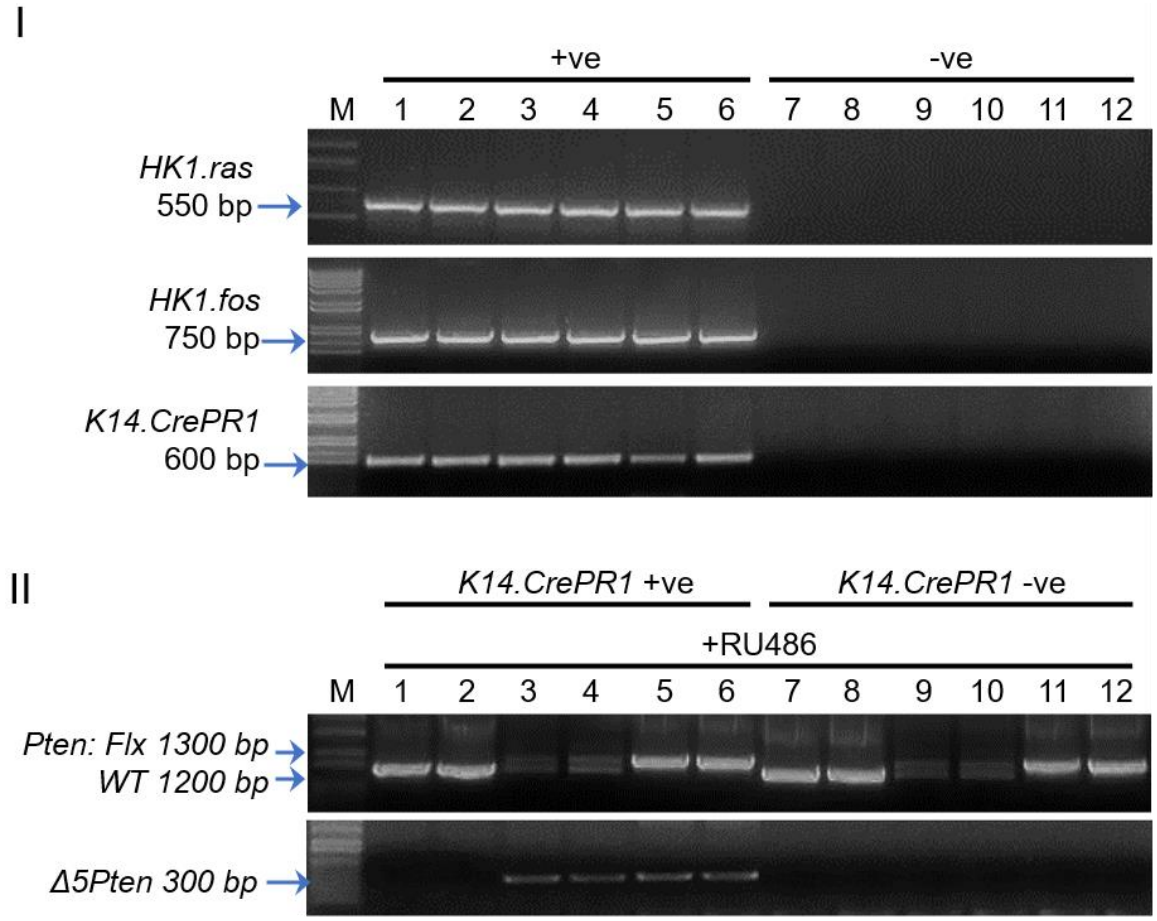

Figure 3-1: PCR analysis identifies transgenic genotypes and successful excision of Pten exon 5.

Panel I: PCR analysis of DNA isolated from tails detects *HK1.ras*, *HK1.fos* and *K14.CrePR1* transgenes (lanes 1-6), including negative controls to confirm specificity and to check for contamination of reagents (lanes 7-12).

Panel II: PCR of biopsy tissue DNA detects the loxP-flanked (exon 5) *Pten* allele at 1300 bp compared to the wild-type 1200 bp band, forming a doublet in heterozygous samples (primers 1 & 2; lanes 3 & 4; 9 & 10). RU486 treatment of *K14.Pten*$^{flx/+}$ and *K14.Pten*$^{flx/flx}$ results in the excision of Pten exon 5 (*Δ5Pten*) at 300 bp band (primers 1 & 3; lanes 3-6). No bands are present in the *K14.Pten*$^{+/+}$ samples (lanes 1 and 2), nor in any samples without the *K14.CrePR1* gene (lanes 7-12).

3.3. Stratifin expression in benign skin phenotypes

3.3.1. Stratifin expression increases in *HK1.fos* and *HK1.ras* hyperplasias and papillomas and is concurrent with increases in p53 and p21 expression

As described in Chapter 1, *HK1.fos* activation in transit amplifying and differentiating cells of the epidermis results in mild hyperplasia upon wound-promotion (ear tagging) which becomes more pronounced, accompanied by keratosis after around 7 months. *HK1.ras* (line 1205, which is very sensitive to wound-promotion) results in immediate neonatal hyperplasia which diminishes in adults but acts as an initiating event in the epidermis so that papillomas are induced by ear tag wound promotion; these regress if the stimulus is lost, i.e., by the tag falling out (Greenhalgh et al, 1993b). *HK1.ras* line 1276, which harbours exactly the same transgene construct, has been shown to be insensitive to wound-promotion but results in papilloma formation when co-expressed with *HK1.fos* (Greenhalgh et al., 1993c), recapitulating the initiation-promotion mechanism seen in DMBA/TPA chemical carcinogenesis (Filler et al., 2007). NB: Promotion experiments in the USA via crossing of *HK1.ras*^{1205} with *HK1.fos* activation produced too severe a phenotype in neonatal pups, as the hyperplasia normally seen in all *HK1.ras* pups was exaggerated and accompanied by hyperkeratosis; thus all *HK1.ras/fos* and *HK1.ras/fos-Δ5Pten* mice produced utilised the *HK1.ras*^{1276} line.

Initially, IHC staining was performed to test for p53 and p21 expression and localisation in normal skin, *HK1.fos* hyperplasias (and HK1.ras hyperplasia, not shown), and *HK1.ras* papillomas. Previously, basal layer p53 expression had been found to increase in older (>5 mo.) hyperplasias and papillomas, consistent with its role in cell cycle regulation, to combat hyperproliferation in the context of these activated oncogenes. Similar increases were seen in p21 expression, which is downstream of p53 and controls cell cycle arrest at the G1/S checkpoint and at G2/M (Niculescu III et al., 1998).

However, both anti-p53 and anti-p21 antibodies used in the previous study (Santa Cruz Biotechnology) were discontinued early in this project, thus

replacements needed to be obtained and verified (Appendix 1, McMenemy et al., in preparation, *Figure S1*). Confirmation of these expression patterns with the new antibodies is shown in *Figure 3-2*. In normal skin, p53 showed only infrequent basal layer positivity, consistent with division of interfollicular stem or transit amplifying cells, while expression of p21 followed an identical pattern of staining (*Figure 3-2A,B*). Expression of both p53 and p21 was increased in basal cells of *HK1.fos* hyperplasia (*Figure 3-2D,E*) and in *HK1.ras* papilloma (Figure 3-2G,H) with noticeable increases in p21 expression in granular cells, consistent with a role in late-stage differentiation.

Against this background, Stratifin expression in normal skin, hyperplasia and papilloma was found to always be strong in suprabasal layers, where it is involved in the normal terminal differentiation programme (Dellambra et al., 1995; Sun et al., 2015). Slight increases in basal layer expression were noted in *HK1.fos* hyperplasia and *HK1.ras* papilloma, related to the observed increase in p53 staining. Following DNA damage, caused here by a marked increase in proliferation driven by *HK1.fos* and *HK1.ras*, p53 is partially stabilised by Chk1 and 2, allowing it to go on to transactivate downstream targets including p21 and Stratifin (Hermeking et al., 1997; Ou et al., 2005). Upregulation of Stratifin provides positive feedback to p53 through removal of its inhibitor, Mdm2, from the nucleus and induction of its autoubiquitination, as shown in Chapter 1 *Figure 1-9* (Lee & Lozano, 2006). These data, therefore, support the hypothesis that Stratifin acts as a tumour suppressor in the initial stages of *HK1.fos* and *ras* hyperplasia and papillomatogenesis.

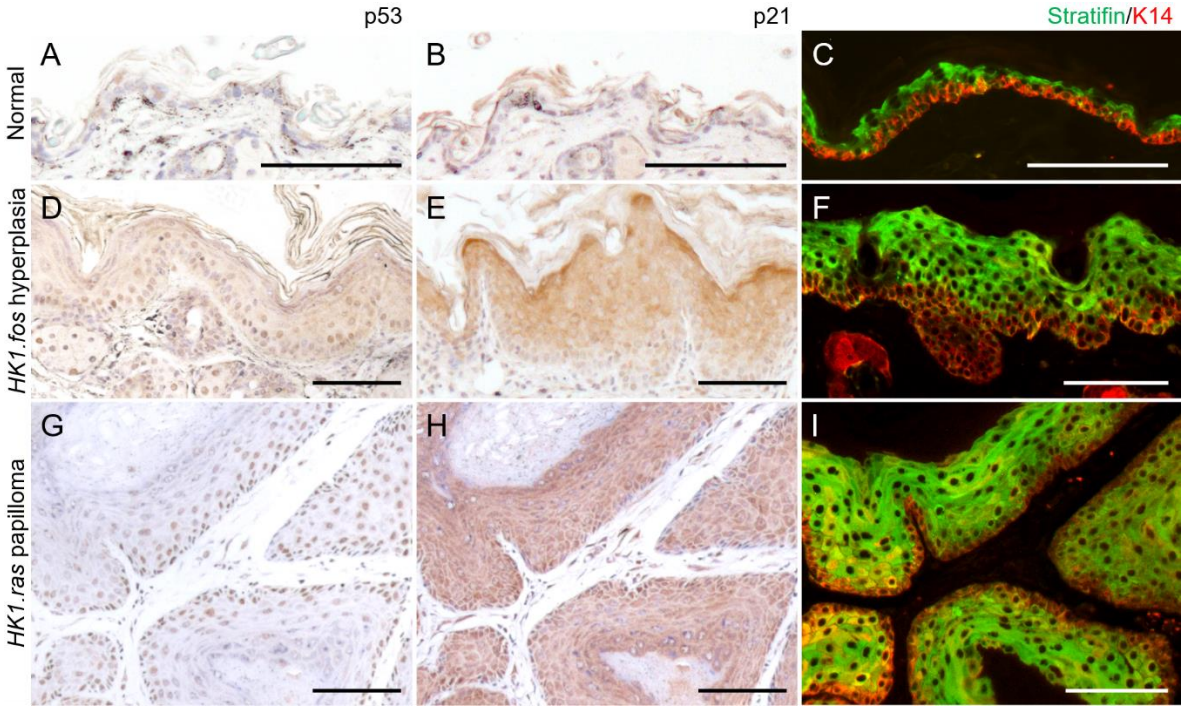

Figure 3-2: Stratifin expression in normal epidermis, benign hyperplasia and papillomas exhibits mainly suprabasal expression with increased basal expression corresponding to that of p53 and p21.

(**A**) Normal ICR skin shows very weak, sporadic p53 staining, similar to (**B**) p21 expression. (**C**) Stratifin is present in all differentiated cells in this slightly thicker (~2 cells) patch of normal skin, with only weak, sporadic basal layer staining. (**D**) p53 abundance is increased slightly in the basal layer of *HK1.fos* hyperplasia in response to increased proliferation driven by the transgene. (**E**) p21 staining in *HK1.fos* hyperplasia is mainly suprabasal with some increasing basal layer positivity. (**F**) In *HK1.fos* hyperplasia, Stratifin is strongly expressed in suprabasal layers and shows a slight increase in basal layer positivity compared to normal, mainly around the plasma membranes. (**G**) p53 positivity in basal cells of *HK1.ras* papilloma is moderate to strong with some positive suprabasal cells. (**H**) p21 staining is strong in basal cells, similar to p53 in *HK1.ras* papilloma, and in suprabasal cells, primarily of the granular layer. (**I**) Stratifin expression is similar in *HK1.ras* papilloma is similar to *HK1.fos* hyperplasia, with slightly more basal layer staining in areas with more p53 expression. *Scale bars approx. 100 µm.*

3.3.2. Stratifin expression is increased in basal keratinocytes in early *HK1.fos-5Pten* hyperplasia and supports p53 expression in later keratoacanthoma in accelerating differentiation

In contrast to hyperplasias produced by *HK1.fos* and *HK1.ras*—and later *HK1.ras* papillomas—induced ablation of Pten activity in *HK1.fos* (*HK1.fos-Δ5Pten*) to deregulate the PI_3K/Akt pathway in this background resulted in keratotic hyperplasia in RU486-treated TGE skin, which developed into keratoacanthoma rather than converting to malignancy (Yao et al., 2008). This was found to be due to very high expression of p53 and p21 in the late-stage hyperplasia and early papilloma as a result of increasing Akt-mediated GSK3β inactivation, causing increased β-catenin activation (Yao et al., 2008; Manning & Toker, 2017). This compensatory p53/p21 activation caused a switch in the phenotype from hyperproliferation to accelerated differentiation, resulting in the highly keratotic KA phenotype to combat malignant conversion (Yao et al, 2008).

Ablation of Pten activity in *HK1.fos* skin appeared to induce an increase in Stratifin expression in basal keratinocytes particularly at the membrane and in the cytoplasm (Appendix 1, McMenemy et al., in preparation, *Figure 2A*) of the hyperplasia, even prior to the increased p53 expression seen later, suggesting p53-independent tumour suppressive roles of Stratifin at this stage. In the later disease, two distinct histotypes were evident; fronds of keratinocytes producing massive hyperkeratosis, overlying an SCC-like proliferative histotype. Stratifin expression was seen to be strong throughout the frond regions, in conjunction with increased p53/p21 expression, and keratin 1 (K1) was found to be spuriously expressed in the basal compartment, consistent with a confused and accelerated differentiation programme (Appendix 1, McMenemy et al., in preparation, *Figure 2C*) and in the inappropriate expression of mK1 in HFs that are the presumed precursors of *HK1.fos/K14.stratifin* SCC (see Chapter 4).

In the proliferative, SCC-like regions, Stratifin expression was notably absent in basal keratinocytes, and this was associated with low abundance of p53 and p21 alongside increased active Akt1 ($pAkt^{ser473}$) in these areas (Yao et al., 2008). These data now suggest that the trigger for elevated p53/p21

expression in response to excessive AKT/βcatenin could involve increased Stratifin expression to commit keratinocytes to differentiate and maintain a benign phenotype (Appendix 1, McMenemy et al., in preparation).

3.4. Stratifin expression persists after p53 loss, mirroring p21 expression but is lost in poorly-differentiated SCC

Taken together, these data suggest a protective role for Stratifin in the early stages of *HK1.ras/fos* papillomatogenesis and in maintaining a differentiating phenotype in *HK1.fos-Δ5Pten* keratoacanthoma to avoid malignancy. Previously, in the *HK1.ras/fos-Δ5Pten* multistage model of carcinogenesis, it was found that p53 expression was lost upon conversion to squamous cell carcinoma. Given the relationship between p53 and Stratifin expression (Chapter 1, *Figure 1-9*) exemplified in the benign phenotypes already discussed, expression of Stratifin was examined in aggressive, late-stage *HK1.ras/fos-Δ5Pten* papillomas which were determined to be converting to a malignant phenotype by K1 expression analysis (Chapter 1, *Figure 1-8G,H*).

As shown in *Figure 3-3*, these data confirmed the previously seen expression pattern of p53, with moderate to strong basal staining in the K1-positive benign regions (*Figure 3-3A,B;* right), becoming weak and negative in the K1-negative carcinoma area (*Figure 3-3A,B*; left). As in previously published data (MacDonald et al., 2014), p53-independent p21 is seen to persist in the well-differentiated carcinoma (*Figure 3-3C*), acting to antagonise further progression to a poorly-differentiated SCC (pdSCC; MacDonald et al., 2014). Immunostaining analysis showed that Stratifin expression was also found to persist in these areas of wdSCC, albeit confined to the suprabasal layers and less abundant when compared to the adjacent benign tissues (*Figure 3-3D left vs right*; Appendix 1, McMenemy et al., in preparation, *Figure 3*). However, with time the most poorly-differentiated regions appear to have lost Stratifin expression completely, concurrent with the p21 expression pattern (*Figure 3-3C*, centre and *D*, centre), and with increasing pAkt^{ser473} at this stage (Appendix 1, McMenemy et al., in preparation, *Figure 6*). This was also identified in *HK1.ras-Δ5Pten* TPA-treated tumours, which are seen to rapidly lose expression of p53,

p21 and Stratifin (Appendix 1, McMenemy et al., in preparation, *Figure 4*) and exhibit an abundance of pAkt^{ser473} (Yao et al., 2006), contributing to development of a hyperproliferative, pdSCC histotype.

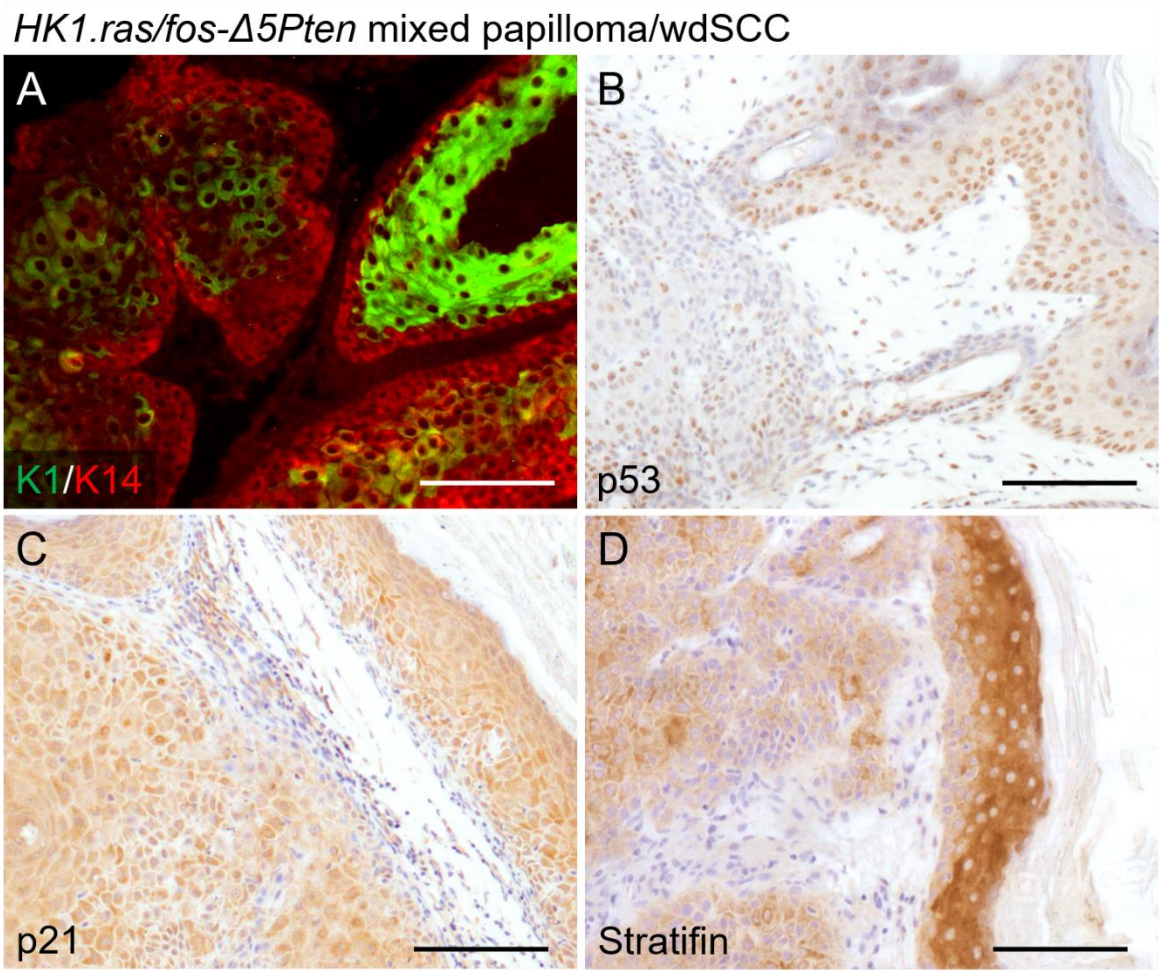

Figure 3-3: p53 loss coincides with K1 loss on malignant conversion in *HK1.ras/fos-Δ5Pten carcinoma* but Stratifin and p21 expression persist in wdSCC.
(**A**) K1 expression (green) is strong in the suprabasal layers of the hyperplastic area (right of image) and is lost, leaving mostly K14 (red) counterstaining in the wdSCC region. (**B**) p53 staining is strong and mostly basal in the benign hyperplastic region (right) but is lost in the adjacent carcinoma tissue (left) (**C**) p21 staining is similar in the hyperplasia (right) and carcinoma (left and bottom) with only some cells beginning to lose positivity as the phenotype becomes more poorly differentiated (centre), as with Stratifin. (**D**) Stratifin is mainly suprabasal with sporadic basal staining in the hyperplasia (right) and is weak to moderate in the carcinoma (left and bottom of image) but not absent as with p53. *Scale bars approx. 100 µm.*

Given the nature of the relationship between Stratifin, p53 and Mdm2 (Lee and Lozano, 2006)—and, indeed, Akt1 (Gottlieb et al., 2002)—expression of activated Mdm2 (pMdm2^{ser166}) was assessed in the benign and malignant phenotypes described to assess the interplay between expression of these proteins in this model (shown in Appendix 1, McMenemy et al., in preparation, *Figure 5*). In normal epidermis, pMdm2^{ser166} expression was found to be primarily

suprabasal, with only sporadic basal layer expression, similar to that of p53 and consistent with its antagonism of p53-mediated apoptosis which constitutes a threat to barrier maintenance in the skin (Gottlieb et al., 2002). In *HK1.ras* papillomas, pMdm2^{ser166} remains mainly suprabasal, whilst absent in many basal layer strands, indicative of suppression by Stratifin expression in these cells to maintain high p53 expression in these regression-prone benign papillomas and thus prevent malignant conversion.

However, in trigenic *HK1.ras/fos-Δ5Pten* wdSCCs, elevated pMdm2^{ser166} expression undergoes a suprabasal-to-basal transition, which was paralleled by the observed reverse basal-to-suprabasal change in Stratifin localisation. This reduction in basal layer Stratifin expression coupled with an increase in pMdm2^{ser166} activity would reduce p53 expression and increase susceptibility to malignant conversion through loss of cell cycle regulation (Appendix 1, McMenemy et al., in preparation, *Figure 5C*).

3.5. Discussion

The purpose of this chapter was to reconfirm the previously observed loss of the tumour suppressor p53 during malignant conversion of *HK1.ras/fos-Δ5Pten* carcinogenesis, and subsequently, to assess the pattern of expression of Stratifin in this model.

3.5.1. The *HK1.ras/fos-Δ5Pten* multistage model of carcinogenesis

Squamous cell carcinoma, unlike BCC, does not arise *de novo*, and instead develops over time from an existing benign neoplasm such as actinic keratosis (AK) (Ratushny et al., 2012). For decades, multistage carcinogenesis has been studied using to two-stage chemical carcinogenesis protocol, involving induction of initiating mutations by topical application of DMBA and subsequent repeated application of the promoting agent, TPA (Abel et al., 2009). This analysis identified an activating mutation in the proto-oncogene Harvey Ras (*HRAS*) gene, $HRAS^{Q61L}$ as a frequently occurring initiating mutation resulting from DMBA treatment, with upregulation of c-Fos (part of the AP-1 transcription factor complex) being common following repeated TPA treatment (Balmain et al., 1984; Greenberg & Ziff, 1984). However, in reality, these chemical agents cause a plethora of mutations and changes to gene activity, making it difficult to elucidate the changes which are associated with stage progression and which have little or no effect on carcinogenesis. Additionally, the process of inducing malignant conversion in benign papillomas by this method is very time consuming (~1 year), the rate of conversion to SCC can be very low and conversion rate varies considerably by mouse strain (Slaga, 1986).

To combat these issues, transgenes were developed which specifically activated the oncogenes H-Ras and Fos in the epidermis promotion vector which allowed for specific analysis of the consequences of their activation and changes in the expression of downstream effectors and antagonists more directly. Studies which targeted H-Ras activation to the proliferative compartment, via use of a K5 promoter for example, resulted in aggressive SCCs at a very early age (Brown

et al., 1998), likely from activation in both interfollicular and follicular stem cell compartments. The HK1 promoter (Chapter 1, *Figure 1-6*), by contrast, activates in the suprabasal layers alongside mK1 during differentiation, and in a subpopulation of basal layer cells, allowing expression in some stem and transit amplifying cells to occur without driving immediate carcinogenesis as seen using K5-promotion. In this manner, both the viral homologues of c-H-ras and c-fos (v-Ha-ras and v-fos) were targeted to the epidermis, alone or in tandem, to study the effects of their activation phenotypes detailed in Chapter 1, Section 1.5.3.) and to allow further genetic manipulation to be performed.

Studies utilising primary cells transfected with v-Ha-ras and v-fos indicated that this pairing was carcinogenic and able to form wdSCC when grafted onto nude mice (Greenhalgh et al., 1990). As mentioned, however, this was not true when the *HK1.fos* and *HK1.ras* transgenes were co-expressed *in vivo*, as the papillomas produced did not show signs of malignant conversion with time (though these were not found to be regression-prone as is the case with *HK1.ras*-only papillomas). This indicated the need for further genetic insult to facilitate conversion to carcinoma, which in this model, was provided by inducible Cre-loxP-mediated excision of Pten exon 5 (detailed in Chapter 1, *Figure 1-7*). This inducible system is useful in that it allows control over timing of conversion and therefore analysis of protein expression changes before and after induction of Pten ablation has occurred.

In previous studies (Yao et al., 2008; MacDonald et al., 2014), induction of p53 expression and that of one of its major downstream effectors, p21, was found to increase in the proliferative cells of *HK1.fos* and *HK1.ras* hyperplasias, *HK1.ras* papillomas, as well as in *HK1.fos-Δ5Pten* keratoacanthomas, wherein very high levels of p53 and p21 were believed to prevent malignancy and maintain an accelerated differentiation phenotype (Yao et al., 2008). Similarly, this expression of TSGs seems to be key in preventing malignancy in *HK1.ras*/*fos* bigenic papillomas, as when Pten is ablated through topical RU486 application, malignant conversion coincides directly with loss of p53 (MacDonald et al., 2014). This finding was re-confirmed here (*Figure 3-3*) with the use of a new anti-p53 antibody due to discontinuation of that used in the previously published data.

Despite the important role Pten plays in inhibition of Akt activation (Hemmings and Restuccia, 2012), it was found that the quantity of Akt in *HK1.ras/fos-Δ5Pten* well-differentiated squamous cell carcinoma remained low in the early stages of malignant conversion; this interesting finding was also seen following Pten ablation in urothelium in a model of bladder carcinoma (Yohn et al., 2011). In both this *HK1.ras/fos-Δ5Pten* model of cutaneous SCC and the bladder cancer model (as well as the *HK1.fos-Δ5Pten* KA), Pten inactivation was accompanied by sustained p21 expression, independent of p53, which antagonised Akt activation and prolonged the well differentiated phenotype. In *HK1.ras/fos-Δ5Pten* and in the more aggressive *HK1.ras-Δ5Pten* + TPA carcinomas, loss of p21 correlated with an increase in Akt activity and a change to a much more poorly differentiated phenotype (Yao et al., 2006; MacDonald et al., 2014).

3.5.2. Endogenous Stratifin expression in *HK1.ras/fos-Δ5Pten* carcinogenesis

Given the correlation between p53 loss and malignant conversion in *HK1.ras/fos-Δ5Pten* carcinogenesis (MacDonald et al., 2014), proteins involved in p53 regulation were analysed. It was found that activated Mdm2 (pMdm2^{ser166})—which directly targets p53 for degradation—translocated from the suprabasal layers to the proliferative basal layers concurrent with p53 loss from these cells. Therefore, the expression of Stratifin, a protein which chaperones Mdm2 from the nucleus to the cytoplasm for degradation to protect p53, was analysed throughout the benign and converted stages of this model to assess its putative roles in the observed aetiology.

In benign *HK1.fos* and *HK1.ras* hyperplasias and papillomas, Stratifin expression was strong in all suprabasal layers, as in normal skin, consistent with its importance in influencing normal keratinocyte terminal differentiation and spatial awareness (Dellambra et al., 1995; Sun et al., 2015; Ling et al., 2010). In these tissues, the expression of p53 in proliferative basal layer cells was seen to increase above the low level found in normal skin, due to the excess proliferation driven by the *HK1.fos* and *HK1.ras* activated oncogenes. Stratifin is

transactivated by p53 following DNA damage (Chapter 1, *Figure 1-9*), which can be caused by hyperproliferation due to accumulation of genotoxic reactive oxygen species generated through oncogene (e.g., H-Ras) activation (Ogrunc et al., 2014). Accordingly, in the later *HK1.fos* hyperplasia and *HK1.ras* papilloma, Stratifin expression was found to be increased in the basal layers (*Figure 3-2*). Concurrently, expression of active Mdm2 (pMdm2^{ser166}) was limited to the suprabasal layers, as increased Stratifin activity in basal cells countered its activity (Appendix 1, McMenemy et al., in preparation, *Figure 5*).

Upon conversion to a malignant wdSCC phenotype (as suggested by loss of Keratin 1 expression and concurrent p53 downregulation, in conjunction with histological changes consistent with carcinoma development), pMdm2^{ser166} activity increased in basal cells and Stratifin expression appeared to be reduced (*Figure 3-3*). Stratifin expression was somewhat maintained in the suprabasal cells of wdSCC, presumably transactivated by p63 (primarily TAp63γ (Trink et al., 2007)) in the absence of p53. At this stage, Stratifin was likely contributing to the maintenance of a well-differentiated state in two modes: performance of normal regulation in supporting proteins such as PKC and CALML5 in the terminal differentiation programme (Dellambra et al., 1995; Sun et al., 2015) and in cell cycle regulation, where it acts in tandem with the CDK-inhibitors p21, p15 and p27 by preventing interaction between cyclin D and CDK4/6 to limit G1/S progression, and later by sequestration of Cdc2/cyclin B at the G2/M checkpoint (Laronga et al., 2000). Stratifin is also a direct inhibitor of Akt activity (Yang et al., 2006) and could therefore be aiding in suppressing pAkt^{ser473} activity in well differentiated *HK1.ras/fos-Δ5Pten SCC*, compensating for Pten loss.

These data are generally suggestive of a protective role of Stratifin in *HK1.ras/fos-Δ5Pten* carcinogenesis, which is consistent with its known roles in negative regulation of the cell cycle and promotion of differentiation (Hermeking et al., 1997; Laronga et al., 2000; Dellambra et al., 1995; Sun et al., 2015), as well as its loss in certain cancers being associated with poor prognosis (Iwata et al., 2000; Umbricht et al., 2001; Ren et al., 2010). However, it is important to note that numerous studies of internal carcinomas (Ide et al., 2004; Neupane and Korc, 2008; Li et al., 2009; Radhakrishnan et al., 2011; Husni et al., 2019), as well as some analysing cutaneous carcinomas (Lodygin et al.,

2003), have observed persistent or increased Stratifin expression in the malignant tissue relative to adjacent benign areas. However, the same researchers who identified upregulated Stratifin in all cutaneous SCCs tested (Lodygin et al., 2003) also found that loss of Stratifin was associated with greater sensitivity to carcinoma induction by DMBA/TPA papillomatogenesis (Winter et al., 2016), further highlighting the extremely contextual nature of Stratifin activity in the process of tumour development.

Further analysis is therefore required in the contexts of Ras and Fos activation, through manipulation of Stratifin expression using a targeted transgenic construct, *K14.stratifin*, which will be detailed in the coming Chapters.

Chapter 4 *K14.stratifin* and *HK1.fos* co-operation in mouse skin carcinogenesis

4.1. Introduction

As outlined in Chapter 1, when v-Fos was transfected into keratinocyte cultures with v-H-ras, the resultant cell lines were malignant, as confirmed by grafting onto nude mice and identified their synergism in skin carcinogenesis (Greenhalgh et al., 1990). Expression of activated v-Fos (c-Fos homologue) targeted to the epidermis by a modified human keratin 1 promoter (HK1) results in mild hyperplasia and hyperkeratosis after >4 months, with wound-promotion eventually eliciting a small papilloma at least 8 months after the ear is tagged. In contrast with the previous *in vitro* findings, *in vivo*, synergy of *HK1.fos* and *HK1.ras* transgenes results only in benign papillomas. These require further genetic insult, for example, via ablation of tumour suppressor gene *Pten*, to elicit malignant conversion (MacDonald et al., 2014). This model thus mimicked classical two-stage chemical carcinogenesis and gave a stability of phenotype ideal to assess stage-specific genetic insults.

In Chapter 3, analysis of multistage carcinogenesis in tri-genic *HK1.ras/fos-Δ5Pten* initially identified 14-3-3σ, commonly called Stratifin, as a potential tumour suppressor, given its loss following malignant conversion. This was consistent with its role in the inhibition of Mdm2-mediated p53 degradation. However, as shown in the submitted manuscript, in certain contexts Stratifin expression persisted into early-stage carcinoma (Appendix 1; McMenemy et al., in preparation, *Figure 5*).

Therefore, to directly investigate the putative tumour suppressor role(s) of Stratifin in this model, a mouse which overexpresses Stratifin in proliferative epidermal cells was purchased from the European Mouse Mutant Archive (B6D2-Tg(KRT14-SFN)44Odo/Cnrm (EM:06111); Cianfarani et al., 2011). This model harbours 14 copies of the *K14.stratifin* transgene construct and overexpresses the full-length human form of the protein—which shares 97.5% identity and 99.2% similarity with the mouse isoform (ClustalW2, EMBL)—in the undifferentiated epidermis and hair follicles. As this epidermal targeting is directed under the control of a Keratin 14 (K14) expression cassette (Vassar et al., 1989), it is referred to here as *K14.stratifin*. The schematic for the *K14.stratifin* transgene construct can be seen in *Figure 4-1A*.

As discussed in detail in Chapter 1, both c-Fos and Stratifin have integral roles in skin morphogenesis and differentiation (Fisher et al., 1991; Dellambra et al., 1995). Stratifin has also been shown to be vital for normal hair follicle integrity and maintenance of epidermal homeostasis (Hammond et al., 2012). Additionally, both proteins are important in tissue remodelling and return to homeostasis following wounding in the skin; Stratifin in particular has been identified in mediating scar-free wound-healing (Pakyari et al., 2013).

Given the overlap in the plethora of functions mediated by Fos and Stratifin in the skin, in relation to neoplasia, differentiation and tissue homeostasis, it seemed likely that they would produce synergistic effects when overexpressed together via the *HK1.fos* and *K14.stratifin* transgenes. In the initial rounds of breeding to introduce Stratifin into the *HK1.ras*, *HK1.fos* and *Pten*$^{flx/flx}$ backgrounds, it became very clear that a unique novel synergism existed between Fos and Stratifin overexpression in this model that challenges the dogma of Stratifin as a TSG.

The main aims of this chapter were to: characterise the *K14.stratifin* mouse phenotype on our outbred ICR background and assess any effects of wound promotion on *K14.stratifin* ear skin; study the novel phenotype elicited by concomitant activation of Fos with Stratifin overexpression in the mouse epidermis (both wound-promoted and not); and to identify changes in the expression and/or localisation of relevant proteins which may be involved in development of the *HK1.fos*/*K14.stratifin* model phenotype.

4.2. Confirmation of genotype and overexpression of Stratifin in presence of *K14.stratifin* transgene

Prior to crossbreeding with the transgenic lines involved in the multistage model, it was important to characterise the phenotype generated by the *K14.stratifin* transgene on the outbred ICR genetic background on which all other transgenes are maintained on in our research. Cianfarani et al. noted that the skin of *K14.stratifin* mice on a BD-1 background was thinner than their normal littermates (measured on tail skin). Additionally, their supplementary

data shows desquamation of tail skin in young adults (6 weeks) and hair loss in older individuals, though the latter is not shown. However, neither desquamation of the tails nor hair loss was observed in any *K14.stratifin* mice on our ICR background by 6 months of age (*Figure 4-1D*) or indeed up to 12 months, suggesting some features identified in the original research may be strain-dependent. Also, mice employed by Cianfarani et al. were not routinely tagged as they are here, thus wound promotion effects in ear epidermis synergistic with *K14.stratifin* transgene expression cannot be compared to their BD-1 counterparts.

Confirmation of genotype was done using PCR analysis of genomic DNA isolated in the first instance from juvenile tail-tip tissue when tagging (3-4 weeks old), and subsequently reconfirmed from adult biopsy tissue prior to further analyses (*Figure 4-1B*).

Since the correct expression of transgenes cannot be inferred from genotyping PCR, and *K14.stratifin* mono-genic mice do not develop an obvious macroscopic phenotype (*Figure 4-1D*), expression of Stratifin was assessed by immunofluorescence analysis in *K14.stratifin* mice compared to normal and hyperplastic *HK1.fos* epidermis (*Figure 4-1C*). Stratifin (green) is always present in the suprabasal layers, consistent with its roles in epidermal differentiation, and is seen here in all samples as expected. In basal cells, the abundance of endogenous Stratifin is generally low and confined to membrane staining, as typified by the expression pattern seen in *HK1.fos* hyperplasia (*Figure 4-1C*, centre).

Conversely, the Stratifin expression profile in *K14.stratifin* skin was much higher and present in the cytoplasm, as evidenced by the yellow colour in the image, due to the overlay of green Stratifin staining and red K14 counterstain in the basal layer (*Figure 4-1C,* bottom). Unfortunately, due to the similarity of the endogenous mouse Stratifin and the transgenic human Stratifin, it is not possible to distinguish the two forms through immunostaining, so the greater intensity and difference in spatial expression is used to confirm correct expression *in vivo*, consistent with the properties of the K14 promoter.

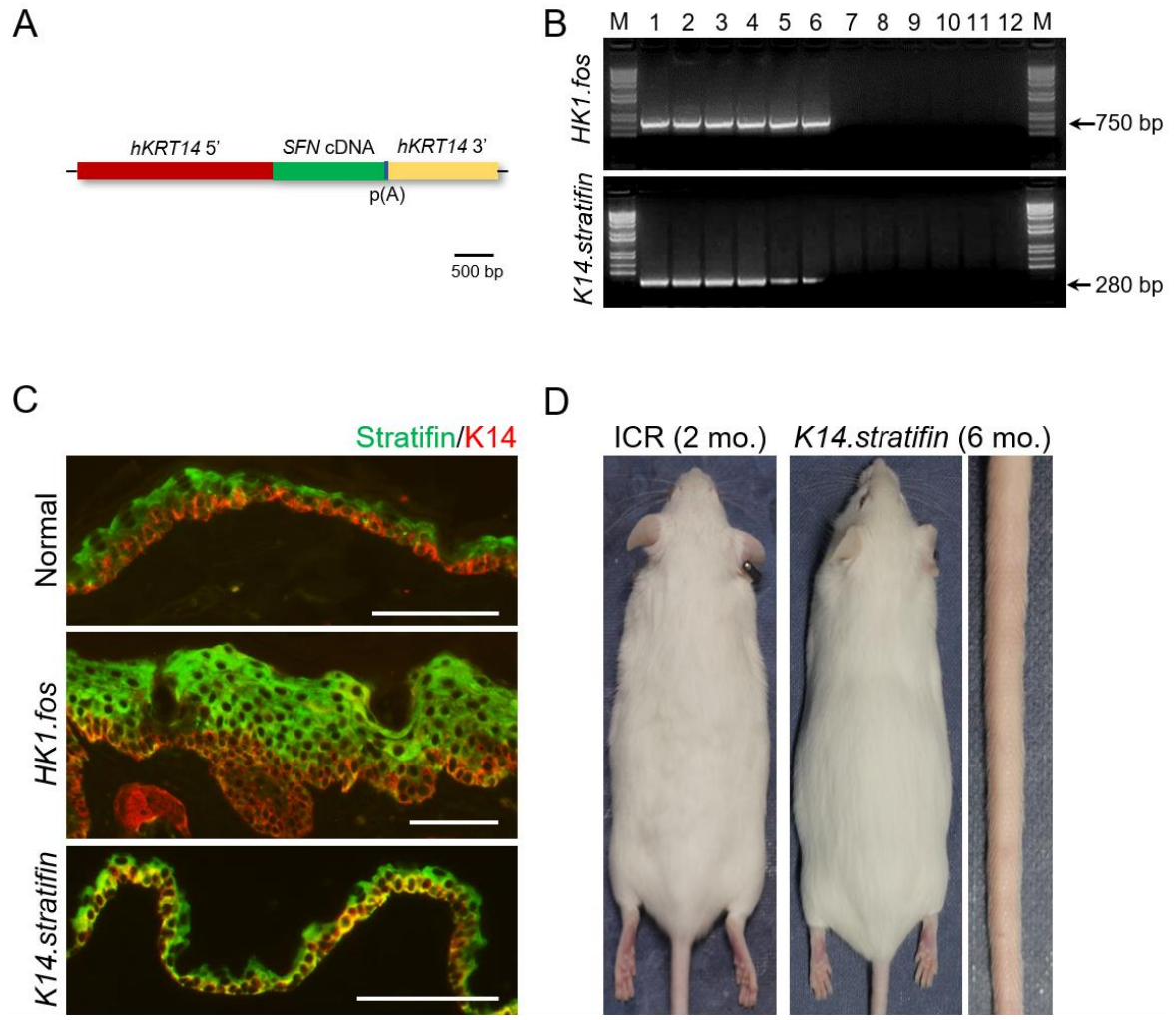

Figure 4-1: Genotyping PCR and confirmation of exogenous Stratifin overexpression and macroscopic phenotype.

(**A**) Schematic of the *K14.stratifin* transgene construct containing a ~2.5kb upstream of the Keratin 14 gene (*KRT14*) TATA box, the full Stratifin gene (*SFN*) coding sequence (cDNA, ~700bp), and the Poly(A) signal and ~700bp downstream sequence from the *KRT14* gene. (**B**) PCR analysis of *HK1.fos* and *K14.stratifin* DNAs confirm genotype via presence of 750 and 280bp bands, respectively, in lanes 1-6 which are absent in negative DNA samples (lanes 7-11) and no DNA control (lane 12). (**C**) Double-label immunofluorescence analysis of Stratifin expression (green), counterstained with K14 (red) to delineate the epidermis. Normal and *HK1.fos* skin display supra-basal Stratifin expression, consistent with roles in differentiation. *K14.stratifin* skin shows both supra-basal expression of endogenous Stratifin and basal-layer expression from the K14-driven promoter. *Scale bars approximately 100 µm.* (**D**) **Left:** 2-month-old non-transgenic ICR mouse **Centre:** 6-month-old *K14.stratifin* mouse exhibiting no noticeable change in hair phenotype associated with epidermal Stratifin overexpression. Right: No tail skin desquamation is apparent at 6 months, as described in Cianfarani et al., 2011 in BD-1 mice, suggesting strain specificity in the phenotype generated by *K14.stratifin* expression.

4.3. Characterisation of *K14.stratifin*, *HK1.fos* and bi-genic *HK1.fos/K14.stratifin* macroscopic and histological phenotypes

As previously described, expression of the *HK1.fos* transgene resulted in an early, mild hyperplasia accompanied by some keratosis (*Figure 4-2A,C*), which progressed to a much more macroscopically evident hyperplasia and hyperkeratosis at around 7 months of age (*Figure 4-2B,D*), which eventually developed into a small papilloma after approximately 12 months.

K14.stratifin mice did not exhibit a pronounced phenotype after tagging (*Figure 4-2E,G*), either macroscopically or on histological analysis. However, at around 6-7 months of age, the tagged ears developed a thickening localised to the tag site, though no hyperkeratosis was evident (*Figure 4-2F,H*). Histology of the thickened area showed that hyperplasia of both the epidermis and dermis were present, with the epidermal hyperplasia generally less pronounced than in age-matched *HK1.fos* epidermis (*Figure 4-2F,H* vs *B,D*).

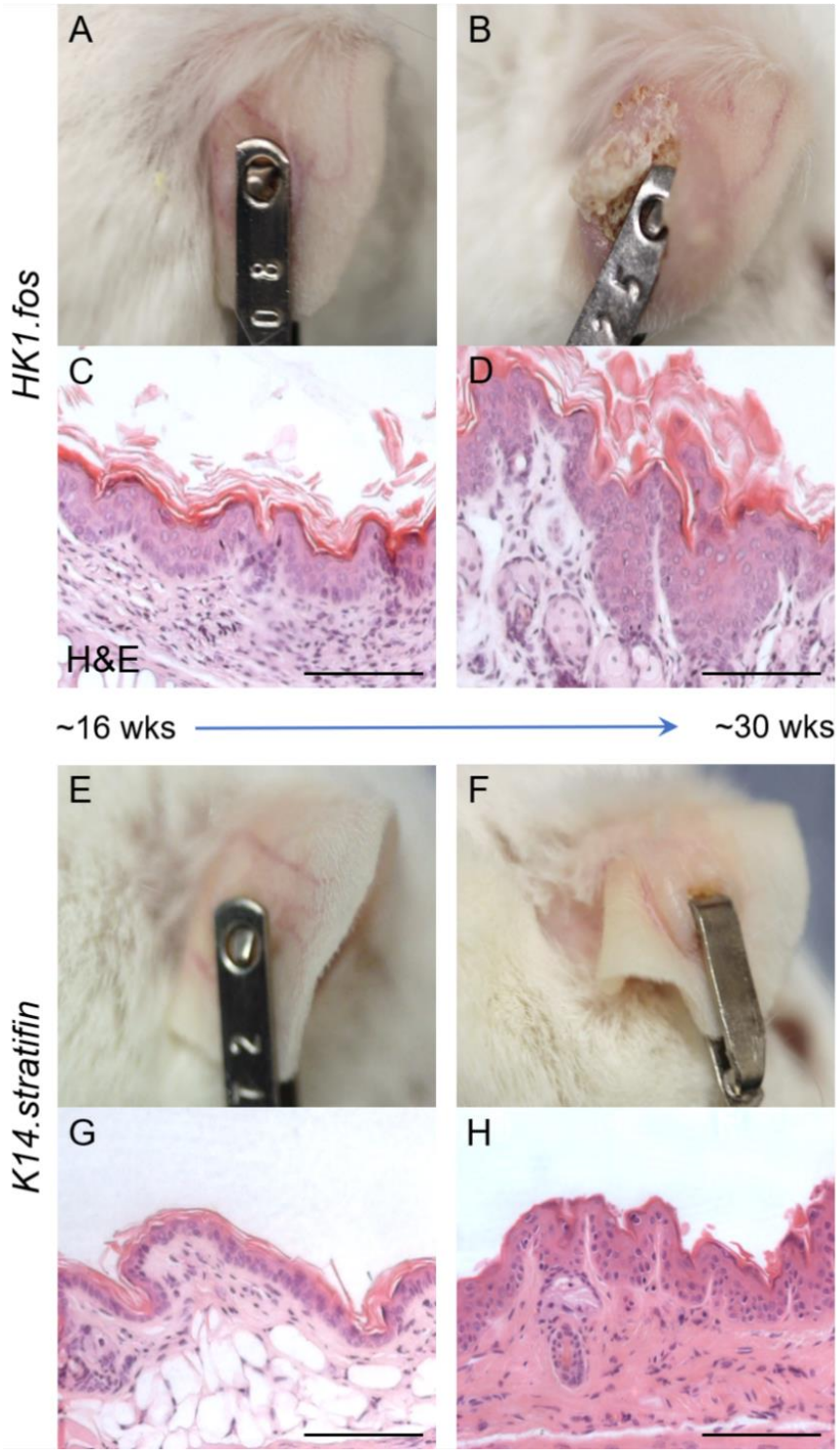

Figure 4-2: Macroscopic and histological appearance of typical *HK1.fos* and *K14.stratifin* tagged ears

HK1.fos tagged ears show only mild hyperplasia and keratosis by about 16 weeks of age, which is not easily visible on gross inspection (**A**) but can be seen on H&E sectioning (**C**). This progresses to greater hyperplasia/hyperkeratosis and papillomatous appearance by 30 weeks (**B** & **D**) and may progress to a papilloma if given enough time (>12 months). *K14.stratifin* tagged ear skin appears grossly and histologically normal (**E** & **G**) at 16 weeks, progressing to a mildly hyperplastic state (**F** & **H**) but lacking the hyperkeratosis seen in *HK1.fos*. The grossly hyperplastic appearance seen in *K14.stratifin* tagged ear skin is a combination of thickened epidermis and dermis, while *HK1.fos* is primarily epidermal. *Scale bars approx. 100 µm.*

In contrast, *HK1.fos/K14.stratifin* bi-genic offspring rapidly produced a distinct and unique phenotype which was quite unexpected. As shown in *Figure 4-3*, *HK1.fos/K14.stratifin* mice developed grossly apparent phenotypes at an early age which quickly exceeded that observed in *HK1.fos* littermates. Those which were most strongly affected had evidence of hyperplasia and keratosis which gave a dusty appearance to the skin (mainly localised to the ears) within 3 days of birth. These strongly phenotypic pups had notable bilateral ear hyperplasia and hyperkeratosis by 3-weeks-old, as seen in the untagged example in *Figure 4-3A,B*. Of those mice which were tagged, regardless of the severity of their phenotype, 100% developed a tagged ear (TGE) tumour (*Figure 4-3E,F*). In many cases, the phenotype was bilateral such that a smaller non-tagged ear (NTE) tumour was also present at biopsy. In cross-section, *HK1.fos/K14.stratifin* tumours invariably appeared very pale with a prominent main blood vessel through the centre, quite unlike the *HK1.ras/fos-Δ5Pten* phenotype (*Figure 4-3I,J*) which had a more expected pink/red, somewhat homogenous cross section.

Several unique features were apparent in *HK1.fos/K14.stratifin* tumour histology from a very early stage (3-week-old hyperplasia/early tumour shown), most noticeably the deposition of keratin throughout the tumour epidermis (yellow arrows in *Figure 4-3C,D,H*). This produced a very distinctive mottled colouration in H&E stained sections when juxtaposed with the pale acanthosis in the suprabasal layers. Additionally, there was a striking reduction in the granular layer which exhibited a speckled appearance before being lost completely in the more advanced regions (*Figure 4-3C,G*: black asterisk). Mitotic figures were also seen in these early examples (circled in *Figure 4-3D*), suggestive of malignant conversion at a much earlier timepoint than in *HK1.ras/fos-Δ5Pten* multistage carcinogenesis, despite only involving overexpression of two genes.

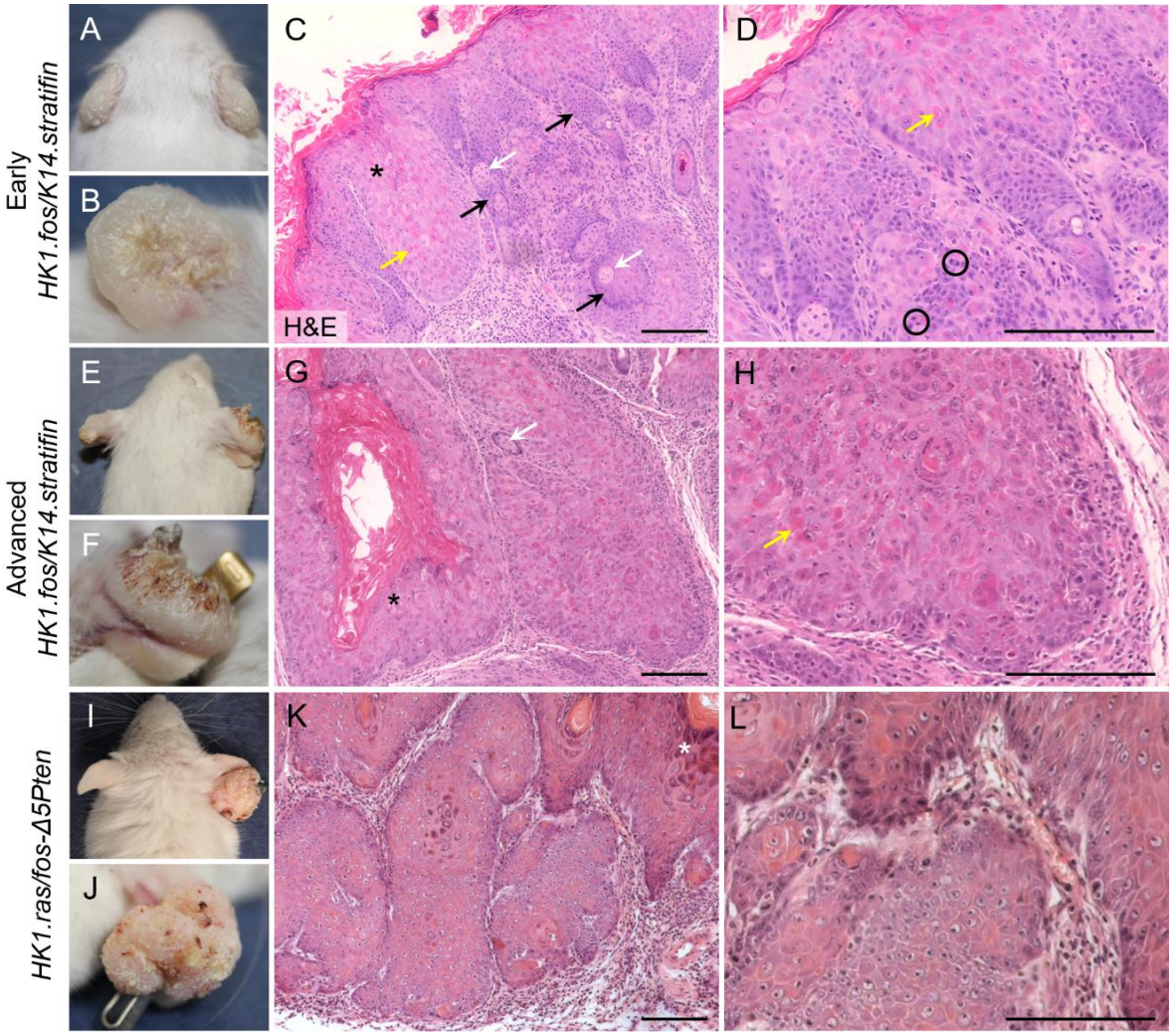

Figure 4-3: Gross and histological appearance of Early and Advanced *HK1.fos/K14.stratifin* tumours contrasted with *HK1.ras/fos-Δ5Pten* wdSCC.
Gross images of a bilaterally affected *HK1.fos/K14.stratifin* mouse at 3-weeks-old (untagged) are shown in **A** and **B**, with prominent thickening of the ears and hyperkeratosis evident. Histology of the ear in low (**C**) and high (**D**) magnification shows hyperplasia, aberrated hair follicles (black arrows) and associated sebocytes (white arrows), intraepidermal keratin deposition (yellow arrows), mitotic figures (black circles) and a loss of normal granular layer (black asterisk). **E** and **F** show macroscopic images of an *HK1.fos/K14.stratifn* mouse with an advanced tumour on the tagged ear (TGE) and smaller tumour on the non-tagged ear (NTE); both are hyperkeratotic. x100 (**G**) and x200 (**H**) powered micrographs of the TGE tumour show some of the features highlighted in **C** and **D** (white arrow and yellow arrows, and black asterisk) though the section is noticeably more poorly differentiated overall. **I** & **J** show an *HK1.ras/fos-Δ5Pten* TGE tumour (no NTE tumour is present) for comparison. Low (**K**) and high (**L**) powered micrographs of the TGE tumour are shown; these do not exhibit the same intraepidermal keratosis seen the *HK1.fos/K14.stratifin* tumours above and the granular layer appears to be thickened (white asterisk) rather than absent in the well differentiated area of this SCC. *Scale bars approx. 100 µm.*

This bigenic genotype clearly impacted the development of hair follicles, as many aberrated follicles were found in the hyperplasia and early tumour stages (in *Figure 4-3C,D*: black arrows), including clusters of sebocytes appearing in conjunction with follicular keratinocytes (*Figure 4-3C,G*: white arrows). Such structures were not apparent in either *HK1.fos* or *K14.stratifin* mono-genic mice, nor in the *HK1.ras/fos-Δ5Pten* wdSCC at any stage. In addition, *HK1.ras/fos-Δ5Pten* wdSCC did not exhibit the intraepidermal keratosis seen in *HK1.fos/K14.stratifin* tumours and the granular layer appeared to be thickened rather than lost (*Figure 4-3K,L*: white asterisk).

More advanced *HK1.fos/K14.stratifin* tumours (*Figure 4-3G,H*) exhibited the same features as the early example, though the aberrant differentiation was widespread, including the loss of most discernible follicular structures, though some sebocytes were still present, unlike in the *HK1.ras/fos-Δ5Pten* control (*Figure 4-3K,L*). All *HK1.fos/K14.stratifin* advanced tumours were hyperkeratotic, often comprising more than 50% of the total tumour volume. Most tumours of this genotype had very little stroma present overall, and many larger regions of stroma had broken and were lost during processing. Given this was common in advanced *HK1.fos/K14.stratifin* tumours, it could indicate a fragile or brittle stroma, which is also distinct from control tumours.

HK1.fos/K14.stratifin hyperplasias and SCCs were also evaluated for expression of Stratifin (*Figure 4-4A,B,D*), where it was found to be strongly expressed in all layers of the epidermis and throughout tumour keratinocytes. At low and moderate magnification (x100 and x200), some areas of the tumour appeared to have lower expression, particularly basal cells (*Figure 4-4B,D*). However, on inspection at high magnification (x400) the proliferating basal cells were tightly packed together, resulting in a less visible cytoplasm and therefore less intense green staining; seen in the narrow spaces between nuclei in the highlighted box in *Figure 4-5D*. In contrast, endogenous Stratifin was largely lost subsequent to malignant conversion in *HK1.ras/fos-Δ5Pten* wdSCC (*Figure 4-4C,E*), though some sporadic cytoplasmic and membranous staining was found to persist in the wdSCC, before disappearing in the pdSCC, as observed rapidly in TPA-treated *HK1.ras-Δ5Pten* pdSCCs (Appendix 1: McMenemy et al., in preparation, *Figure 4*).

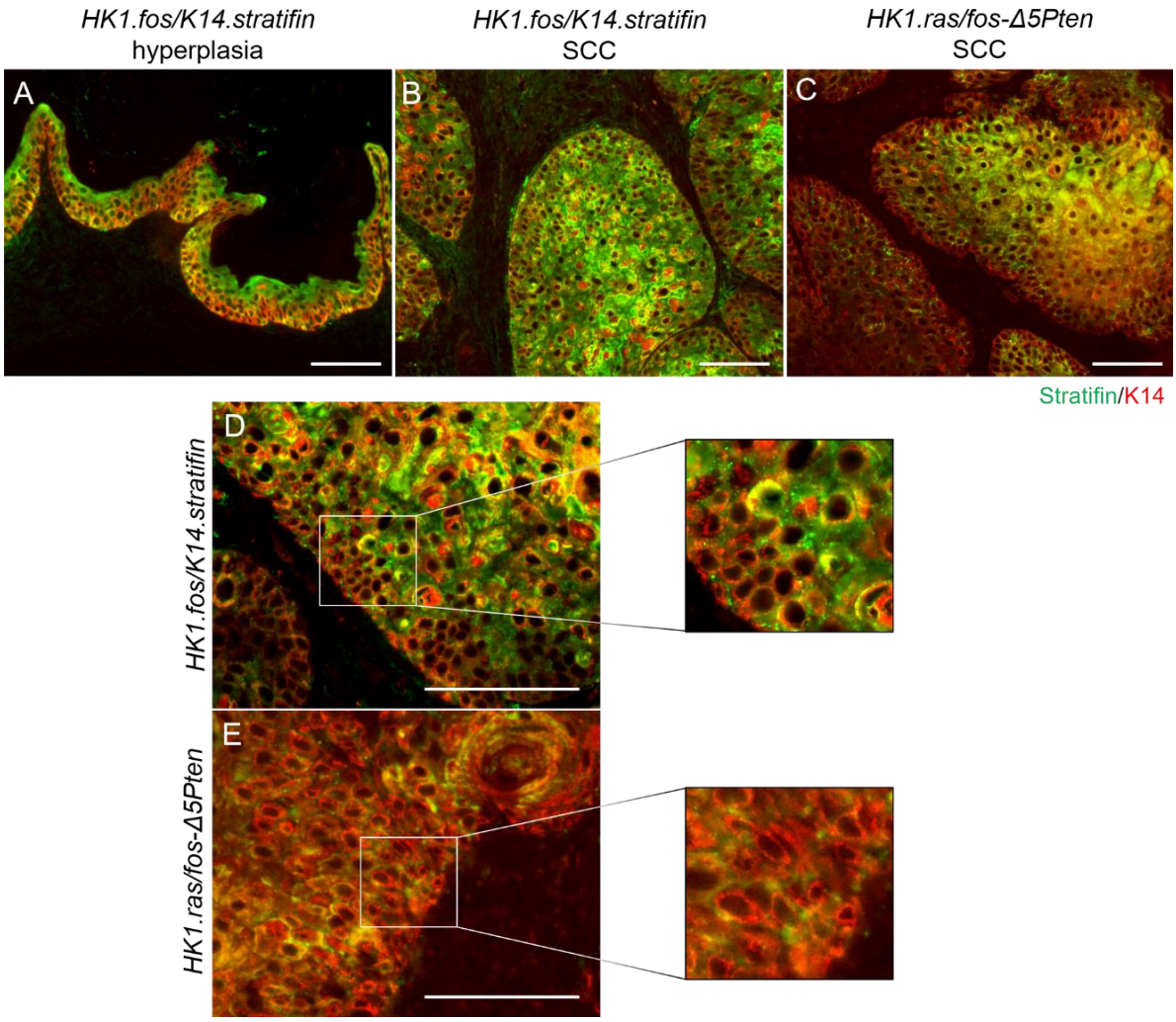

Figure 4-4: Exogenous Stratifin expression is maintained throughout *HK1.fos/K14.stratifin* tumorigenesis.
(**A**) *HK1.fos/K14.stratifin* hyperplasia shows Stratifin (green) in all layers of the epidermis. Similarly, (**B**) malignant *HK1.fos/K14.stratifin* SCC shows strong staining throughout, compared to (**C**) *HK1.ras/fos-Δ5Pten* SCC where endogenous stratifin expression is lost. (**D**) Higher magnification of *HK1.fos/K14.stratifin* SCC displays clusters of apparently negative basal cells; highlighted to show that where *K14.stratifin* staining appears reduced, this due to the tightly packed nature of the invasive cells, with little cytoplasm. (**E**) At higher magnification, *HK1.ras/fos-Δ5Pten* SCC show sporadic, mainly membranous Stratifin expression. Keratin 14 (red) is used as a counterstain. *Scale bars approx. 100 µm.*

All *HK1.fos*/*K14.stratifin* tumours exhibited nearly identical epidermal histology to one another. However, as alluded to earlier, there was variation in the rate at which tumours developed, whether wound-promotion was required for tumour development, and whether the tumour was noticeably distinct from adjacent, grossly normal ear tissue or if the entire ear was affected. These phenotypes were termed Mild, Moderate, and Strong (*Table 4-1*). The reasons for this variation in phenotype were not immediately apparent, but homozygosity of either the *HK1.fos* or *K14.stratifin* transgenes was not found to correlate with the pattern of severity.

However, macroscopic observation of the ears of strongly phenotypic mice indicated redness and warmth consistent with inflammation, though there were no signs of infection from open wounds nor visible pus. This led to examination of the histology for signs of immune infiltration, which did appear to correlate well with the categories; the number of visible immune cells in the tumour stroma increased from mild to strong phenotype, consistent in both tagged (TGE) and non-tagged (NTE) ear sections, depicted in *Figure 4-5*. Also noticeable was the increased depth of the basal layer with strength of phenotype, and an apparent reduction in the characteristic intraepidermal keratin deposits in the Strong phenotype, consistent with less differentiation and more proliferation.

	Mild	**Moderate**	**Strong**
Tagged Ear (TGE) Tumour	2-10 mm	6-10 mm	Whole ear affected
Non-Tagged Ear (NTE)	Normal or very mild gross phenotype. Mild hyperplasia on histology	Hyperplasia and keratosis or tumour < 8 mm	Whole ear affected
Age at Biopsy	8-20 weeks	8-16 weeks	≤ 8 weeks
Frequency	26.1% (6/23)	56.5% (13/23)	17.4% (4/23)

Table 4-1: Description of Mild, Moderate and Strong *HK1.fos/K14.stratifin* phenotypes and their frequency of occurrence.

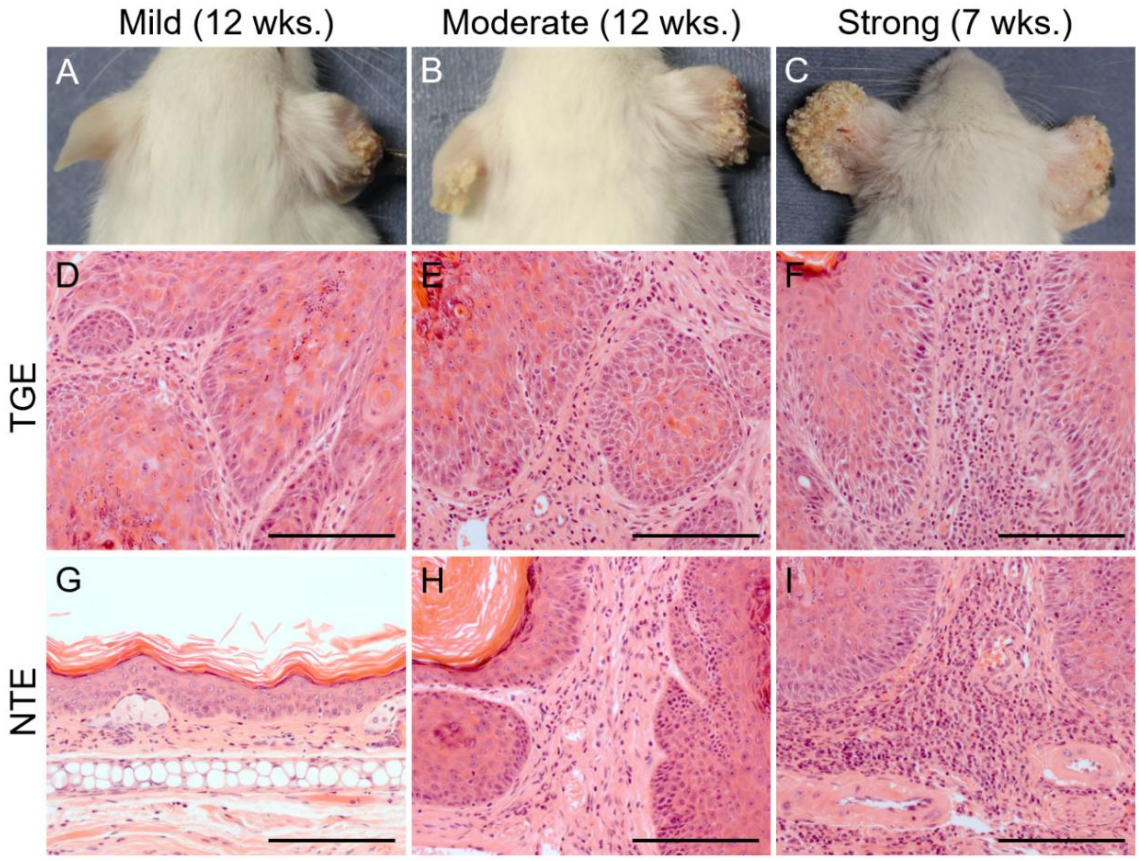

Figure 4-5: Gross and histological differences between Mild, Moderate and Strong *HK1.fos/K14.stratifin* phenotypes and their correlation with extent of immune cell infiltrate.

(**A**) Mild *HK1.fos/K14.stratifin* phenotype, with a tumour on the tagged/wound-promoted ear (TGE) on the right and grossly normal non-tagged ear (NTE) on the left. (**D**) Histology of the TGE tumour including immune infiltrate in the stroma; (**G**) NTE with only mild hyperplasia and low abundance of immune cells. (**B**) Moderate phenotype, TGE tumour comparable to that in (**A**) and gross hyperkeratosis overlying a very small tumour on the NTE. (**E** and **H**) TGE and NTE histology, respectively, with similar features in the tumour and extent of immune infiltrate despite the gross size difference. (**C**) Strong phenotype which required biopsy at an earlier stage (7 wks. vs 12 wks. in **A** and **B**), with bilateral tumours of similar appearance. Histology of TGE and NTE (**F** and **I**), are indistinguishable regardless of wound-promotion status, and of immune infiltrate is high in both. *Scale bars approx. 100 µm.*

Determining the type of immune cells present with certainty would require more specific staining to be performed for specific markers. However, H&E analysis did allow for identification of eosinophils due to their distinctive red cytoplasm, which appeared to be present to some degree in all *HK1.fos/K14.stratifin* tumours.

4.4. *HK1.fos/K14.stratifin* tumours display several characteristics of malignancy

The loss of normal differentiation and presence of mitotic figures seen on H&E histological examination of *HK1.fos/K14.stratifin* tumours were suggestive of malignant conversion to SCC. To explore this further, sections of hyperplasia and tumours from *HK1.fos/K14.stratifin* mice were analysed for differentiation marker loss that correlate with conversion to SCC. Here, Keratin 1 has been examined by immunofluorescence staining, shown in green in *Figure 4-6*.

In *HK1.fos/K14.stratifin* hyperplasia/papilloma (*Figure 4-6A,C*) most suprabasal cells are strongly positive for Keratin 1, indicating a benign phenotype at this stage. However, when compared directly with the *HK1.ras/fos* papilloma (8 weeks post-tagging; *Figure 4-6B,D*), it is clear that the proliferative basal layers (denoted by Keratin 14 counterstaining in red) had already expanded to 2 or more cells deep, compared with the older, wound-promoted control papilloma wherein only one, distinct layer of undifferentiated cells was present.

Furthermore, in the intermediate tumour (*Figure4-6E,G*; 7-weeks-old) *HK1.fos/K14.stratifin* tumours exhibited loss of K1 positivity in a large proportion of cells, to a similar degree to that seen in the older *HK1.ras/fos-Δ5Pten* wdSCC (*Figure 4-6F,H*). It is also worth noting that the pattern of K1 loss displayed a much less smooth transition than in *HK1.ras/fos-Δ5Pten* wdSCC aetiology, reflective of the highly unusual differentiation pattern in this *HK1.fos/K14.stratifin* phenotype.

At the advanced stages (*Figure 4-6I,K*; 11 weeks) wound-promoted tumours displayed regions devoid of Keratin 1 positivity, indicating a highly undifferentiated, malignant phenotype, similar to that in the aggressive TPA-promoted *HK1.ras-Δ5Pten* SCC (*Figure 4-6J,L*). This was completely unexpected, given the well-documented TSG roles of Stratifin, coupled with the fact that it only involves two genetic “hits”, unlike the multistage and TPA-promoted control SCCs, which also take longer to develop than *HK1.fos/K14.stratifin* SCCs.

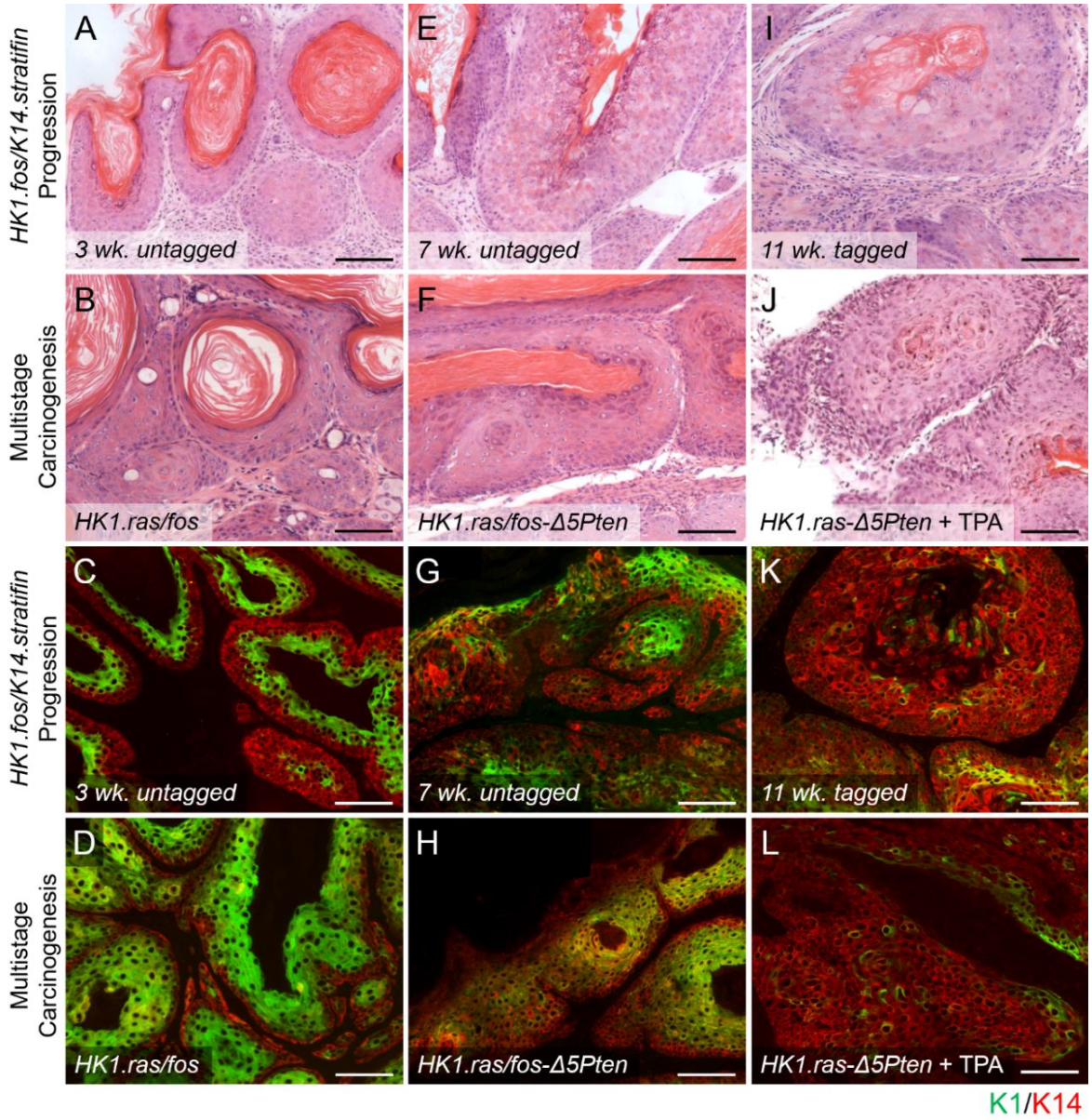

Figure 4-6: Loss of Keratin 1 staining indicates malignancy in *HK1.fos/K14.stratifin* tumours, similar to *HK1.ras/fos-Δ5Pten* and *HK1.ras-Δ5Pten+TPA* carcinogenesis despite distinct histological features.

(**A**) *HK1.fos.K14.stratifin* untagged ear (3 wks.) shows similar hyperplasia/papilloma development to (**B**) *HK1.ras/fos* tagged ear (12 wks.) but with unique histological features such as intra-epidermal keratin deposition, and (**C**) a reduction in suprabasal Keratin 1 (K1; green) staining and expansion of the undifferentiated K14-positive basal layers (red), indictive of early-stage malignant conversion, which is not observed in (**D**) benign *HK1.ras/fos* early papilloma which displays strong K1 staining in all suprabasal layers. (**E**) *HK1.fos/K14.stratifin* NTE tumour (7 wks.) shows novel dysplasia in all layers compared to (**F**) *HK1.ras/fos-Δ5Pten* papilloma/wdSCC which lacks the unusual *HK1.fos/K14.stratifin* aetiology at a similar stage of malignant conversion, as indicated by the comparable extent of K1 loss in (**G**) *HK1.fos/K14.stratifin* SCC and (**H**) *HK1.ras/fos-Δ5Pten* SCC. (**I**) *Older HK1.fos.K14.stratifin* TGE SCCs (11 wks.; 7 wks. post-tag). exhibit anomalous differentiation with no visible granular layer, intraepidermal keratin, acanthosis in the supra-basal layers, and expanding proliferating invasive layer with hyperchromatic nuclei consistent with **(K)** loss of most K1 expression and a novel SCC histotype. These novel features are absent in (**J**) aggressive, TPA-promoted *HK1.ras-Δ5Pten* poorly-differentiated SCCs, although some features are similar, such as loss of granular differentiation and abundant immune cell infiltrate and are (**L**) K1-negative. *Scale bars approx. 100 µm.*

Given confirmation of malignancy via K1 immunofluorescence showing a loss of normal differentiation, coupled with the histological features described, including presence of mitotic figures, analysis of the degree of proliferation was carried out. This was done using 5-bromo-2'-deoxyuridine (BrdU) labelling; a thymidine analogue which is incorporated into the DNA of dividing cells. Mice were injected intraperitoneally with 125 mg/kg approximately 2 hours before being sacrificed, thus, any positivity detected indicated cells which divided during that time frame. This is expressed as positive cells per mm of basement membrane (cell mm/BM) (*Figure 4-8*).

As shown in *Figure 4-7*, the number of positive cells in normal skin was found to be very low at ~2 cells/mm basement membrane, rising to ~10 cells mm/BM in *HK1.fos* hyperplasia (*Figure 4-7A,B*). Importantly, in both of these genotypes, positivity is almost exclusively confined to the basal layer (i.e., cells which are directly attached to the basement membrane). In the malignant control, an *HK1.ras/fos-Δ5Pten* wdSCC, both basal and suprabasal cells are positive, and the numbers in both categories are much higher than in the benign samples shown, with approximately 40 and 25 positive cells per mm in basal and suprabasal layers, respectively (*Figure 4-7C*; *Figure 4-8*).

In moderately developed and two more advanced *HK1.fos/K14.stratifin* SCCs, the occurrence of basal cell positivity was very high in some areas, where almost every nucleus was positive, with a dearth in others (compare *Figure 4-7D* with the lower half of *E*, for example). This resulted in a lower mean basal figure than for *HK1.ras/fos-Δ5Pten* carcinoma, at ~30 cells/mm. However, there was a much greater spread in the counts, ranging from less than 20 to nearly 60 in *HK1.fos/K14.stratifin*, compared with between around 30 and 50 in the *HK1.ras/fos-Δ5Pten* control. The difference is even more dramatic in the suprabasal counts, as evidenced in the boxplot in *Figure 4-8*, with several areas far exceeding the mean (outlier points on plot, labelled) and others having negligible positivity. This suggests that despite a similar histology across these tumour sections, there was significant heterogeneity in the *HK1.fos/K14.stratifin* phenotype with regards to cellular activity.

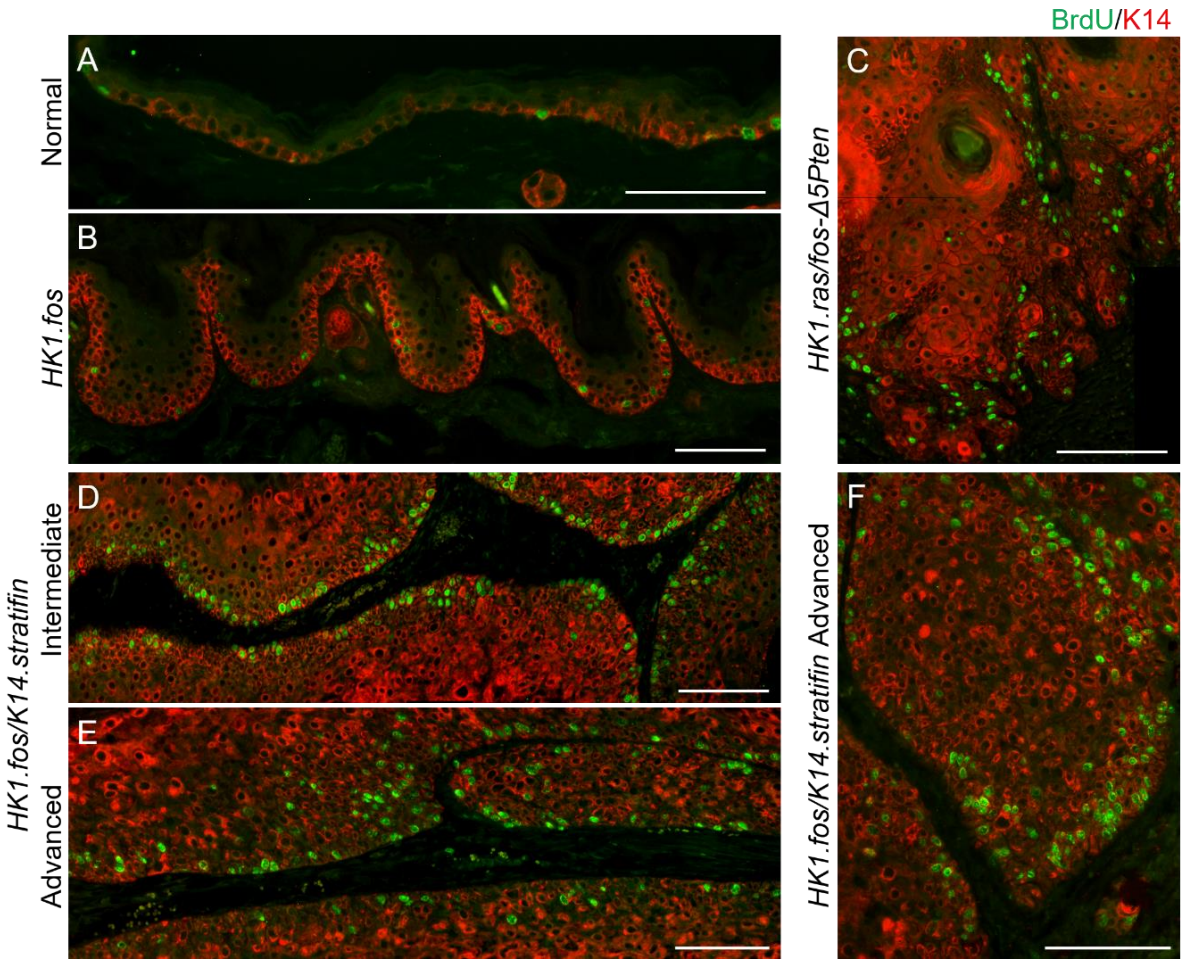

Figure 4-7: *HK1.fos/K14.stratifin* shows high mitotic index on BrdU labelling with greater suprabasal staining corresponding with more malignant tumour regions. BrdU labelling for mitotic index in 7-month Normal mouse ear skin (**A**), *HK1.fos* hyperplasia (**B**), *HK1.ras/fos-Δ5Pten* SCC (**C**), and *HK1.fos/K14.stratifin* SCC (**D-F**). Well-differentiated *HK1.fos/K14.stratifin* SCC (**D**) shows predominantly basal layer staining, with a high rate of positivity. More poorly differentiated areas of *HK1.fos/K14.stratifin* SCCs (**E** & **F**) have both frequent basal and suprabasal layer staining, similar to *HK1.ras/fos-Δ5Pten* SCC (**C**). *Scale bars approx. 100 µm.*

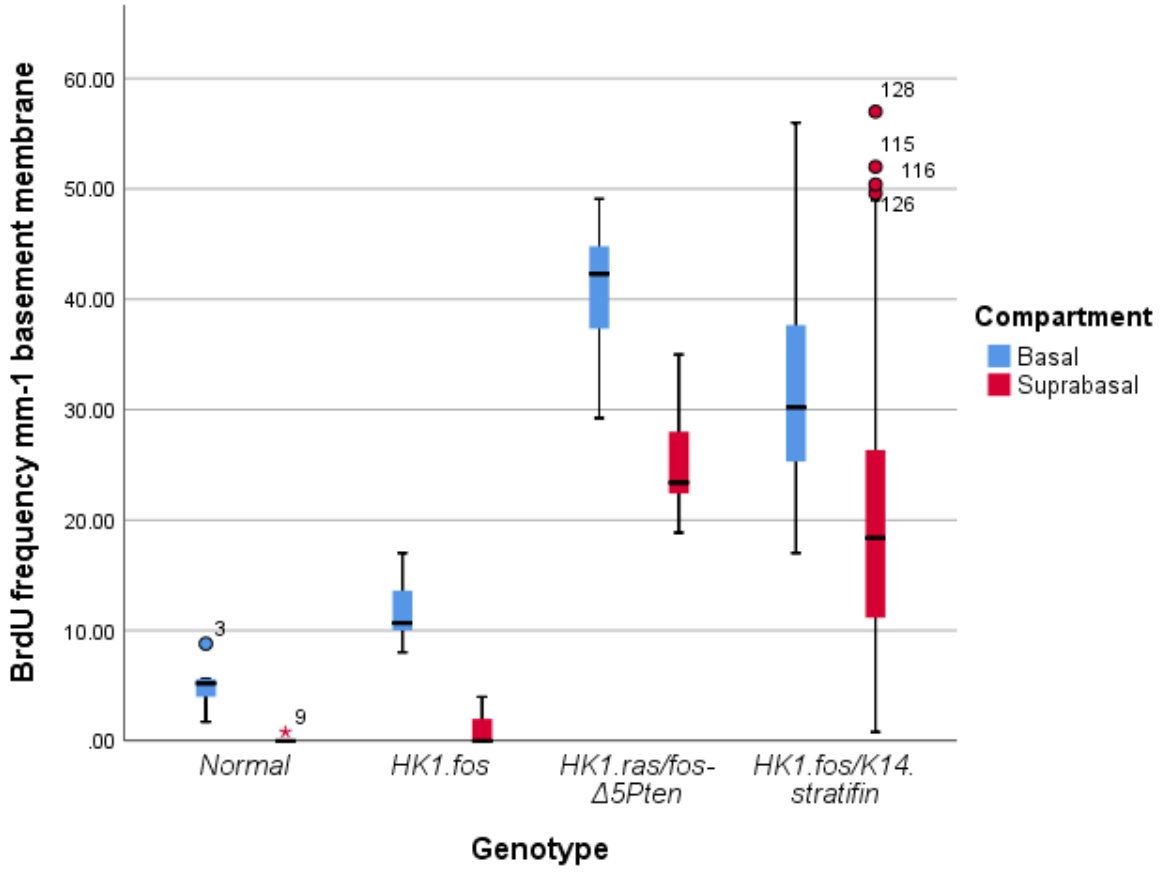

Figure 4-8: Mitotic index in *HK1.fos/K14.stratifin* tumours is comparable to *HK1.ras/fos-Δ5Pten* SCC but with greater variation within tumour samples.
Boxplot showing basal and suprabasal frequencies of BrdU staining in Normal, *HK1.fos*, *HK1.ras/fos-Δ5Pten* and *HK1.fos/K14.stratifin* samples. Number of mice in each category: Normal *n*=2; *HK1.fos* *n*=2; *HK1.ras/fos-Δ5Pten* *n*=2; *HK1.fos/K14.stratifin* *n*=3. Multiple areas of each section for each genotype were assessed and the number of positive cells per 1 mm basement membrane was calculated in each. Note: variation within the tumour sections (both *HK1.ras/fos-Δ5Pten* and *HK1.fos/K14.stratifin*; latter more pronounced, as shown by the whiskers) was large due to tumour heterogenicity (malignancy vs benign/hyperplasia).

4.5. *HK1.fos/K14.stratifin* SCCs retain p53 positivity and are unaffected by conditional p53 knockout

To investigate the mechanisms underlying the variation in mitotic index, sections were next stained for the tumour suppressor protein, p53. This protein has an important role in governing cell cycle progression and as described in detail in the introduction, is supported by Stratifin as the latter chaperones its inhibitor (Mdm2) out of the cytoplasm to prevent p53 degradation (Lee and Lozano, 2006).

In the *HK1.ras/fos-Δ5Pten* and TPA-promoted *HK1.ras-Δ5Pten* models of SCC, the abundance of p53 increases in basal cells during the hyperplasia and papilloma stages and is lost following conversion to malignancy, as described in the Introduction and further in Chapter 3. A p53 negative TPA-promoted *HK1.ras-Δ5Pten* SCC is shown in Panel I of *Figure 4-9* for reference.

Despite the positive feedback relationship between p53 and Stratifin, the formation of highly proliferative malignant tumours in *HK1.fos/K14.stratifin* mice, it was thought that p53 was likely to be lost in these tumours at the malignant stage, as in controls. Contrary to this hypothesis, the early and moderately developed *HK1.fos/K14.stratifin* SCCs tested showed very strong p53 positivity in multiple layers of the epidermis, with both stronger staining and a greater number of positive cells than in *HK1.fos* hyperplasia, as indicated in *Figure 4-9 Panel I vs Panel II*.

In the most advanced regions of *HK1.fos/K14.stratifin* tumours, where differentiation was poorest, some loss in positivity was observed, but this was primarily a reduction in the strength of staining present, as truly negative cells were few in number (*Figure 4-9 Panel II:C,F*). This appears to indicate that the mechanisms in place to increase p53 are present in the advanced stages of *HK1.fos/K14.stratifin* tumorigenesis. However, there is clearly a disconnect which prevents it from initiating cell cycle arrest, as evidenced by the high mitotic index of these tumours.

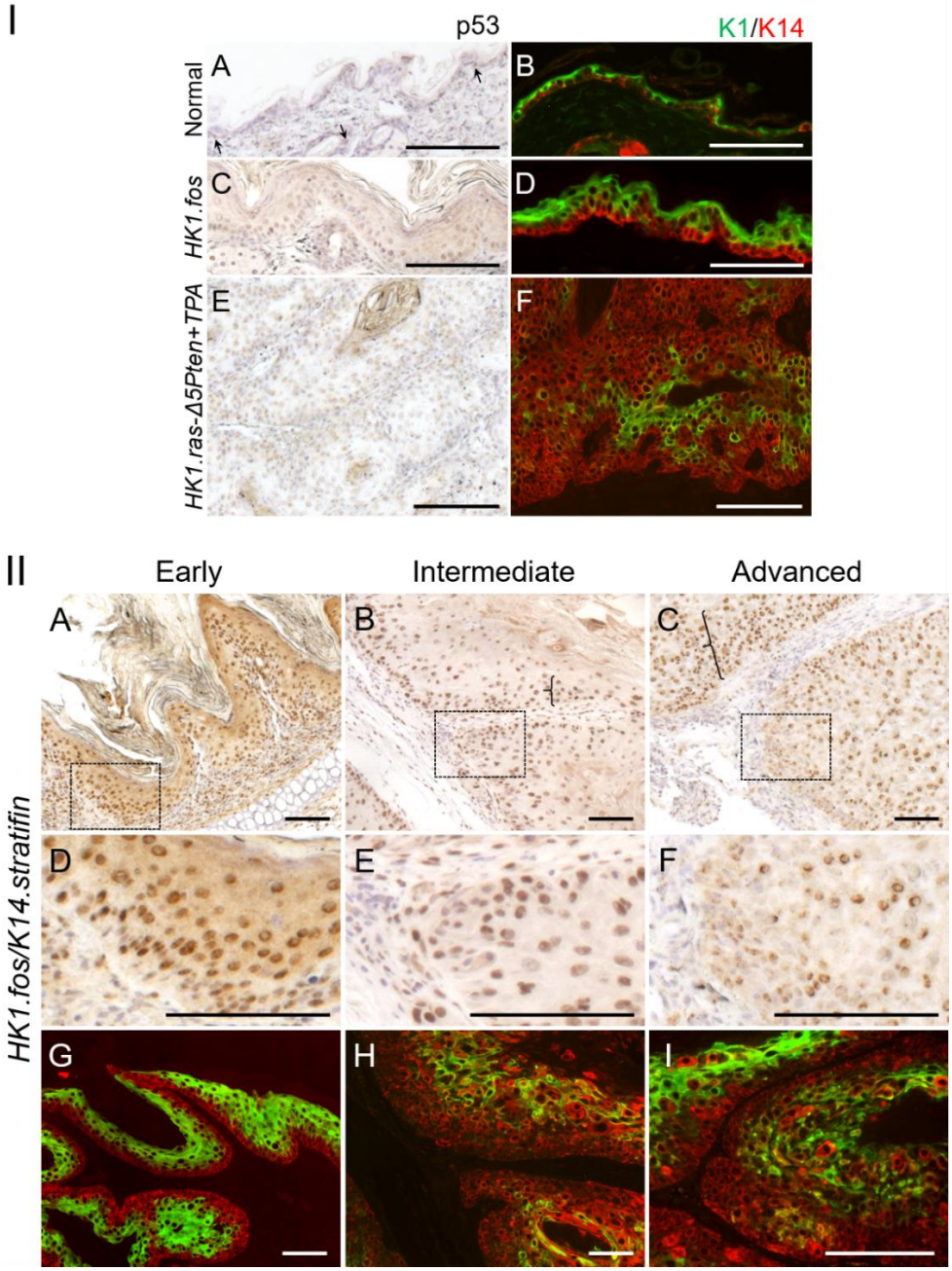

Figure 4-9: Immunostaining shows persistence of p53 in *HK1.fos/K14.stratifin* tumours after K1 loss indicates malignant conversion has occurred.

Panel I: In Normal skin (**A**), p53 staining is negligible with only sporadic staining in both epidermis and follicles (arrows). *HK1.fos* hyperplasia (**C**) shows staining in approx. half of basal layer nuclei; all staining is light to moderate. *HK1.ras-Δ5Pten* + TPA SCC shows very low abundance of p53 (**E**). Keratin 1 (green) and Keratin 14 (red) staining is shown in **B**, **D** and **F** to indicate the malignant status of the sections assessed for p53.

Panel II: (**A-C**) Low and (**D-F**) high magnification of p53 expression during *HK1.fos/K14.stratifin* tumour progression indicated by (**G-I**) reducing K1 expression in serial sections. (**A**) Early (3 weeks) ear hyperplasia/early tumour shows p53 staining in high numbers of positive cells with moderate to strong staining in multiple layers; boxed section is enlarged in **D**; while K1 staining indicates a benign tumour (**G**). (**B**) p53 staining remains strong at 7 weeks (boxed area in **E**) despite tumour converting to SCC as indicated by K1 expression (**H**). Positive p53 cells are ~4 layers deep (bracket, **{**). (**C**) Advanced tumours show strong p53 positivity, now in multiple layers (bracket, **{**); while (**F**) staining appears reduced in aggressive invasive areas, although no regions appear wholly negative. *Scale bars approx. 100 µm.*

To explore the role of p53 in this model of carcinogenesis, *HK1.fos*/*K14.stratifin* mice were crossed with mice harbouring the *K14.CreP1* transgene and floxed (flanked by loxP sites) copies of the endogenous p53 gene ($p53^{flx/flx}$) (Marino et al., 2000). Here, following topical treatment with RU486 in an identical fashion to *Pten* ablation outlined earlier, Cre recombinase acts to remove exons 2-10 of the *TP53* gene, resulting in functional ablation of the p53 protein.

This generated mice heterozygous (*K14.fos.*$p53^{flx/+}$*.stratifin*; *n*=8) and homozygous (*K14.fos.*$p53^{flx/flx}$*.stratifin*; *n*=14) for the floxed p53 allele, as well as control littermates lacking the *K14.CrePR1* gene. Cohorts of these mice were treated with either RU486 to activate Cre recombinase activity, thereby ablating p53 activity, or EtOH as a vehicle control. The cohort of mice which were either heterozygous or homozygous for the floxed allele but which lacked *K14.CrePR1* was also treated with RU486 to control for any effects of the treatment itself. Mice were first treated topically with RU486 (or EtOH vehicle) at the time of ear tagging, then 1-3 subsequent times, dependent on age at biopsy.

Determination of genotype (from tail tip DNA) was performed by PCR using primers spanning one of the two loxP sites in the p53 gene (*Figure 4-10A*, blue arrowheads), which produced either the wild-type (WT) band on gel electrophoresis if no loxP sequences were present, a WT and larger “floxed” (flanked by loxP; FLX) band if the mouse was heterozygous, or a single FLX band if it was homozygous (*Figure 4-10B*). Genotype was reconfirmed following biopsy using either ear or back tissue that had been treated with RU486 (or vehicle control). Confirmation of p53 exon 2-10 ablation was done using the 1F and 10R primers which span the entire floxed region of the gene, producing a ~550 bp band following successful excision (*Figure 4-10B*). The wild-type band was rarely observed in this PCR due to the length of the flanked area (~6 kb).

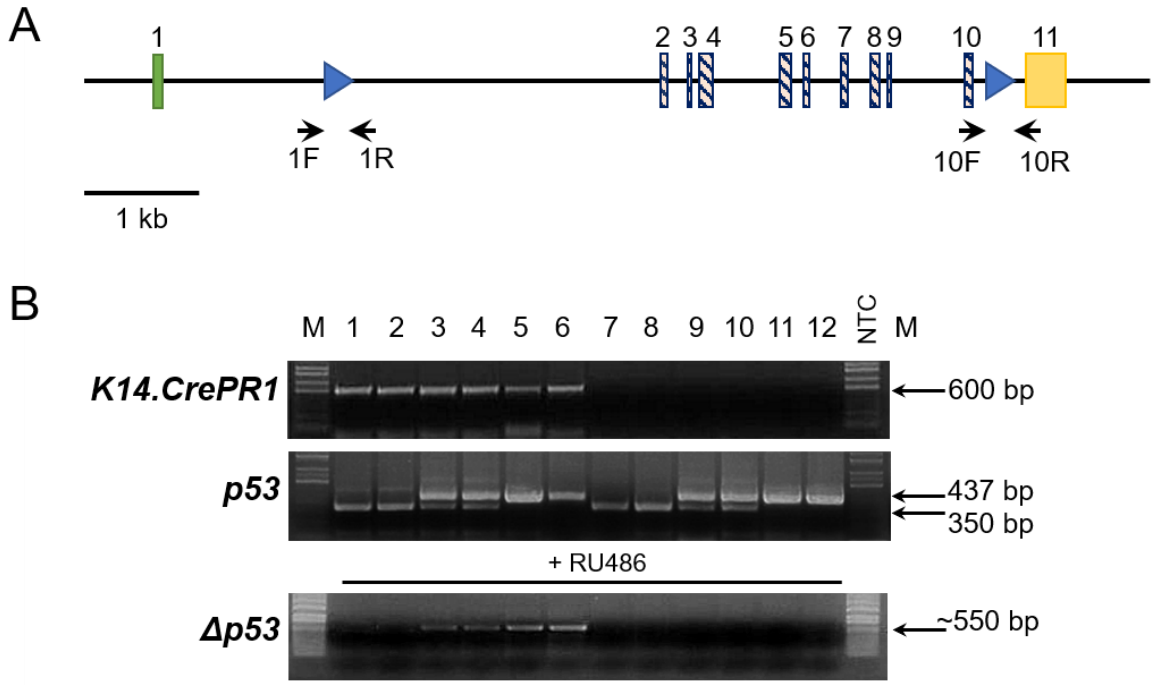

Figure 4-10: Schematic showing floxed regions of TP53 together with PCR confirmation of floxed status and confirmation of Cre-mediated gene recombination. (**A**) Map of *TP53* (which encodes the p53 tumour suppressor protein) with exons numbered (1-11). Blue arrowheads represent *loxP* sites downstream of exon 1 and exon 10. Genotyping can be performed with either the 1F/1R or 10F/10R pair to determine whether loxP sites are present (i.e., the allele is floxed; $p53^{flx}$). Genotyping following RU486 treatment to activate Cre-recombinase is done using the 1F/10R primer pair which spans the entire excised region (*Adapted from Marino et al., 2000)*. (**B**) **Top:** Electrophoresis gel showing *K14.CrePR1* positive samples (lanes 1-6; 600 bp band) and negative (7-12) samples. **Centre:** Gel showing wild-type p53 samples (lanes 1,2, 7 and 8; 350 bp), samples heterozygous for the floxed allele (lanes 3, 4, 9 and 10; 350 and 437 bp), and homozygous floxed samples (lanes 5, 6, 11 and 12; 437 bp). **Bottom:** All samples were treated with RU486 to activate Cre if present. Lanes 1 and 2 are negative because those samples are $p53^{+/+}$; Lanes 3-6 show a band at around 550 bp as these possessed both the *K14.CrePR1* transgene and at least one copy of the $p53^{flx}$ allele. Notice the band is visibly weaker in the $p53^{flx/+}$ samples than in the $p53^{flx/flx}$ as only half of the p53 alleles can be recombined in the heterozygote. Lanes 7-12 are negative because they lack the *K14.CrePR1* transgene.

Loss of a potent TSG would normally be hypothesised to cause a worsened phenotype, e.g., more rapid conversion to SCC. However, the analysis in *HK1.fos*/*K14.stratifin* tumours, indicating increased abundance of p53 in this genotype did not inhibit tumour formation, suggested that any observed effects may be less dramatic than seen in previous models (Greenhalgh et al., 1996). Concurrent with this hypothesis, this analysis found no discernible difference between *HK1.fos*/*K14.stratifin*, *K14.fos.*$p53^{flx/+}$*.stratifin* and *K14.fos.*$p53^{flx/flx}$*.stratifin* whether treated with RU486 or not (*Figure 4-11*). This, again, suggests that p53 is uncoupled from Stratifin regulation as the aetiology of SCC appears independent of p53 status in these mice.

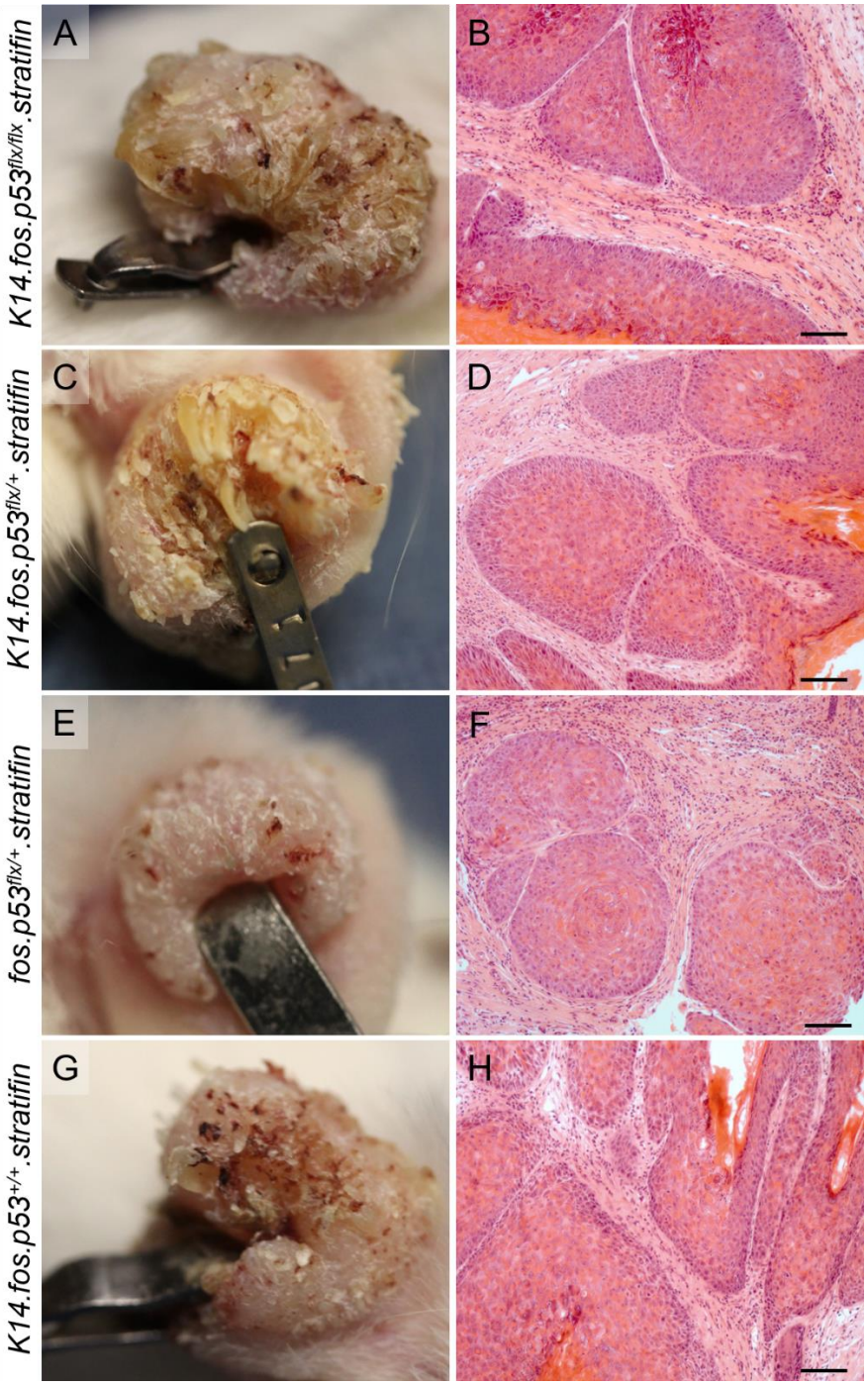

Figure 4-11: Induced p53 loss does not result in a different histotype in *HK1.fos/K14.stratifin* tumorigenesis.
(**A**) *K14.fos.p53$^{flx/flx}$.stratifin* (*n*=14) tumour is indistinguishable macroscopically from (**C**) *K14.fos.p53$^{flx/+}$.stratifin* (*n*=8), (**E**) *fos.p53$^{flx/flx}$.stratifin* (no Cre, thus p53 is intact; *n*=5) and (**G**) *K14.fos.p53$^{+/+}$.stratifin* (*n*=5) tumours. **B**, **D**, **F** and **H** show micrographs (100x) of the same genotypes which also show no appreciable difference correlated with p53 status. *Scale bars approx. 100 µm.*

4.6. Hair follicle keratinocytes are the likely site of origin of *HK1.fos/K14.stratifin* tumours

In early (3-week-old) *HK1.fos*/*K14.stratifin* hyperplasia/papilloma (*Figure 4-3*) numerous aberrated follicles were evident. Follicular involvement has not been observed in *HK1.fos* hyperplasia/papilloma, nor in *K14.stratifin* skin or TGE hyperplasia. This aspect of *HK1.fos*/*K14.stratifin* carcinogenesis was therefore explored further through histological analysis of early and mid-stage tumours.

Initially, in normal and *HK1.fos* hyperplastic skin, histological appearance of hair follicles and associated structures showed that the keratin of hair shafts was not stained with haematoxylin or eosin, unlike that in the *Stratum corneum* (*Figure 4-11 Panel I A,C*). Hair shafts within their follicles were observed as nearly colourless circles or rings with a central pink core, depending on the stage in the follicle cycle and the region which was transected, e.g., in transverse section through the upper isthmus and infundibulum regions showing trichilemmal keratin differentiation surrounding the pink centre of the shaft (El-Domyati et al., 2017). This transverse section means the associated sebocytes are also visible adjacent to the follicles. In *HK1.ras*/*fos-Δ5Pten* carcinogenesis, clearly demarcated, laminated keratin pearls form in the papilloma stage (above; *Figure 4-6B*). In the subsequent carcinoma, the loss of normal differentiation signals impacts the ordered structure of the pearls, which become more amorphous (*Figure 4-12 Panel I D,E*).

HK1.fos/*K14.stratifin* tumours are invariably hyperkeratotic and initial analysis of early-intermediate tumours identified some structures which at first appear to be keratin pearls (centre of image; *Figure 4-12 Panel II: A*. However, closer inspection revealed than most such structures were in fact follicles in which the outer root sheath (ORS) had become massively hyperplastic. Here, hair shafts could be observed in an oddly normal infundibular-like structure at the centre of the hyperplasia (highlighted in *Figure 4-12 Panel II C,D*) Elsewhere, hair shafts appeared to be trapped within the keratosis of cystic structures, while sebocytes were incorporated into masses of tumour keratinocytes (*Figure 4-11 Panel II: E*). These features strongly suggest a hair follicle cell of origin in *HK1.fos*/*K14.stratifin* tumour aetiology.

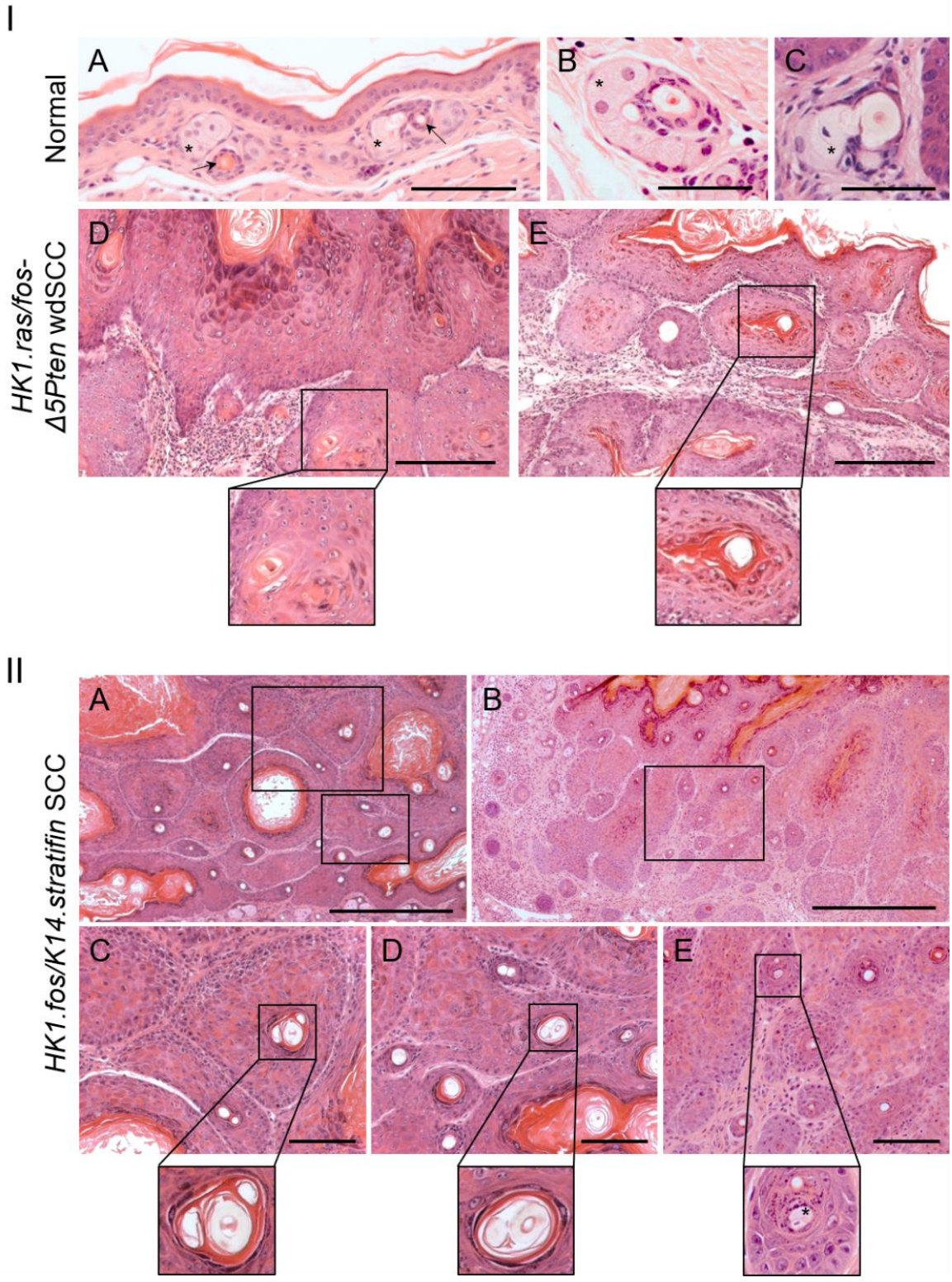
I
Normal
A
B
C
HK1.ras/fos-Δ5Pten wdSCC
D
E
II
HK1.fos/K14.stratifin SCC
A
B
C
D
E

Figure 4-12: *HK1.fos/K14.stratifin* SCCs possess anomalous hair shafts surrounded by tumour tissue suggests histological structures derive from aberrant follicle development.

Panel I: (**A** and **B**) Normal mouse skin and **(C)** *HK1.fos* hyperplasia exhibits typical quiescent (telogen) hair follicles (arrows) with sebocytes (asterisks). At higher magnification, the pink core of the hair shaft is apparent in the centre of the unstained hair keratin (off-white ring). (**D**) *HK1.ras/fos-Δ5Pten* and (**E**) *HK1.ras-Δ5Pten*+TPA SCCs show epidermoid cysts resulting from changes to differentiation signals during carcinogenesis and although similar (boxes), these histotypes lack features associated with hair follicles.
Panel II: (**A** and **B**) Low magnification images of *HK1.fos/K14.stratifin* SCCs exhibit many lobular structures with central rings visible typical of HFs. In addition, normal hair follicles are present adjacent to the main tumour body, most with a relatively normal appearance. (**C**-**E**) Higher magnification of lobular boxed areas show apparent hair shafts present in the centre of tumour tissue, seen more clearly in the excerpts; with (**E**) showing a lobular area with a clear follicle remnant, closely adjacent to a group of sebocytes (asterisks). Several other HF-like histotypes are present in **E** (top right). *Scale bars approx. 100 µm.*

To further investigate the suspected follicular origin of *HK1.fos/K14.stratifin* SCCs, immunofluorescence was performed for Keratin 17, a keratin which can be associated with hyperplasia and wound healing, but which is always present in the ORS of hair follicles (McGowan et al., 2002). This was confirmed in normal skin, where staining was confined to the follicle and was not found to be present in the intrafollicular epidermis or sebocytes. Analysis of *HK1.ras/fos-Δ5Pten* carcinogenesis found positivity only within follicle remnants in the tumour stroma, not in the tumour mass. Both are depicted in *Figure 4-12 Panel I*.

In stark contrast to *HK1.ras/fos-Δ5Pten* carcinogenesis, the majority of K17 positive staining in *HK1.fos/K14.stratifin* tumours was seen in rings within the tumour epidermis, akin to the placement of follicles seen in H&E in the previous figure. Staining also confirmed the nature of the trapped hair shafts seen in H&E, as depicted in the serial sections in *Figure 4-12 Panel II: C and D*, below. DAPI was also used here to confirm the presence of parakeratosis in this early tumour (white oval) which further highlights the abnormalities in differentiation. This expression pattern also supports a follicular cell of origin in *HK1.fos/K14.stratifin* carcinogenesis.

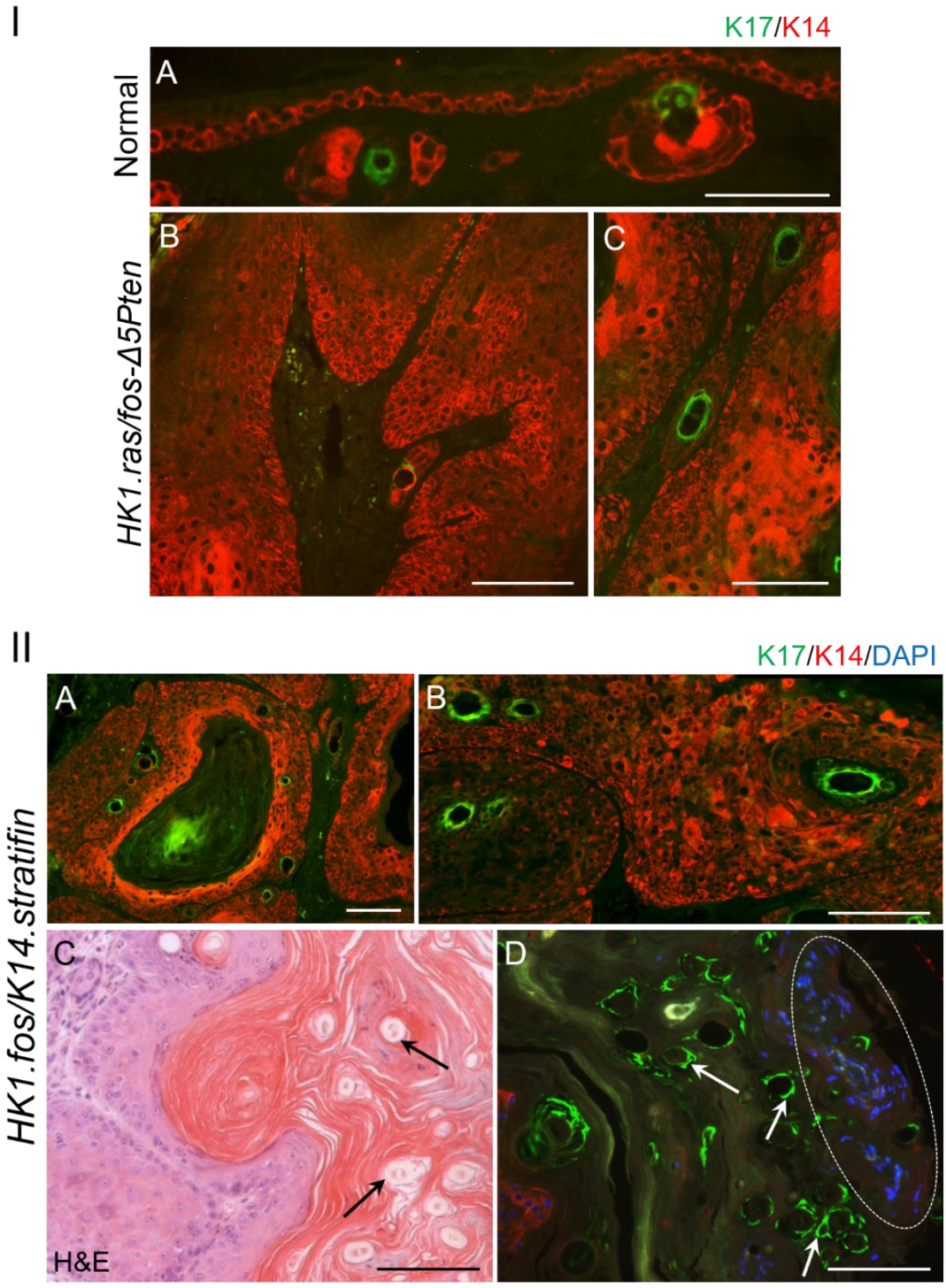

Figure 4-13: Keratin 17 expression, a marker for hair follicle outer root sheath (ORS) cells, supports the follicular origin of *HK1.fos/K14.stratifin* tumours.
Panel I: A shows normal skin in which follicles are cut perpendicular to the hair shaft, thereby appearing as a green ring situated between $K14^{+ve}$ (red) sebocytes. **B** and **C** show low- and high-power micrographs, respectively, of a *HK1.ras/fos-Δ5Pten* wdSCC in which K17 staining is clearly localised to a few follicular structures in the tumour stroma.
Panel II: Low (**A**) and high (**B**) power micrographs (100x & 200x, respectively) show that *HK1.fos/K14.stratifin* SCCs exhibit numerous areas of $K17^{+ve}$ staining (green circles) within the tumour, not distinct in the stroma as in **Panel I**. H&E staining of *HK1.fos/K14.stratifin* tumours possess hair shafts (cut in cross section) that have been trapped in the keratosis (black arrows) and (**D**) serial sections show K17 is associated with this parakeratotic-like trapped hair phenotype (arrows), as well as formal parakeratosis, indicated by DAPI staining (white oval). *Scale bars approx. 100 µm.*

Having established that the keratinocytes giving rise to *HK1.fos*/*K14.stratifin* carcinogenesis were likely to be follicular in origin, a literature search was performed to identify any known tumour types classed as Squamous Cell Carcinomas which develop from follicles, distinct from benign trichofolliculoma or trichilemmoma (a common neoplasm in Cowden Syndrome) (Hanssen and Fryns, 1995).

This identified several case studies in which Follicular Squamous Cell Carcinomas (fSCC) were described (Shendrik et al. 2012; Misago et al., 2012; Carr et al., 2014). Some variation was observed in the histopathology of the tumours presented between and within these papers, though all described trichilemmal differentiation being present, highlighted in the human tumour shown in *Figure 4-14A* (Shendrik et al. 2012; reproduced with permission), highlighted in *B* for direct comparison with the very similar pattern of keratin deposition in the mouse *HK1.fos*/*K14.stratifin* tumour in *F*. Several other similarities were identified, including the juxtaposition of highly acanthotic regions with packed areas of proliferative cells (*C*/*G* and *D*/*H*, respectively). All *HK1.fos*/*K14.stratifiin* tumours also showed increased angiogenesis in the tumour stroma, often accompanied by extravasation of red blood cells which is also apparent in the human fSCC shown. Furthermore, as described in *Figure 4-6*, a high degree of immune infiltration is frequently observed in *HK1.fos*/*K14.stratifin* SCCs, which is also evident in the human fSCC as highlighted in *Figure 4-14E*.

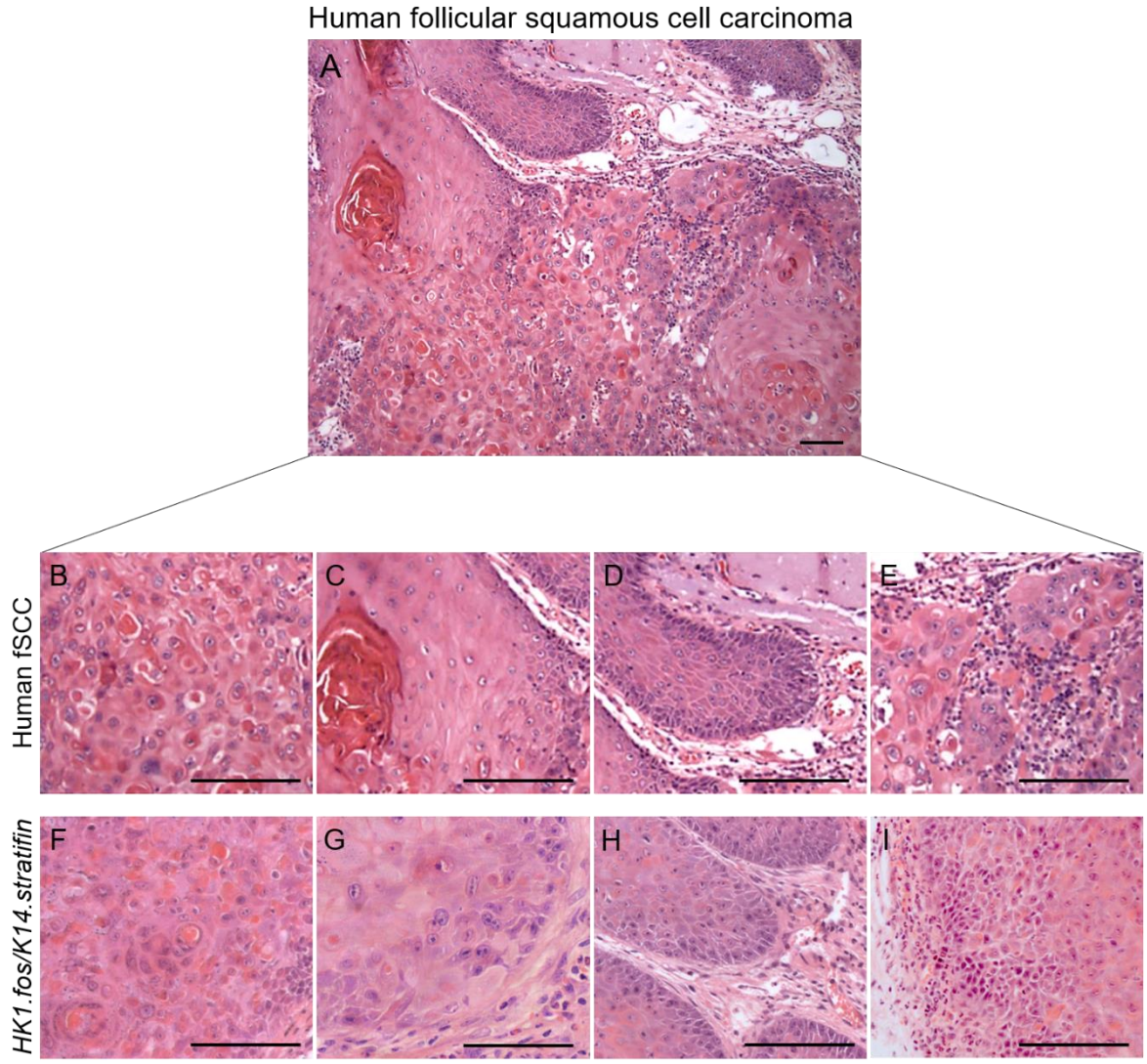

Figure 4-14: *HK1.fos/K14.stratifin* carcinogenesis recapitulates many features seen in human follicular squamous cell carcinoma.
(**A**) Human follicular squamous cell carcinoma, fSCC (Shendrik, et al., 2012; reproduced with permission). Notable features include intraepidermal keratin deposits/trichilemmal differentiation (**B**), acanthosis (**C**), tightly packed proliferative basal cells and increased angiogenesis (**D**) and immune infiltration and invasion (**E**). These characteristics are reproduced in *HK1.fos/K14.stratifin* SCCs, as highlighted in the lower row (**F**-**G**). *Scale bars approx. 100 µm.*

4.7. Changes in cell-cell adhesion may promote invasion of malignant *HK1.fos/K14.stratifin* tumours

In order to assess cell-cell adhesion in the tumour, immunofluorescence staining was performed for ß-catenin, a major component of adherens junctions in normal epidermis. ß-catenin is also an important protein in the canonical WNT-signalling pathway, involved in embryogenesis, hair follicle growth and development, and carcinogenesis as it can act as a transcription factor for numerous downstream targets involved in these processes.

Strong suprabasal membrane staining with some sporadic basal layer positivity was seen in both *HK1.fos* hyperplasia, with little to no cytoplasmic or nuclear staining evident, consistent with its role in adherens junctions and a lack of TF activity (*Figure 4-15A*). The staining pattern was found to be almost identical in tumour-adjacent hyperplastic regions of *HK1.fos/K14.stratifin* samples tested (*Figure 4-15C*), suggesting cell-cell adhesion is not greatly altered in the early stages of carcinogenesis, and ß-catenin does not appear to be involved as a TF at this stage.

In *HK1.ras/fos-Δ5Pten* carcinogenesis, membrane staining was found to be reduced, mainly in the proliferative cells and invasive front, while the change in colour from red to orange suggested cytoplasmic (and likely nuclear) staining was present in these SCCs (*Figure 4-15B*). In later *HK1.fos/K14.stratifin* tumours, membrane staining was much less pronounced, and what was present indicated the lack of organisation in the tumour epidermis; cell sizes appeared to vary widely and not conform to distinct layers.

DAPI staining was then utilised to assess whether the loss of membrane staining corresponded with an increase in nuclear activity. Analysis showed many cyan-coloured cells in the basal layers (where both green ß-catenin and blue DAPI staining co-localised) where membrane staining was very indistinct if present at all (*Figure 4-15E,F*). Sporadic nuclear positivity was also seen in some suprabasal cells. This was confirmed using the ColorInspector 3D plugin for ImageJ, wherein specific nuclei were isolated for colour analysis. Using this method, pixels were plotted on three axes (green, red and blue); in the nuclei

which appeared to be β-catenin positive, a roughly equal quantity of green and blue positive pixels were detected, while in the seemingly negative nuclei tested, almost no colour other than blue was present, as expected (*Figure 4-15G*). This indicated that there was an increase nuclear localisation of β-catenin in the advanced stages of *HK1.fos*/*K14.stratifin* tumorigenesis, concurrent with the visible loss in distinct membranous positivity, suggestive of increased β-catenin TF activity and reduction in cell-cell adhesion. Together, these findings indicate a role for altered β-catenin activity in progression of *HK1.fos*/*K14.stratifin* tumours to a more advanced stage and an increase in invasive potential.

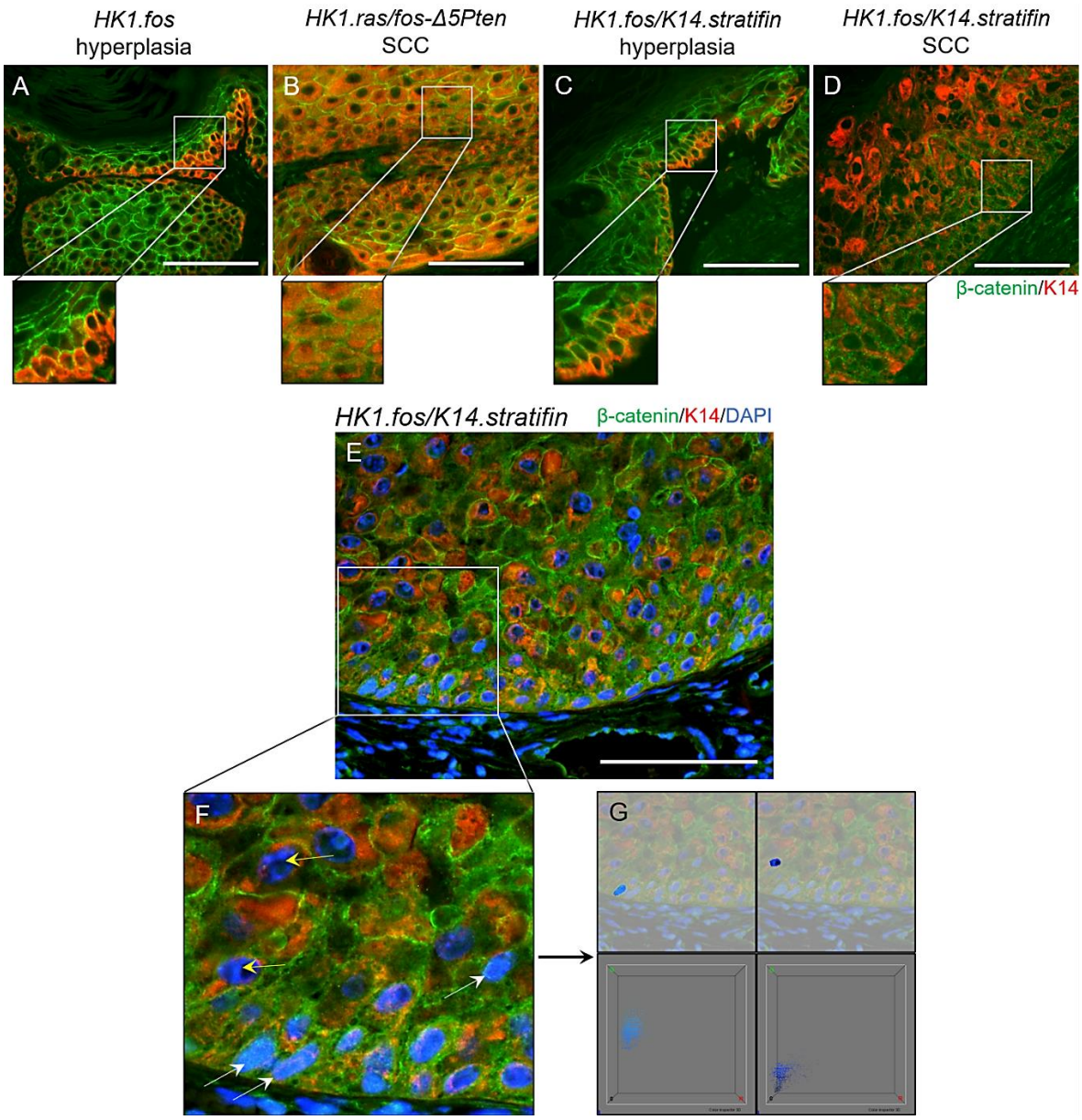

Figure 4-15: Immunofluorescence staining shows anomalous β-catenin expression aids *HK1.fos/K14.stratifin* progression to SCC.

(**A**) *HK1.fos* hyperplasia shows membranous β-catenin localisation in the suprabasal layers with sporadic expression in basal layer keratinocytes. (**B**) *HK1.ras/fos-Δ5Pten* wdSCC shows reduced membranous staining in proliferative basal cells with increasing cytoplasmic positivity. (**C**) *HK1.fos/K14.stratifin* hyperplasia shows near identical β-catenin expression profile to that seen in *HK1.fos*. (**D)** Advanced *HK1.fos/K14.stratifin* SCC now shows loss of β-catenin staining at the membranes of the proliferative layer keratinocytes, with diffuse cytoplasmic and nuclear positivity. (**E**) At higher magnification, such aggressive *HK1.fos/K14.stratifin* SCCs now counterstained with DAPI show the appearance of cyan nuclei, indicating green β-catenin staining colocalised with blue DAPI. (**F**) Nuclear β-catenin expression is further confirmed by appearance of cyan nuclei (white arrows) compared to a lack of nuclear β-catenin in the less aggressive cells that retain membranous expression (yellow arrows). (**G**) ImageJ plugin *ColorInspector 3D* image analysis (lower plots) shows that roughly equal levels of blue and green are present in the cyan nucleus (highlighted), whereas the upper (membrane positive) cell is completely blue and lacks discernible nuclear β-catenin expression. *Scale bars approx. 100 µm.*

4.8. Homeostasis of the keratin filament network is greatly disrupted in *HK1.fos/K14.stratifin* carcinogenesis and may contribute to SCC progression

In *HK1.fos*/*K14.stratifin* tumours, histological analysis showed that the normal differentiation programme was clearly aberrated. For instance, whilst Keratin 1 expression was used as a marker of malignant conversion (*Figure 4-6*), it was also noted that K1 was lost from the lower suprabasal layers at an early stage in the benign hyperplasia/early papilloma. However, when Keratin 1 expression was assessed in *K14.stratifin* skin, it was also found to be spuriously expressed in hair follicles. As described in Chapter 1, Keratin 1 is an early differentiation marker expressed in the spinous layers (with the protein persisting somewhat in the granular layers without further RNA expression). To explore this further, back skin from normal ICR and *K14.stratifin* mice were assessed since many more follicles are present there than in ear skin. Sections were chosen for comparison where follicles were at a similar stage of their cycle and where the transverse section had captured them at a similar level in each (judged based on the appearance on the H&E stained sections).

As shown in *Figure 4-16*, K1 staining (green) is totally confined to the differentiating cells of the epidermis, whereas strong expression was seen in the hair follicles of the *K14.stratifin* counterpart and epidermal expression did not appear to be limited to the supra-basal epidermis, though this was harder to evaluate given the very thin nature of mouse skin.

To better assess where the spurious expression was present, *K14.stratifin* back skin (where HFs were in telogen) was cut giving sections in which the follicles were cut longitudinally, allowing examination of most of the follicle length. This staining showed clear expression in the ORS cells and, importantly, in the bulge cells. The bulge is located in the area highlighted in *Figure 4-16C* close to the bottom of the follicle, rather than to the side as in an anagen-stage follicle. This is the site of one of the main stem cell pools in hair follicles, as discussed in Chapter 1.

In order to confirm the basal layer K1 staining that appeared to be present in *K14.stratifin* back skin, a 7-month-old tagged ear hyperplasia was assessed. Here, there was very poor demarcation between the basal and suprabasal layers as a large proportion of basal cells were found to spuriously express K1, while numerous cells in the lower suprabasal layers lacked K1 staining (appearing red in the image in *Figure 4-16D* where only K14 staining is present). This clearly indicated the presence of a disordered differentiation pattern resulting from *K14.stratifin* expression coupled with wound-promotion.

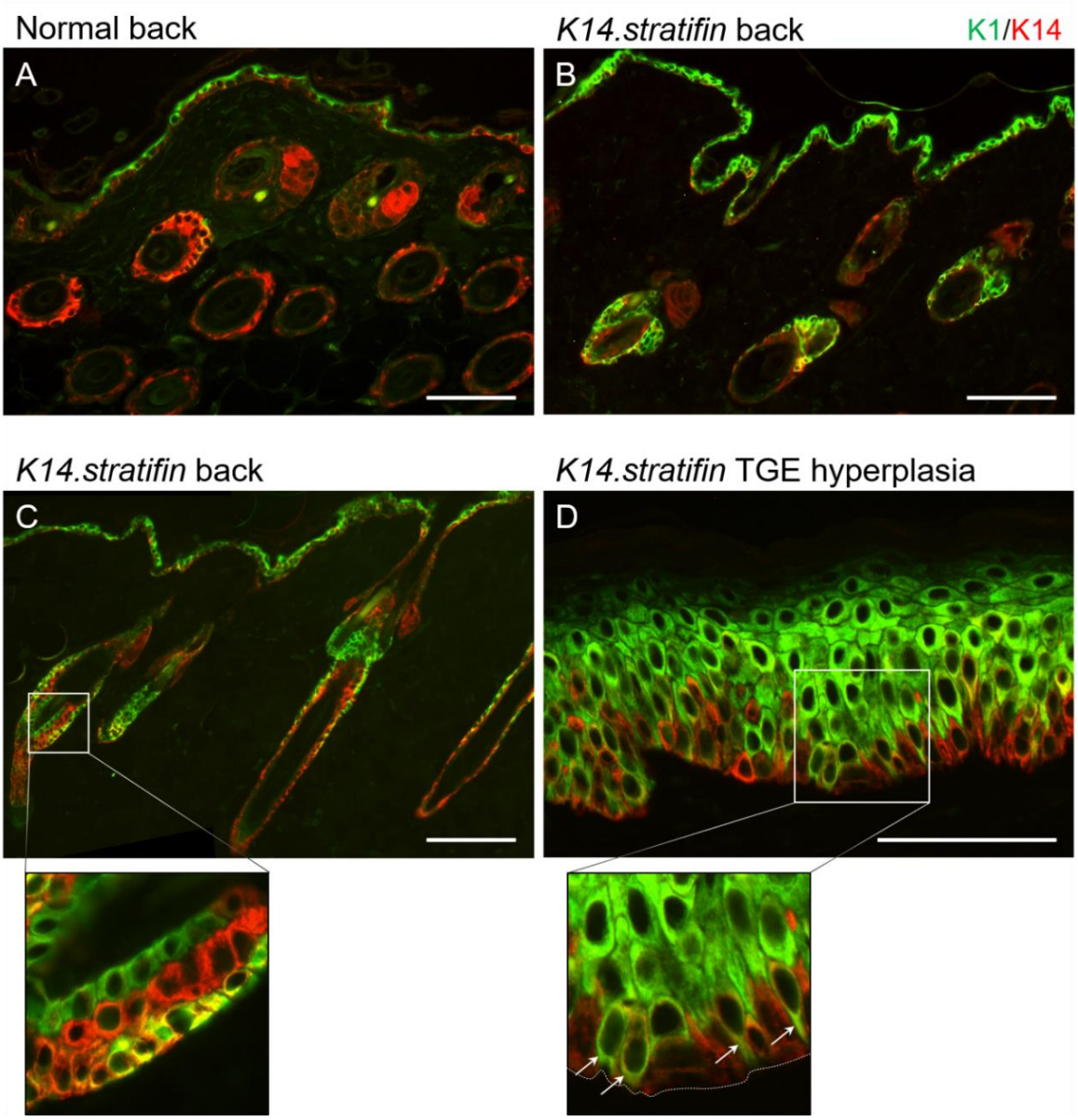

Figure 4-16: Exogenous Stratifin expression results in spurious Keratin 1 expression in hair follicles and basal layer keratinocytes.
(**A**) Keratin 1 (green) staining in normal 6-month-old ICR back skin with Keratin 14 (red) counterstaining to identify undifferentiated intrafollicular keratinocytes and hair follicles; no K1 positivity is observed in the follicles pictured. (**B**) Age-matched *K14.stratifin* back, with very clear K1 positivity in the follicles and strong epidermal staining. (**C**) 7-month *K14.stratifin* back in which follicles can be observed in longitudinal cross section, in which K1 staining is visible in multiple follicle cell layers. (**D**) 7-month *K14.stratifin* TGE hyperplasia in which K1 is spuriously expressed in a high proportion of basal layer cells, indicated by arrows in the highlighted box (white dotted line indicates basement membrane). *Scale bars approx. 100 µm.*

Since keratins function as polymerised dimers in a basic-acidic pair, the partner of Keratin 1, Keratin 10, was assessed to evaluate whether it was also expressed outside of the suprabasal epidermis. This was done using a guinea-pig anti-K10 antibody to allow co-localisation analysis with the rabbit anti-K1 antibody, therefore K10 appears as red in the following figures, while K1 is still green.

As shown in *Figure 4-17*, co-localisation was found to be imperfect in *HK1.fos* hyperplasia, though most suprabasal cells expressed both K1 and K10, with K10 staining appearing slightly stronger (*Figure 4-16A*). In contrast, in *K14.stratifin* skin, K1 appeared to be more widely expressed than K10, with only K1 present in basal layer cells and follicles, while K10 was limited to suprabasal cells (*Figure 4-17B*). In the benign *HK1.ras/fos-Δ5Pten* papilloma there was little sign of divergence in localisation, though in the later wdSCC K10 appeared to persist slightly longer than K1 in the lower suprabasal layers (*Figure 4-17C,D*).

While, overall, those controls which lacked the *K14.stratifin* transgene did not show excessive loss of co-localisation, all stages of *HK1.fos/K14.stratifin* carcinogenesis showed extensive divergence of K1 and K10 expression patterns.

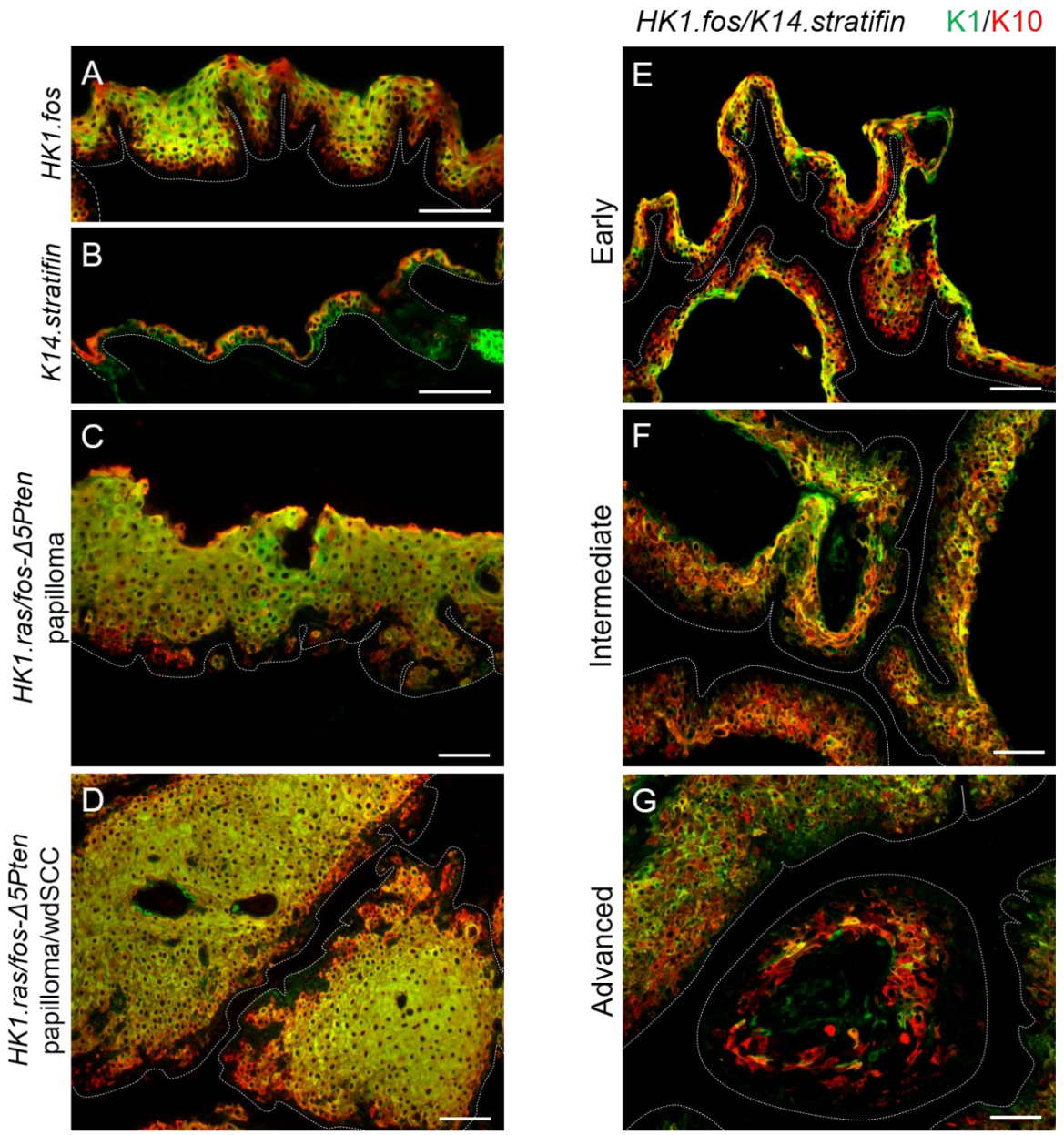

Figure 4-17: Keratin partners K1 and K10 diverge in localisation in *K14.stratifin* skin and in *HK1.fos/K14.stratifin* tumours.
(**A**) *HK1.fos* hyperplasia demonstrates colocalization of both K1/K10; similar to normal (not shown). (**B**) *K14.stratifin* back skin exhibits a divergence in expression as K1 is expressed in the basal layer and in follicles, while K10 expression is confined to differentiating supra-basal cells, as expected. (**C**) Tri-genic *HK1.ras/fos-Δ5Pten* papillomas exhibit only slight divergence which becomes increased in (**D**) wdSCCs as K1 expression begins to diminish with tumour progression. (**E**) *HK1.fos/K14.stratifin* hyperplasia now exhibits an early divergence as K1 expression diminishes and K10 remains strong - unlike *HK1.fos* controls. (**F**) Intermediate *HK1.fos/K14.stratifin* SCC and (**G**) advanced SCC all exhibit marked divergence as K10 expression persists whilst K1 expression is lost in the context of a highly confused differentiation programme. White dashed lines indicate basement membrane position. *Scale bars approx. 100 µm.*

As it can be difficult to manually assess subtleties in colour distribution, especially when there are differences in the intensity of the signal due to differing degrees of expression, the Colocalisation Threshold plugin for ImageJ was utilised (*Figure 4-18; 4-19*). This allowed for objective assessment of red-green distribution, with and without taking intensity into account.

Multiple images were assessed using the plugin for each skin or tumour sample. The plugin output a colocalised image, wherein pixels with a value above the threshold for both the red and green channels appeared in greyscale, while any pixels with an above-threshold value in only one of those channels appeared as green or red. Additionally, a scatterplot was generated for each showing each pixel value plotted on a set of axes (Y = green; X= red). The plot is colour coded from blue through red to white to indicate increasing numbers of pixels of those red-green values. Representative examples of each control genotype are shown in *Figure 4-18*.

As shown in *Figure 4-18A-C*, the *K14.stratifin* skin showed very poor correlation as evidenced by the coloured patches in the co-localised image as compared to the far better co-localisation seen in both *HK1.fos* and benign *HK1.ras/fos-Δ5Pten* papilloma (*Figure 4-18D-F* and *G-I*). The co-localised images controls show that very few cells were not positive for both K1 and K10 to some degree, despite areas in the full colour image of the *HK1.fos* hyperplasia appearing to be negative for K1 staining. Colocalisation appears slightly poorer in the later trigenic papilloma/wdSCC (*Figure 4-18J-L*); however, as with the earlier example of this genotype, the scatterplot suggests strong correlation in expression pattern.

Subsequently, *Figure 4-19* depicts co-localisation of K1 and K10 in advancing stages of *HK1.fos/K14.stratifin* carcinogenesis. It is clear from the green and red patches in the co-localisation images that the expression pattern of these proteins diverged greatly from the that of the controls which lack *K14.stratifin* expression. This is supported by the much more diffuse nature of the scatterplots at all stages, indicating that this divergence was an early event, unlike K1 (and K10) loss which is correlated with malignant changes.

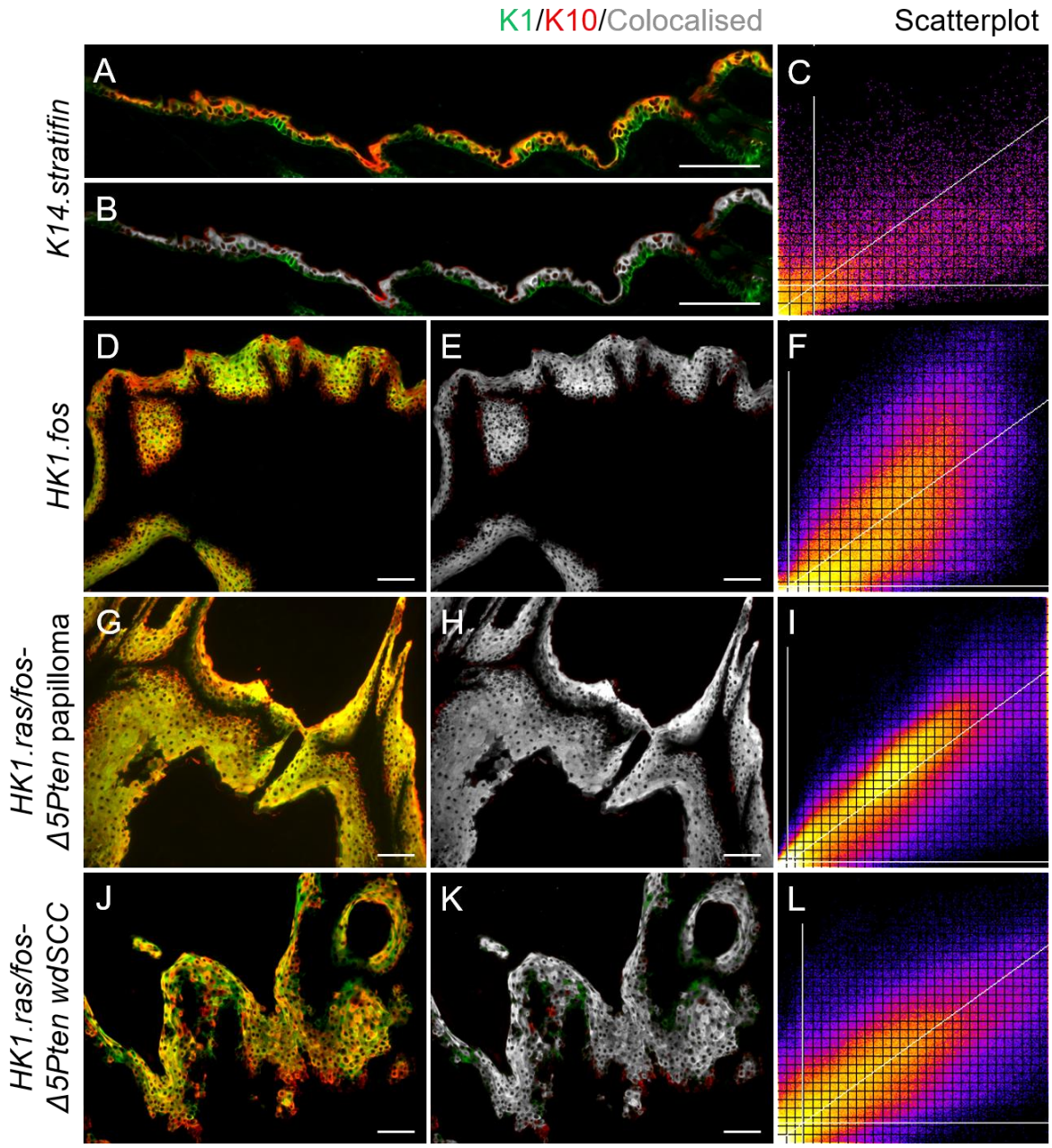

Figure 4-18: Keratin 1 and 10 expression localisation is closely correlated in *HK1.fos* and *HK1.ras/fos-Δ5Pten* samples but diverges in *K14.stratifin* skin.
(**A**-**C**) 5-month *K14.stratifin* back skin, K1 (green) is present in basal cells where K10 is not, indicated by the green cells in (**B**) and the diffuse scatterplot in (**C**). (**D**-**F**) 7-month *HK1.fos* ear hyperplasia shows better correlation between K1 and K10 staining, with the Colocalised image in (**E**) largely greyscale and less diffuse scatterplot in **F**. (**G**-**I**) *HK1.ras/fos-Δ5Pten* papilloma which has not converted to wdSCC shows very good correlation between K1 and K10 staining, with few red areas and no green seen in (**H**). (**J**-**L**) Later *HK1.ras/fos-Δ5Pten* papilloma/wdSCC shows slight disparity in correlation but the colocalised image (**K**) is still mainly greyscale and the scatterplot (**L**) shows good correlation. *Sale bars approx. 100 µm.*

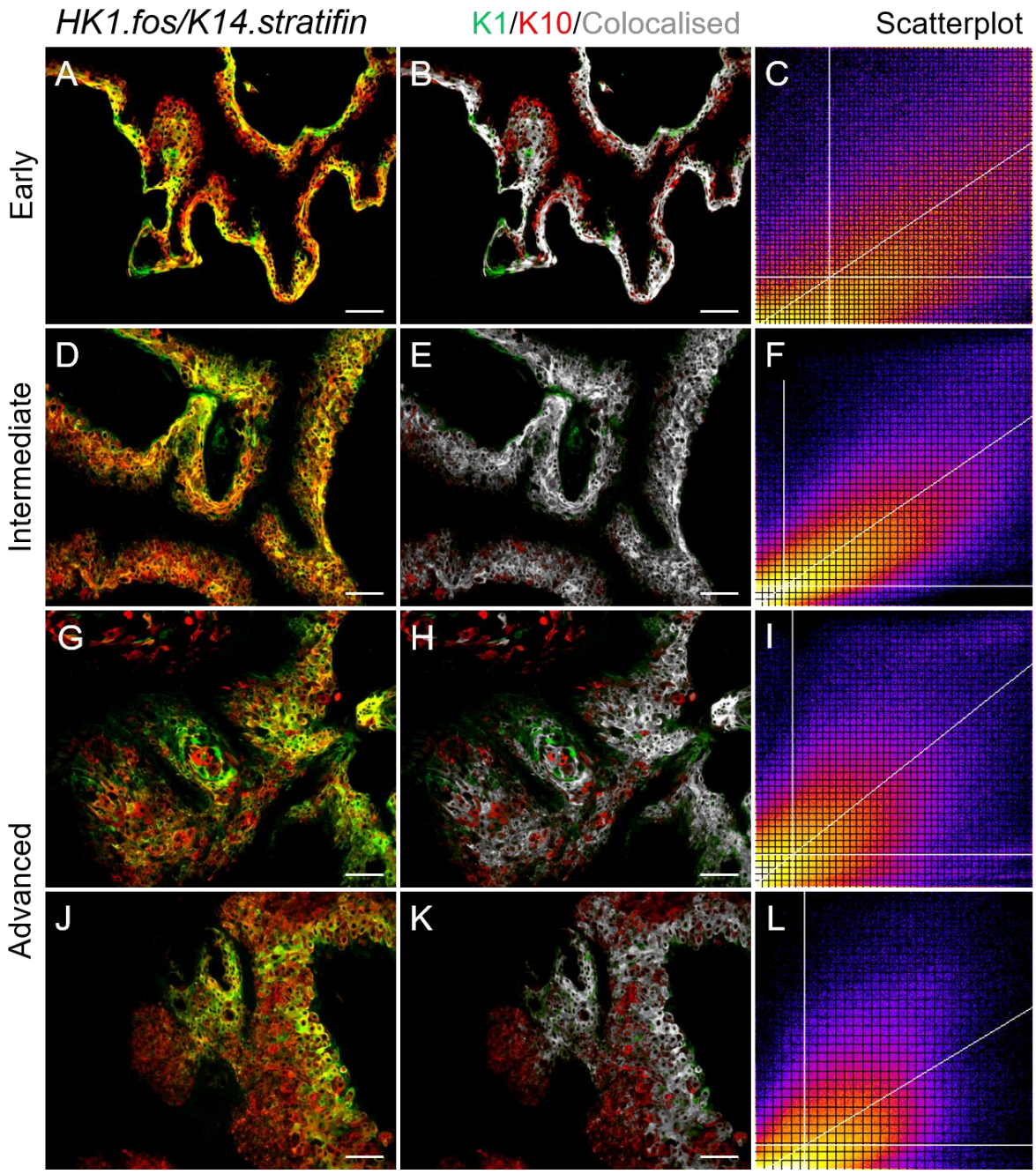

Figure 4-19: Stage-specific expression analysis confirms poor Keratin 1 and Keratin 10 correlation throughout *HK1.fos/K14.stratifin* tumour development.
Full colour images of (**A**) Early, (**D**) Intermediate and (**G** and **J**) Advanced *HK1.fos/K14.stratifin* tumours are shown for reference. (**B**, **E**, **H** and **K**) Co-expression of K1 and K10 in *HK1.fos/K14.stratifin* tumours is poor, as indicated by the red and green areas seen in the colocalised images, where the colocalised areas (grey) make up a much smaller fraction of the total area compared to tri-genic controls in *Figure 4-18*. (**C**, **F**, **I** and **L**) Poor co-localisation is also shown by the scatterplots, in which many blue data points far from the line of best fit indicate many pixels with only green or red values, i.e., no colocalisation. The more strongly correlated values also appear quite spread out and mainly in the lower left region (low intensity values) and do not lie closely along the line of best fit, especially in the advanced tumours (**I** and **L**). *Scale bars approx. 100 µm.*

In earlier analyses, the K14 expression pattern was seen to be unusual in *HK1.fos/K14.stratifin* tumours when compared to controls, with a patchy staining appearance at low magnification and rings which did not appear to come close together observed at higher magnification. β-catenin staining was also useful to investigate this further, as shown in *Figure 4-20*.

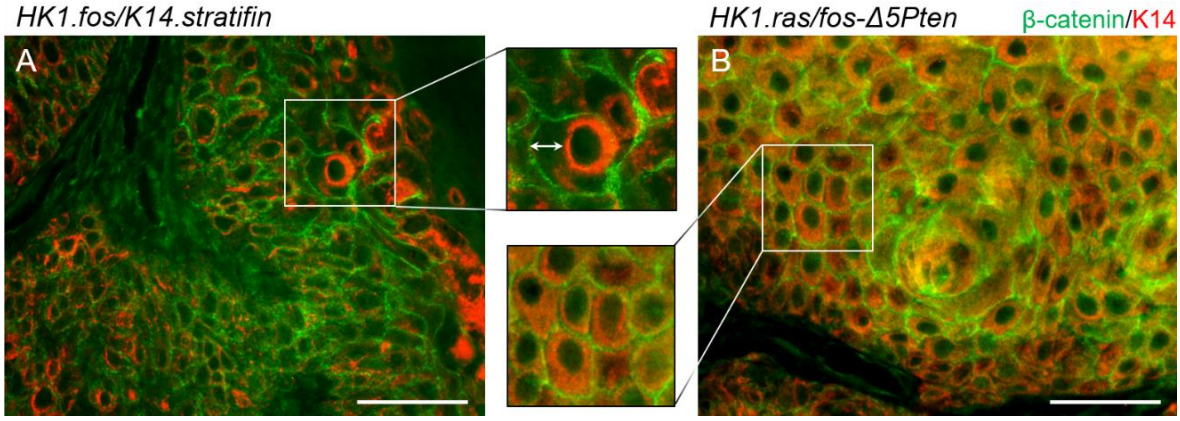

Figure 4-20: Keratin 14 exhibits perinuclear localisation indicating membrane detachment in advanced *HK1.fos/K14.stratifin* SCC.
β-catenin (green) was used to indicate positions of cell membranes (specifically, adherens junctions). In A, an advanced *HK1.fos/K14.stratifin* SCC, Keratin 14 (red) has clearly collapsed or aggregated in the perinuclear region and does not span the space between the nuclear membrane and the cell membrane, indicated by the double-headed arrow in the highlighted box. **B** shows an *HK1.ras/fos-Δ5Pten* wdSCC in which there are no examples of K14 exhibiting perinuclear localisation; the highlighted box clearly shows the red K14 staining filling the whole cytoplasmic area. *Scale bars approx. 100 μm.*

This highlighted a unique phenotype, wherein K14 had become localised into the perinuclear region, which has not been seen in any other transgenic phenotype, including *K14.stratifin*. β-catenin membrane positivity strongly suggested that cell-cell adhesion was present in these areas, however, K14 was clearly no longer attached to the cell membrane. Staining of Keratins 1, 10 and 17 (as well as K6 and K16, not shown) do not show this perinuclear localisation, indicating that this is specific to Keratin 14, and perhaps its partner K5, though this is yet to be assessed.

4.9. Discussion

This chapter characterised the phenotypes generated by concomitant overexpression of Fos and Stratifin in mouse skin. Resultant *HK1.fos/K14.stratifin* mice produced tumours with highly unusual aetiology which is believed to recapitulate an under recognised form of cutaneous squamous cell carcinoma arising from the hair follicle (HF), termed follicular squamous cell carcinoma (fSCC). This appears to be the first evidence of direct co-operation between Fos activation and Stratifin overexpression in the causal aetiology of squamous cell carcinomas in general and, in particular, in fSCC. These data clearly show that Stratifin can have significant oncogenic potential when overexpressed in certain contexts, separate to the apparent tumour suppressive functions observed earlier in *HK1.ras.fos/Δ5Pten* carcinogenesis.

4.9.1. The *HK1.fos/K14.stratifin* model

This model combines expression of the activated *v-Fos* oncogene (*c-Fos* homologue; Curran et al., 1982) with overexpression of human Stratifin (Cianfarani et al., 2011), targeted to the epidermis. This was achieved using the HK1 promoter to drive Fos expression; HK1 is a modified form of the human Keratin 1 where the keratin coding region is replaced by oncogenic FBR/J v-Fos to create the *HK1.fos* transgene (Chapter 1 *Figure 1-6*) which is expressed in all suprabasal cells and a subset of proliferative interfollicular cells (Rosenthal et al., 1991; Rothnagel et al., 1993). Importantly, while mK1 and other differentiation-related genes are reduced during carcinogenesis, HK1 expression continues throughout malignancy.

The K14 promoter which drives human Stratifin expression in the epidermis is targeted to undifferentiated cells in the basal layer of the interfollicular epidermis and to hair follicles (Vassar et al., 1989), especially the layers of the outer root sheath (which also contains the bulge region; an important stem cell niche), in accordance with the mK14 expression pattern (Coulombe et al., 1989). While *HK1.fos* expression elicits epidermal hyperplasia and hyperkeratosis after approximately 7 months, *K14.stratifin* expression does

not produce a particularly keratotic phenotype (*Figure 4-2*), though both epidermal and dermal hyperplasia are seen, the latter may be influenced by Stratifin secreted into the stroma from keratinocytes, where it acts on fibroblasts to encourage remodelling (Ghahary et al., 2005; Ghaffari et al., 2006; Ghaffari et al., 2010), though the generation of hyperplasia through this interaction does not appear to have previously been described in the literature and may involve novel processes.

Based solely on these promoters, the majority of cells expressing both *HK1.fos* and *K14.stratifin* should be those 30% of cells in the basal layer of the interfollicular epidermis wherein *HK1.fos* is expressed, which may include interfollicular stem or transit amplifying cells. However, analysis of mK1 expression in *K14.stratifin*-expressing skin showed that K1 was aberrantly expressed in hair follicle cells (*Figure 4-16*), notably including cells of the bulge region. Given that HK1 is sensitive to the same activating cues as mK1 (Rosenthal et al, 1991; Rothnagel et al., 1993), it is reasonable to assume that in the presence of the *K14.stratfin* transgene, *HK1.fos* is also active in these follicular cells—which is not the case in other models involving *HK1.fos*, including *HK1.ras/fos-Δ5Pten* carcinogenesis.

4.9.2. *HK1.fos/K14.stratifin* mice elicit a novel malignant histotype

Unlike *HK1.fos* and *K14.stratifin* parental phenotypes (*Figure 4-2*), bigenic *HK1.fos/K14.stratifin* mice developed hyperplasia and hyperkeratosis early, which did not always require wound-promotion, as most mice developed either hyperplasia and hyperkeratosis or a tumour on the non-tagged ear (*Figure 4-3*). Tumorigenesis occurred at the tag site in all tagged mice, with those biopsied early (prior to tagging) exhibiting wound-independent hyperplasia and hyperkeratosis of the ear skin at 3 weeks (*Figure 4-3A,B*). Variation in the extent of the phenotype was observed (likely influenced by outbred nature of these ICR mice); however, all individuals shared common gross and histological features independent of the difference in overall severity. *HK1.fos/K14.stratifin* mice developed hyperplasia and hyperkeratosis to a stronger degree and much more rapidly than *HK1.fos* monogenic controls (*Figure 4-3 vs 4-2*). When wound-

promotion was applied (ear tag), 100% of mice developed a tumour at the tag site, which were invariably highly keratotic on the surface; in cross-section, these all exhibited a very pale interior with a distinct large central blood vessel.

Histological analysis suggested that this pale colour reflected the highly keratotic nature of these tumours. This also identified a unique histotype characterised by an abundance of intraepidermal keratin deposition, early disruption to and loss of the granular layer in many places, acanthosis in the suprabasal region juxtaposed with areas of highly proliferative cells with many mitotic figures visible, and an obvious disruption to the hair follicle (HF) morphology in the early stages (*Figure 4-3C,D*). Further histological and immunofluorescence analysis identified a definite link between the observed changes in HF morphology and the development of these highly unusual tumours, for example the presence of hair shafts within tumour lobes (*Figure 4-12*) and rings of Keratin 17 positive cells (a marker for outer root sheath keratinocytes) (*Figure 4-13*) placed these structures at the forefront of the tumour aetiology.

Given that histological analysis identified blatant disruption to the epidermal architecture, cell-cell adhesion was assessed using immunofluorescence analysis of ß-catenin expression (*Figure 4-15*). ß-catenin is a multifunctional protein: it is an integral part of adherens junctions, in which it binds E-cadherin and α-catenin and is thus present at the plasma membrane (Hartsock & Nelson, 2007). Aside from this, it plays an important role in the canonical Wnt signalling pathway as a transcription factor (TF) during embryogenesis and stem cell regulation/fate determination, including in hair follicle development (Willert & Nusse, 1998; Lien et al., 2014). ß-catenin therefore has implications in carcinogenesis both in changes to cell-cell adhesion that may facilitate cell migration/invasion, and as a TF promoting cell growth and proliferation, and possibly aberrant differentiation.

In *HK1.fos/K14.stratifin* tumours, immunofluorescence analysis showed that while ß-catenin was still present at the membranes (*Figure 4-15D-F*), it was weaker than in either *HK1.fos* or earlier *HK1.fos/K14.stratifin* hyperplasias (*Figure 4-15A,C*), suggesting some loss of cell-cell adhesion may contribute to the highly unusual structure of the *HK1.fos/K14.stratifin* epidermis and fSCCs.

Subsequently, DAPI was used as a counterstain to assess the nuclear localisation of ß-catenin in areas where the quantity was clearly increased in the cytoplasm (*Figure 4-15E,F*). This showed that there were clearly positive nuclei present, confirmed using the ColorInspector 3D plugin for ImageJ (*Figure 4-15G*); positive staining was mostly confined to the basal cells, whilst there was only sporadic suprabasal positivity, where cells retained a higher degree of membranous staining, albeit in cells with unusual morphology. This echoes other studies into the roles of ß-catenin activation in carcinomas (Brabletz et al., 1998; Miyazawaet al., 2000) in which the majority of ß-catenin positivity was found at the invasive front, despite homogeneity in the mutational status of the tumours (e.g., germline APC mutation), leading the authors to suggest a role of the tumour microenvironment in its localised upregulation. Activation of ß-catenin has also been observed in *HK1.fos/ras-Δ5Pten* SCCs, with work ongoing to elucidate its roles in this model and in *HK1.ras/ROCK* carcinogenesis (Masre et al., 2020).

In this study, there are multiple ways in which *K14.stratifin* expression could contribute to this ß-catenin activation. Stratifin is now well-known to be released from keratinocytes into the dermis to facilitate remodelling of the stroma, leading to changes in expression and activity of fibroblasts which could in turn, influence basal keratinocyte gene expression (Maas-Szabowski et al., 1999; Lai et al., 2011). Alternatively (or in addition), Stratifin has been shown to sequester GSK3ß (which binds cytoplasmic ß-catenin, preventing its activation) during embryonic development, thereby facilitating increased Wnt/ß-catenin signalling (Chang et al., 2012); the high degree of Stratifin overexpression in basal cells via targeted expression of the *K14.stratifin* transgene (coupled with *HK1.fos* activation) may create a context for this activity to re-emerge in the adult tissue, contributing to tumorigenesis and possibly increasing the invasive potential. Finally, the apparent follicular origin of *HK1.fos/K14.stratifin* tumours may mean that the Wnt signalling pathway is intrinsically more active in these cells, given its importance in follicle growth and homeostasis (Lien et al., 2014), again contributing to the unique aetiology.

4.9.3. *HK1.fos/K14.stratifin* carcinogenesis: a potential model for follicular squamous cell carcinoma (fSCC)

The combination of abrupt terminal differentiation throughout the epidermis causing a uniquely mottled appearance in H&E, loss of the granular cell stage of the differentiation process, and excessive keratosis lead to a review of the literature to identify any proliferative skin diseases exhibiting similar characteristics.

The majority of interfollicular histopathologies and malignancies observed did not share much similarity with the *HK1.fos/K14.stratifin* histotype, however, given the notable aberration of HF morphogenesis, the search was extended to include proliferative diseases of hair follicles and associated malignancies. Again, most of these (e.g., trichofolliculoma) did not fit the features observed in this study, but a non-malignant condition known as a trichilemmal (pilar) cyst did share some morphological features, such as the lack of granular layer and highly irregular border between cells and abundant keratosis (Ramaswamy et al., 2013). Moreover, a more aggressive form, proliferating trichilemmal cyst, which only occasionally converts to malignant state, showed particular similarity.

This, therefore, led to the specific search to determine whether a form of squamous cell carcinoma which develops from HF keratinocytes is possible; thus, identifying several case studies and characterisations of follicular (or trichilemmal/tricholemmal) squamous cell carcinoma, which is believed to be an often-misdiagnosed skin malignancy, frequently mistaken for BCC (Misago et al., 2012; Shendrik et al., 2013; Carr et al., 2014). As shown in *Figure 4-14*, this *HK1.fos/K14.stratifin* mouse model appears to recapitulate many of the features identified in human fSCC (Shendrik et al., 2013; reproduced with permission). Upon staining sections of the fSCC with an anti-keratin 17 antibody, Misago et al. also found well circumscribed rings of positive staining akin to those observed in this study via immunofluorescence (*Figure 4-13*).

However, none of these studies investigated the expression of Stratifin in the tumours presented, despite its well-known roles in HF morphogenesis and maintenance, and numerous examples of its upregulation in carcinomas,

including some cutaneous SCCs (Lodygin et al., 2003; Herron et al., 2005; Hammond et al. 2012; Neupane & Korc, 2008). This mouse model could, therefore, represent an opportunity to shed light on the underlying mechanisms of this poorly recognised neoplasia and may represent a possible druggable target for therapeutic intervention as an alternative or adjunct to surgical excision.

4.9.4. Immune infiltrate in severity of phenotype

The macroscopic phenotypes generated in *HK1.fos/K14.stratifin* mice were divided into Mild, Moderate, and Strong with regards primarily to the rate of phenotype development (early hyperplasia and hyperkeratosis, and later tumour development) and whether or not the non-tagged ear (NTE) was phenotypic. In Mild individuals, no phenotype was visible until after tagging (wound-promotion) which elicited a small tumour over a period of several weeks; Moderate mice developed a tumour on the TGE which could be of any size but was clearly a tumour with adjacent grossly normal ear skin, while the non-tagged ear exhibited some degree of hyperplasia and hyperkeratosis, or a small tumour (relative to the TGE tumour). Strongly phenotypic individuals exhibited hyperplasia on both ears prior to wound-promotion, which developed into tumours involving the whole ear, with little to no normal adjacent skin visible (*Figure 4-5C*).

Histological analysis of the three levels of phenotype severity indicated that the abundance of immune infiltrate was correlated with the degree of tumour development. In mild individuals, the non-phenotypic NTEs had no obvious increase in the number of visible immune cells (on H&E) compared to normal skin, while moderate and strong phenotypes both had much increased immune cell infiltrate. As shown in *Figure 4-5*, with the TGE of Moderately phenotypic mice noticeably more inflamed than the NTE, whilst both the TGE and NTE of Strongly phenotypic siblings possessed similarly high numbers of infiltrating immune cells. It was difficult to quantify the number of immune cells reliably, as many *HK1.fos/K14.stratifin* tumours, particularly in the advanced stages, had lost a large portion of their stroma during processing, with only the

tissue closest to the epidermis left intact in many cases. A more focussed study into the inflammation in non-wounded skin (i.e., NTE) may be possible, as the majority of tumours in this group did not exceed the intermediate phenotype in which stroma was generally intact.

Through studies investigating its implication in scar-free wound-healing, Stratifin has been implicated as an anti-inflammatory 14-3-3 isoform (Rahmani-Neishaboor et al., 2012). However, some studies investigating its expression on epithelial carcinomas have indicated an upregulation in its expression is associated with areas of inflammation in the tumour (Nakajima et al., 2003; Robin et al., 2020). However, there appears to be a dearth in the literature regarding the specific correlation between Stratifin expression in carcinomas and the associated degree of inflammatory response in these metastatic contexts. Very preliminary data involving two intermediate *HK1.fos*/*K14.stratifin* tumours compared to relevant controls showed a possible increase in the number of infiltrating Mast cells (CD34+; not shown), which are pro-inflammatory and known to release chemoattractants to recruit eosinophils and T lymphocytes to the area (Krystel-Whittemore et al., 2016); based on histopathology, both eosinophils and lymphocytes make up a large proportion of the infiltrating immune cells (*Figure 4-5*). Unfortunately, a proper investigation into this aspect of *HK1.fos*/*K14.stratifin* tumorigenesis was outside of the time frame of this project, though presents an interesting avenue for future study.

4.9.5. Involvement of p53 expression in *HK1.fos/K14.stratifin* tumorigenesis

The key role played by Stratifin in regulation of the p53-Mdm2 interaction was described in Chapter 1 (*Figure 1-9*) and revisited in Chapter 3 given their relative expressions in *HK1.ras*/*fos-Δ5Pten* carcinogenesis, which appeared to support TSG roles. In light of the finding that p53 expression was lost on malignant conversion in the multistage model, it had been hypothesised that maintaining p53 expression in proliferating cells by means of Stratifin overexpression could prevent such conversion. These *HK1.fos*/*K14.stratifin* data clearly demonstrated an oncogenic mechanism and, given the highly unusual

nature of *HK1.fos*/*K14.stratifin* carcinogenesis compared with this multistage model, the hypothesis seemed unlikely to hold true in this context.

Surprisingly, the level of p53 was found to be moderate or high throughout the early and intermediate stages of *HK1.fos*/*K14.stratifin* carcinogenesis, with some fading of this positivity only in the advanced tumour stages (*Figure 4-9 Panel II*). These data did indeed appear to show that p53 expression was maintained in the presence of exogenously increased Stratifin activity; however, unlike the outcome hypothesised based on the role of p53 as a master cell cycle regulator, maintenance of its expression was totally insufficient to prevent tumorigenesis and malignancy in this *HK1.fos*/*K14.stratifin* fSCC phenotype. Indeed, tumours of this genotype were found to arise and convert to carcinoma very quickly, as confirmed by Keratin 1 loss (*Figure 4-6*), in spite of strong p53 expression in the early stages (*Figure 4-9*), thus it was concluded that p53 function had somehow been uncoupled from its normal roles. Alternate possibilities such as the presence of a gain-of-function (GOF) p53 mutant was deemed to be a very unlikely cause of carcinogenesis in this study, given the lack of strong staining or tumorigenesis in monogenic parents and siblings of *HK1.fos*/*K14.stratifin* mice, as well as the eventual fading of p53 expression here, which is not seen in GOF models. Furthermore, these results were obtained in rounds of breeding over several years, with only *HK1.fos*/*K14.stratifin* bigenic mice exhibiting this staining pattern. Genetic sequencing will be conducted on frozen tissue samples to confirm this.

Since p53 expression appeared unhampered and its degradation was reduced in the presence of high Stratifin activity due to the *K14.stratifin* transgene, inhibition of downstream effectors of p53 is likely to explain its impotence in the context of *HK1.fos*/*K14.stratifin* carcinogenesis. Given the vast number of effectors targeted by p53 for transcriptional activation, this conclusion is somewhat vague. Preliminary data suggested that expression of the G1/S (and to a lesser extent, G2/M) inhibitor p21, an important downstream target of p53, is maintained in *HK1.fos*/*K14.stratifin* carcinogenesis, as previously detected in *HK1.ras*/*fos-Δ5Pten* SCCs (MacDonald et al., 2014).

However, this analysis was not performed on a large number of samples and has not yet been validated by further IF or IHC analysis.

4.9.6. *HK1.fos/K14.stratifin* phenotypes are associated with major disruption to keratin expression and localisation

The Keratin 1 and 10 intermediate filament proteins are the most abundant proteins in the suprabasal layers of the epidermis (Moll et al., 2008), whose transcription is activated by separation of divided cells from the basement membrane (BM) and upregulation of TAp63 isoforms (Trink et al., 2007) and subsequent increase in Notch1 signalling (Blanpain et al., 2006). This allows Keratin 1 analysis to be a useful marker for loss of differentiation during malignant conversion, as lower K1 expression is correlated with a resistance to normal differentiation cues (BM detachment and increased Ca^{2+} concentration (Banno and Blumenberg, 2014; Bilke et al., 2012)). When immunofluorescence analysis was performed to assess K1 expression in *K14.stratifin* skin (both thin back skin and wound-promoted TGE hyperplasia), it was found that K1 was aberrantly expressed in both basal cells and HF keratinocytes, while very few cells of normal basal epidermis are $K1^{+ve}$ and no HF cells should express this keratin (Roop et al., 1987).

Interestingly, despite being obligate heterodimers, there are known differences in their transcriptional regulation, functions and degradation. For example, initial induction of Keratin 10 mRNA expression lags behind that of K1 during embryogenesis, with K1 mRNA consistently more abundant throughout development, including in adulthood (Ouellet et al., 1990), and K10 induction during differentiation has been shown to require the transcription factor AP-2 (Maytin et al., 1999), while the K1 gene has multiple AP-1 binding sites instead (Rothnagel et al. 1993). Additionally, Keratin 10 knockout results in a normal epidermis (Reichelt et al., 2001), albeit one which experiences much faster cell turnover, while Keratin 1 knockout has been found to be perinatally lethal (Roth et al., 2012), indicative of their diverging functions. Furthermore, Keratin 1-null mice exhibited an increase in interleukin 18 (of the IL-1 group) and upregulation of anti-microbial peptides which indicates a link to immune regulation not

observed in K10. On the other hand, Keratin 10 has been shown to prevent Akt and PKCζ activity, thereby acting in a tumour suppressor capacity (Paramio et al., 2001). With regards to their removal, K10—but not K1—is targeted for degradation by Mdm2 in Varicella zoster virus-infected skin and in the autosomal recessive congenital ichthyosis family of genetic diseases, leading to uncoupling of their expression (specifically, increased K1 and downregulated K10) (Tommasi et al., 2020; O'Shaughnessy et al., 2010; Youssef et al., 2014).

In this study, Keratin 1 loss was used as a marker of loss of differentiation and transition to a malignant SCC. However, it was noticed that from an early stage in *HK1.fos*/*K14.stratifin* carcinogenesis, expression and localisation of K1 and K10 was uncoupled, to a far greater degree than observed in *HK1.ras*/*fos-Δ5Pten* multistage carcinogenesis (*Figures 4-16, -17, 18*). The reasons for this are unclear, since the loss in Keratin 1 also appeared to be accompanied by an increase in Keratin 14 expression in suprabasal cells (*Figure 4-6*), indicative of the more proliferative, less well-differentiated phenotype. In this model, Mdm2 activity is repressed by high *K14.stratifin* expression (as evidenced by much higher-than-normal p53 expression throughout carcinogenesis), thus, Mdm2-mediated degradation is not likely to be implicated in the discrepancy between K1 and K10 staining seen in *HK1.fos*/*K14.stratifin* carcinogenesis. However, the fact that this mechanism exists to reduce K10 independent of K1 in other disease states suggests that they can be selectively targeted for removal, thus, it is plausible that K1 is actively degraded in this tumour context by another molecule. Given that K10 has independent roles of K1 in tumour suppression (via inhibition of Akt and PKCζ activities (Paramio et al., 2001)) while K1 appears to have influence in immunoregulation (Roth et al., 2012), the discrepancy in their expression may be reflective of these independent roles and slight differences in their transactivation.

Finally, through its use as a counterstain, it was found that Keratin 14 uniquely exhibited perinuclear localisation in intermediate and advanced stage *HK1.fos*/*K14.stratifin* tumours. This peculiar phenomenon was confirmed using ß-catenin as membrane marker (*Figure 4-20*) which showed that, while cells were clearly distorted, total loss of cell-cell adhesion did not explain this perinuclear localisation. Keratin IFs attach to desmosomal plaques at the plasma

membrane; thus, it was initially hypothesised that desmosomal dysregulation or loss may be implicated. However, since no other Keratins analysed (K1, K10, K17, and K6/K16 (not shown)) displayed the same untethering from the membrane, this theory doesn't appear to fit the data. The only instances in the literature of this staining pattern appear to be in cases where a keratin mutation has occurred, preventing correct IF formation in cases of Epidermolysis Bullosa Simplex (Keratin 5; Livingston et al., 2001) and Epidermolytic Hyperkeratosis (Keratin 10; Huber et al., 1994). In this study there is no reason to believe that a Keratin mutation has occurred, however, post-translational modifications like phosphorylation have are known to be required for correct filament assembly, thus, disruption of this process could have the same profound effect. These results, therefore, appear to suggest some form of direct targeting of K14, preventing normal filament organisation and association with the desmosomes. Alternatively, this finding could indicate a novel protein-protein interaction involving K14 independent of K5, as is the case with K16-iRHOM2 (Maruthappu et al., 2017), thus indicating a very interesting focus for further research which could have more wide-ranging implications in other epithelial disease aetiologies.

4.9.7. Future directions

It will be important to validate the *HK1.fos*/*K14.stratifin* genotype as a model of human follicular squamous cell carcinoma (fSCC). This will require acquisition of fSCC samples, which is likely to prove difficult due to the under-recognised nature of this SCC subtype (Misago et al., 2012; Shendrik et al., 2013; Carr et al., 2014), thus, initially this will involve reaching out to the authors of studies cited here, before inevitably requiring a much larger cohort of samples.

The first such validation experiments will examine the expression of both c-Fos and Stratifin; however, since both of these proteins have been shown to be elevated in classic cSCCs (Lodygin et al., 2003), further analysis is required to confirm the fSCC phenotype. This will involve similar analyses to those already performed on mouse samples, including initial histopathological assessment to look for the unique features found in all *HK1.fos*/*K14.stratifin* tumours assessed

(e.g., trichilemmal differentiation), which are absent in the *HK1.ras/fos-Δ5Pten* multistage model of more classic SCCs. Mouse ear skin undergoes an initial anagen growth phase between 2 and 15 days post partum, then enters an extended quiescent (telogen) phase, unlike that of the body where the hair follicles grow in roughly monthly cycles, coordinated into waves around the body (Wang et al., 2017). Ear skin again differs, in that even when HFs re-enter anagen, they do not do so in a coordinated manner, but do so sporadically and individually. Since these *HK1.fos/K14.stratifin* tumours are believed to be of follicular origin, and tumours of the follicles are more likely to arise during active growth (Miller et al., 1993), this long quiescence may further account for the differences in phenotype severity; if the tumour does not arise early, prior to tagging, then it may not be generated until the next time a HF enters its growth cycle. This could be tested by inducing anagen at a specific site by plucking the hairs; known to stimulate the follicle to enter anagen (Wang et al., 2017).

Further analyses will look for the cause of divergence in post-mitotic keratin (K1/K10) expression, which is evident early in these tumours, though also appears in aggressive *HK1.ras/K14.stratifin* Type 2 tumours (see Chapter 5); divergent K1/K10 expression may become a reliable marker for aggressive Stratifin-driven oncogenesis. More investigation is required into the reasons for K14 filament accumulation in the perinuclear region (Figure 4-20), which remains specific to this *HK1.fos/K14.stratifin* fSCC phenotype.

While this model appears to be the result of two genetic “hits”, in reality, the nature of Fos as part of the major transcription factor complex, AP-1, means that the exact underlying gene expression changes which contribute to *HK1.fos/K14.stratifin* carcinogenesis are unclear. Thus, to identify such changes in expression which underpin the disease pathology, transcriptomic or proteomic approaches may be required, given the scope of influence of AP-1, coupled with the vast array of interaction partners of Stratifin. This could potentially identify new interactions and allow identification of novel proteins or pathway interactions to develop targeted treatment strategies. Furthermore, given previous research has identified Stratifin as a vital component in normal HF development and implicated it in having roles in the bulge region stem cell

niche, this approach may elucidate Stratifin-mediated interactions governing SC physiology and how the overexpression of Stratifin, here, in conjunction with activated Fos induces carcinogenesis.

Additionally, the role of the immune system is patently apparent in these *HK1.fos*/*K14.stratifin* tumours, as it has been observed that the stronger phenotypes are correlated with greater immune cell infiltrate. However, understanding which components are involved and how requires much more study, likely in collaboration with scientists in the field of onco-immunology to properly elucidate the mechanisms of immune cell recruitment and their interactions with keratinocytes in tumour promotion.

Finally, since p53 ablation had no observable effect on *HK1.fos*/*K14.stratifin* tumorigenesis (despite high abundance of the protein in the wild-type tumours), work is ongoing to assess the impact of p21 knockout (Appendix 2; *Figure S2*). This is one of the main downstream effectors of cell cycle arrest mediated by p53 but can also be induced by p53-independent mechanisms (such as by TGF-β), as seen in *HK1.ras*/*fos-Δ5Pten* carcinogenesis in which both p21 and Stratifin persisted beyond p53 loss (Appendix 1; McMenemy et al., in preparation). Preliminary results suggest the development of these tumours is similar to wild type but with a more aggressive histological appearance, with all mice assessed so far resembling the strongly phenotypic p21WT fSCC tumours. Given the natural variability in the severity of phenotype in *HK1.fos*/*K14.stratifin* tumours, however, a larger cohort of mice will be needed to confirm this finding.

4.9.8. Conclusions

HK1.fos/*K14.stratifin* mice generate tumours of varying size and speed of development but with remarkably similar histopathology despite their outbred background. These tumours appear to recapitulate the histological features of human fSCCs, an underrecognized subset of cutaneous SCC. The relatively stable nature of the phenotype on an outbred genetic background implies that this model could be useful in studying the underlying mechanisms of disease

pathogenesis and potentially inform new treatment modalities specific to this tumour type.

Chapter 5 *K14.stratifin* and *HK1.ras* co-operation in mouse skin carcinogenesis

5.1. Introduction

As detailed in Chapter 4, co-operation of *HK1.fos* and *K14.stratifin* transgene constructs caused development of malignant tumours of follicular origin in bi-genic mice. This chapter deals with the phenotypes resulting from concomitant expression of *HK1.ras* and *K14.stratifin* transgenes.

HK1.ras mice develop benign papillomas on the tagged ear due to the tumour-promotion effects of wounding, which regress over time if the tag is removed. Rarely, papillomas have been found to develop on other areas of the body which do not require wounding to initiate papillomatogenesis. Such papillomas are believed to remain benign but exhibit a more aggressive histological phenotype than those at ear tag.

As previously discussed, *K14.stratifin* mice appear grossly normal throughout development, with only tagged ears generally exhibiting visible hyperplasia after 5 months of age, though mild hyperplasia is seen on histological examination at an earlier stage.

While *HK1.fos*/*K14.stratifin* mice developed tagged ear tumours in 100% of cases, the follicular origin of this type of carcinogenesis was unusual. This was thought to be related to the synergistic effects of these proteins in the hair follicle (HF), since both already have roles in HF development. While *H-Ras* has been shown to be carcinogenic when expressed in the HF via a K5 promoter (Brown et al., 1998) it is not otherwise believed to play a part in fate determination of HF stem cells or differentiation, unlike Fos proteins (Fisher et al., 1991).

Here, the aims were to characterise the phenotypes generated by co-expression of the *HK1.ras* and *K14.stratifin* transgenes using histological and immunostaining analyses of several proteins of interest to inform the stage in malignant progression and identify possible effectors of the pathology. Further, this protein analysis was used to attempt to identify the reasons underpinning the two distinct disease aetiologies seen in *HK1.ras*/*K14.stratifin* mice.

5.2. Initial results that suggested a protective effect of *K14.stratifin* on the *HK1.ras* phenotype

HK1.ras mice were crossed with *K14.stratifin* mice and, whilst little effect could be observed in neonatal skin (pups remained wrinkly and became normal as juveniles, as in *HK1.ras*), preliminary data based on the first bigenic litter generated suggested that the *K14.stratifin* transgene elicited a tumour-suppressive effect on *HK1.ras* papillomatogenesis (*Figure 5-1*). When biopsied, *HK1.ras* monogenic controls had developed the expected papilloma at tag, approximately 8 mm in diameter. In contrast, whilst two bigenic *HK1.ras*/*K14.stratifin* mice exhibited papillomas of a similar size to their *HK1.ras* siblings, three had much smaller papillomas which were more V- or C-shaped than standard *HK1.ras* papillomas, as depicted in *Figure 5-1*.

Figure 5-1: Initial results showed smaller papilloma size in *HK1.ras/K14.stratifin* bi-genic mice compared with *HK1.ras* age-matched controls.
Three (middle) *HK1.ras/K14.stratifin* mice show smaller papillomas relative to *HK1.ras* siblings (right) at ~10 weeks post-tag, with the two remaining more similar to the *HK1.ras* controls.

Initial examination suggested that these tumours were largely benign, though some differences were immediately apparent compared with *HK1.ras* papillomas. For example, the centre of the biopsied tumours had a grossly glassy or jelly-like appearance compared to control papillomas which appear largely matte due to the presence of keratin pearls throughout the structure. Histological examination suggested that the gross cross-sectional appearance resulted from a high stroma content in the *HK1.ras*/*K14.stratifin* tumours, with few keratin pearls evident and some histological features challenging their apparently benign aetiology (*Figure 5-3*). Subsequently, this initial trend for smaller tumours became evidently only part of the story, with the emergence of many more aggressive (Type 2; see below) tumours in a large number of mice.

5.3. *HK1.ras/K14.stratifin* tumours fall into two distinct phenotypes based on growth rate, appearance at biopsy and histopathology

While preliminary data suggested a putative logical, protective role for Stratifin in suppressing *HK1.ras* papillomatogenesis, increased numbers of mice generated (*n*=40) indicated that this was incorrect.

As mentioned above, *HK1.ras* mice typically develop wound-dependent papillomas at ear tag in all cases, generally between 8- and 10-weeks post-tag; should the tag fall out, these papillomas regress (or do not commence if this wound-promotion fails prior to their formation) (Greenhalgh et al., 1993a). However, in very few cases and dependent upon the background substrain of ICR, *H-ras* activation may produce wound-independent papillomas at other body sites, with a completely different aetiology and appearance. In this model, under UK Home Office guidelines, these rapidly-growing tumours quickly approach acceptable limits and are therefore biopsied. As they remain benign at biopsy, they are termed type 2 papillomas, lacking signs of carcinoma but exhibiting some dysplasia and are not regression-prone like their Type 1 TGE counterparts.

In *HK1.ras*/*K14.stratifin* bi-genic mice, these wound-independent tumours occurred frequently on the body, most commonly at the base of the tail where the hyperplasia and hyperkeratosis present at birth never regressed before tumour formation; a result which suggests early co-operation between activated H-ras and Stratifin overexpression. These tumours grew rapidly from inception to a size and appearance which necessitated biopsy within 2 weeks, whereas the sporadic Type 2 papillomas on *HK1.ras* littermates could legitimately remain for up to 8 weeks. Additionally, a subset of tumours on the TGE mimicked this rapid growth and large, aggressive appearance, while others grew much more slowly and were macroscopically more akin to *HK1.ras* papillomas. This was the first indication that two distinct types, designated Type 1 and Type 2 in this chapter, also existed in the *HK1.ras*/*K14.stratifin* genotype and despite a dissimilar aetiology, both exhibited evidence of SCC development.

As shown in *Figure 5-2*, in the absence of a wound-promotion stimulus, NTE tumours did not develop in any mice in this cohort. Type 1 TGE tumours frequently developed the "dumbbell" shape (*Figure 5-1B*) and grew slowly, ranging from 12-17 weeks at biopsy. Type 2 TGE tumours were much larger at an earlier stage in development than their Type 1 counterparts, with obvious hyperkeratosis and inflammation apparent. In cases where the tag was lost (*n*=4) these tumours did not regress, indicating a wound-independent phenotype. Type 2 tumours on the body frequently appeared at the tail base (*n*=7), with others on the dorsum, flank, shoulders or lower abdomen (*n*=5). This type differed in outward appearance, with some like that shown in *Figure 5-1E,F* exhibiting a relatively benign, lobular structure, while others had a much smoother, dome-like shape. No mice were homozygous for the *HK1.ras* gene, (since homozygosity creates an unacceptable degree of hyperplasia and hyperkeratosis in neonatal mice which compromises viability of juveniles (Greenhalgh et al., 1993), and no link between *K14.stratifin* homozygosity and tumour type was apparent.

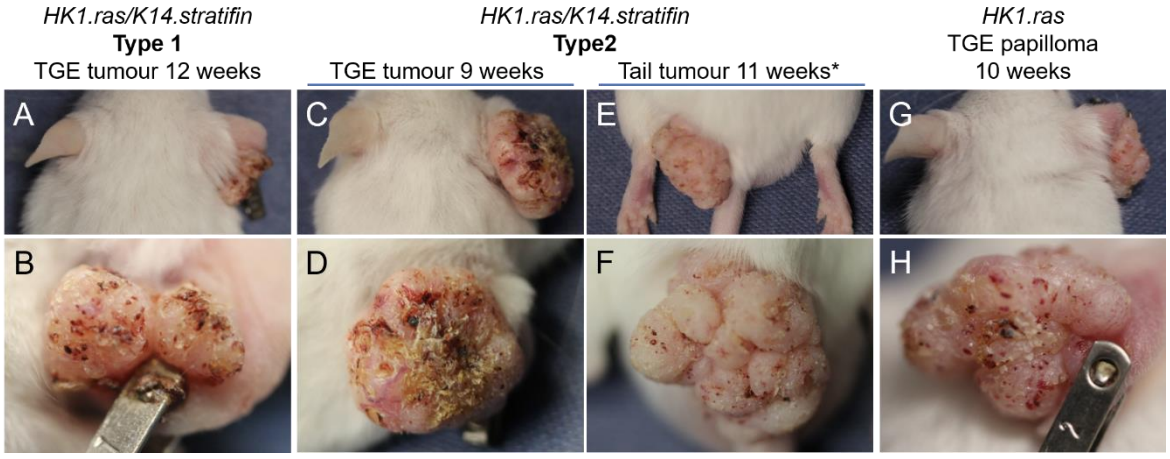

Figure 5-2: Type 1 and Type 2 *HK1.ras/K14.stratifin* tumours are grossly distinguishable.
(**A**) Type 1 *HK1.ras/K14.stratifin* phenotype showing grossly normal non-tagged ear (NTE) and small tumour on tagged ear (TGE) at 12 wks./8 wks. post-tag. (**B**) Close-up of TGE tumour showing dumbbell shape and mild surface keratosis common to Type 1 tumours. (**C**) Type 2 *HK1.ras/K14.stratifin* phenotype showing grossly normal NTE and large, flattened tumour on TGE at 9 wks./5 wks. post-tag. (**D**) Close-up of TGE tumour showing very keratotic centre. (**E**) Type 2 *HK1.ras/K14.stratifin* phenotype showing rounded tumour at tail base at 11 wks. (**F**) Close-up shows seemingly lobular structure and little keratosis. (**G**) *HK1.ras* with grossly normal NTE and TGE papilloma at 10 weeks. (**H**) Close-up showing slightly keratotic surface and multi-lobed structure.

Histological analysis (H&E) assessed the morphological features in each tumour type, compared with each other and *HK1.ras* controls, as shown in *Figure 5-3*. Despite their outward similarity to *HK1.ras* papillomas, Type 1 *HK1.ras*/*K14.stratifin* tumours exhibited a very different cross-sectional appearance (*Figure 5-3A vs G*). In these tumours, the structure generally comprised a large area of stroma, surrounded by a relatively thin layer of hyperplastic and papillomatous tumour epidermis, very different to the ratio seen in *HK1.ras* papillomas, which do not contain as much stroma relative to the outer epidermis and keratin pearls. On closer examination (*Figure 5-3B*), it was also apparent that the normal stratification of the epidermis was highly disrupted in these *HK1.fos*/*K14.stratifin* tumours, with an increase in proliferative cells and keratosis present in the spinous layers, somewhat akin to that seen in the *HK1.fos*/*K14.stratifin* phenotype but with clear overall differences. Here, the granular layer was also found to be reduced or missing entirely, with hyperkeratosis observed in all examples. The *HK1.ras*/*K14.stratifin* histotype appeared to be a mix of dysplastic but generally benign papilloma and clear indications of malignant conversion, with frequent mitotic figures present, particularly in invasive regions, where the delineation between epidermis and dermis at the basement membrane (BM) was lost. These Type 1 *HK1.ras*/*K14.stratifin* tumours thus represent a mixed phenotype of benign papilloma, albeit with unusual dysplasia and high stromal content, and clear carcinoma *in situ* or early wdSCC given the increasing signs of invasion.

Analysis of Type 2 tumours from ear and body sites showed some variation in these *HK1.ras*/*K14.stratifin* features present and all were found to exhibit widespread malignancy and quite aggressive SCC (*Figure5-3C,F*). Such features included a high degree of hyperkeratosis both on the tumour surface and in misshapen keratin pearl structures which were not generally seen in Type 1 tumours. These also exhibited a large expansion of the proliferative basal compartment which, in some cases, involved a clear separation of the cells suggestive of oedema or possible loss of cell-cell adhesions. Uniquely, this tumour type produced “ghost cell” keratosis, a failure of proper cornification in which the nuclear envelope was not fully collapsed and the cornified cell overall retained its shape as in life (*Figure 5-3D*; circled).

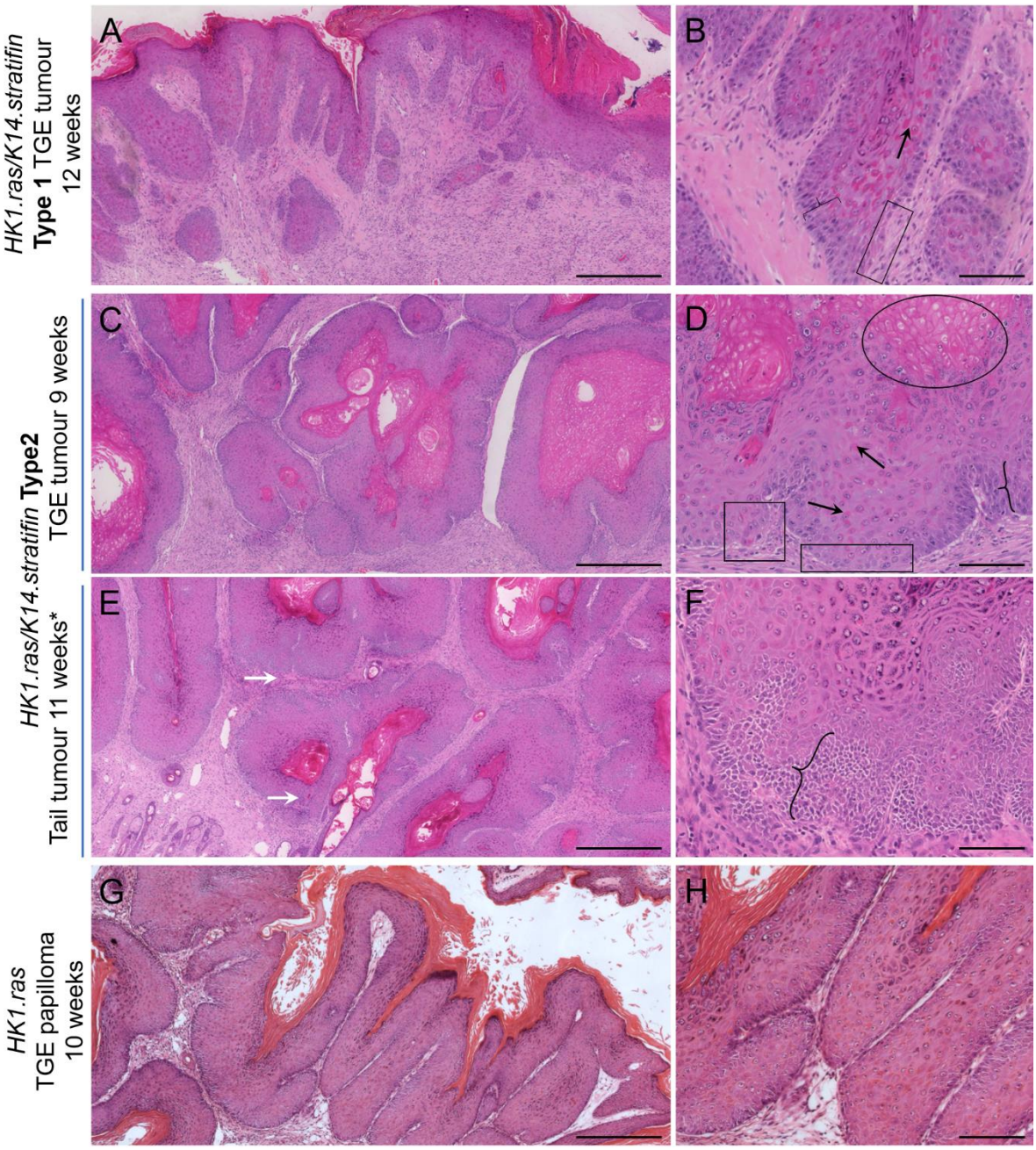

Figure 5-3: Histological analysis shows Type 1 HK1.ras/K14.stratifin tumours are less aggressive than Type 2 tumours, but both have features of malignant conversion. (**A**) Low magnification (40x) H&E histology of Type 1 *HK1.ras/K14.stratifin* tumour showing a hyperplastic epidermis surrounding inflamed stroma which constitutes a large proportion of the tumour mass. (**B**) High mag. (200x) showing intra-epidermal keratosis (arrow), increase in proliferative layers (bracket; **{**) and loss of basement membrane (BM) integrity in places (box). (**C**) Low mag. (40x) Type 2 *HK1.ras/K14.stratifin* TGE tumour showing more hyperplastic epidermis than in (**A**) with large keratin pearls and a high immune infiltrate. (**D**) High mag. (200x) shows unusual "ghost cell" keratosis (oval), a lack of granular layer cells, less intra-epidermal keratosis than in Type 1 (arrows), expanded proliferative compartment (bracket; **{**) and loss of BM integrity with signs of invasion (boxes). (**E**) High mag. (200x) shows expanded proliferative compartment (bracket; **{**) and gaps visible between cells. Invading keratinocytes and immune infiltrate are seen in the lower left. (**G**) *HK1.ras* papilloma showing clearly stratified layers and ordered keratosis. This also shows a much lower stromal content than in *HK1.ras/K14.stratifin* tumours. (**H**) High mag (200x) shows the single proliferative layer and presence of granular cells clearly, with no invasion. *Scale bars: (**A, C, E, G**) approx. 500 µm; (**B, D, F, H**) approx. 100 µm.*

Additionally, the inflammatory response appeared to be much greater in all Type 2 tumours than Type 1. Indeed, their presence may have been integral to invasion in some Type 2 tumours, where the infiltrating immune cells participated in BM disruption, facilitating invasion (*Figure 5-3F*).

	Tumour development*	Histology	Immune cell infiltration	Wound dependent?
Type 1	Slow (≥ 8 weeks)	Papilloma, carcinoma *in situ* & wdSCC	Low/Moderate	Yes
Type 2	Fast (≤ 2 weeks)	wdSCC & carcinoma	High	No

Table 5-1: Characteristics of Type1 and Type 2 *HK1.ras/K14.stratifin* tumours based on macroscopic appearance/growth rate and histological observations.
Tumour development refers to time from first appearance of tumour to date of biopsy, not age of mouse. Frequency of tumours reflects how many mice had each tumour type, not number of tumours total (several mice had > 1 Type 2 tumour). Type 2 category includes all Type 2 TGE and body tumours biopsied. 5 mice were biopsied between 4 and 9 weeks old due to rapid growth of Type 2 tumours on the body, prior to expected development of a Type 1 TGE tumour; 100% of mice were expected to develop a TGE of either Type >9 weeks old. 9 mice had both a TGE tumour (of either Type) and at least 1 Type 2 body tumour.

To assess whether the difference in phenotype was linked to *K14.stratifin* transgene expression, immunofluorescence analysis was performed to assess Stratifin abundance in Type 1 and Type 2 *HK1.ras/K14.stratifin* tumours compared with *HK1.ras* control papillomas (*Figure 5-4*). This showed strong Stratifin expression in all layers of the tumour epidermis in both types of *HK1.ras/K14.stratifin* neoplasia (*Figure 5-4A,B*), in contrast with strong staining in only the suprabasal layers of *HK1.ras* papilloma, in which only weak basal layer staining was observed (*Figure 5-4C*). The comparable staining pattern and intensity in Type 1 and Type 2 *HK1.ras/K14.stratifin* tumours therefore did not appear to be linked to weak or patchy *K14.stratifin* expression.

All mice used in this study were outbred on an ICR background which could account for some difference in the observed phenotypes; however, several *HK1.ras/K14.stratifin* mice developed both a Type 1 TGE tumour and a Type 2 tumour at another site, indicating that this was not the only factor accounting for the difference.

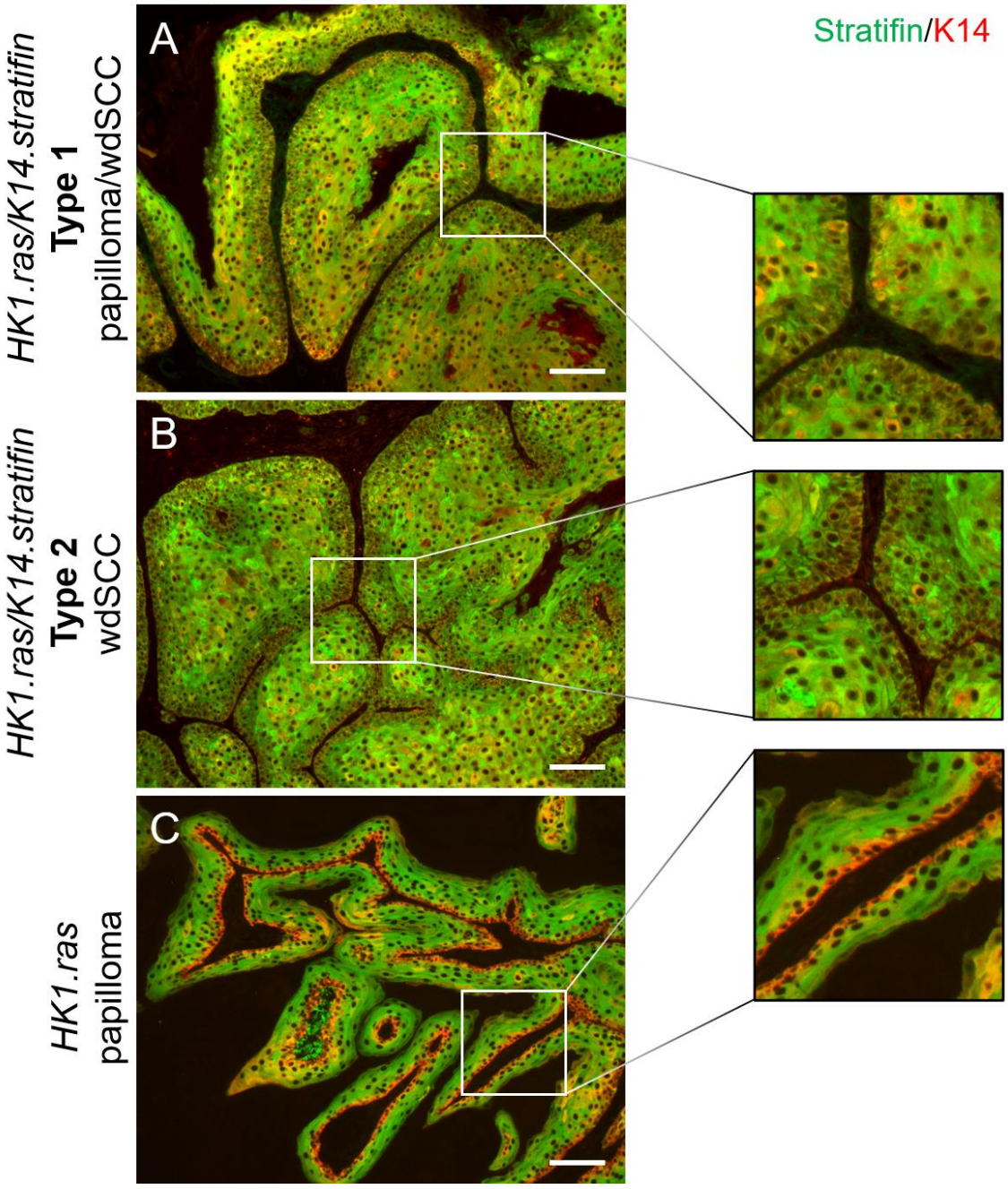

Figure 5-4: Elevated Stratifin expression is present in both Type 1 and Type 2 *HK1.ras/K14.stratifin* tumours.
(**A**) Type 1 *HK1.ras/stratifin* TGE tumour showing Stratifin (green) in all layers of the epidermis, highlighted in the boxed area to show strong basal layer staining from expression of the *K14.stratifin* transgene. (**B**) Type 2 *HK1.ras/K14.stratifin* tail tumour showing strong Stratifin staining in all layers, highlighted in the boxed area. (**C**) *HK1.ras* papilloma showing mainly strong suprabasal Stratifin staining with some basal layer staining, highlighted in the boxed area showing a lack of strong basal layer staining in the absence of the *K14.stratifin* transgene. *Scale bars approx. 100 µm.*

5.4. All *HK1.ras/K14.stratifin* tumours undergo malignant conversion with differential expression of markers indicative of Type 1 and 2 derivation

Histological analysis indicated signs of malignancy in Type 1 and aggressive SCC in Type 2 *HK1.rasK14.stratifin* tumours, including increased proliferation, loss of stratification and areas of invasion (*Figure 5-3A-F*). To further evaluate this progression to SCC, Keratin 1 staining was performed on typical Type 1 and Type 2 *HK1.ras/K14.stratifin* tumours and their profiles were compared with benign *HK1.ras* papillomas (*Figure 5-5*).

These results supported histological analysis, that at the time of biopsy, Type 1 tumours did not exhibit widespread malignant conversion, indicated by the largely K1-positive suprabasal layers (*Figure 5-5A*). However, large areas of these tumours did show a reduction in K1 staining intensity and areas of patchier K1 loss compared to *HK1.ras* papilloma controls (*Figure 5-5A vs C*). Additionally, areas such as that highlighted in the boxed area in *Figure 5-5A* exhibited greater K1-loss, suggesting development of localised carcinoma *in situ* which appeared to be becoming invasive.

In contrast, Type 2 *HK1.ras/K14.stratifin* tumours exhibited a more aggressive aetiology with widespread K1 loss (*Figure 5-5B*). All Type 2 tumours grew rapidly and, based on this K1 loss coupled with histological analysis, converted to malignancy within this short time frame. This was unusual given that this only required overexpression of two genes to elicit these aggressive SCCs. However, the contextual differences which cause development of Type 2 tumours instead of the slower-growing, wound-dependent Type 1 variety is unclear, though it may depend upon expression in hair follicle stem cells, given that *K14.stratifin* has been shown to direct mK1 activation in follicle cells (Chapter 4; *Figure 4-15*) and targeting of activated Ras to HFs has been found to elicit aggressive SCCs (Brown et al., 1998).

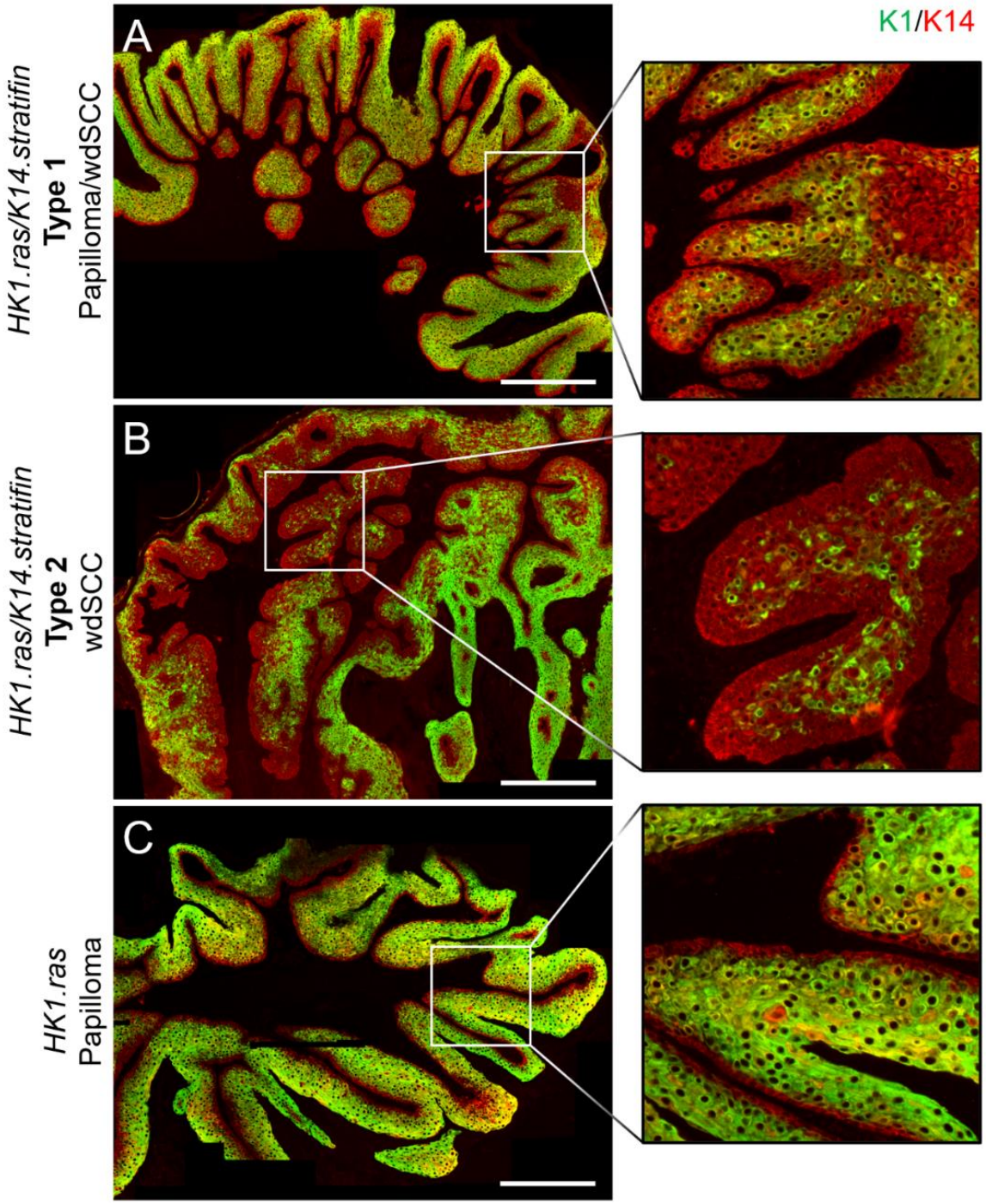

Figure 5-5: Keratin 1 loss indicates that both Type 1 and Type 2 *HK1.ras/K14.stratifin* tumours exhibit conversion to wdSCC.
(**A**) Type 1 *HK1.ras/K14.stratifin* TGE tumour showing reduced Keratin 1 staining (green) with increased depth of basal proliferative compartment, indicated by Keratin 14 (red) counter-staining. A patch of carcinoma *in situ* is shown at higher magnification in the boxed area. (**B**) Type 2 *HK1.ras/K14.stratifin* tumour showing widespread K1 loss, highlighted in the boxed area, indicating malignancy. (**C**) *HK1.ras* papilloma with strong suprabasal K1 staining and a single layer of proliferative K14 positive cells, indicative of a benign papilloma. *Scale bars approx. 500 µm.*

To explore this further and gain an idea of the extent of proliferation, the mitotic index was assessed of *HK1.ras*/*K14.stratifin* tumours, by labelling dividing cells with BrdU, as described in Chapter 4 (*Figure 5-6A-D*). Here, basal layer positivity was found to be similar in both Type 1 and Type 2 tumours, with mean counts of 27.7 and 35.1 cells/mm BM, respectively, compared with a mean of only 15.9 in the *HK1.ras* papillomas assessed. The difference in suprabasal positivity was more marked between the *HK1.ras*/*K14.stratifin* tumour Types, with means of 9.1 and 23.5, in Type 1 and Type 2 tumours, respectively. Both groups had much higher mean suprabasal values than in *HK1.ras* papillomas, which were found to have few suprabasal positive cells, with a mean of only 3.9 cells/mm BM. The range in values was also found to be larger in both *HK1.ras*/*K14.stratifin* tumour types than in *HK1.ras* papillomas, indicative of heterogeneity in the tumours assessed, whereas the number of dividing cells in *HK1.ras* was found to be much more consistent across the sections. This is seen in the boxplot (*Figure 5-6*) where the 95% CI of *HK1.ras*/*K14.stratifin* tumours is much greater than in controls, as denoted by the whiskers.

These data suggest that, whilst the amount of proliferation in each was comparable, BrdU-positivity was extensive throughout the Type 2 tumour, consistent with the disordered nature of differentiation and proliferation, compared to Type 1 in which division was largely confined to basal layer cells.

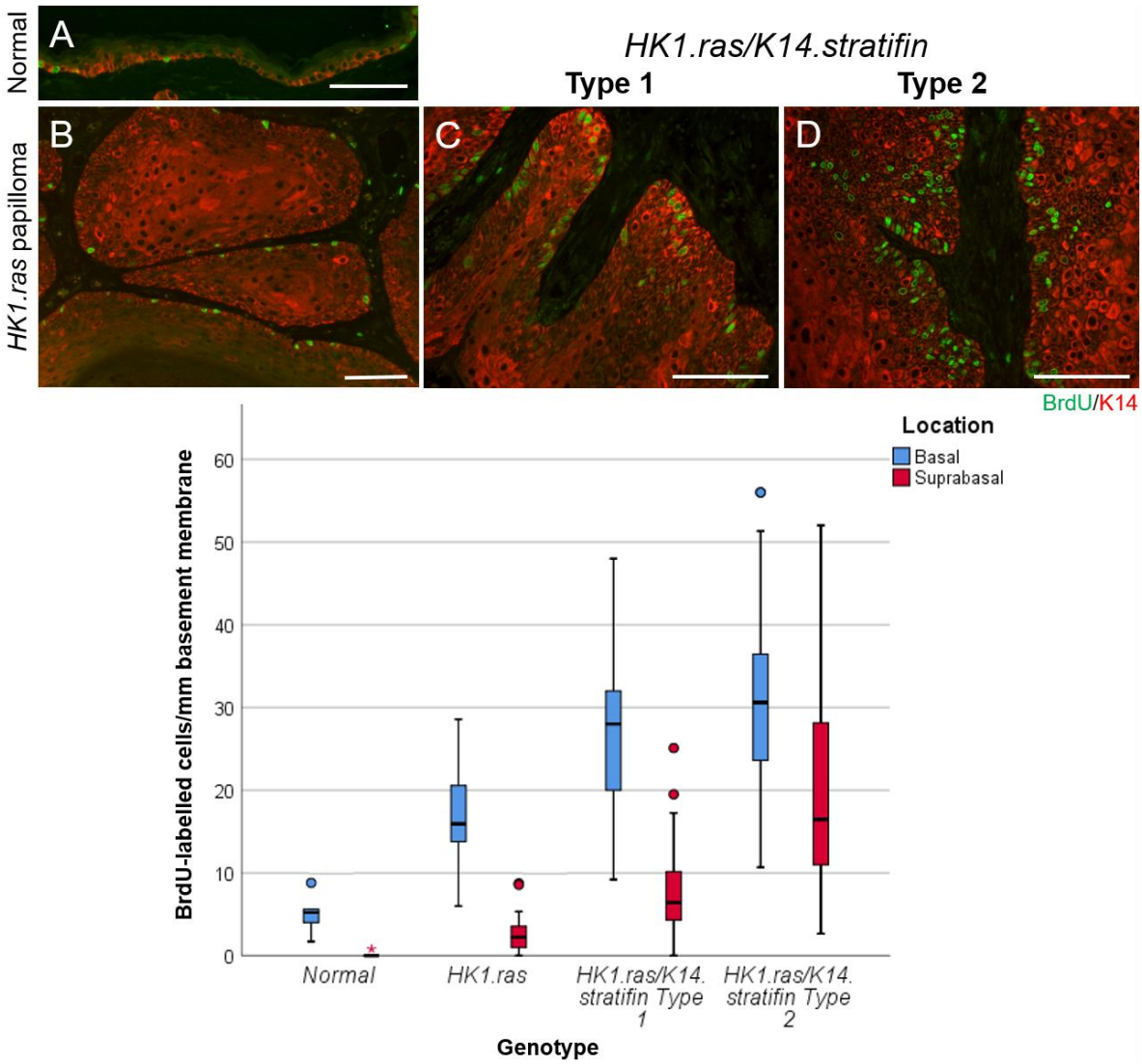

Figure 5-6: BrdU labelling indicates the mitotic index is high in both Types of *HK1.ras/K14.stratifin* tumours compared to HK1.ras papillomas.

(**A**) BrdU labelling showing low mitotic index in Normal ICR skin (*n*=2), with approx. 5 labelled cells per mm basement membrane (BM) in the basal layer and no supra-basal positivity, as shown in the box plot. (**B**) BrdU labelling in *HK1.ras* (*n*=2) is approx. 15/mm BM with very little supra-basal labelling (**C**) Mitotic index in **Type 1** *HK1.ras/K14.stratifin* tumours (*n*=4) is approximately 30 cells/mm BM in the basal layer with supra-basal labelling approximately 7 cells/mm BM. Variation in labelling is much greater than in *HK1.ras*, as shown by whiskers in the boxplot depicting 95% CI. (**D**) Labelling in **Type 2** *HK1.ras/K14.stratifin* tumours (*n*=3) is >30 in the basal layer and approx. 15 in the supra-basal layers. Variation in positivity is especially apparent in the suprabasal counts due to low positivity in benign regions and a high number of positive cells in SCC regions. *Scale bars approx. 100 µm.*

5.5. *HK1.ras/K14.stratifin* invasive potential may be linked to changes in cell-cell adhesion and cancer-associated fibroblast activity

Skin neoplasms undergo stages of development, from normal skin through hyperplasia, and from there may develop into a benign tumour such as a papilloma before progression to carcinoma. The well-charactered *HK1.ras* expression model results in the formation of papillomas when subject to wound or chemical promotion. Histopathological and immunofluorescence analyses show that these papillomas exhibit clear epidermal stratification with little dysplasia and overall, relatively normal features of differentiation. Conversely, *HK1.ras/K14.stratifin* tumours exhibited dysplasia from an early stage, with several unusual histological features such as intra-epidermal keratosis and ghost cell cornification, along with the more common signs of carcinoma *in situ* such as increased proliferation and loss of stratification, as shown in *Figure 5-3*.

In addition to *in situ* features, both Type 1 and Type 2 *HK1.ras/K14.stratifin* tumours exhibited signs of invasion, even in areas which were not entirely undifferentiated, as indicated by the presence of K1 in some suprabasal cells (*Figure 5-7D-F*). Here, both collective cell invasion in the form of finger-like projections into the tumour stroma together with broader "pushing" invasive fronts and several hot spots of individual cell invasion (in more advanced Type 2 SCCs) wherein cells appear to scatter into the stroma following basement membrane (BM) degradation (*Figure 5-7A, B and C*).

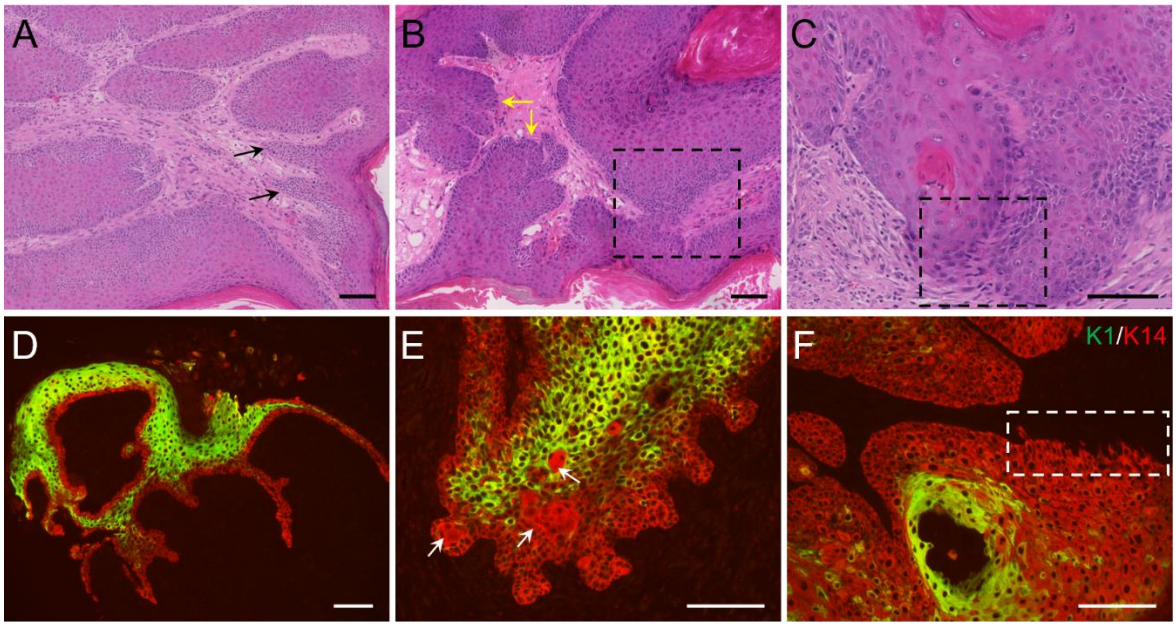

Figure 5-7: *HK1.ras/K14.stratifin* tumours exhibit multiple forms of invasion.
(**A**) Type 1 *HK1.ras/K14.stratifin* tumour exhibiting collective invasion in the form of finger-like protrusions into the stroma (black arrows) (**B**) Type 1 *HK1.ras/K14.stratifin* tumour showing broad "pushing" invasive fronts (yellow arrows) as well as more diffuse invasion (black dashed box) (**C**) Type 2 *HK1.ras/K14.stratifin* ear tumour exhibiting diffuse, individual cell invasion where BM integrity has been lost. (**D**) Type 1 *HK1.ras/K14.stratifin* tumour: $K1^{-ve}/K14^{+ve}$ (red) cells are seen invading into the surrounding stroma via multiple finger-like projections from an otherwise seemingly benign ($K1^{+ve}$; green) region. (**E**) Type 1 *HK1.ras/K14.stratifin* tumour: $K1^{-ve}$ cells show invasion via pushing tumour borders from an area where K1 is seen to be fading more so than in **A**. Sebocytes are visibly trapped among the tumour keratinocytes (white arrows) indicating aberration of hair follicle structures. (**F**) Type 2 *HK1.ras/K14.stratifin* tail tumour: patches of basal keratinocytes (white box) are invading individually where BM integrity has failed. *Scale bars approx. 100 µm.*

5.5.1. Differences in E-cadherin expression facilitate multimodal invasion in *HK1.ras/K14.stratifin* SCCs

These findings prompted analysis of two components with major roles in the regulation of tumour cell invasion. Firstly, a keratinocyte component, E-cadherin, which has a vital role in cell-cell adhesion and mediation of collective invasion, whose loss permits individual cell invasion and more aggressive SCC. Secondly, the potential role of keratinocyte-releasable Stratifin in recruitment of cancer-associated fibroblasts that express Tenascin-C, thereby facilitating keratinocyte invasion through stromal dynamism, as recently observed in ROCK2/H-Ras-mediated carcinogenesis (Masre et al, 2017; 2020). Tumour cell invasion is a highly complex process involving extracellular matrix (ECM) remodelling in conjunction with acquisition of cellular abilities involving actinomyosin mechanotransduction and alterations in cell-cell adhesion, similar to what is observed during wound-healing.

During collective invasion, observed here in the more well-differentiated Type 1 *HK1.ras/K14.stratifin* SCCs and in less advanced areas of Type 2 tumours (*Figure 5-8A,B,D*), E-cadherin—a major component of adherens junctions which connect the actin cytoskeleton of adjacent cells—is known to maintain expression in the leading cells (Krakhmal et al., 2015); this allows the formation of finger-like projections (*Figure 5-7A* and *Figure 5-8D*) and broader invasive fronts (*Figure 5-7B*). Epithelial-mesenchymal transition is a set of processes resulting in loss of epithelial characteristics in invasive cells; loss of E-cadherin positivity at the cell membranes is therefore one of the earliest changes seen in EMT. During EMT, the loss of cell-cell adhesion allows individual cell invasion to occur, as observed in *Figure 5-8C*, where E-cadherin is cytoplasmic rather than membranous, and notably, Keratin 14 (red) expression is greatly reduced.

Nuclear positivity for E-cadherin has been observed in some advanced human carcinomas and has been found to inhibit ß-catenin TF activity. However, this inhibition is ablated if E-cadherin is acetylated at its ß-catenin binding site (Zhao et al., 2019). Without testing for acetylation, it was not possible to determine the actions of nuclear E-cadherin apparently observed in some *HK1.ras/K14.stratifin* samples (*Figure 5-8C*).

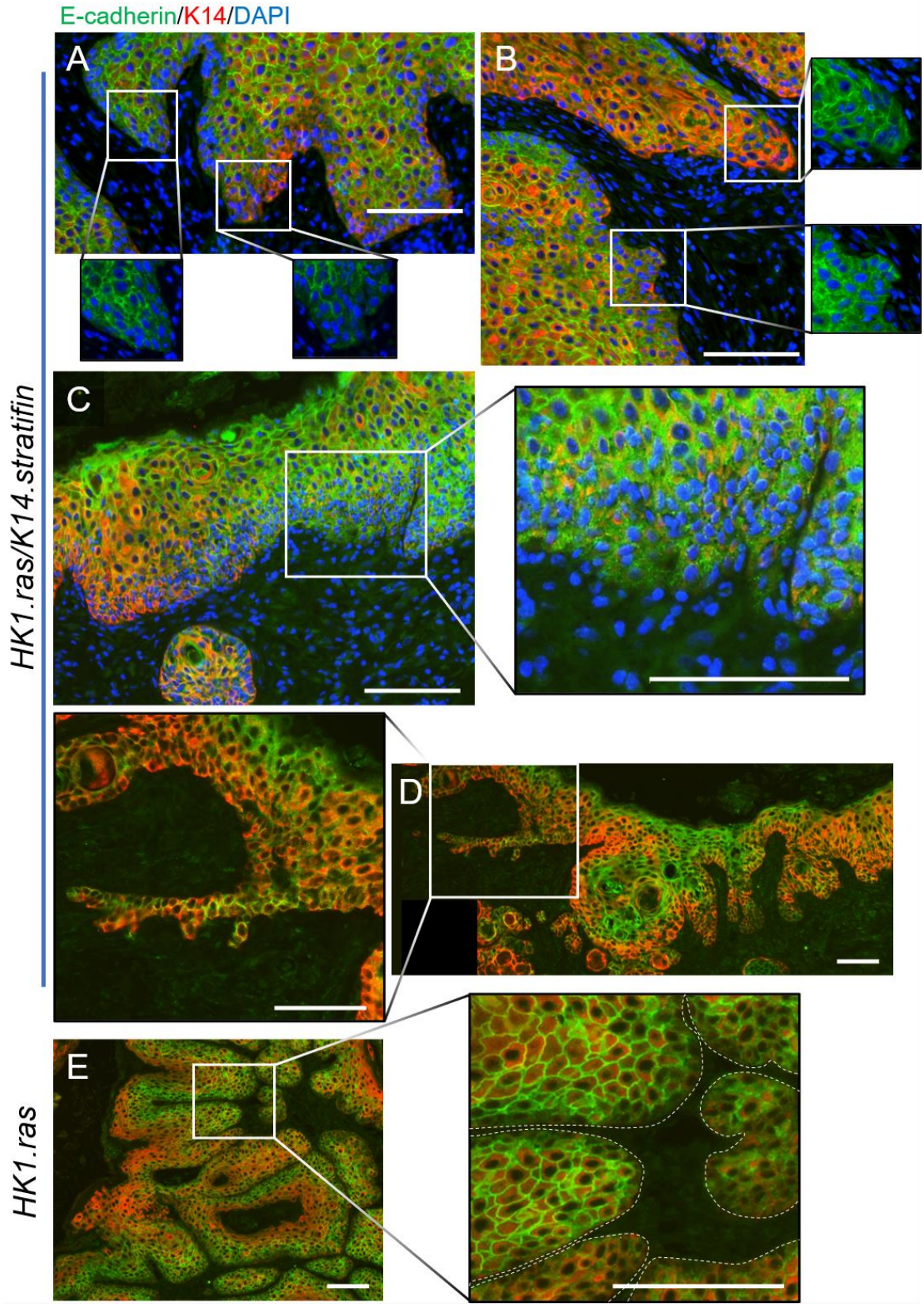
E-cadherin/K14/DAPI
A
B
C
D
E
HK1.ras/K14.stratifin
HK1.ras

Figure 5-8: E-cadherin staining shows differences in expression at various invasive sites in *HK1.ras/K14.stratifin* carcinogenesis.
(**A**) *HK1.ras/K14.stratifin* ear tumour showing basal E-cadherin (green) expression at the membranes in some collectively invading areas (left box) and reduced positivity in others with more irregular morphology (right box). Suprabasal membranes are mostly positive but show some patchiness in intensity. (**B**) *HK1.ras/K14.stratifin* ear tumour showing an area of tumour with very low expression of E-cadherin in all layers, especially at the invasive front (top box) juxtaposed with an area of relatively strong staining (lower box), where cell size is also much smaller. (**C**) *HK1.ras/K14.stratifin* ear tumour showing reduced E-cadherin to the left of the image and diffuse cytoplasmic staining (and possibly nuclear, given cyan colour of some, combined with DAPI) in the highlighted area. Keratin 14 (red) expression is also reduced in the boxed area and invasion appears more individual than collective here, suggestive of epithelial-mesenchymal transition in these cells (**D**) Finger-like invasion in a nearby area of the same tumour as in **C**, showing clear membranous E-cadherin positivity in the invading cells, highlighted in the boxed area. The centre of the image also shows an aberrated follicular structure while to the left other pushing invasive fronts are E-cadherin positive. (**E**) *HK1.ras* papilloma showing strong membranous E-cadherin staining throughout the supra-basal layers and negligible staining in the basal layer, highlighted in the boxed area (white dashed lines represent BM). *Scale bars approx. 100 µm.*

5.5.2. Tenascin-C is upregulated in *HK1.ras/K14.stratifin* tumour stroma, indicating presence of CAFs which may facilitate invasion

Invasion occurs not just due to activity within the tumour keratinocytes themselves, but also due to changes in the tumour microenvironment. Specifically, crosstalk between cancer cells in the epidermis and the tumour stroma can result in the development of cancer-associated fibroblasts (CAFs). CAFs are not themselves mutated but exhibit changes in their behaviour and secretory phenotype as a result of paracrine signalling from the tumour epidermis and can facilitate invasion through the BM by both physical and protease-mediated mechanisms (Goetz et al. 2011; Glentis et al, 2017).

Stratifin has been found to be secreted into the dermis by keratinocytes, inducing fibroblasts to undertake matrix remodelling as an important step in wound-healing (Ghaffari et al., 2006; Ghahary et al., 2007). Here, Stratifin binds aminopeptidase N/CD13 on dermal fibroblasts, resulting in upregulation of AP-1 signalling and increased expression of various matrix metalloproteinases (MMPs) which break down stromal components including collagens and fibronectin (Ghaffari et al., 2006; Lai et al., 2011). This is interaction is thus hypothesised to play a role in the invasion commonly seen in *HK1.ras*/*K14.stratifin* SCCs.

Tenascin-C (TENC), a large matrix glycoprotein, has been identified as a reliable marker of CAFs in tumour stroma, with increased expression significantly associated with increased invasion and metastasis in several carcinomas (Jahkola et al., 1998; Cai et al., 2017), as well as induction of EMT and blood vessel invasion (Sun et al., 2019). Moreover, increased Stratifin expression has been identified in invasive colorectal cancer cells where the tumour stroma exhibited high TENC positivity (Ide et al. 2007), suggesting a link between their expressions and co-operation in inducing invasion and thus was investigated in both types of *HK1.ras*/*K14.stratifin* tumours.

Here, expression of TENC in Type 1 and 2 *HK1.ras*/*K14.stratifin* SCCs—both of which have been shown to be invasive—was compared with that in non-invasive benign *HK1.ras* papillomas (*Figure 5-9*). In all *HK1.ras*/*K14.stratifin* SCCs tested (*n*=5) TENC expression was found to be moderate to strong throughout the tumour stroma (*Figure 5-9A,C,D,E*), compared with mostly weak staining in *HK1.ras* papillomas (*Figure 5-9F,G*). Strongest staining was observed close to the dermo-epidermal junction in all samples, though staining was weak or negative in *HK1.ras* papillomas in the stroma farthest from the epidermis whereas it remained moderate or strong in the comparative regions in *HK1.ras*/*K14.stratifin* carcinomas (*Figure 5-9C,E vs G*). Where areas of benign hyperplasia existed adjacent to *HK1.ras*/*K14.stratifin* tumours, the majority of the stroma exhibited very weak or negative staining, with some patches of positivity along the dermo-epidermal junctions (*Figure 5-9B, arrows*). This may be indicative of an early role in matrix remodelling in *HK1.ras*/*K14.stratifin* tumours as an integral part of their aetiology, as was previously observed in *HK1.ras*/*ROCK2* carcinogenesis (Masre et al., 2017; 2020).

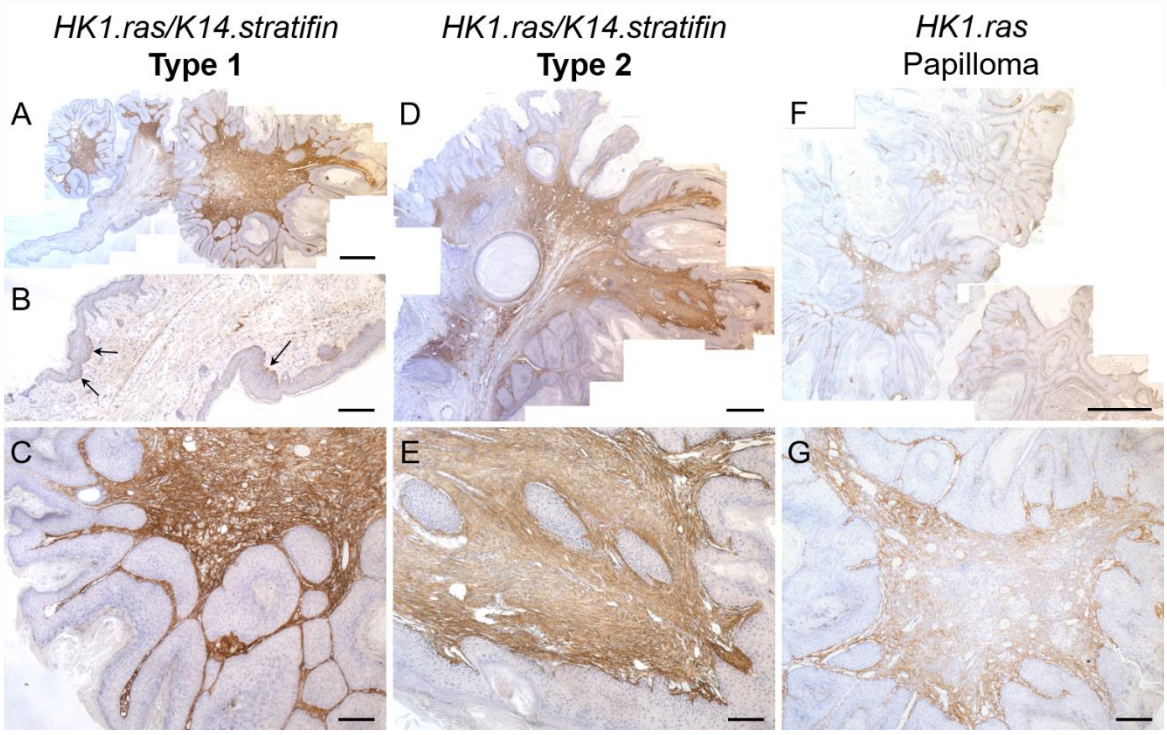

Figure 5-9: Tenascin C expression is markedly stronger in all *HK1.ras/K14.stratifin* tumours compared to *HK1.ras* controls.

(**A**) Type 1 *HK1.ras/K14.stratifin* tumour showing strong Tenascin C (TENC) staining in the tumour versus weak or no staining in the adjacent hyperplastic ear. (**B**) Magnification of the hyperplastic area in **A**, showing sporadic staining only at the dermo-epidermal (arrows). (**C**) Close-up of part of the tumour portion in **A**, showing strong stromal staining for TENC throughout the stroma. (**D**) Type 2 *HK1.ras/K14.stratifin* tumour exhibiting moderate to strong staining throughout the stroma, except in the hyperplastic area to the lower left of the image. (**E**) Close-up of **D**: moderate to strong staining throughout, especially at the dermo-epidermal junctions and surrounding the 3 tumour islands in the centre of the image (**F**) *HK1.ras* papilloma exhibiting weak staining throughout the stroma and moderate staining at the dermo-epidermal junctions. (**G**) Close-up of **F**: TENC expression is mainly confined to the stroma close to the epidermis, staining weakly in the central portion. *Scale bars: **A**, **D** and **F** approx. 500 µm; **B**, **C**, **E** and **G** approx. 100 µm.*

5.6. *HK1.ras/K14.stratifin* tumours exhibit strong p53 expression into malignancy but Types 1 and 2 differ in p21 localisation

In Chapter 4, it was shown that the major tumour suppressor p53 persisted though *HK1.fos/K14.stratifin* tumorigenesis, in contrast to *HK1.ras/fos-Δ5Pten* multistage tumorigenesis in which p53 loss coincided with malignant conversion (MacDonald et al., 2014). This persistence was assumed to be due to overexpression of Stratifin through the *K14.stratifin* transgene due to the protective effect exerted through Stratifin's inhibition of Mdm2 activity. However, whilst expression of the gene appeared to be responsible for the persistence of p53 in those fSCCs, p53 appeared uncoupled from its TSG roles. Hence, while *HK1.ras/K14.stratifin* tumour aetiology was shown to be rather different to the HK1.fos/K14.stratifin fSCC tumours, it was hypothesised that if a similar persistence occurred in *HK1.ras/K14.stratifin* tumours this may influence the aetiology of Type 1 wdSCC and aggressive Type 2 SCCs.

Here, *HK1.ras/K14.stratifin* tumours of both types showed moderate to strong p53 staining in the expanded basal compartment where K1 was still present in suprabasal cells, or throughout the epidermis when K1 expression was absent. This was observed in both Type 1 wdSCC and Type 2 SCC of this genotype (*Figure 5-10A,B*). In contrast, *HK1.ras* activation elicited an increase in p53 abundance in the basal layer, as depicted in *Figure 5-10G*, with low or negligible expression in the suprabasal layers, since the increase in proliferation was mainly confined to basal cells.

Since this strong p53 response did not appear to prevent excessive proliferation or malignant conversion in either Type 1 or Type 2 *HK1.ras/K14.stratifin* tumours, one of its main downstream effectors, p21, was assessed. p21 acts in the nucleus to halt the cell cycle at the G1/S checkpoint by sequestration of cyclin-dependent kinases 4 and 6 (CDK4/6) and was found to mimic p53 localisation in *HK1.ras* papilloma, shown in *Figure 5-10H*.

In both Type 1 and 2 tumours, p21 staining was moderate in the cytoplasm across the whole epidermis, though only Type 1 showed strong nuclear staining in the proliferative layers (*Figure 5-10C*). Of note, Type 2 tumours showed only sporadic nuclear p21 staining in basal cells, despite moderate cytoplasmic staining throughout, indicating the protein was being transcribed but was not active in the nuclei (*Figure 5-10D*). The areas contrasted in *Figure 5-10A/B* and *C/D* were both determined to be carcinoma rather than papilloma by the absence of Keratin 1 staining, shown in *E* and *F*, respectively. This lack of functional p21 could partly explain the more widespread carcinoma and aggressive histology seen in Type 2 tumours; a conclusion also supported by persistent endogenous Stratifin/p21 antagonism of pAKT1 observed in *HK1.ras/fos-Δ5Pten* carcinogenesis (Appendix 1, McMenemy et al., in preparation), explored further later in this chapter.

Evidence suggests that strong expression of p53 in this genotype was insufficient to suppress tumorigenesis and progression to carcinoma, even where p21 was induced and located in the nucleus, thus, presumably functional.

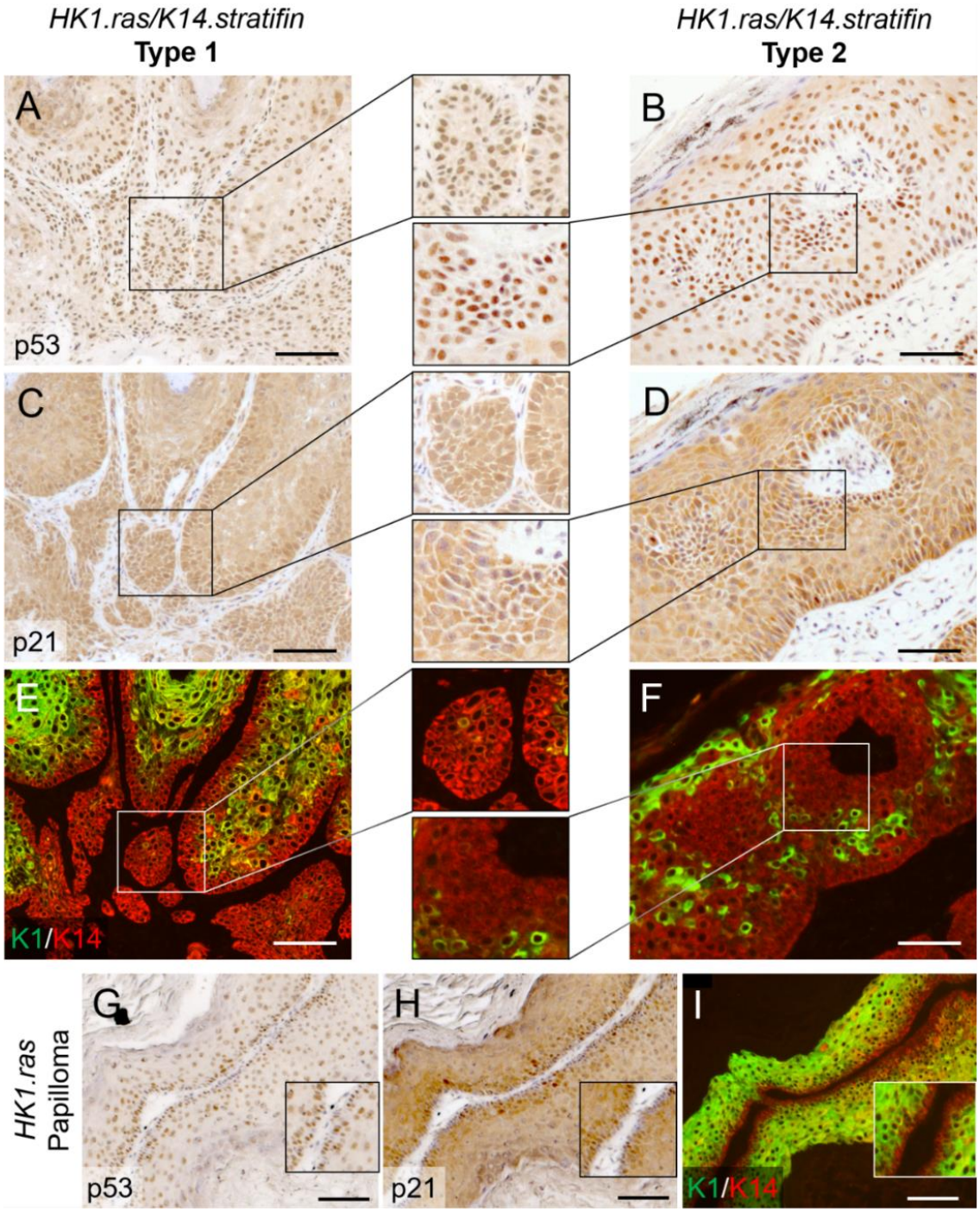

Figure 5-10: Both Type 1 and Type 2 *HK1.ras/K14.stratifin* tumours exhibit strong p53 positivity but have differing p21 expression.

(**A**) Type 1 *HK1.ras/K14.stratifin* tumour showing strong nuclear p53 expression in multiple layers of cells, shown at higher magnification in the boxed area. (**B**) Type 2 *HK1.ras/K14.stratifin* tail tumour showing similar very strong nuclear p53 staining throughout the epidermis. (**C**) Type 1 tumour showing moderate cytoplasmic p21 staining in all layers and moderate to strong p21 nuclear expression in the multiple basal layers. (**D**) Type 2 tumour showing moderate cytoplasmic staining in all layers with strong cytoplasmic staining in the basal layers but a lack of nuclear p21 expression in most basal cell, as shown in the highlighted box. (**E** & **F**) Confirmation of malignancy as indicated by the lack of K1 (green) staining in the areas tested for p53 and p21. (**G**) *HK1.ras* papilloma showing moderate nuclear p53 staining mainly confined to basal layer cells, similar to the pattern of p21 staining (**H**) which also displays some cytoplasmic staining mainly in the basal and granular layers. (**I**) Strong suprabasal K1 staining confirms benign nature of this *HK1.ras* papilloma. *Scale bars approx. 100 µm.*

To investigate this further, expression of active Akt1 (pAkt1^{ser473}) was assessed in both *HK1.ras*/*K14.stratifin* tumour types. Akt can be phosphorylated at several sites, though the main activating residues are Thr308 and Ser473; Thr308 is always activated prior to Ser473, thus assessing pAkt1^{ser473} indicated expression of the fully active form (Hemmings and Restuccia, 2012).

Akt can indirectly inhibit p53 by phosphorylating Mdm2 at ser166/186/188, thereby increasing its ubitquin ligase activity to antagonise p53 (Mayo & Donner, 2001). However, Stratifin directly inhibits Mdm2 (Lee and Lozano, 2006), reflected in the very high p53 expression in both Type 1 and Type 2 *HK1.ras*/*K14.stratifn* tumours (*Figures 5-10A,B* and *5-11A,D*). Akt is also a direct inhibitor of p21 by phosphorylation of p21 at position Thr145 which results in cytoplasmic localisation (Zhou et al., 2001), which is consistent with the pattern of p21 expression seen in Type 2 *HK1.ras*/*K14.stratifin* tumours (*Figures 5-10D* and *5-11E*).

Seemingly in direct contradiction with what was hypothesised, it was found that pAkt1^{ser473} expression was much higher in Type 1 tumours than Type 2 (*Figure5-11C vs F*); however, this may be consistent with the roles of Akt in differentiation, rather than proliferation (Calautti et al., 2005; Naeem et al., 2015). It was noted than in both types, pAkt1^{ser473} expression was localised to the perinuclear regions of positive cells or indeed, in the nuclei (*Figure 5-11C,F*). Nuclear Akt has been shown to have a myriad of roles, including suppression of apoptosis and senescence, and inhibiton of cell cycle inhibitors including p21, p27 and p300, among others (Martelli et al., 2012).

Stratifin has been shown to directly bind and inhibit Akt activity (Yang et al., 2006), and may partly account for the low pAkt1^{ser473} expression seen here in Type 2 *HK1.ras*/*K14.stratifin* tumours, since despite, apparently comparable overall Stratifin expression driven by the *K14.stratifin* transgene in Type 1 and Type 2 tumours, Stratifin activity is known to be highly context-dependent, such that it may act in contridictory fashions given small changes in signalling (Li et al., 2009). This however, leaves the question of why p21 is not active in the nuclei of Type 2 tumours, which may be integral to their more aggressive phenotype.

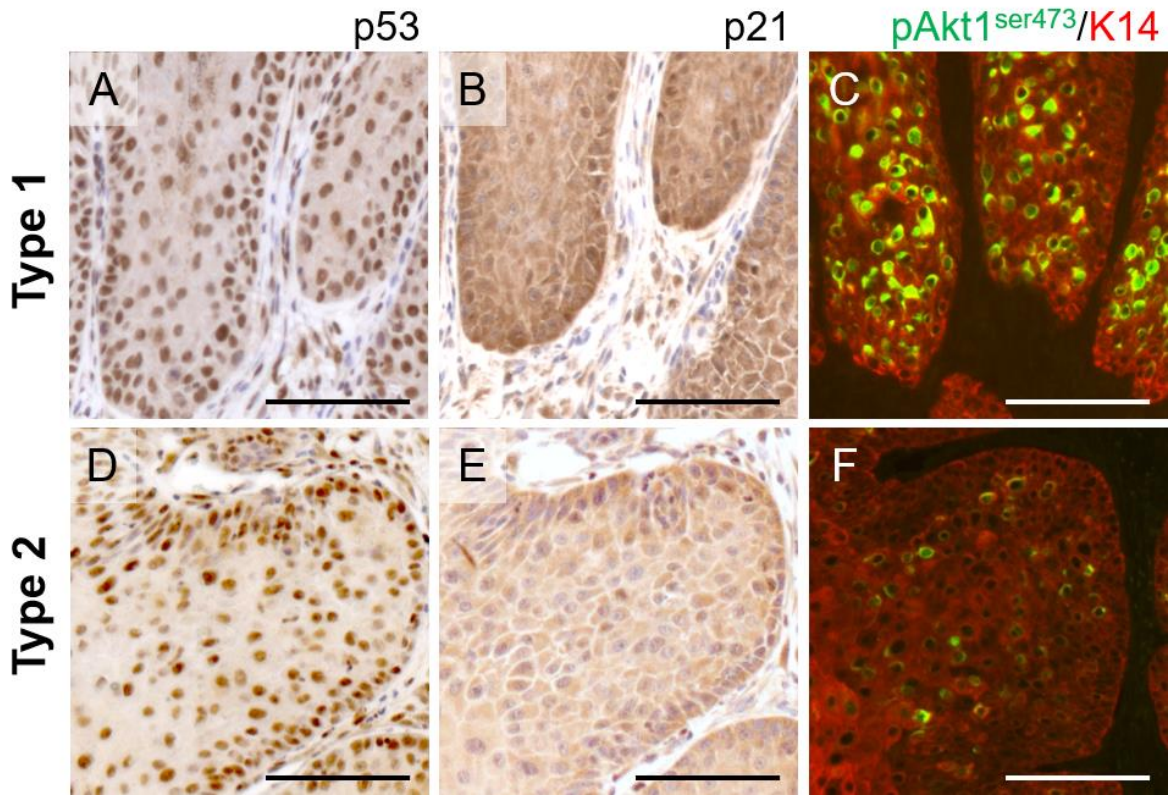

Figure 5-11: pAkt1^{ser473} expression is stronger in Type1 *HK1.ras/K14.stratifin* tumours than in Type 2 and thus does not account for cytoplasmic p21 localisation in Type 2 SCCs.

(**A**) Type 1 *HK1.ras/K14.stratifin* tumour confirming strong p53 positivity throughout epidermis (**B**) Same area as in **A**, also confirming concurrent strong p21 expression and both cytoplasmic and nuclear localisation (**C**) Surprisingly strong pAkt1^{ser473} expression concomitant with strong p53/p21 in Type 1 *HK1.ras/K14.stratifin* tumour, exhibiting primarily perinuclear and nuclear expression. (**D**) Type 2 *HK1.ras/K14.stratifin* tumour showing similarly strong p53 expression to the Type 1 tumour in **A.** (**E**) Moderate cytoplasmic p21 expression but a lack of nuclear p21 is seen in this area, dented by blue haematoxylin counterstained nuclei with few positive nuclei visible (**F**) Very little pAkt1^{ser473} expression suggesting this is not responsible for the cytoplasmic localisation of p21 in Type 2 *HK1.ras/K14.stratifin* SCCs. *Scale bars approx. 100 µm.*

5.7. Ablation of p53 repeats experiments showing that its expression is paradoxically required for *HK1.ras*-driven tumour formation, but *K14.stratifin* expression elicits malignancy in the p53-null hyperplasia

Prior studies by Greenhalgh et al. (1996) identified a paradoxical anti-tumorigenesis effect of p53 knockout (via gene-targeting) in mice expressing *HK1.ras*, *HK1.fos* and *HK1.TGF-a*. These results were also recapitulated in *HK1.ras* and *HK1.fos* mice through use of a Cre-mediated excision of exons 2-10 of p53, targeted to the epidermis either constitutively (*K5.Cre*; Tarutani et al., 1997) or induced in the manner previously described for excision of *Pten* exon 5 (*K14.CrePR1*). The mechanisms underpinning this paradox of inhibiting wound-dependent papillomatogenesis have remained elusive and continue to be investigated.

As shown in *Figure 5-10*, p53 expression in *HK1.ras*/*K14.stratifin* phenotypes was found to be both stronger and present in more layers of the tumour epidermis than in *HK1.ras* papillomas, where expression was mostly limited to basal cells, consistent with the confinement of proliferating cells to the basal layers in benign tumours (*Figure 5-6C*). Taken together with the data regarding the p53 paradox in *HK1.ras* papillomatogenesis, it was hypothesised that p53 expression may be required for generation of the tumours seen in *HK1.ras*/*K14.stratifin* mice, despite its well-known status as a major TSG.

To investigate this, *HK1.ras*/*K14.stratifin* mice were mated with mice harbouring floxed p53 alleles ($p53^{flx/flx}$) as well as the *K14.CrePR1* transgene (designated $K14.ras.p53^{flx/flx}.stratifin$), required for excision of the floxed segment following repeated topical RU486/Mifepristone application. This generated mice which were homozygous ($K14.ras.p53^{flx/flx}.stratifin$, n=14) and heterozygous ($K14.ras.p53^{flx/+}.stratifin$, n=6) for the floxed allele, as well as controls either lacking the *K14.CrePR1* regulator transgene ($ras.p53^{flx/flx}.stratifin$, n=4; *and* $ras.p53^{flx/+}.stratifin$, n=4) or *K14.stratifin* ($K14.ras.p53^{flx/flx}$ n=7, and $K14.ras.p53^{flx/+}$, n=4). A subset (n=2 per cohort) of those with the *K14.CrePR1* transgene were not treated with RU486 to ensure the

phenotypes observed were due to Cre-mediated p53 ablation, while the remaining mice were treated between 2 and 4 times. Previous experiments with *HK1.ras* mice (n>60, over many years) suggested the paradoxical effect was only present if p53 ablation occurred prior to initial papilloma growth (either by wound-promotion or TPA-treatment (Greenhalgh et al., 1996), or if a *K5.Cre* promoter was employed, which is constitutively active throughout development. Thus, all mice in this study received their first RU486 treatment on the day they were tagged (wound-promotion). Determination of genotype was performed as described in Chapter 4: *Figure 4-9*. Interestingly, no mice in this cohort developed wound-independent (Type 2) papillomas/SCCs.

The first of the *K14.ras.p53$^{flx/flx}$.stratifin* mice generated (*n*=2, Figure 5-12) and control littermates were treated with RU486 3 times (first at tag) and biopsied at 4-months-old. Macroscopically, *K14.ras.p53$^{flx/flx}$.stratifin* exhibited only hyperplasia at the tag site, though this was clearly inflamed, unlike the *K14.ras.p53$^{flx/flx}$* littermates which showed almost no gross phenotype (Figure 5-12), supporting paradoxical tumour suppression in this loss-of-function genotype (Greenhalgh et al., 1996), whereas *K14.ras.p53$^{flx/+}$* and *ras.p53$^{flx/flx}$* exhibited typical papillomatogenesis over 8-10 weeks (not shown).

No clear difference in macroscopic phenotype was observed between *K14.ras.p53$^{flx/+}$.stratifin* mice and p53 wild-type mice, as all developed keratotic tumours at tag (Figure 5-12; top row, labelled) which did not regress when the tag was lost (see the third mouse in the heterozygous group, Figure 5-12). *K14.ras.p53$^{flx/+}$.stratifin* tumours grossly appeared more inflamed and keratotic than *K14.ras.p53$^{flx/+}$* papillomas (Figure 5-12; top row), consistent with the phenotype observed in *HK1.ras*/*K14.stratifin* ear tumours and reflective of the recessive nature of this TSG, wherein both copies generally need to be either altered or lost to produce a significant change in phenotype (Venkatachalam et al., 1998).

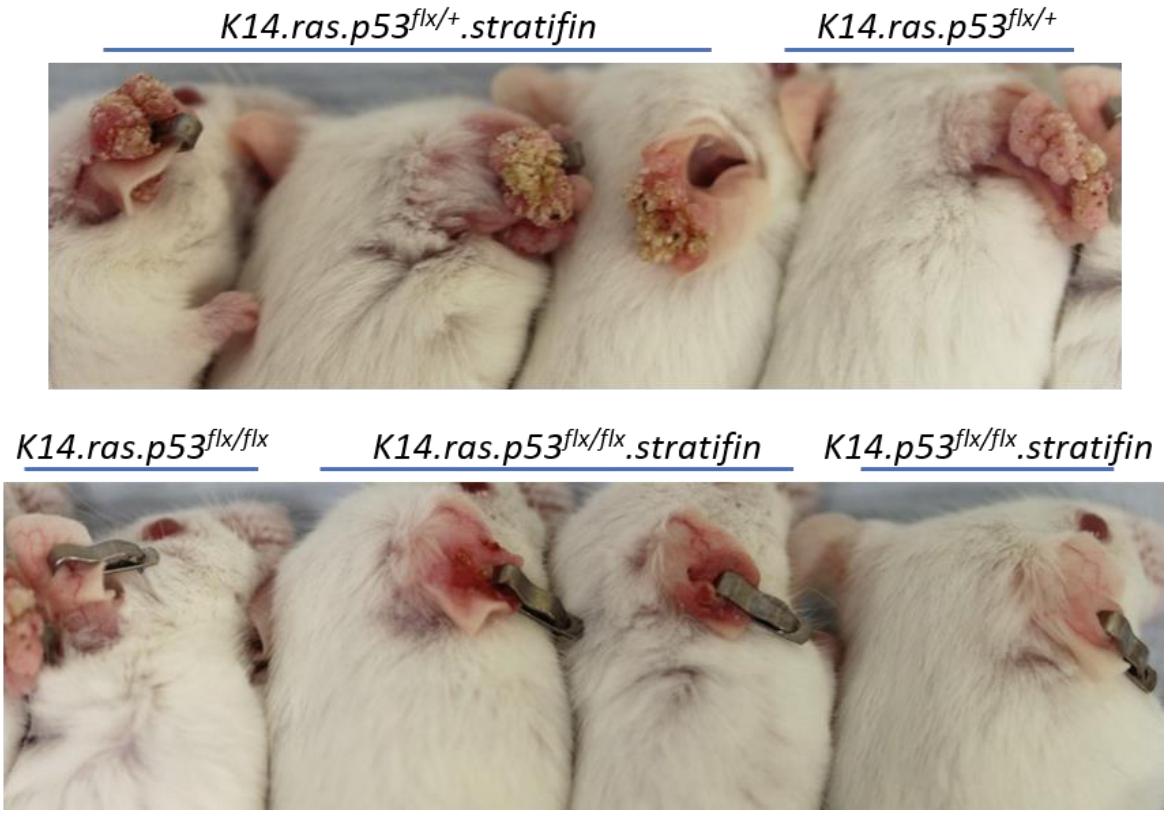

Figure 5-12: Initial results showed *K14.ras.p53$^{flx/flx}$.stratifin* mice did not develop tumours but instead exhibited inflamed hyperplasia not seen in *K14.ras.p53$^{flx/flx}$*.
First set of *K14.ras.p53$^{flx/flx}$.stratifin* mice generated alongside their various age-matched controls at 20 weeks/17 weeks post-tag. All mice received 3 topical treatments of RU486 to activate *K14.CrePR1* activity to each ear and a shaved portion of the back between the tag date and biopsy. **Top row:** 3 x *K14.ras.p53$^{flx/+}$.stratifin* mice exhibiting keratotic papillomas/possible SCCs at tag. The third mouse lost the tag several weeks prior to biopsy with no noticeable tumour regression in that time. 1 x *K14.ras/p53$^{flx/+}$* papilloma showing less keratosis than those with the *K14.stratifin* transgene. **Bottom row:** 1 x *K14.ras.p53$^{flx/flx}$* mouse lacking any gross phenotype, due to previously described paradoxical inhibition of papillomatogenesis by p53 ablation. 2 x *K14.ras.p53$^{flx/flx}$.stratifin* lacking any tumour development but exhibiting an inflammatory hyperplasia at ear tag. 1 x *K14.p53$^{flx/flx}$.stratifin* mouse showing some hyperplasia at tag without the obvious inflammation seen in *K14.ras.p53$^{flx/flx}$.stratifin*.

Histological analysis of the initial *K14.ras.p53$^{flx/flx}$.stratifin* hyperplastic ears (*Figure 5-12*) showed that despite lacking overt tumour development, the TGEs showed signs of malignancy. The sections exhibited a very high degree of immune infiltrate in the stroma, which was expanded as had previously been identified in *HK1.ras/K14.stratifin* SCCs. Unlike the heterozygous or wild-type p53 controls (*K14.ras.p53$^{flx/+}$.stratifin* or *K14.ras.p53$^{+/+}$.stratifin*) and parental *HK1.ras/K14.statifin*) tumours, *K14.ras.p53$^{flx/flx}$.stratifin* did not exhibit hyperkeratosis and, indeed, may be considered hypokeratotic in places (*Figure 5-13C,D*), suggesting this combination inhibited the normal terminal differentiation programme, supported by the apparent lack of granular cells in some areas (*Figure 5-13E,F*).

K14.ras.p53$^{flx/flx}$.stratifin hyperplasias were found to exhibit extensive invasion, both collective in the form of pushing borders (*Figure 5-13E*; immune infiltrate appears to be facilitating BM disruption) and finger-like projections (*Figure 5-13F*), as well as a trend towards aggressive SCC and even epithelial-mesenchymal transition/spindle cell carcinoma, seen in *Figure 5-13D*. Here, invading cells have a very elongated shape and less cohesion than the collective projections in *F*, with the leading cells nearly indistinguishable from fibroblasts in the surrounding stroma. This phenotype is quite different to the age-matched *K14.ras.p53$^{flx/+}$.stratifin* tumours or *K14.ras.p53$^{flx/+}$* papillomas analysed (*Figure 5-13G and H*, respectively). Age-matched *K14.ras.p53$^{flx/flx}$* TGEs showed only mild hyperplasia and no signs of invasion (*Figure 5-13I*).

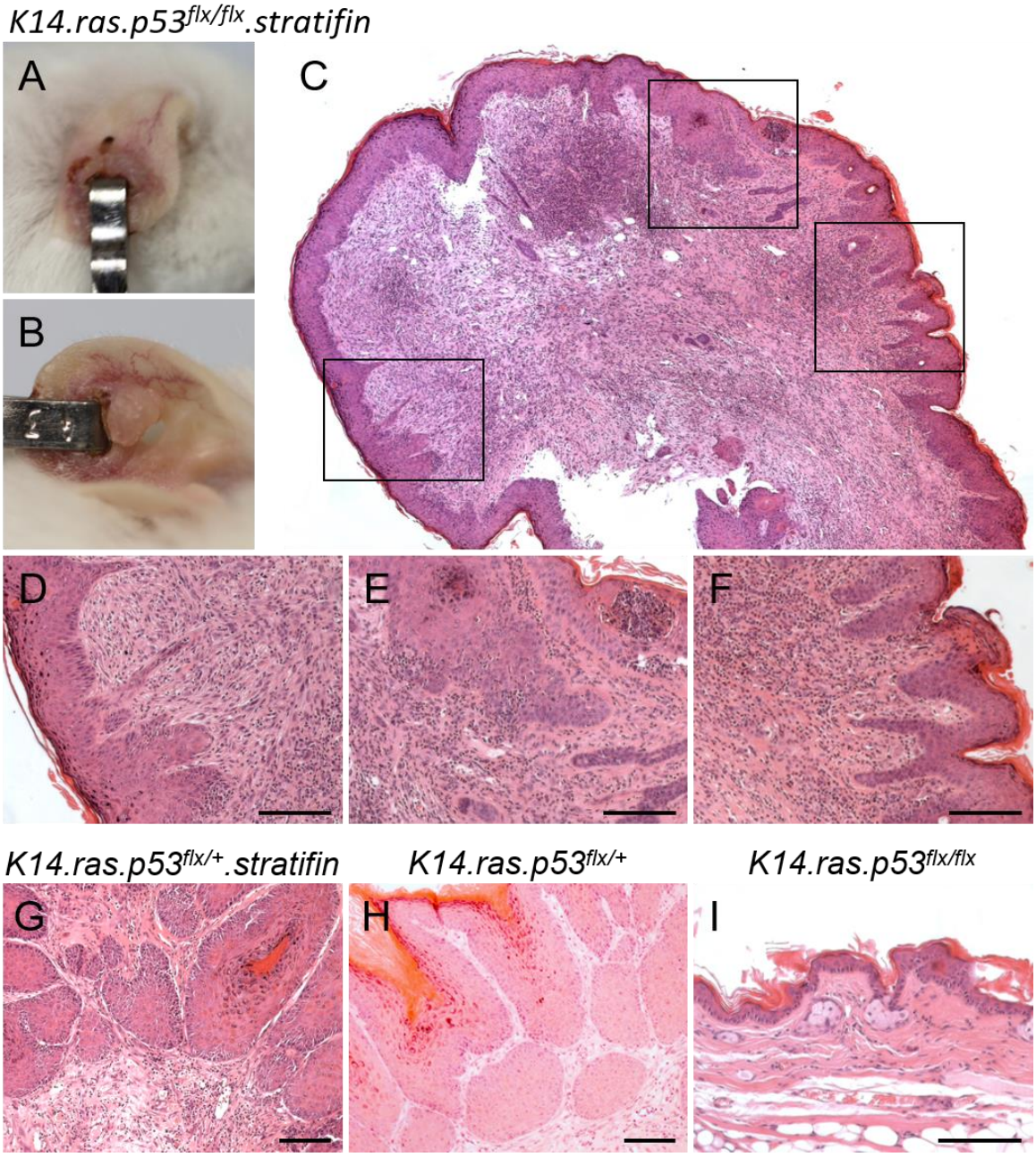

Figure 5-13: *K14.ras.p53$^{flx/flx}$.stratifin* hyperplasia exhibits a high degree of immune infiltrate and invasion.

(**A**) Outer surface of *K14.ras.p53$^{flx/flx}$.stratifin* hyperplasia surrounding the ear tag site, showing signs of inflammation (**B**) Inner surface of **A**, showing a slightly larger hyperplastic area (**C**) Histological overview of the same ear hyperplasia showing a large proportion of stroma with a very high number of infiltrating immune cells, especially in the patch near the top of the image which appears dark due to the density of immune cells in the region. (**D**) Highlighted from C, showing elongated invasive cells (top, centre) consistent with a trend towards partial or full epithelial-mesenchymal transition phenotype. (**E**) Collectively invading cells with immune infiltrate apparently contributing to BM destruction, further promoting keratinocyte invasion. (**F**) Collective invasion in the form of finger-like projections, similar to that described in p53-competent *HK1.ras/K14.stratifin* tumours. (**G**) *K14.ras.p53$^{flx/+}$.stratifin* tumour indistinguishable from *HK1.ras/K14.stratifin-p53WT* tumours (**H**) *K14.ras.p53$^{flx/+}$* papilloma outwardly similar to **G** but lacking signs of malignancy and unusual differentiation (**I**) *K14.ras.p53$^{flx/flx}$* mild hyperplasia typical of this genotype, showing far fewer immune cells than in the counterparts expressing K14.stratifin. *Scale bars approx. 100 µm.*

Further breeding generated more *K14.ras.p53*$^{flx/flx}$*.stratifin* (*n*=12) which exhibited some variation compared with the initially observed phenotype, above. Again, none of these mice had developed a tumour macroscopically comparable with their heterozygous or WT control siblings, though several produced small tumours (*Figure 5-14*; *Table 5-2*) at the tagged, RU486-treated ear. The histology of these TGE sections showed only one mouse had developed an actual tumour with papilloma-type features, e.g., keratin pearls and some surface keratosis (*Figure 5-14A,B*), though even this developed areas or carcinoma and invasion (*Figure 5-14C*).

The rest developed either inflamed hyperplasia similar to that shown in *Figure 5-13A-F*, a very small (<5 mm) tumour (*Figure 5-14D-F*), or small (≤8 mm) tumour (*Figure 5-14G-I*), as detailed in *Table 5-2*. When the histology of these was examined, it was found that most of their mass was comprised of stroma (*Figure 5-14D-I*) in all cases, suggesting the papilloma-like tumour in *Figure 5-14A-C* may be an outlier, possibly influenced by unknown genetic or epigenetic differences that facilitate escape from the described p53-paradox which could not be assessed within the scope of this project yet remain under scrutiny.

With the exception of a single outlier (*Figure 5-14A-C*), these data suggest that p53 competency is a requirement for development of *HK1.ras*-driven tumorigenesis, consistent with that described by Greenhalgh et al. (1996). However, given the invasive nature of all *HK1.ras*/*K14.stratifin* tagged ear sections analysed, the lack of overt tumour formation is unconnected with the malignant potential of lesions generated by this *K14.ras.p53*$^{flx/flx}$*.stratifin* genotype. Collectively, these data also show that *K14.stratifin* expression cannot overcome the initial paradox to elict overt benign tumours, however, the histotypes suggest the beginnings of invasion that may circumvent this apparent protection and once overcome, would rapidly lead to aggressive tumours possibly exhibiting extensive EMT to metastatic spindle cell carcinoma.

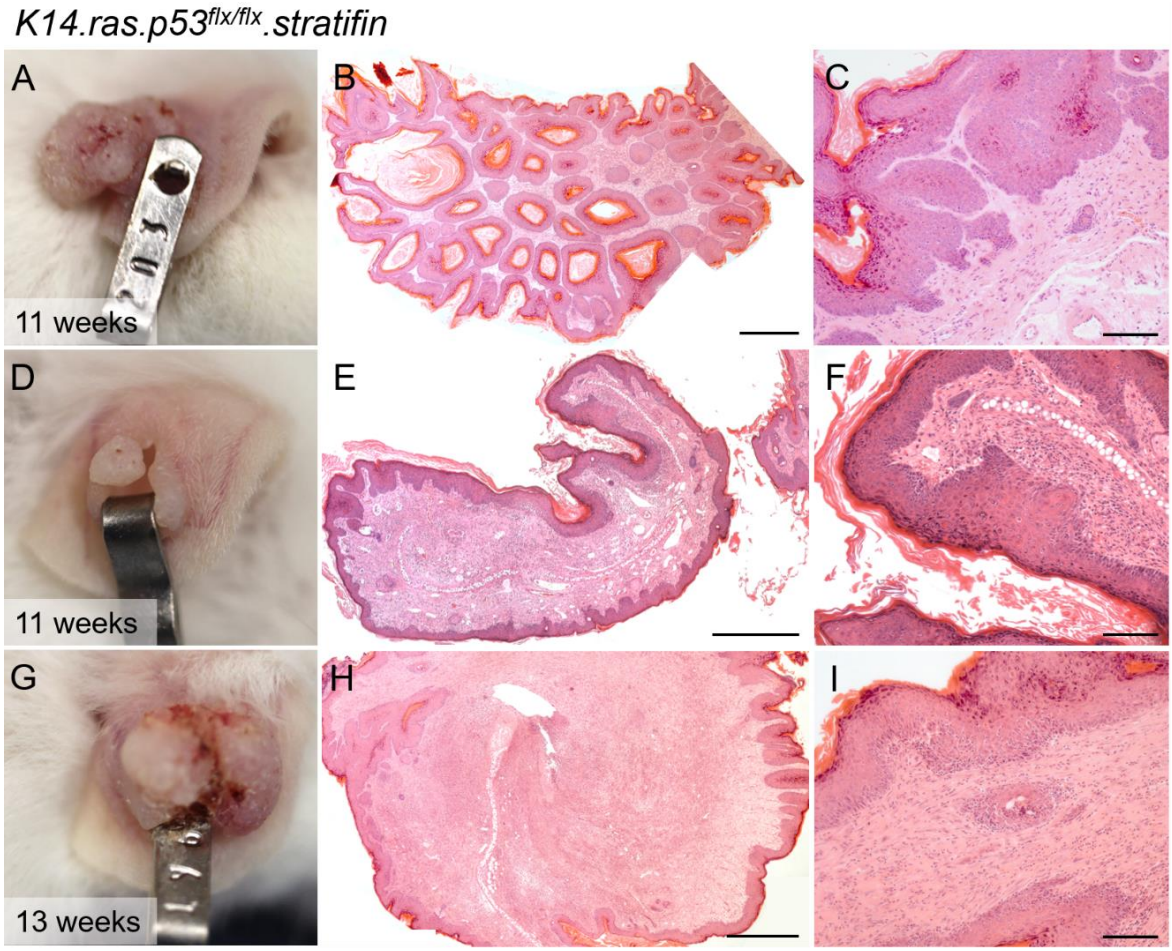

Figure 5-14: Later *K14.ras.p53$^{flx/flx}$.stratifin* mice developed small tumours which also showed signs of invasion.
(**A**) *K14.ras.p53$^{flx/flx}$.stratifin* small papilloma at 11 wks./7 wks. post tag with mild surface keratosis. (**B**) Histology of **A** shows a fairly benign papilloma appearance with keratin pearls throughout and largely stratified epidermis, however, the area in the top right of the image is highlighted in (**C**) and shows a loss in differentiation and presence of invading cells contrary to the benign appearance of the rest of the structure. (**D**) *K14.ras.p53$^{flx/flx}$.stratifin* at 11 wks./7 wks. very small tumour not much larger than the hyperplasia in *Figure 5-12*, lacking any surface keratosis. (**E**) Histology of **D** showing hyperplastic epidermis surrounding a tiny tumour mostly comprised of stroma. Many patches of epidermis are invasive, like that highlighted in (**F**). (**G**) *K14.ras.p53$^{flx/flx}$.stratifin* at 13 wks./9 wks. with unusually large tumour for the genotype exhibiting a very smooth, rounded appearance dissimilar to a papilloma or classic SCC. (**H**) Histology of **G** showing hugely hyperplastic stroma with epidermal hyperplasia surrounding it of a similar appearance to that in **E**. Again, this is quite invasive, as seen to the far left of the image. It also exhibits a large immune infiltrate, seen as an especially dark band close to the central cartilage and other dark patches throughout the stroma. (**I**) Higher magnification of an invasive region of **H** including a small tumour island. *Scale bars: **B**, **E**, **H** approx. 500 µm; **C**, **F**, **I** approx. 100 µm.*

Phenotype	Frequency
Inflamed hyperplasia (lots of stroma)	4/14 (28.6%)
Papilloma (some invasion)	1/14 (7.1%)
Very small tumour (<5 mm ø)	5/14 (35.7%)
Small tumour (≤8 mm ø; mostly stroma)	4/14 (28.6%)

Table 5-2: Frequency of observed *K14.ras.p53$^{flx/flx}$.stratifin* TGE phenotypes.

5.8. Type 1 *HK1.ras/K14.stratifin* tumours exhibit only minor loss of K1/K10 co-localisation but Type 2 tumours show similar extensive divergence to that seen in *HK1.fos/K14.stratifin* SCC

In Chapter 4, it was shown that Keratin partners 1 and 10 greatly diverge in expression and localisation in *HK1.fos*/*K14.stratifin* SCCs from an early stage. While noted that *HK1.fos* hyperplasias exhibited minor loss in K1/K10 co-localisation, the divergence seen in *K14.stratifin* skin was much more apparent, suggesting that Stratifin overexpression was the driver for this phenomenon.

Here, *HK1.ras*/*K14.stratifin* tumours were assessed for K1.K10 co-localisation in the same manner. Immunofluorescence examination (*Figure 5-15*) showed that both Type 1 and Type 2 tumours exhibited differences in co-localisation when compared with *HK1.ras* papillomas (*Figure 5-15 A,B vs C*), and the divergence was much more striking in Type 2 than Type 1 tumours (*Figure 5-15 B vs A*).

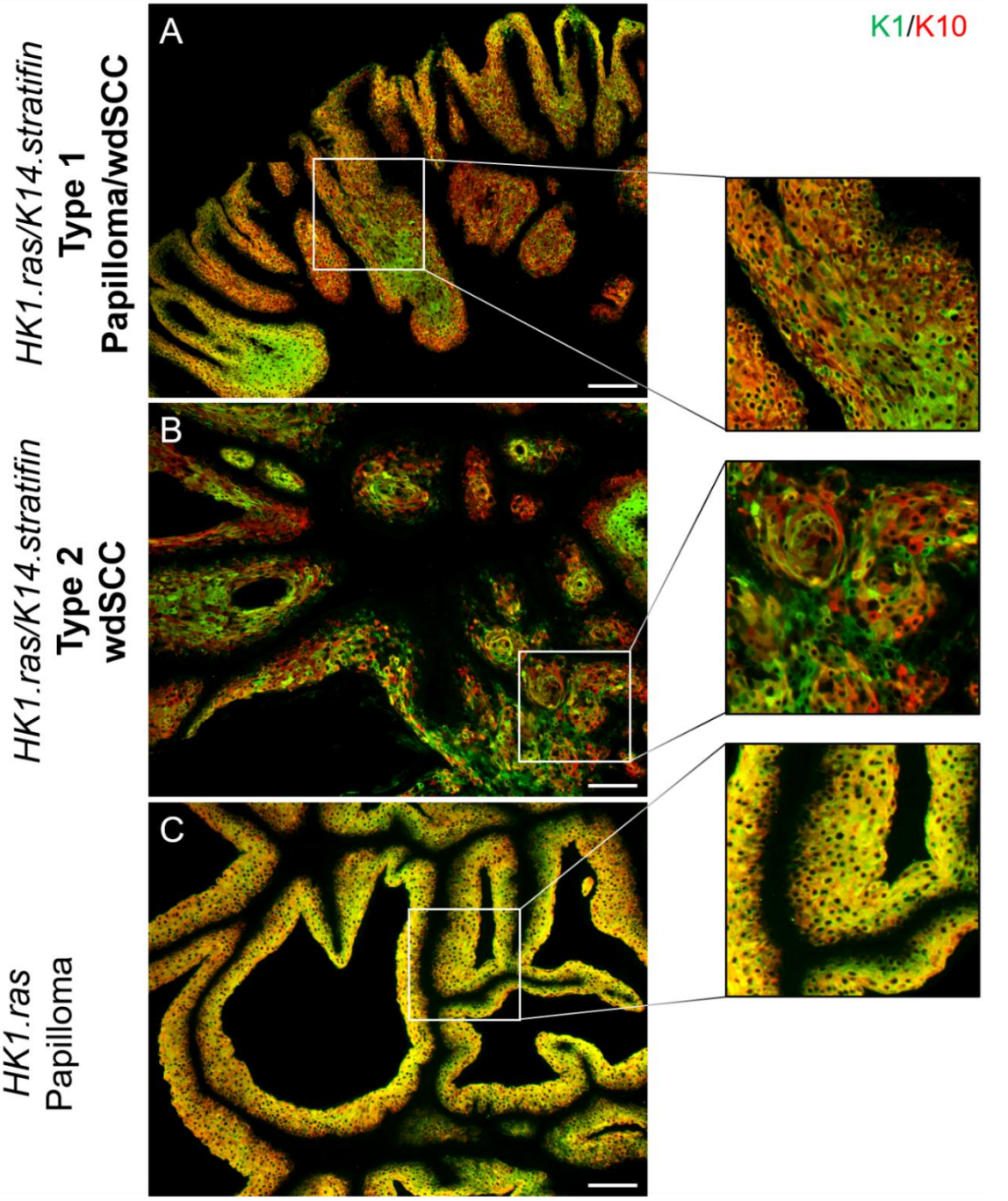

Figure 5-15: Expression of Keratin 1 and Keratin 10 is mostly co-localised in Type 1 *HK1.ras/K14.stratifin* but diverges extensively in Type 2 SCCs.
(**A**) Type 1 *HK1.ras/K14.stratifin* tumour showing well co-localised K1 (green) and K10 (red) expression in some areas (lower left of image) diverging in some patches (centre right). Highlighted area shows a moderate level of co-localisation. (B) Type 2 *HK1.ras/K14.stratifin* tail tumour shows similar K1 and K10 expression but poor colocalization throughout; highlighted in the boxed area. (**C**) *HK1.ras* papilloma shows apparent yellow staining indicative of very good co-localisation throughout. *Scale bars approx. 100 µm.*

To determine the extent of the difference in K1/K10 co-localisation between *HK1.ras*/*K14.stratifin* tumours and *HK1.ras*, and between the two *HK1.ras*/*K14.stratifin* tumour types, the Colocalization Threshold plugin was employed, as described in Chapter 4, for objective image analysis.

This analysis now found that Type 1 *HK1.ras*/*K14.stratifin* tumours actually did show a co-localisation pattern more akin to that of the *HK1.ras* controls when only position of positive cells was considered, ignoring intensity of the signal (*Figure 5-16 Panel I: A,B vs H,I*). Thus, co-localisation in space of Keratins 1 and 10 is consistent with controls, though further assessment would be required to determine if the expression of each was comparable in these tumours, for example through western blotting or by RT-PCR to determine whether the difference lies at the level of transcription or post-transcriptional repression mechanisms.

In contrast, Type 2 tumours differed significantly in K1/K10 co-localisation (*Figure 5-16 Panel II:B*) from control *HK1.ras* papillomas (*Figure 5-16 Panel I: C-F vs H,I*). In some Type 2 tumours, such as the TGE SCC shown in *Figure 5-16C*, Keratin 10 expression was found to persist after K1 was lost in some regions, as indicated by the large red area in the image, similar to the pattern observed in *HK1.fos*/*K14.stratifin* SCCs (*Figure 4-18*). In other Type 2 tumours, however, the overall abundance of K1 and K10 was comparable, though many cells were either K1 or K10 positive, as denoted by the patches of red and green cells in the colocalised image (*Figure 5-16E*), and reflected by the scatterplot, which is diffuse but does not have a strong skew to either colour.

Manders overlap coefficients (thresholded values only) (Manders, Verbeek and Aten, 1993) were assessed in all *HK1.ras*/*K14.stratifin* tumours tested and compared with *HK1.ras* papillomas and *HK1.ras*/*fos-Δ5Pten* SCCs. Here, tM1 (percentage of red pixels which also had a green value over threshold) and tM2 (percentage of green pixels which also had a red value over threshold) were close to 1 (100%) for both the *HK1.ras*/*K14.stratifin* Type 1 tumours and the control *HK1.ras* papillomas, with only one of the 3 *HK1.ras*/*fos-Δ5Pten* SCCs tested showing a drop in value for each, through variation was also greater in that sample. Type 2 *HK1.ras*/*K14.stratifin* tumours showed much lower mean

tM1 and tM2 values, though far more variation was seen than in any other group (*Figure 5-16 Panel II C,D*), hindering numerical analysis. When Pearson's correlation coefficients were compared between genotypes, there was no significant difference found between *HK1.ras* and *HK1.ras/K14.stratifin* tumours (Mann-Whitney U; p = 0.336), but a highly significant difference was detected between Type 2 tumours and *HK1.ras* papillomas ($p \ll 0.001$) (*Figure 5-16 Panel II B*). These data, therefore, support earlier analyses indicating that *HK1.ras/K14.stratifin* tumours have distinct aetiologies despite both showing evidence of malignant conversion and invasion.

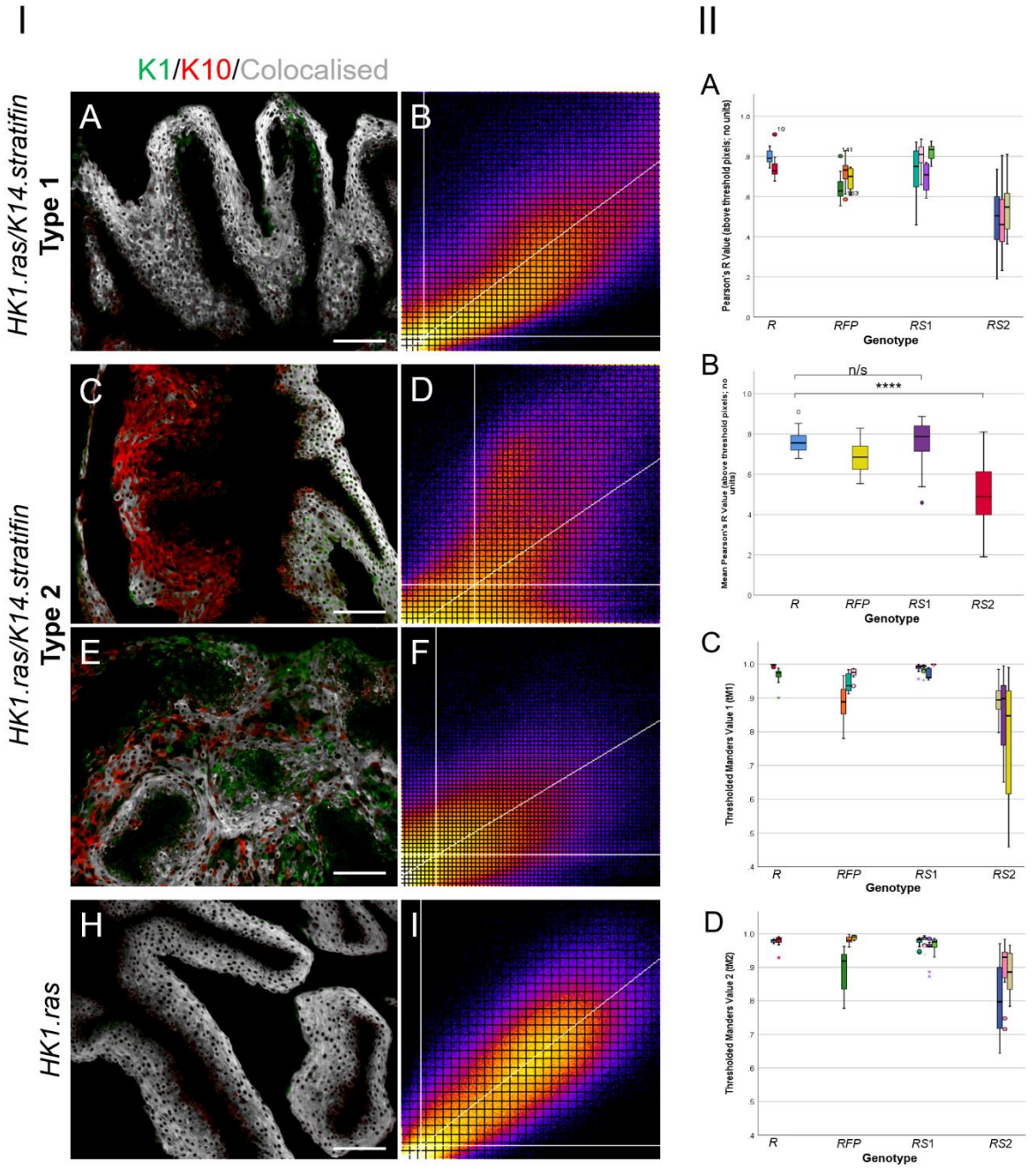

Figure 5-16: Image analysis confirms that HK1.ras/K14.stratifin Type 1 tumours exhibit similar K1/K10 co-localisation to controls while Type 2 tumours diverge significantly.

Panel I: (**A**) K1-K10 co-localisation image of a typical *HK1.ras/K14.stratifin* Type 1 tumour showing mostly co-localised pixels (grey). (**B**) Scatterplot of the pixels in **A** confirming similar degree of co-localisation as in *HK1.ras* control (**H** and **I**). (**C**) K1-K10 co-localisation image of a *HK1.ras/K14.stratifin* Type 2 ear tumour showing poor co-localisation mainly due to loss of K1 (green) while K10 (red) persists juxtaposed with a hyperplastic region exhibiting good correlation (grey, right of image). (**D**) Scatterplot confirms poor correlation between red and green pixels in **C**. (**E**) K1-K10 co-localisation image of a *HK1.ras/K14.stratifin* Type 2 tail tumour showing poor co-localisation but without the bias towards more K10 positivity seen in **C**. (**F**) Scatterplot shows relatively similar numbers of red and green pixels, but the diffuse nature of the plot indicates the low correlation in their expression. (**H**) *HK1.ras* papilloma showing very well correlated K1 and K10 expression, supported by the scatterplot (**I**). Scale bars approx. 100 µm.

Panel II: (**A**) Pearson's R value for above-threshold pixel correlation in *HK1.ras* (*R*, *n*=2), *HK1.ras/fos-Δ5Pten* (*RFP*, *n*=3), *HK1.ras/K14.stratifin* Type 1 (*RS1*, *n*=4) and *HK1.ras/K14.stratifin* Type 2 (*RS2*, *n*=3) showing consistently lower correlation in *RS2*. (**B**) Mean Pearson's R values for the 4 categories (*R*, *RFP*, *RS1* and *RS2*) showing no significant difference between the mean values of *R* and *RS1* ($p = 0.336$), but highly significant difference between *R* and *RS2* ($p \ll 0.001$), using Mann-Whitney U non-parametric test. (**C**) Manders thresholded overlap coefficient 1, tM1 (i.e., percentage of red pixels above threshold also had a green value above threshold), showing colocalisation approaching 1 (100%) in *R* and *RS1*, with one *RFP* sample exhibiting a value ~0.9. RS2 sample means are all >0.8 but the spread of data is far greater than in the other groups, with 95% CI ranging between ~0.5 and 1 in the last sample set. (**D**) tM2 (i.e., percentage green pixels above threshold which also have an above threshold red value), showing all values closer to 1 in all groups, confirming slight bias towards K10 retention when K1 is lost; clearest in *RS2*. Note that y-axes in **C** and **D** begin at 0.4.

5.9. Discussion

This chapter explored the effects of Stratifin overexpression, via the *K14.stratifin* transgene, on the benign, wound-dependent papilloma phenotype produced in *HK1.ras* mice. As outlined in co-operation with Fos, an initial pre-conception was that these mice would exhibit an inhibition of papilloma formation, given the observations in *HK1.ras*/*fos-Δ5Pten* mice as well as the increased papillomatogenesis seen in DMBA/TPA-treated 14-3-3σ knockout mice (Winter et al., 2016). However, again, the converse proved to be true, as the expression of *HK1.ras* in follicles due to *K14.stratifin* expression led to SCC aetiologies, though distinct from *HK1.fos*/*K14.stratifin* fSCC.

5.9.1. Type 1 and Type 2 *HK1.ras/K14.stratifin* tumours

As discussed above, loss of endogenous Stratifin expression, paralleled by loss of p21 and increased Akt activity, in *HK1.ras/fos-Δ5Pten* carcinogenesis resulted in tumour progression to a more poorly differentiated phenotype, suggestive of a tumour suppressive effect; consistent with tumour suppressive roles as inferred from the knockout model results (Winter et al., 2016). In contrast, co-expression of *K14.stratifin* with *HK1.fos* resulted in fast-growing malignant tumours which recapitulate histological features of fSCC, indicating an oncogenic role for Stratifin. Unlike *HK1.fos* mice, which develop hyperplasia and hyperkeratosis at the wound-promoted tag site after several months, *HK1.ras* mice (of the 1205 line) typically produce wound-dependent papillomas around 8 weeks after tagging. These papillomas remain benign and are prone to regression if the tag is removed or if given enough time (Greenhalgh et al., 1993a). These mice, therefore, gave an ideal opportunity to study either inhibition of papillomatogenesis or, as it turned out, a role in papilloma conversion, independent of its functioning in p53 protection.

As shown in *Figure 5-1*, the initial bigenic litter produced papillomas on the tagged ear (TGE) similar in size or slightly smaller than the *HK1.ras* monogenic controls. However, in cross-section, these *HK1.ras/K14.stratifin* tumours were found to be pink with a glassy appearance through the centre, unlike the dull, pale appearance of *HK1.ras* papillomas created by their high keratosis content.

With much greater numbers (n>40), it became apparent that two distinct phenotypes were generated by the *HK1.ras/K14.stratifin* genotype. The first was a wound-dependent tumour (termed Type 1) which grew slowly (>8 weeks) and outwardly resembled a small to moderately sized *HK1.ras* papilloma, though different in cross-section (as in *Figure 5-1*). Secondly, a rapidly growing (<2 weeks from initiation) wound-independent tumour (Type 2) which formed either at the tag site or elsewhere on the body, commonly at the tail base where the juvenile hyperplasia and hyperkeratosis common to *HK1.ras* pups did not regress, or areas subject to bite or scratch wounds.

This result recapitulated the two types of DMBA-initiated (*HRAS* activated) papillomas generated followed by TPA treatment in the classic two-stage carcinogenesis SCC model: researchers found that the earliest papillomas to develop were not reliant on continued TPA treatment after initial promotion and were much more likely to convert to SCC following repeated promotion, whereas later emerging papillomas would regress more readily if TPA treatment was halted and converted at a lower rate than the early variety with continued promotion (Hennings et al., 1985).

Similarly, while in *HK1.ras* mice the vast majority of papillomas require prolonged wound-promotion (ear tag) to prevent regression, a small subset of papillomas with more aggressive—though still benign—histology can emerge, induced by a single wounding event (e.g., bite) which do not readily regress over time (Greenhalgh et al., 1993a). The difference in these types has been linked to the dose and type of initiation and promotion agents in chemical carcinogenesis (Ewing et al., 1988); their mutational landscape and epidermal targets (HF or interfollicular stem cells (Type 2) versus transit amplifying cells (Type 1)). Since the frequency of spontaneous Type 2 tumour development seems to be markedly increased in *HK1.ras*/*K14.stratifin* mice (below), this suggests the synergy between Ras and Stratifin activation creates a highly initiated epidermis, similar to SENCAR (sensitive to carcinogenesis) mouse strain (Slaga, 1986).

This also may translate to the level of *HK1.ras* expression in the basal cells, possibly linked to whether stem or transit amplifying cells are the tumour initiation site. It is also possible that other co-operating mutations are present in these persistent papillomas, which further prime them for conversion to carcinomas in the presence of other genetic or chemically promoting factors (Greenhalgh et al., 1993a).

One hypothesis to consider is the role of the immune system in the regression of wound-dependent papillomas. Continual immunosurveillance should ordinarily detect abnormally dividing cells and counter tumour progression; supported by the fact that immunocompromised individuals are at much greater risk of developing SCCs (Hampton, 2005; Bottomley et al., 2019).

However, a pro-inflammatory immune response is also known to be cancer-promoting (Grivennikov et al., 2011) and, as seen in *HK1.fos*/*K14.stratifin* tumours (Chapter 4, *Figure 4-5*), as well as in other models involving the *K14.stratifin* construct (see Chapter 6), this transgene appears to be associated with very high immune infiltration. While the type of immune response observed has not been characterised in-depth, higher numbers of immune cells in the stroma appear to correlate with more aggressive histology in *HK1.ras*/*K14.stratifin* tumours, as was found in *HK1.fos*/*K14.stratifin* fSCCs and which was thought to contribute to the development of these fSCCs in non-wounded skin.

Unlike in *HK1.ras* monogenic controls in which promotion-independent papillomas are rare, *HK1.ras*/*K14.stratifin* mice frequently developed this type of tumour, with approximately half of the 40 mice so far assessed having at least one rapidly-growing tumour on the body or at the tag site. This suggests that *K14.stratifin* expression can co-operate with *HK1.ras* expression in the skin to promote tumorigenesis in certain contexts. Furthermore, in a study of lung adenocarcinoma—in which Stratifin overexpression appears to be a common finding—researchers found that Stratifin associated with ubiquitin-specific protease 8 (USP8) and stabilised receptor tyrosine kinases, such as EGFR, which is upstream of Ras in the canonical MAPK pathway (Kim et al., 2018). Thus, by this mechanism, Stratifin may increase endogenous Ras signalling (as well as the other MAPK pathways) in the basal layer, where *HK1.ras* is only present in around 30% of cells (Greenhalgh et al., 1993a), resulting in a much stronger signal in this proliferative compartment. Furthermore, as shown in *Figure 4-15*, *K14.stratifin* expression results in spurious mK1 expression in hair follicle cells, notably in the stem cells of the bulge, suggesting HK1 is also anomalously expressed in this compartment, as it is sensitive to the same transcriptional promotion signals as mK1 (Rosenthal et al., 1991; Rothnagel et al., 1993). It is known that targeting activated H-Ras to all basal and HF keratinocytes results in aggressive SCC formation at an early stage (Brown et al., 1998), thus, these mechanisms by which *K14.stratifin* is able to elicit both endogenous and exogenous H-Ras activation in proliferative basal and HF cells could help explain the higher incidence of wound-independent Type 2 tumours as well as their rapid growth and aggressive histology.

However, while the aetiology of Type 2 tumours was clearly more aggressive, Type 1 tumours also exhibited histological signs of malignancy (*Figure 5-3A,B*) including increased basal layer proliferation (supported by BrdU labelling, *Figure 5-6C* & Graph), loss of BM integrity and invasion (further explored in *Figure 5-7*), and invariably exhibited a high stromal content which has been associated with poorer prognosis in other carcinomas (Wu et al., 2016). Thus, while exhibiting quite different aetiologies in terms of growth rate, wound-dependence and histological appearance, both Type 1 and Type 2 *HK1.ras/K14.stratifin* tumours do show features of conversion to SCC. This was assessed further using K1 loss as a marker for malignancy (*Figure 5-5*) as was shown previously (Greenhalgh et al., 1993a; MacDonald et al., 2014). It was found that some loss of K1 was evident in Type 1 tumours, mainly from the lower suprabasal layers, though an overall reduction in staining intensity was apparent throughout. Some areas of these Type 1 tumours (such as that highlighted in *Figure 5-5A*) showed greater loss and were indicative of the development of carcinoma *in situ*, while areas of collective invasion (*Figure 5-7A,B*) were also devoid of K1 positivity. Concurrent with the more advanced gross and histological phenotype, Type 2 tumours exhibited far more widespread and complete loss of K1 positivity (*Figure 5-5B*) and were more invasive, with a higher degree of individual cell invasion than in Type 1 tumours (*Figure 5-7C*).

5.9.2. Involvement of the tumour stroma and changes in cellular adhesion in *HK1.ras/K14.stratifin* invasion

Since invasion was found to be common to both *HK1.ras/K14.stratifin* tumour Types, proteins which are implicated in promoting and facilitating this were examined. Stratifin is now well-known to have roles in influencing extracellular matrix remodelling; it is secreted by keratinocytes in the epidermis, binds to the CD13/APN receptor on dermal fibroblasts and upregulates their AP-1 activity to induce production of multiple matrix metalloproteinases (Medina et al., 2007; Ghahary et al., 2005; Ghaffari et al., 2006; Ghaffari et al., 2010; Lai et al., 2011). In the process of wound-healing, this is very useful in reducing fibrosis and improving the healing process, but in the context of carcinogenesis, it is ideal for increasing invasion and promoting

the development of cancer-associated fibroblasts (CAFs) (Kalluri & Zeisberg, 2006). CAFs can mediate keratinocyte movement into the dermis through paracrine signalling, direct mechanical interaction, alterations to the stroma structure and chemical signalling environment (Räsänen & Vaheri, 2010; Glentis et al., 2017).

Furthermore, Stratifin has been identified at the invasive front in multiple carcinomas, which has been correlated with an upregulation in Tenascin-C (TEN-C) expression in the stroma (Ide et al., 2007). Higher TEN-C expression in tumours has been implicated in more active tumour invasion as well as a prognostic marker of recurrence and metastasis (Jahkola et al., 1998; Cai et al., 2017; Sun et al., 2019). Thus, TEN-C expression was analysed in both Type 1 and Type 2 *HK1.ras*/*K14.stratifin* tumours, using *HK1.ras* papillomas as benign, non-invasive controls (*Figure 5-9*). In both types of *HK1.ras*/*K14.stratifin* tumour, TEN-C expression was moderate to strong throughout the tumour area, while the benign *HK1.ras* papilloma exhibited much weaker staining with some sporadic moderate staining around parts of the dermo-epidermal junction. Only the histologically normal and mildly hyperplastic adjacent ear tissue in the Type 1 *HK1.ras*/*K14.stratifin* tumour exhibited weak staining, again with some positivity at the dermo-epidermal junction, akin to the staining pattern in normal skin (Midwood et al., 2016). This highlights both the wound-dependency of the Type 1 tumours (since tissue farther from the tag was much less phenotypic), and the role of the activated stroma in the invasion which is common to all *HK1.ras*/*K14.stratifin* tumours.

In these bigenic *HK1.ras*/*K14.stratifin* mice, multiple modes of tumour cell invasion were evident on histological examination. Collective cell invasion was most commonly observed in Type 1 tumours but was also seen in Type 2, while the trend was reversed with regards to individual cell invasion which appeared more commonly in aggressive Type 2 tumours (*Figure 5-7*). Collective cell invasion, perhaps surprisingly, requires the maintenance of cell-cell adhesion, thus E-cadherin—a key component of adherens junctions—is often retained in these projections (Krakhmal et al., 2015; Hesse et al., 2016), but must be lost to facilitate individual cell invasion. Collectively invading cells may be aided by CAFs; thus, they do not require mutations or gene expression

changes which allow them to navigate the BM and stroma themselves (Gaggioli et al., 2007; Glentis et al., 2017). Indeed, CAF-mediated invasion may actually require E-cadherin in the cancer cells, as one study showed that adhesion between E-cadherin present in cancer cells (derived from vulvar SCC) formed adhesions with N-cadherin in CAFs, allowing the fibroblasts to mechanically guide the SCC keratinocytes to invade a surrounding matrix (Labernadie et al., 2017). This, therefore, may allow invasion to occur at an earlier stage in tumorigenesis before further accumulation of mutations has occurred that allow escape from anoikis and therefore individual amoeboid or spindle cell invasion. Reduction in E-cadherin at the plasma membranes, along with reduction in K14 expression (*Figure 5-8A,B,C*) is associated with a shift towards individual cell invasion and a more aggressive SCC phenotype including epithelial-mesenchymal transition (Hesse et al., 2016).

5.9.3. Expression of p53 and p21 and p53 ablation in *HK1.ras/K14.stratifin* tumours

Given the relationship between Stratifin and p53 regulation, IHC was performed to assess the p53 expression in Type 1 and Type 2 *HK1.ras/K14.stratifin* tumours compared with *HK1.ras* papillomas (*Figure 5-10*). Previous results showed that loss of p53 was correlated with conversion to wdSCC in *HK1.ras/fos-Δ5Pten* multistage carcinogenesis (MacDonald et al., 2014), while in *HK1.fos/K14.stratifin* fSCCs, p53 expression persisted throughout carcinogenesis, fading only in advanced tumours (Chapter 4, *Figure 4-9*). This latter result was most likely due to the high level of Stratifin expression from the *K14.stratifin* transgene, but clearly did not confer protection from tumorigenesis, thus it was concluded that antagonism of its TSG roles occurred downstream. Here, it was hypothesised that a similar protection of p53 may occur in *HK1.ras/K14.stratifin* tumours, although similarly failing to prevent generation or conversion of tumours to SCC. IHC staining showed that this was indeed the case, with both Type 1 and Type 2 tumour variants exhibiting strong nuclear p53 staining in multiple layers of the epidermis, contrasted with the more moderate staining in *HK1.ras* papillomas where it was almost exclusively confined to basal layer cells (*Figure 5-10A,B vs G*). Unlike in

HK1.fos/*K14.stratifin* fSCC, the expression of p53 in advanced Type 2 *HK1.ras*/*K14.stratifin* tumours did not show signs of fading.

Since presence of p53 did not confer an anti-tumour effect in this genotype, one of its major downstream effectors, p21, was also assessed to identify possible differences between Type 1 and Type 2 *HK1.ras*/*K14.stratifin* SCCs. Here, there was a striking difference in p21 localisation, with only Type 1 tumours exhibiting nuclear staining, which followed the pattern of p53 expression, whereas in Type 2 tumours p21 was excluded from the nucleus, showing only cytoplasmic staining in most cells (*Figure 5-10C vs D*). In order to perform its functions in cell cycle arrest, p21 must be localised to the nucleus, thus this discrepancy between the two Types could help to explain the higher mitotic index (*Figure 5-6*) and more aggressive tumour aetiology. This is also interesting since Stratifin has previously been shown to support the functions of p21 in its TSG roles, antagonising cell cycle progression by binding CDK4/6 at G1/S and the Cdc2/cyclin B1 complex at G2/M (Laronga et al., 2000). Here, however, much like p21 its expression is almost exclusively cytoplasmic (*Figure 5-4*), perhaps explaining the lack of tumour suppressive functions seen in these *K14.stratifin*-expressing tumour models.

To elucidate possible reasons for this p21 cytoplasmic localisation, expression of pAkt1^{ser473} was assessed by immunofluorescence analysis, since Akt can prevent nuclear localisation of p21 via phosphorylation (Zhou et al., 2001). However, expression of pAkt1^{ser473} was found to be expressed to a greater degree in Type 1 tumours than in Type 2 and was primarily expressed in suprabasal cells (*Figure 5-11*) possibly more indicative of its roles in the terminal differentiation process than in proliferation (Calautti et al., 2005). This is contrary to the pdSCCs generated in *HK1.ras*/*fos-Δ5Pten* mice following p21 loss, wherein pAkt^{ser473} is strongly expressed (though absent in the earlier wdSCC stage) (MacDonald et al., 2014). The lack of pAkt^{ser473} in suprabasal cells of Type 2 *HK1.ras*/*K14.stratifin* tumours may also explain the development of "ghost cells" found on histology in many examples of this tumour type (*Figure 5-3C,D*), as Akt1 is required for proper nuclear degradation in the normal cornification process (Naeem et al., 2015). Another, related, protein possibly implicated in the carcinogenesis process which has not been analysed yet is mTOR, which

Stratifin is able to upregulate through an interaction involving keratin 17 in the cytoplasm directly, without involvement of Akt (Kim et al, 2006).

To further explore the involvement of p53 in this system, a Cre-mediated gene-switch was employed to induce p53 ablation as in *HK1.fos*/*K14.stratifin* mice in Chapter 4. As explained above, when p53 is ablated in *HK1.ras* mice (prior to papilloma formation), papillomas paradoxically fail to form despite wound-promotion (Greenhalgh et al., 1996); a finding which has been repeated in both knockout and inducible Cre-mediated excision models (Greenhalgh et al., unpublished) and was repeated in this study as control *K14.ras.p53*$^{flx/flx}$ mice exhibited only mild hyperplasia (*Figures 5-12 and 5-13I*). Given the co-operation between *HK1.ras* and *K14.stratifin* to produce malignant tumours, it was hypothesised that *K14.stratifin* expression may subvert the paradoxical tumour-inhibitory effect of p53 knockout.

The majority of *K14.ras.p53*$^{flx/flx}$*.stratifin* mice did not develop overt tumours, though the hyperplasia at ear tag was noticeably more inflamed than in *K14.ras.p53*$^{flx/flx}$ controls (*Figure 5-12*). Histological examination showed that *K14.ras.p53*$^{flx/flx}$*.stratifin* hyperplasias had a high level of immune cell infiltration, abundant stroma, and were clearly invasive despite the lack of a benign tumour stage. These data further support the unusual paradoxical requirement for p53 competency to develop a benign *HK1.ras*-driven papilloma and indicate that the invasion and immune cell recruitment seen in *HK1.ras*/*K14.stratifin* tumours are unconnected to their strong p53 expression. In gastric and pancreatic cancer studies where high Stratifin expression was observed, it was noted that the abundance of p53 and Stratifin were not correlated with one another (Neupane & Korc, 2008; Mühlmann et al., 2010), indicating that in these cases of human carcinomas in which Stratifin appears to be oncogenic, its functions are also uncoupled from the role it plays in p53 upregulation, as observed here.

5.9.4. Keratin 1 and 10 expression differs between Types 1 and 2

In Chapter 4, aberrations in Keratin filament expression, and both tissue and cellular localisation were found in *HK1.fos*/*K14.stratifin* fSCCs. The

perinuclear collapse of Keratin 14 (Chapter 4, *Figure 4-20*) was not apparent in any *HK1.ras*/*K14.stratifin* tumour and thus appears to be a unique aspect of *HK1.fos*/*K14.stratifin* carcinogenesis. However, aberrant basal layer and follicular Keratin 1 expression was also observed in *HK1.ras*/*K14.stratifin* hyperplasias and carcinomas, indicating this to be a common feature in mice expressing the *K14.stratifin* construct.

Therefore, as in Chapter 4, co-localisation of Keratin 1 and Keratin 10 was analysed by fluorescence analysis and quantified using the *Colocalisation Threshold* ImageJ plugin (*Figures 5-15 & 5-16*). Here, a discrepancy in the localisation of K1 and K10 expression between tumours designated Type 1 and Type 2 based on histology, mitotic index, and Keratin 1 expression was found.

Type 1 *HK1.ras*/*K14.stratifin* immunofluorescence exhibited a mottled appearance in full colour images, which suggested a reduction in co-localisation compared with *HK1.ras* papillomas which were more uniformly yellow due to consistent red/green overlap. However, Colocalisation Threshold analysis showed that the co-expression of these keratins was very good in terms of spatial distribution (*Figure 5-16 Panel I A*), thus, the fluctuations seen in *Figure 5-15A* are likely to be tied to a difference in the level of expression, with Keratin 1 exhibiting a lower intensity in most of the tumour than K10. This perhaps reflects the slight differences in their timing and mechanism of transactivation in normal skin, with AP-1 TFs important in *KRT1* activation, while AP-2 is implicated in *KRT10* transcription. AP-1 is directly downstream of Ras-MAPK, thus its abundance is likely altered in *HK1.ras*-mediated tumorigenesis, while AP-2 is regulated by stress response pathway proteins and retinoic acid and has primarily pro-differentiation and pro-apoptotic roles (Lüscher et al., 1989; Wajapeyee et al., 2006). This difference could help to account for the evidently higher Keratin 10 expression in Type 1 *HK1.ras*/*K14.stratifin* tumours, while the loss of K1 causes a greater inflammatory response (Roth et al., 2012), contributing to the evident immunogenicity of all *K14.stratifin*-expressing tumours.

Keratin 10 is also an antagonist of Akt (Paramio et al., 2001), possibly contributing to the patchy Akt expression in Type 1 tumours and negligible

staining in Type 2, especially in areas where K10 was retained while K1 was lost (*Figures 5-11 & 5-16 Panel I*). Expression of K10 is not ubiquitously higher in all Type 2 tumours, however, with some (*Figure 5-16C*) showing strong K10 staining in the absence of K1, while others (*Figure 5-16E*) exhibiting a more even total expression of each protein, albeit with very poor co-localisation. As in *HK1.ras* Type 2 papillomas (Greenhalgh et al., 1993a), this may occur due to differences in other mutations which have occurred in the skin to facilitate wound-independent growth of these tumours or could reflect the initiating cell type. Activated Akt1 expression was previously seen to increase during progression of *HK1.ras/fos-Δ5Pten* wdSCCs to pdSCC following loss of p21 (Macdonald et al., 2014) and Stratifin (Chapter 3) expression.

Both Pearson's correlation coefficients and Manders thresholded overlap coefficients were obtained for the K1/K10 co-localisation data, showing a clear distinction between *HK1.ras* papilloma controls and Type 2 *HK1.ras/K14.stratifin* tumours (Pearson's $p < 0.001$), with a similar difference between Types 1 and 2 observed. Conversely, no significant change in localisation between Type 1 tumours and *HK1.ras* papilloma controls was found (*Figure 5-16* Panel II), though further study is needed to probe the reasons for the discrepancy in the relative expressions of these partner keratins in Type 1 tumours. These data further support the hypothesis that Type 1 and Type 2 tumours are different entities which share some common histological features (e.g., inflammation and invasion) due to the expression of *HK1.ras* and *K14.stratifin* genes, though other factors, including spontaneous mutations or changes to gene expression/protein degradation are likely to play a role in the different aetiologies observed.

5.9.5. Future directions

From extensive previous research using DMBA/TPA chemical carcinogenesis and transgenic Ras activation using the HK1 promoter, it has been established that H-Ras activation is an initiating event which primes the skin for tumorigenesis when subjected to wound, genetic (e.g., Fos activation or Pten ablation), or chemical promotion (e.g., TPA). Here, it was found that spontaneous, aggressive tumours formed in *HK1.ras/K14.stratifin* mice at much

greater frequency than is observed in *HK1.ras* mice, suggesting that Stratifin overexpression in proliferative cells acts as a novel promoting agent. Given the large number of proteins which Stratifin activity is known to modify, these tumours would ideally be analysed using transcriptomic and proteomic analyses to further explore pathways involved in this model of carcinogenesis. This approach could allow identification of the mechanisms of promotion and potentially elucidate novel interactions which may, in turn, identify novel therapeutic targets applicable to both skin and internal carcinomas involving Stratifin activation.

Additionally, differences in the precise cells in which *HK1.ras* is expressed (Greenhalgh et al., 1993a; Brown et al., 1998) may be important in the generation of spontaneous/wound-independent carcinomas in conjunction with *K14.stratifin* expression. For example, hair follicle cells which normally do not express the HK1 constructs have been found to express mK1 when *K14.stratifin* is expressed, leading to the hypothesis that *HK1.ras* is spuriously expressed in these cells in *HK1.ras*/*K14.stratifin* mice. This could be investigated using *in situ* hybridisation (ISH) to detect *HK1.ras* mRNA transcripts, which differ slightly from mouse c-H-Ras as the construct is based on v-H-Ras (which additionally contains an HK6 tag). Recently, a technique has been described which allows for exon-specific RNA ISH to be performed reliably, such that even sequences which have a high degree of homology, such as splice-variants, are distinguishable from one another, making this a more feasible tool to use in this application than may otherwise have been possible (Guo et al., 2018). Alternatively, probes detecting intron-specific pre-mRNA sequences may be a useful alternative (Gainer et al., 2016), as more sizeable differences exist in these regions of the transgenic versus cellular transcripts.

In addition, the reasons for the discrepancy between wound-dependent Type 1 *HK1.ras*/*K14.stratifin* and Type 2 aggressive, spontaneous SCCs is presently unknown and requires further study. Since the mice used in this study are outbred, it is possible that differences in the genetic or epigenetic background of individuals contributes to the two different phenotypes observed, with differences in the immune responses also possibly playing a role. Here proteomic analysis is almost certainly necessary to elucidate this mechanism and

again these stage specific tumours provide an ideal opportunity to apply these techniques. Moreover, this approach may shed light on the so-called "p53 paradox" where loss clearly inhibits wound-associated papillomatogenesis in the HK1.ras model (Greenhalgh et al., 1996) an effect that continues in the *HK1.ras/K14.stratifin* model. Thus, despite presence of exogenous elevated Stratifin, it apparently failed to overcome this intriguing phenotype of paradoxical p53 loss. Indeed, as outlined above in *HK1.fos/K14.stratifin* tumorigenesis p53 ablation had no discernible effect on fSCC tumorigenesis (despite high abundance of the protein in the wild-type tumours). Here proteomic analysis is almost certainly necessary, as no clear reasoning for p53 ablation to result in tumour suppression is evident from its known functions.

Furthermore, as for *HK1.fos/K14.stratifin* tumorigenesis, the impact of p21 knockout is ongoing and, unlike the paradoxical tumour suppressive effect of p53 ablation, preliminary results show development of more rapid, larger *HK1.ras/K14.stratifin/p21*$^{-/-}$ SCC (Appendix 2; *Figure S3*). This seems consistent with *HK1.ras/fos-Δ5Pten* carcinogenesis, where both p21 and Stratifin persisted beyond p53 loss yet became lost in aggressive TPA-promoted SCC concomitant with high levels of uniform AKT activation (Appendix 1; McMenemy et al., in preparation *Figure 6*), thus, analysis of the AKT/mTOR pathways are a logical future step. This also appears to fit with the observations that aggressive Type 2 *HK1.ras/K14.stratifin* tumours lacked nuclear p21 staining, while less aggressive Type 1 tumours showed strong nuclear localisation (*Figures 5-10 & 5-11*). Finally, to assess whether p21 maybe responsible in part to compensate for p53 loss resulting in a lack of papillomas *K14.ras.p53*$^{flx/flx}$*.stratifin*, breeding is ongoing to create the *K14.ras.p53*$^{flx/flx}$*.stratifin.p21*$^{-/-}$ compound genotype in another attempt to solve the "p53 paradox".

5.9.6. Conclusions

Co-expression of activated H-Ras alongside Stratifin overexpression in skin results in two distinct tumour phenotypes of different aggressiveness but which both exhibit indicators of malignant conversion and invasion. Type 2 tumours are often spontaneously generated, suggesting Stratifin is a promoting agent in skin,

similar to the effects of TPA-treatment in classic 2-stage chemical carcinogenesis. The reasons for the different phenotypes remain to be elucidated but may lie in the expression of H-Ras in different stem cell niches.

Chapter 6 Ablation of tumour suppressors p53 and Pten in *K14.stratifin* skin

6.1. Introduction

In Chapters 4 and 5, p53 expression was seen to be high in both *HK1.fos*/*K14.stratifin* and *HK1.ras*/*K14.stratifin* tumours, despite histological signs of carcinoma development and loss of differentiation marker keratin K1, again indicative of malignancy. This contrasted with the findings of p53 loss in *HK1.ras*/*fos-Δ5Pten* carcinogenesis; indeed, when p53 function was ablated in *HK1.fos*/*K14.stratifin* mice, the resultant phenotype was indistinguishable from those which were p53 competent. In addition, whilst in *HK1.ras*/*K14.stratifin* mice tumours no longer formed in the same way as in the p53 wild-type counterparts, histological analysis identified the beginnings of widespread invasion in these hyperplasias, despite the lack of tumour formation. This latter observation suggested the lack of p53 still prevented *HK1.ras*-derived papilloma formation, as documented previously (Greenhalgh et al., 1996). However, this genetic combination appeared to create a context which bypassed the intermediate benign stage and elicited progression to malignant invasion.

Stratifin has a well-known role in protection of p53 by inhibiting its main antagonist, the E3 ubiquitin-ligase Mdm2, from tagging it for degradation (Lee & Lozano, 2006). This interplay likely explains why an abundance of p53 was seen in both *HK1.fos*/*K14.stratifin* and *HK1.ras*/*K14.stratifin* carcinogenesis (Chapter 4 *Figure 4-9* and Chapter 5 *Figure 5-10*). However, more complexity in the system is evident, given the uncoupling of p53 expression from tumorigenesis in *HK1.fos*/*K14.stratifin* mice, and the apparent requirement for p53 to be present in order to form *HK1.ras*/*K14.stratifin* tumours. Here, *K14.p53$^{flx/flx}$.stratifin* mice were generated to further investigate the effect of Stratifin overexpression separate to its interaction with p53, without the added complexity of an activated oncogene (Fos or Ras) to drive tumorigenesis.

Furthermore, to assess the possible tumour suppressive or tumour promoting effects of *K14.stratifin* expression in the context of a deregulated PI_3K/Akt pathway, *K14.Pten$^{flx/flx}$.stratifin* mice were created. Stratifin itself is known to be a direct inhibitor of Akt activity (Chalhoub & Baker, 2009), thus, taken in isolation, its overexpression on a Pten-null background was hypothesised to potentially rescue the phenotype, at least partially. However,

the plethora of other roles of Stratifin in cell cycle regulation, cell-cell adhesion, matrix remodelling, and differentiation obviously complicate this simplistic hypothesis. In particular, both Pten and Stratifin dysregulation are known to cause hair follicle defects (Herron et al., 2005; Hammond et al., 2012; Suzuki et al., 2003) and, in the case of Pten, benign tumours (trichilemmoma; Brownstein et al., 1979; Liaw et al., 1997). Additionally, previous work using this model for Pten exon 5 ablation found, unexpectedly, that Akt1 expression did not immediately increase following Cre-mediated excision (MacDonald et al., 2014). This was believed to be due to antagonism by p21 upregulation, with lack of Akt1 activity being linked to an increase in mTOR activity (downstream of Akt) which, with Mdm2, bypassed the compensatory p53/p21 increase to elicit the hyperplastic and hyperkeratotic phenotype observed (MacDonald et al., 2011).

Finally, *K14.stratifin* was expressed in a combined Pten-null/p53-null background. The *K14.p53*$^{flx/flx}$*.Pten*$^{flx/flx}$ genotype, with loss of function of two major TSGs, should prime the keratinocytes for oncogenesis, though alone it produces a surprisingly mild phenotype: a testament to the resilience of skin to transformation. Here, therefore, *K14.stratifin* overexpression was included in the genotype to assess whether it would produce oncogenic effects in this context, or if some of its known tumour-suppressive roles would maintain the benign phenotype.

The main aims of this chapter were to: assess any phenotype which arose from the overexpression of Stratifin in conjunction with p53 loss, separate to Fos or Ras expression, given the close relationship between these proteins and the unusual findings in the previous chapters regarding p53 expression and ablation; assess phenotypic changes in the Pten ablation model when Stratifin is overexpressed and use immunostaining to identify protein changes which may be relevant to the aetiology observed; combine these tumour suppressor ablation models with Stratifin overexpression to further assess its oncogenic potential in the absence of major TSGs.

6.2. *K14.p53$^{flx/flx}$.stratifin* mice developed invasive hyperplasia at ear tag but not overt tumours

In Chapter 1, the positive feedback loop between p53 and Stratifin expression was described in detail (*Figure 1-9*). In both *HK1.fos*/*K14.stratifin* and *HK1.ras*/*K14.stratifin* tumours, p53 was found to be very highly expressed, even in clearly malignant areas of the tumours, indicative of the protective effect of Stratifin (Lee & Lozano, 2006). However, p53 activity seemed to be uncoupled from *HK1.fos*/*K14.stratifin* tumorigenesis, with no change in the phenotype elicited by p53 ablation compared with p53 competent tumours. In *K14.ras.p53$^{flx/flx}$.stratifin*, while p53 ablation paradoxically prevented overt tumour formation—itself a counter-intuitive finding—malignant conversion occurred in the resultant hyperplasias, with extensive invasion evident.

To investigate the effects of *K14.stratifin* overexpression separately from oncogene expression and also separate to any effects elicited by the elevated expression of p53 observed, *K14.stratifin* mice were crossed with mice harbouring floxed p53 alleles as described in Chapter 4, with either inducible (*K14.CrePR1*) or consitutive (*K5.CreP*) Cre-recombinase to excised the floxed exons (*n*=22 and 4, respectively). Of those, none developed tumours (either wound-promoted or spontaneous), though all developed some degree of hyperplasia at the tag site. This hyperplasia was, in many cases, not grossly distinct from control mice (*Figure 6-1*).

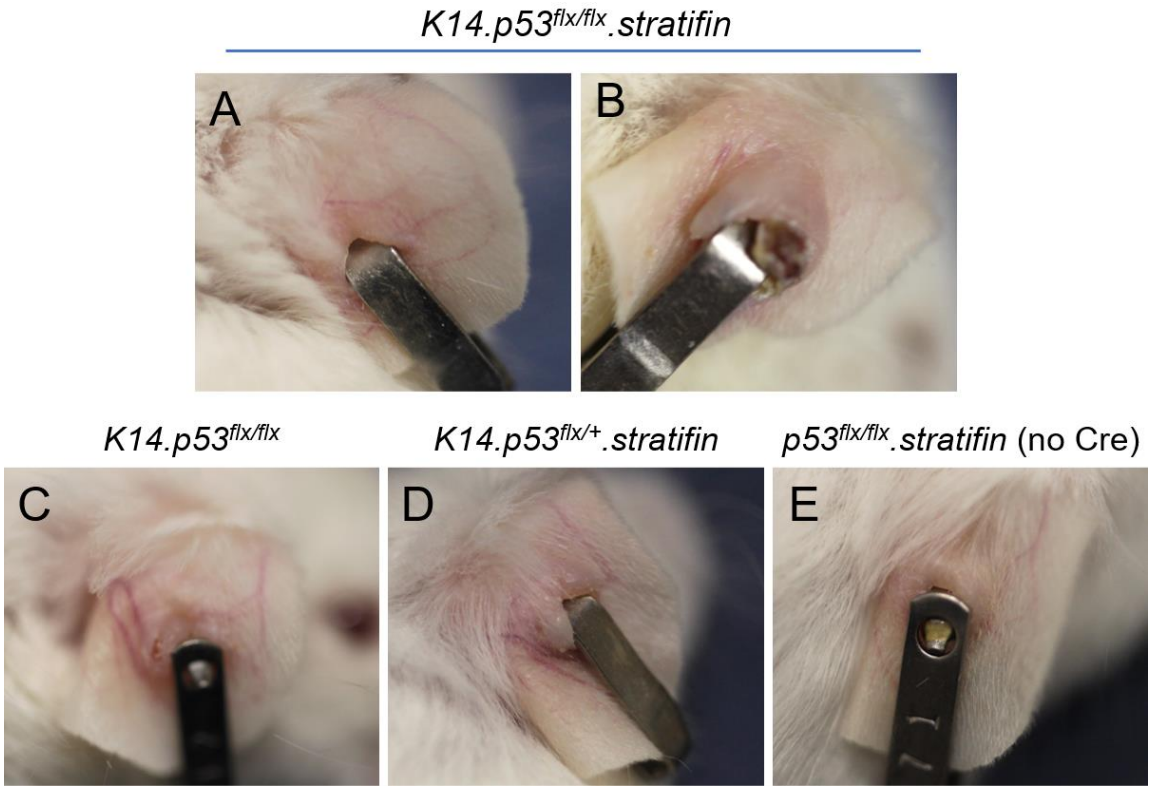

Figure 6-1: *K14.p53$^{flx/flx}$.stratifin* mice do not develop tumours but localised hyperplasia at the tag site.
(**A**) *K14.p53$^{flx/flx}$.stratifin* TGE with minor hyperplasia at tag site. (**B**) *K14.p53$^{flx/flx}$.stratifin* TGE showing greater hyperplasia surrounding a scabbed wound at the tag. (**C**) Age-matched *K14.p53$^{flx/flx}$* mouse showing slightly thickened skin at tag, similar to (**E**) *K14.p53$^{flx/+}$.stratifin* and (**F**) *p53$^{flx/flx}$.stratifin* (no Cre control) tagged ears. All mice pictured are 20-weeks-old and received RU486 treatment 3 times. *K5.p53flx/flx.stratifin* mice produced identical results (not shown).

The lack of appreciable difference in the appearance of *K14.p53$^{flx/flx}$.stratifin* (*n*=22), *K14.p53$^{flx/+}$.stratifin* (*n*=8), *K14.p53$^{flx/flx}$* (*n*=12), or *p53$^{flx/flx}$.stratifin* (*n*=7; no Cre control) cohorts suggested that *K14.stratifin* expression had little impact on the p53-null background, either from inducible ablation in adults or throughout development in *K5.p53$^{flx/flx}$.stratifin* individuals.

However, histological examination of these hyperplasias showed that *K14.p53$^{flx/flx}$.stratifin* skin displayed more pronounced hyperplasia, extensive dysplasia, hyperchromatic nuclei in proliferative cells, and the beginnings of widespread invasion (*Figure 6-2A-C*). In contrast, *K14.p53$^{flx/flx}$* epidermis was not found to be greatly hyperplastic, with only occasional thickened areas seen at the tag site mainly due to increased stromal thickness. In this regard, whilst *K14.p53$^{flx/flx}$.stratifin* showed a similar degree of stromal depth increase, measured from the average level of the basement membrane to that of the ear cartilage (*Figure 6-2A; bracket*). The immune cell recruitment was much greater in *K14.p53$^{flx/flx}$.stratifin* TGE skin compared with non-*K14.stratifin* controls (*Figure 6-2A-C vs D*), as seen in *HK1.fos*/*K14.stratifin* and *HK1.ras*/*K14.stratifin* phenotypes previously.

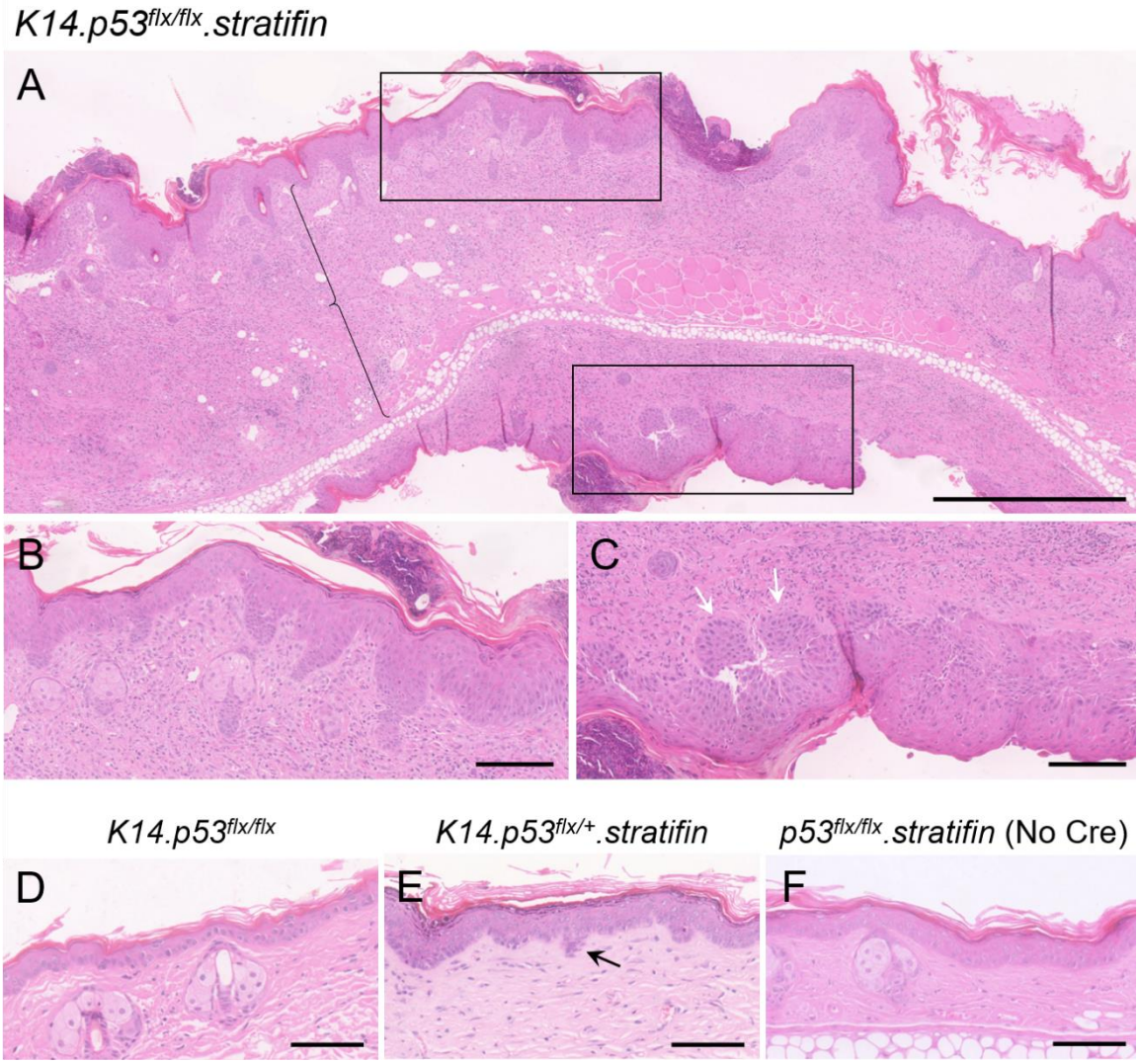

Figure 6-2: *K14.p53$^{flx/flx}$.stratifin* wound-promoted skin exhibits epidermal and dermal hyperplasia and keratinocyte invasion.
(**A**) *K14.p53$^{flx/flx}$.stratifin* TGE (20 wks.; RU486 x3) showing hyperplastic epidermis and greatly increased stromal depth (epidermis to ear cartilage; bracket, **{**). The epidermis shows signs of invasion, indicated in boxed areas highlighted in **B** and **C**. (**B**) Collectively invading cells are evident at several points. (**C**) Right of picture shows total loss of differentiation and invasive spread into the stroma. Also highlighted (white arrows) are the very hyperchromatic nuclei common in this genotype. Age-matched controls: (**D**) *K14.p53$^{flx/flx}$* TGE showing relatively normal appearance, though basal layer nuclei appear somewhat hyperchromatic. (**E**) *K14.p53$^{flx/+}$.stratifin* slightly hyperplastic and dysplastic epidermis with more pronounced granular layer than other genotypes, showing some signs of becoming invasive (arrow), though less pronounced than in **A**. (**F**) *p53$^{flx/flx}$.stratifin* no Cre control displaying mild hyperplasia associated with *K14.stratifin* expression by this time point (5 months) without hyperkeratosis or hyperchromatism associated with p53-null genotypes. *Scale bars: **A** approx. 500 µm; **B**-**F** approx. 100 µm*.

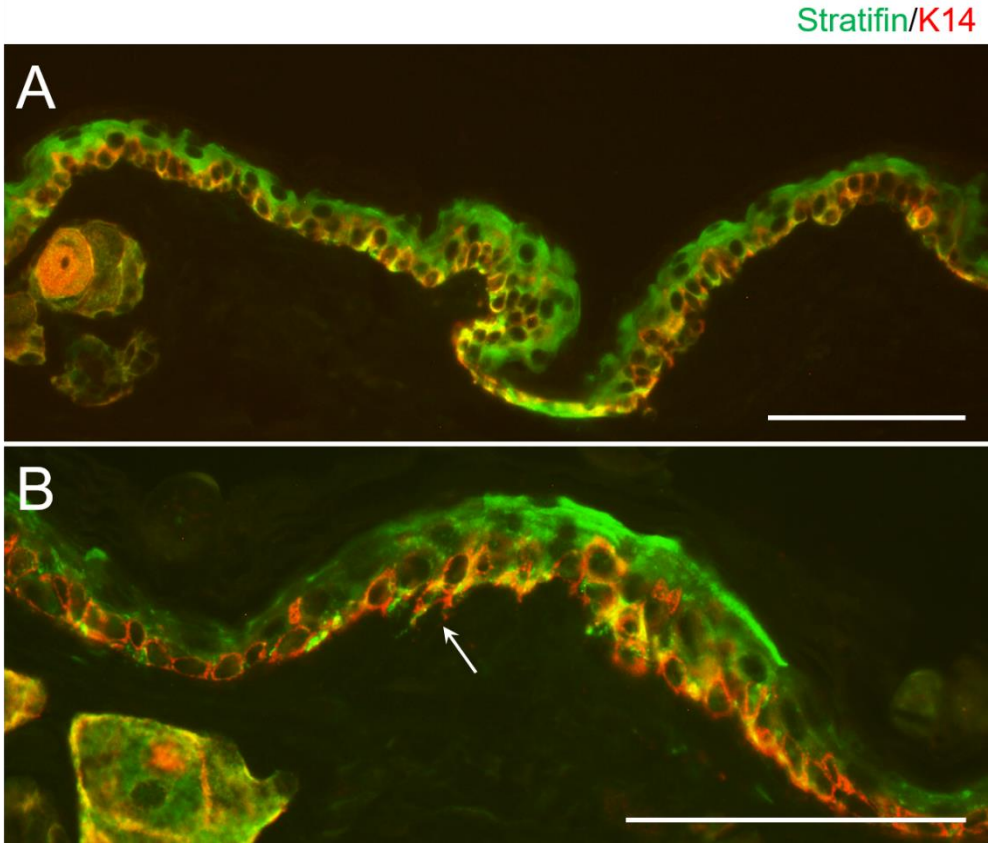

Figure 6-3: Stratifin is strongly expressed in *K14.p53$^{flx/flx}$.stratifin* skin, including in invading cells.
(**A**) Strong Stratifin expression (green) is apparent throughout the *K14.p53$^{flx/flx}$.stratifin* epidermis (16 wks.), indicated by yellow colour where it is co-expressed with the K14 counterstain (red). (**B**) Higher magnification (x400) highlights invasive cells expressing Stratifin (white arrow) despite early-stage hyperplasia.

6.3. *K14.Pten$^{flx/flx}$.stratifin* mice displayed an exacerbated *K14.Pten$^{flx/flx}$* phenotype and produced carcinoma without tumour formation

Mice harbouring inducible Cre-recombinase to excise floxed Pten exon 5 (*K14.Pten$^{flx/flx}$*; alternatively, *K14.PtenΔ5*) have been studied extensively in our ICR mouse background. Alone, *K14.Pten$^{flx/flx}$* mice have been found to develop mild epidermal hyperplasia and hyperkeratosis, mimicking the skin pathologies associated with Cowden Syndrome; a familial cancer predisposition syndrome primarily caused by defects in the *PTEN* gene and resulting in benign hamartomas, but with a significantly increased risk of aggressive internal carcinomas in adults (Gammon et al., 2016). In conjunction with *HK1.fos* expression, the resultant phenotype induced a compensatory burst of p53 and

p21 that switched proliferation to one of differentiation, which recapitulated aetiology of keratoacanthomas (KAs) (Yao et al., 2008), a type of benign skin tumour which is often difficult to distinguish on histological examination from carcinoma *in situ,* but which regresses over time, unlike carcinoma (Ko, 2010).

To investigate the effects of elevated Stratifin expression on the *Pten*-null phenotype, *K14.stratifin* were crossed with *K14.Pten$^{flx/flx}$* mice, generating *K14.Pten$^{flx/flx}$.stratifin* (*n*=19), *K14.Pten$^{flx/+}$.stratifin* (*n*=7), *K14.Pten$^{flx/flx}$* (*n*=9), *K14.Pten$^{flx/+}$* (*n*=5), as well as controls lacking *Cre*-recombinase.

K14.Pten$^{flx/flx}$.stratifin mice were found to develop similar macroscopic features to their *K14.Pten$^{flx/flx}$* counterparts, including a generally scruffy appearance of the coat, as well as ear hyperplasia and keratosis. However, these effects were far more pronounced in the ears of the *K14.Pten$^{flx/flx}$.stratifin* mouse (*Figure 6-4A, B*) which were clearly far more hyperplastic and hyperkeratotic at 15 weeks than the *K14.Pten$^{flx/flx}$* littermate (*E, F*). Indeed, the phenotype of *K14.Pten$^{flx/flx}$* mice more closely resembled that of *K14.Pten$^{flx/+}$.stratifin* with regards to the wound-promoted skin of the tagged ear—though *K14.Pten$^{flx/+}$.stratifin* produced a less pronounced fur phenotype than *Pten*-null mice overall (*Figure 6-4C,D* vs *E,F*). These results suggested that overexpression of Stratifin in *K14.Pten$^{flx/flx}$* mice exacerbated the gross phenotypic effects of total Pten deficiency in the skin.

Subsequently, histology of *K14.Pten$^{flx/flx}$.stratifin* skin was analysed and compared with that of *K14.Pten$^{flx/flx}$*. Not only did this confirm an exacerbation of the benign hyperproliferative and hyperplastic phenotype, but identified features consistent with carcinoma development, including poorly defined strata and loss of BM integrity, leading to individual cell invasion (*Figure 6-5A,B*). By contrast, *K14.Pten$^{flx/flx}$* hyperplasia (and that of *K14.Pten$^{flx/+}$.stratifin*) was noticeably milder and stratification was largely maintained, with a clearly visible granular layer that is largely absent in *K14.Pten$^{flx/flx}$.stratifin* (*Figure 6-5E,F vs A,B*). Inflammation in *K14.Pten$^{flx/flx}$.stratifin* skin was also found to be much greater (*Figure 6-5A,B*), as had been hinted at by the reddening of both the TGE and NTE of these mice compared to littermates lacking *K14.stratifin* expression (*Figure 6-4A,B vs E,F*).

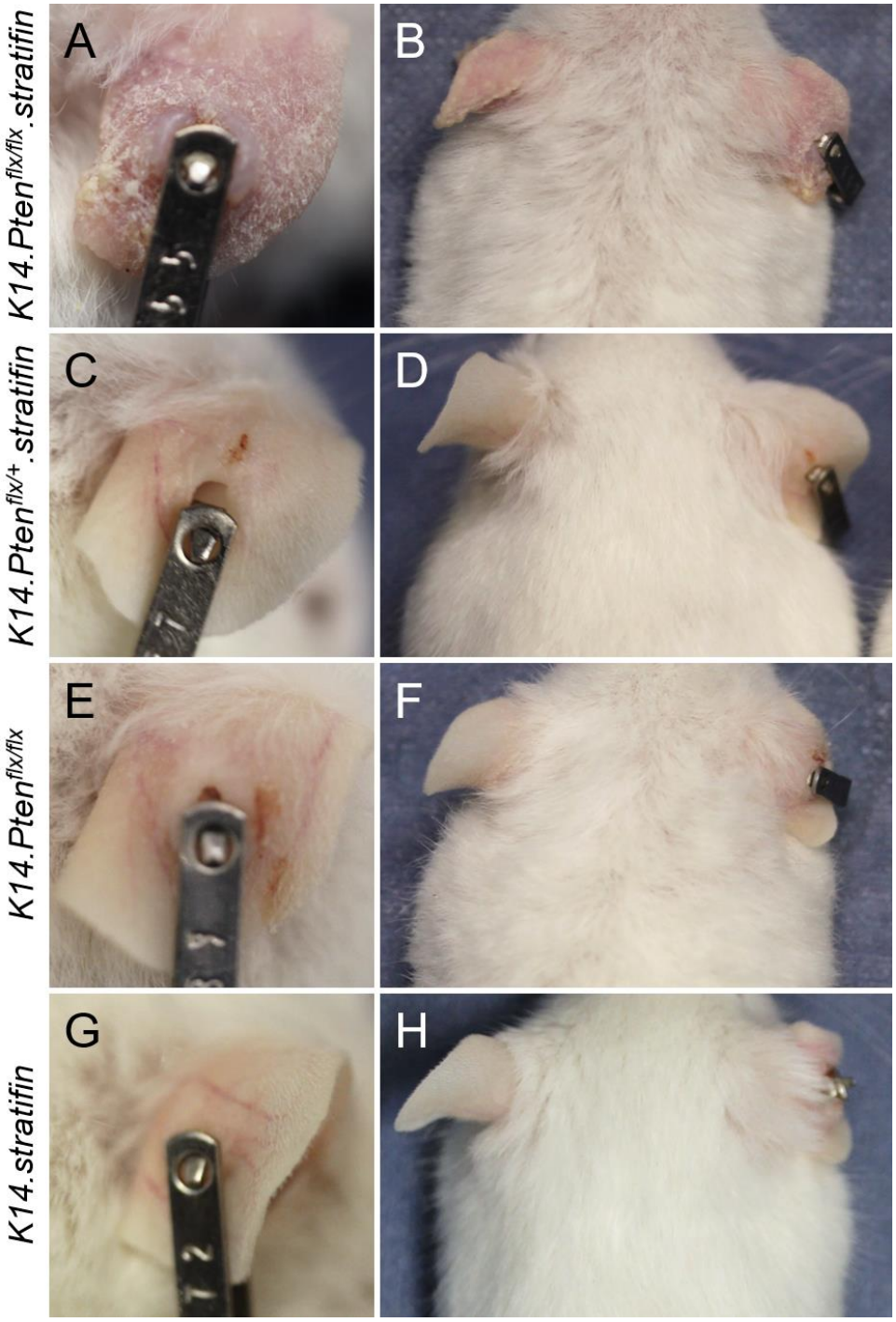

Figure 6-4: Expression of *K14.stratifin* strongly exacerbates the *K14.Pten*$^{flx/flx}$ gross phenotype.
(**A**) *K14.Pten*$^{flx/flx}$*.stratifin* TGE (15 wks.) showing obvious hyperplasia and keratosis over the whole ear surface, with particularly hyperplastic skin close to the tag site (**B**) Overview of the same mouse showing a similar hyperplasia and hyperkeratosis is present without wound-promotion on the NTE, and a generally thin and scruffy appearance to the fur, with skin visible over the crown of the head. (**C**) *K14.Pten*$^{flx/+}$*.stratifin* (21 wks.), showing much more mild hyperplasia at tag and very little keratosis (**D**) Overview of mouse in **B**, showing grossly normal NTE and no apparent hair phenotype present. (**E**) *K14.Pten*$^{flx/flx}$ mouse (15 wks.) with almost identical TGE phenotype as in **C** (**F**) Overview of mouse in **E** shows some mild keratosis at the base of the NTE and a generally scruffy appearance to the coat. (**G**) *K14.stratifin* mouse showing slight hyperplasia at tag, with little to no visible keratosis present. (**H**) Overview of *K14.stratifin* mouse (15 wks.) showing normal fur and no NTE phenotype present.

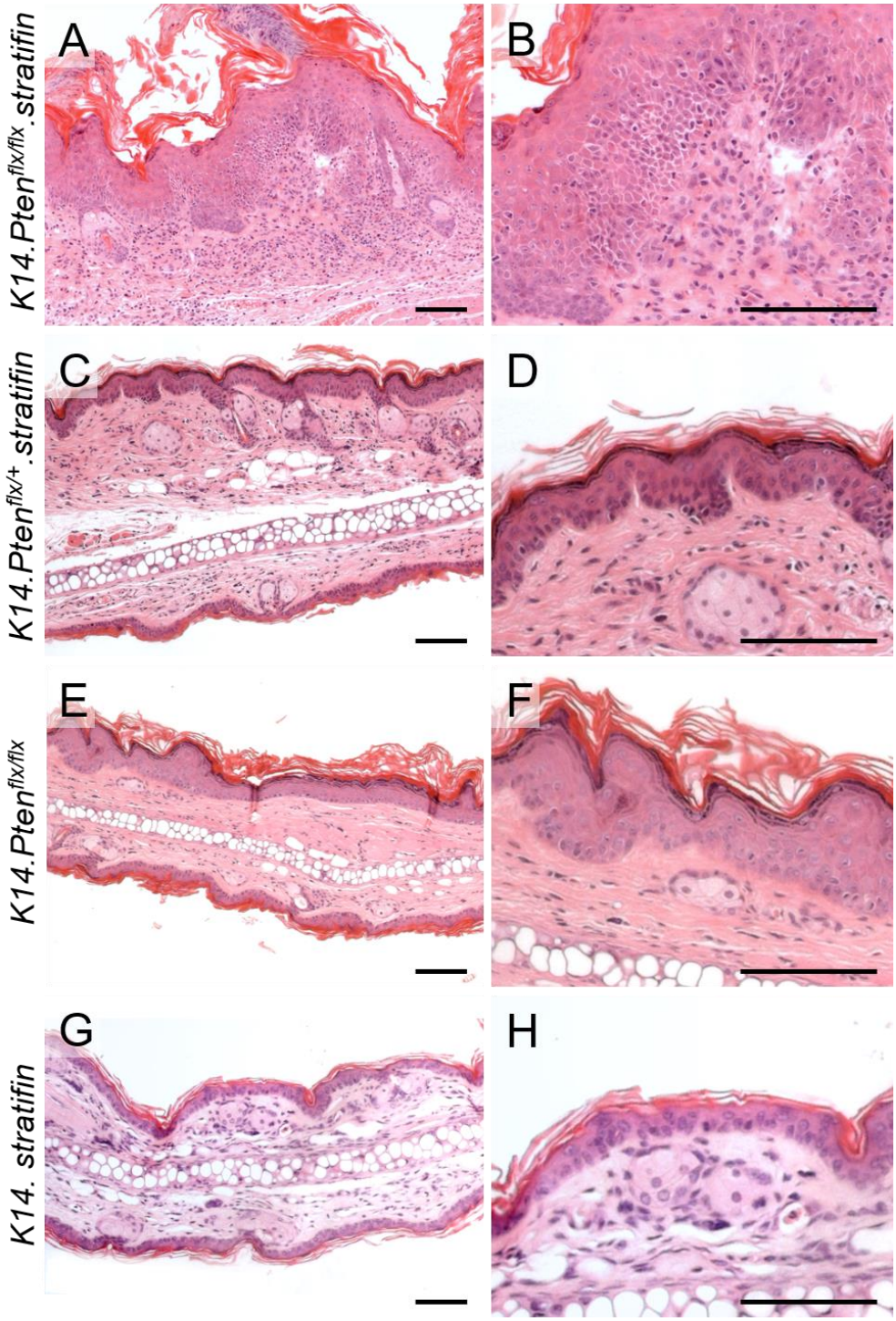

Figure 6-5: *K14.Pten*$^{flx/flx}$*.stratifin* mice develop invasive carcinoma without overt tumour formation.

(**A**) *K14.Pten*$^{flx/flx}$*.stratifin* (15 wks.) histology shows very hyperplastic epidermis and hyperkeratosis; layers are poorly defined with few granular cells present. The central area of the image shows invasive carcinoma with many proliferative keratinocytes and high numbers of immune cells in the surrounding stroma. (**B**) Higher magnification of the carcinoma area of **A**, highlighting the large number of proliferative cells which appear to be poorly interconnected and invasive. (**C**) *K14.Pten*$^{flx/+}$*.stratifin* TGE (21 wks.) showing well-ordered mild hyperplasia, seen at higher magnification in (**D**). (**E**) *K14.Pten*$^{flx/flx}$ TGE displaying moderate hyperplasia and a hyperkeratosis. (**F**) High magnification shows clearly demarcated layers and lack of immune infiltrate seen in **B**. (**G**) *K14.stratifin* TGE at 15 weeks which is not yet hyperplastic. (**H**) Higher magnification shows largely normal appearance. *Scale bars approx. 100 µm.*

A notable feature of the *K14.Pten$^{flx/flx}$.stratifin* was the exaggerated dishevelled appearance of the fur, in particular on the ventral surface (*Figure 6-6*). Here, the coat appeared less dense and the hair shafts where less sleek than in normal mice, resulting in a woolly appearance; a phenotype is not observed in *Pten*-heterozygous mice expressing Stratifin. Both Stratifin and Pten are known to be involved in hair follicle morphogenesis and thus in production of normal hair shafts (Hammond et al., 2012; Suzuki et al. 2003), thus, this phenotype is most likely due to concurrent deregulation of these proteins (by overexpression and ablation, respectively), causing aberrant follicle formation, though no carcinogenesis. Histological analysis of RU486-treated *K14.Pten$^{flx/flx}$.stratifin* back skin supports this, with hair follicles and shafts visibly distorted when compared with that of the *K14.Pten$^{flx/flx}$* control, wherein the hair is clearly smooth and straight with no visible follicle changes (*Figure 6-6F vs G*).

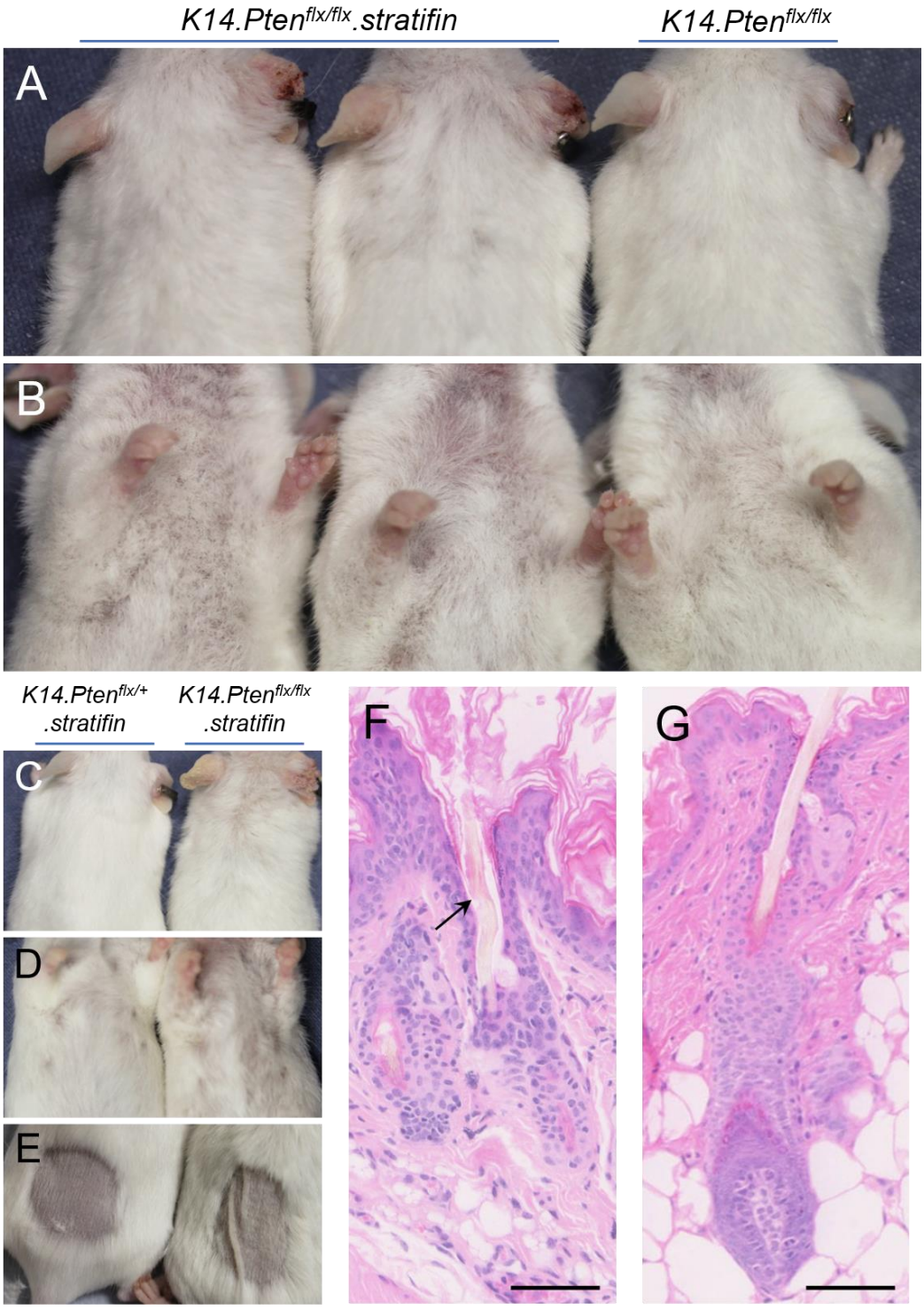

Figure 6-6: *K14.Pten*$^{flx/flx}$*.stratifin* mice exhibit a more pronounced hair phenotype than age-matched K14.Pten$^{flx/flx}$.

(**A**) 2 x *K14.Pten*$^{flx/flx}$*.stratifin* littermates (15 wks.) displaying strong TGE phenotypes including hyperplasia and hyperkeratosis with some inflammation, and milder NTE phenotype. Fur over the crowns is noticeably thinner than *K14.Pten*$^{flx/flx}$ control (15 wks.; far right) and dorsal fur appears dishevelled, whereas this is less pronounced in the *K14.Pten*$^{flx/flx}$ littermate shown. (**B**) More pronounced fur phenotype on the ventral side, where the *K14.Pten*$^{flx/flx}$*.stratifin* mice have a thin coat with a woolly appearance; not so apparent in the *K14.Pten*$^{flx/flx}$ mouse (far right). (**C**) **Left:** *K14.Pten*$^{flx/+}$*.stratifin* littermate with normal coat and very mild TGE phenotype showing little macroscopic effect of Pten heterozygosity and *K14.stratifin* expression. **Right:** *K14.Pten*$^{flx/flx}$*.stratifin* (15 wks.) with a similar phenotype to the mice in **A**. (**D**) **Left:** *K14.Pten*$^{flx/+}$*.stratifin* has normal ventral coat.

Right: *K14.Pten$^{flx/flx}$.stratifin* also showing the dishevelled ventral fur as above. (**E**) **Right:** Shaved patch where RU486 is applied to induce full Cre-recombinase activity, showing a thickened, folded skin apparently lacking elasticity in the *K14.Pten$^{flx/flx}$.stratifin* mouse (**Right**), compared with the *K14.Pten$^{flx/+}$.stratifin* mouse (**Left**) which appears grossly normal. (**F**) *K14.Pten$^{flx/flx}$.stratifin* RU486-treated back skin with incorrect follicle morphogenesis producing poorly structured hair shaft (arrow), compared with (**G**) *K14.Pten$^{flx/flx}$* RU486-treated skin showing normal, straight hair production. *Scale bars approx. 100 µm.*

6.4. *K14.Pten$^{flx/flx}$.stratifin* hyperplasia shows loss of K1 consistent with early malignant conversion yet an unexpected pAkt1^{ser473} expression pattern

Prior to further analysis, RU486-treated, hyperplastic *K14.Pten$^{flx/flx}$.stratifin*, *K14.Pten$^{flx/+}$.stratifin* and control *K14.Pten$^{flx/flx}$* tagged ear sections were assessed for expression of Stratifin (*Figure 6-7*). These results showed that Stratifin expression was strong throughout the *K14.Pten$^{flx/flx}$.stratifin and K14.Pten$^{flx/+}$.stratifin* siblings, especially in proliferative areas with heightened K14 expression, seen as the bright yellow cells in *Figure 6-7A* and *B*. Compared to untreated controls, elevated endogenous Stratifin expression was found in the basal layer of *K14.Pten$^{flx/flx}$* TGE skin (*Figure 6-7C*), though clearly less pronounced than that seen in *K14.stratifin*-expressing epidermis (*Figure 6-7A,B*). Furthermore, this staining was punctate in places especially along the BM and cell membranes, possibly indicative of Stratifin's roles in spatial awareness and desmosome/hemidesmosome maintenance (Li et al., 2007; Reitscher et al. 2018; Roberts et al., 2013).

This, therefore, may indicate that at this lower level of upregulation, Stratifin performs tumour suppressive activities in Pten-null skin, helping to ensure stratification despite loss of a major TSG; a finding also observed in *K14.fos.Pten$^{flx/flx}$* keratoacanthoma (Appendix 1: McMenemy et al., manuscript in preparation, Figure 2). This supports evidence for the highly context-dependent nature of Stratifin function in carcinogenesis; dubbed a "double-edged sword" (Li et al., 2009).

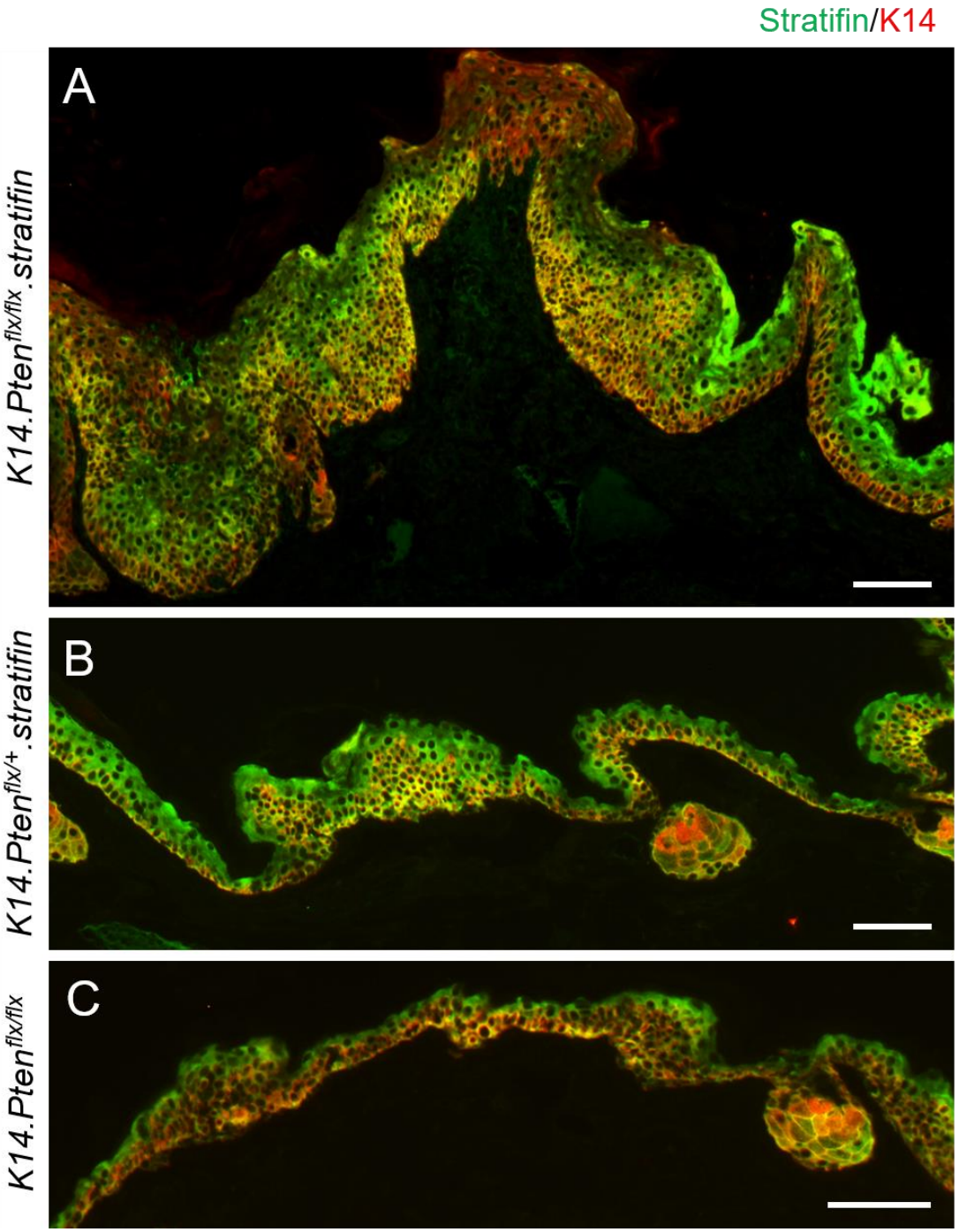

Figure 6-7: Strong Stratifin expression is apparent throughout *K14.Pten$^{flx/flx}$.stratifin* and *K14.Pten$^{flx/+}$.stratifin* epidermis, while *K14.Pten$^{flx/flx}$* exhibits elevated endogenous Stratifin expression in basal cells.

(**A**) Strong Stratifin expression (green) is detected throughout *K14.Pten$^{flx/flx}$.stratifin* hyperplastic epidermis, with large areas of yellow indicating the expanded proliferative compartments which are K14^{+ve} (red) in areas of carcinoma. Some green staining appears to be present in the stroma (upper centre) which may indicate presence of keratinocyte-releasable Stratifin. (**B**) *K14.Pten$^{flx/+}$.stratifin* milder hyperplasia is also strongly Stratifin^{+ve} throughout, again showing yellow hyperproliferative patches of K14^{+ve} cells extending into suprabasal layers (**C**) *K14.Pten$^{flx/flx}$* mild hyperplasia also shows more Stratifin staining in the basal layer than was previously detected in normal and *HK1.fos* or *HK1.ras* epidermis, though notably less than in mice expressing *K14.stratifin*, indicated by the orange-yellow colour compared with the bright yellow in **A** and **B**. *Scale bars approx. 100 µm.*

Subsequently, Keratin 1 expression was assessed (***Figure 6-8***), given the apparent malignant nature of *K14.Pten$^{flx/flx}$.stratifin* TGE skin. Indeed, many areas of hyperplasia determined to have progressed to carcinoma (without formation of an overt tumour) by histological analysis were devoid of K1 staining, while K1^{+ve} regions exhibited an expanded basal proliferative compartment, indicating a transient pre-malignant stage (***Figure 6-8A***).

In contrast, *Pten*-heterozygous skin expressing *K14.stratifin* (***Figure 6-8B***), K1 staining was found to be strong throughout most of the suprabasal layers with an expanded basal compartment visible in some of the most hyperplastic regions, indicating a largely benign phenotype at this stage (15 weeks). However, K1 positive cells occurred frequently in the basal layer in this genotype, as had previously been identified in skin expressing only the *K14.stratifin* transgene (Chapter 4*, Figure 4-15*), which when combined with the generally expanded basal layers, gave the impression of a confused differentiation programme. No K1 positive basal cells were seen in either *K14.Pten$^{flx/flx}$* (22 wks.; ***Figure 6-8C***) or *K14.Pten$^{flx/+}$* (not shown), consistent with it being a direct result of high anomalous basal layer Stratifin expression.

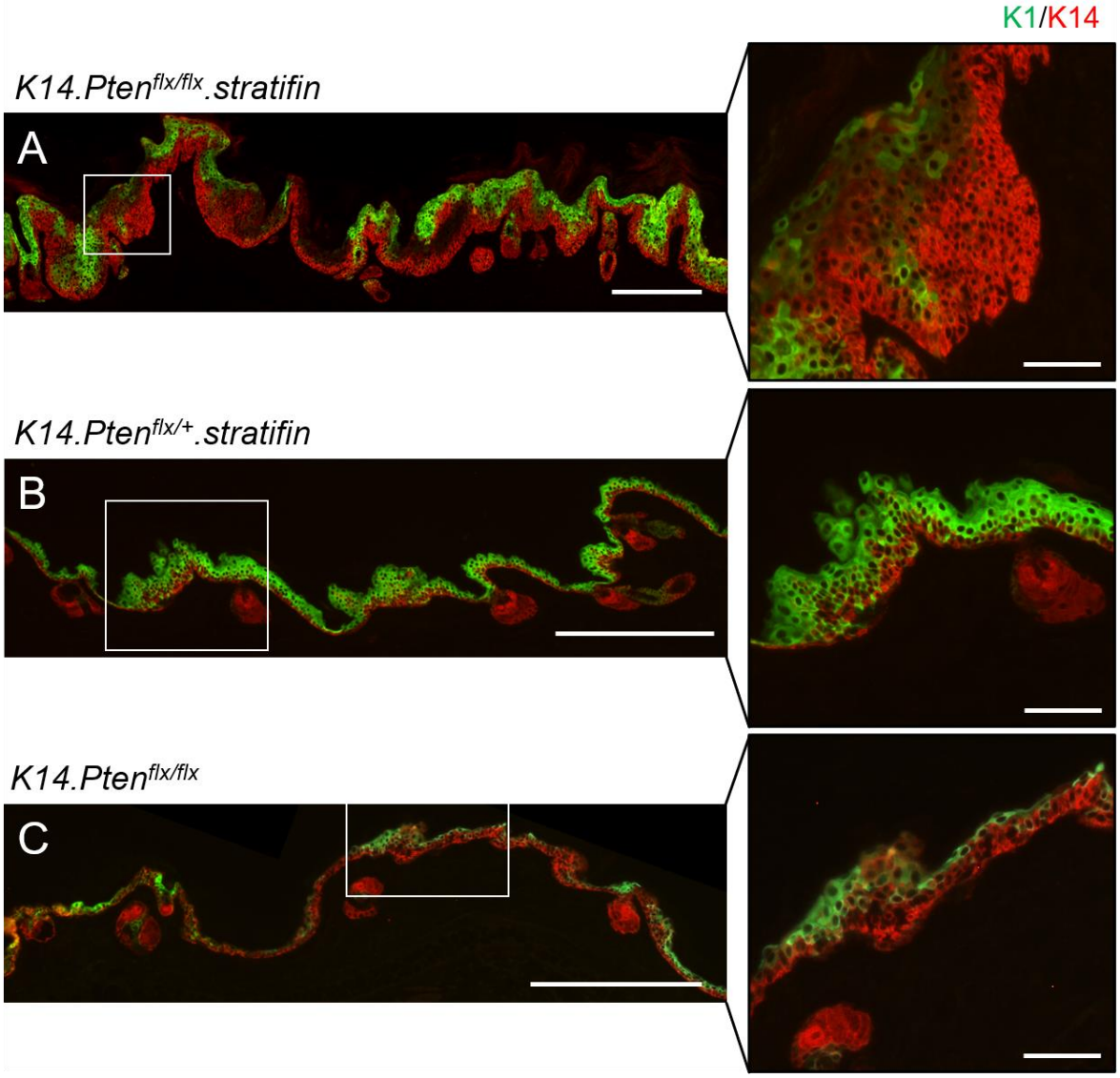

Figure 6-8: *K14.Pten$^{flx/flx}$.stratifin* wound-promoted skin shows Keratin 1 loss consistent with histological signs of malignant conversion, while *K14.Pten$^{flx/+}$.stratifin* shows spurious basal cell K1 expression.
(**A**) *K14.Pten$^{flx/flx}$.stratifin* TGE hyperplasia showing suprabasal K1 (green) to the right of the image above an expanded basal compartment which is K14^{+ve} (red). Areas to the left are largely K1-ve, highlighted in the boxed area showing strong K14 expression in much of the epidermis and only weak, sporadic suprabasal K1 positivity, indicating malignancy. (**B***) K14.Pten$^{flx/+}$.stratifin* wound-promoted skin maintains suprabasal K1 expression and thus is benign. However, spurious basal layer K1 expression is seen throughout, as exhibited in the highlighted box, similar to *K14.stratifin* skin shown in Chapter 4. (**C**) *K14.Pten$^{flx/flx}$* TGE skin exhibits a much lower degree of hyperplasia than the sections in A and B, with K1 expression mainly strong in areas which are 3 or more cells thick, as in the highlighted box. No basal layer K1 is seen in this genotype. *Scale bars: **A**, **B** and **C** approx. 500 µm; highlighted boxes approx. 100 µm.*

The most well-known tumour suppressive function of Pten is its inhibition of Akt activation via dephosphorylation of PIP_3 (Chalhoub & Baker, 2009). Therefore, in this *K14.Pten$^{flx/flx}$* model, it would be assumed that in ablating phosphatase activity by excision of exon 5, phosphorylated Akt1 would be elevated. However, previous studies in this model have shown that pAkt1 is absent in benign *K14.Pten$^{flx/flx}$* skin (MacDonald et al., 2011). This was determined to be the result of an increase in the p53 and p21 activity following Pten ablation to antagonise Akt1 activity, further observed in *HK1.fos-Δ5Pten* keratoacanthomas (Yao et al., 2008). However, instead, in both *HK1.fos-Δ5Pten* KA and *HK1.ras/fos-Δ5Pten* wdSCC, mTOR activation increased dramatically following loss of Pten activity, thereby contributing to the hyperplastic phenotype seen in *K14.Pten$^{flx/flx}$* skin (manuscript in preparation). Thus, given this lack of Akt activation, it is noteworthy that Stratifin has also been shown to directly antagonise Akt activity, similar to its inhibition of Mdm2 (Yang et al., 2006). Therefore, elevated endogenous Stratifin expression in basal *K14.Pten$^{flx/flx}$* keratinocytes may be performing the dual functions of protecting p53 through Mdm2 inhibition and suppressing Akt activity in lieu of functional Pten.

Here, a lack of pAkt1^{ser473} activation was indeed observed in *K14.Pten$^{flx/flx}$* TGE skin (*Figure 6-9E*) as was the case in *K14.Pten$^{flx/+}$.stratifin*. Conversely, in *K14.Pten$^{flx/flx}$.stratifin* TGE hyperplasia/carcinoma, the benign areas (as determined by histological analysis and K1 positivity) displayed pAkt1^{ser473} positivity in the suprabasal layers (*Figure 6-9A,B*), following the pattern of K1 expression in this section (*Figure 6-8A*).

This is consistent with the roles of Akt in differentiation in suprabasal epidermis and prevention of p53-mediated apoptosis which could result in ulceration if left unchecked (Naeem et al., 2015; Kermer et al., 2000; Ogawara et al., 2002), rather than its oncogenic roles in proliferative cells, in which it appears to be absent here (*Figure 6-9A,C*). Taken together, these results indicate that while pAkt1^{ser473} is detected in *K14.Pten$^{flx/flx}$.stratifin* hyperplasia, it is acting in a pro-differentiation role in the premalignant hyperplasia (Calautti et al., 2005), not in promoting progression to carcinoma, as may have been anticipated.

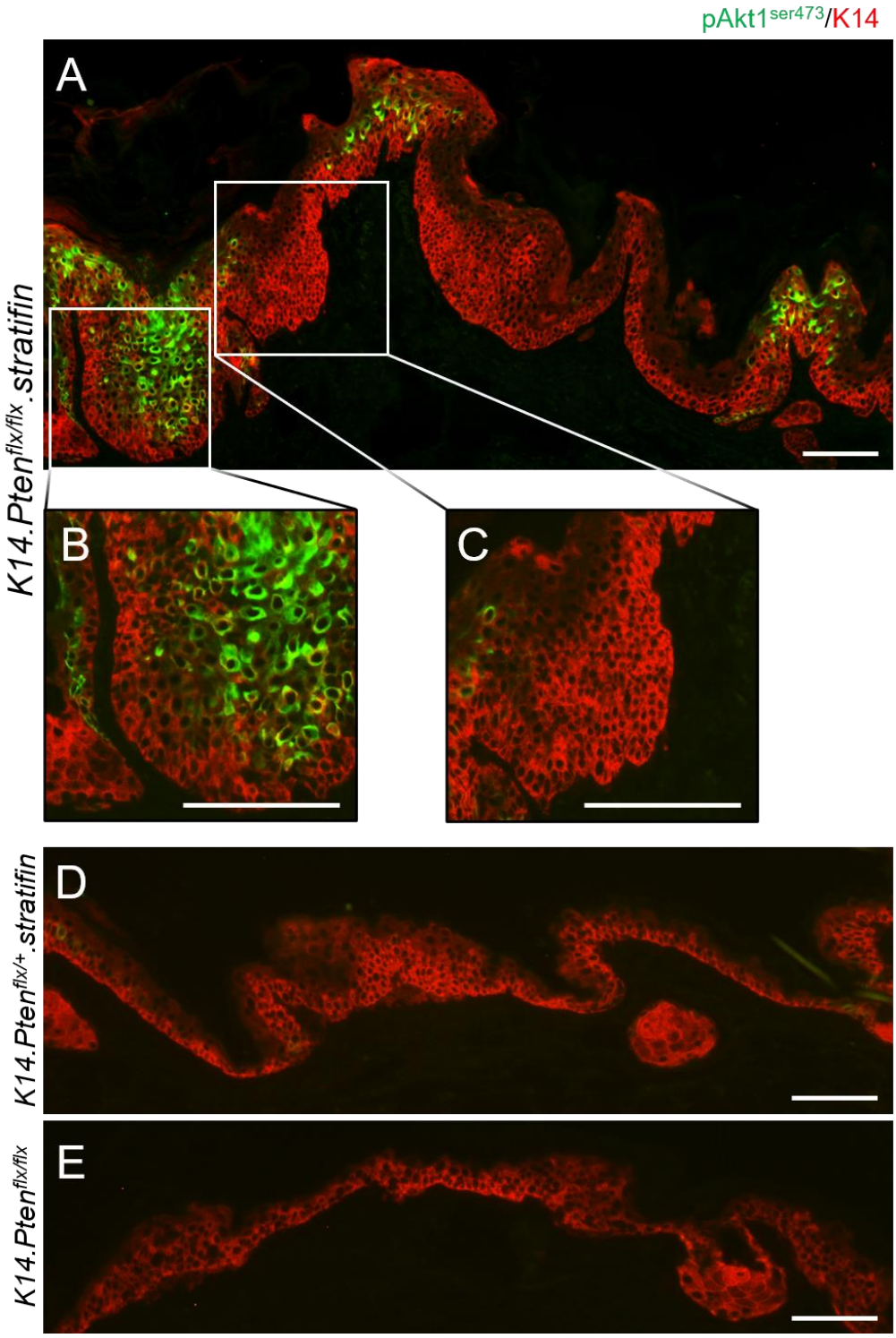

Figure 6-9: Expression of pAkt1^{ser473} is limited to patches of suprabasal cells in *K14.Pten$^{flx/flx}$.stratifin* carcinoma and is strikingly absent in both *K14.Pten$^{flx/+}$.stratifin* and *K14.Pten$^{flx/flx}$* genotypes.

(**A**) *K14.Pten$^{flx/flx}$.stratifin* exhibits strong suprabasal pAkt1^{ser473} expression in areas of benign hyperplasia (K1 positive; *Figure 6-8A*), as highlighted in the left-hand box, magnified in **B**, but expression is strikingly absent in areas of carcinoma as in the adjacent box, magnified in **C**. In this genotype, the pAkt1 expression pattern appears to mimic that of Keratin 1. (**D**) *K14.Pten$^{flx/+}$.stratifin* shows no pAkt1 positivity, suggesting a very different cellular context than in the full Pten-null counterparts, as pAkt1 expression blatantly does not follow that of K1 in this genotype. (**E**) *K14.Pten$^{flx/flx}$* also shows a total absence of pAkt1 positivity, as has previously been reported in this genotype. *Scale bars approx. 100 µm.*

6.5. *K14.p53$^{flx/flx}$.Pten$^{flx/flx}$.stratifin* mice quickly developed wound-independent keratotic lesions and non-keratotic carcinomas

The data suggest that *K14.stratifin* plays oncogenic roles in both p53 and Pten-null mice, with evidence of functions both in initiation (since neither *K14.p53$^{flx/flx}$* or *K14.Pten$^{flx/flx}$* mice alone develop carcinoma) and in promotion to an invasive phenotype in each case. Notably, although both *K14.p53$^{flx/flx}$.stratifin* and *K14.Pten$^{flx/flx}$.stratifin* mice developed carcinoma, as evidenced by histological analysis on which hallmarks such as hyperproliferation and invasion were apparent, neither genotype developed overt tumours either as a result of wound-promotion or spontaneously. Although, *K14.Pten$^{flx/flx}$.stratifin* mice had a much greater degree of hyperplasia and more widespread malignant changes compared with *K14.p53$^{flx/flx}$.stratifin*, and necessitated biopsy earlier on average due to welfare reasons mainly related to phenotypic face skin.

Subsequently, *K14.stratifin* was introduced to a dual *K14.Pten$^{flx/flx}$.p53$^{flx/flx}$* background, producing *K14.Pten$^{flx/flx}$.p53$^{flx/flx}$.stratifin* (*n*=9) and *K14.Pten$^{flx/flx}$.p53$^{flx/flx}$* mice along with various heterozygous and no-Cre controls. In all cases, mice in the *K14.Pten$^{flx/flx}$.p53$^{flx/flx}$.stratifin* cohort necessitated biopsy at an early stage; an average of 13.6 weeks (range: 11-19 weeks); approximately 9 weeks after the first dose of RU486 when the mice were tagged. This was due to the development of wound-independent tumour formation and/or development of ulcers in the head and neck region (*Figure 6-10A*; *Figure 6-11B,C*). None of the mice developed a pronounced gross wound-promoted phenotype on the TGE, though this may be reflective of the short time frame.

As shown in *Figure 6-10A* and more clearly in Figure *6-11B,C*, the areas surrounding these wound-independent tumours were devoid of hair growth, even where the skin was only hyperplastic. This, given the aberration of hair follicle (HF) development (and hair shaft production) in *K14.Pten$^{flx/flx}$.stratifin* skin (*Figure 6-6F*) indicated that such tumour formation was again related to HF keratinocytes.

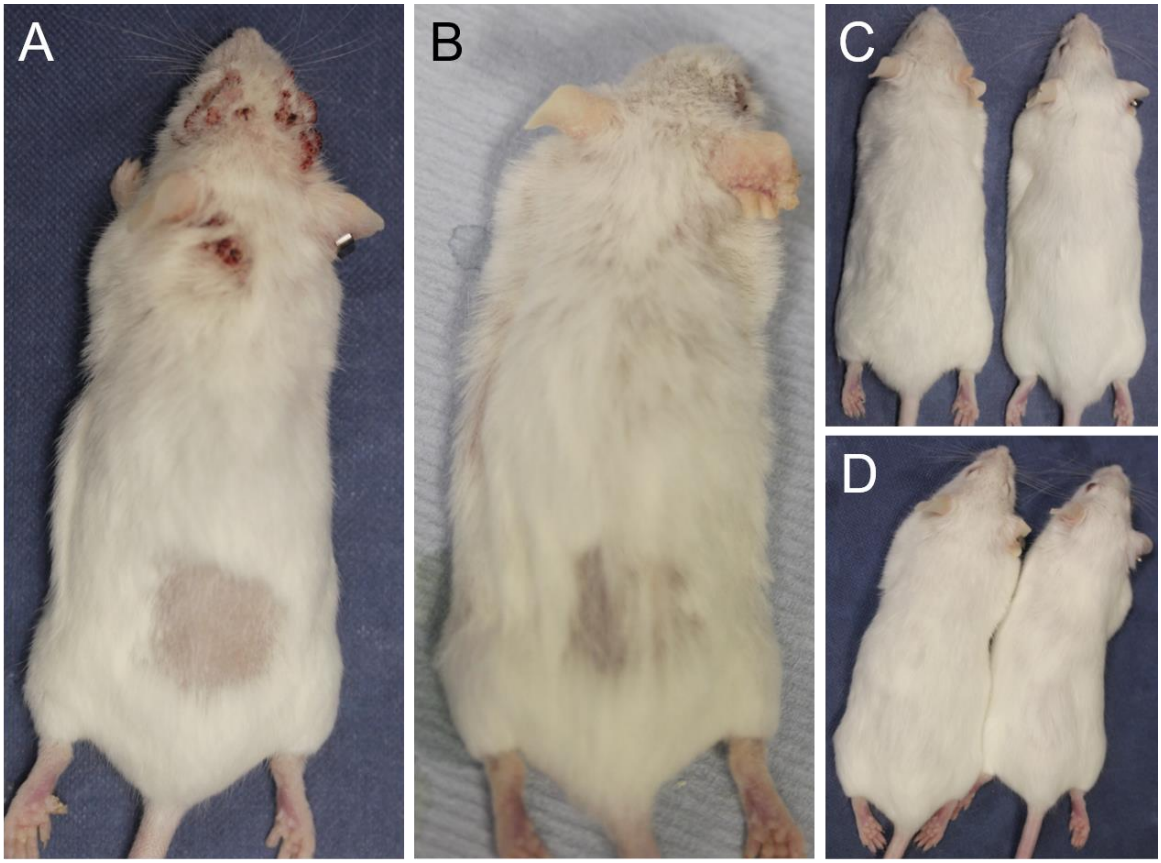

Figure 6-10: *K14.p53$^{flx/flx}$.Pten$^{flx/flx}$.stratifin* mice develop multiple wound-independent tumours necessitating biopsy at an early stage, precluding development of macroscopic TGE phenotype.

(**A**) *K14.p53$^{flx/flx}$.Pten$^{flx/flx}$.stratifin* mouse at 14 wks. displaying development of multiple keratotic and scabbed tumours around the head area which were inadvertently treated with RU486. The face phenotype necessitated biopsy at this early stage, such that the TGE phenotype was still relatively mild. (**B**) *K14.p53$^{flx/flx}$.Pten$^{flx/flx}$* mouse at 22 wks. displaying a slightly exaggerated *K14.Pten$^{flx/flx}$* phenotype with no tumour formation. (**C**) **Left:** *K14.p53$^{flx/+}$.Pten$^{flx/flx}$.stratifin* mouse at 14 wks. displaying expected *K14.Pten$^{flx/flx}$* phenotype with no effect of p53-heterozygosity. **Right:** *K14.p53$^{flx/flx}$.Pten$^{flx/flx}$.stratifin* mouse at 14 weeks showing no macroscopic phenotype at this stage. (**D**) *p53$^{flx/flx}$.Pten$^{flx/flx}$.stratifin* no-Cre control mice treated with RU486 at 14 wks., also showing a normal phenotype.

Examination of the histology of *K14.Pten$^{flx/flx}$.p53$^{flx/flx}$.stratifin* TGE skin (*Figure 6-11A,D,E*), keratotic tumour distal to the NTE (*Figure 6-11B,F*), and non-keratotic face tumours (*Figure 6-11C,G*) identified several distinct histotypes which all featured malignant regions. The TGE skin close to the tag showed a combination of the features typically seen in *K14.p53$^{flx/flx}$.stratifin* and *K14.Pten$^{flx/flx}$.stratifin* wound promoted skin, i.e. hyperchromatic nuclei in a highly expanded proliferative compartment, loss of stratification, extensive (invasion despite the short time frame), increased neoangiogenesis, and high immune infiltrate in the stroma (*Figure 6-11D*). Conversely, ear tip skin, far from the actual tag wound, was not found to be actively invading but exhibited dysplasia and a loss of distinct skin layers (*Figure 6-11E*).

Histology of the keratotic tumours pictures in *Figure 6-11B* showed a hyperkeratotic phenotype with a much more pronounced granular layer than in the TGE skin. Several hyperplastic follicle structures were observed in these tumours (*Figure 6-11F;* left and centre) and while the overall strcuture was actually more benign in appearance, some clusters of invasive keratinocytes had already begun to form disordered tumour islands (*Figure 6-11F*; black arrow).

Histology of the non-keratotic tumours of the face (seen in Figure 6-11C) exhibited a far more poorly-differentiated phenotype (*Figure 6-11G*); likely explaining the lack of keratosis visible macroscopically. Here, several indications of follicular involvement were pesent, including structures with intraepidermal keratosis surrounding circular lumens which bear some similarity to that seen in advanced *HK1.fos/K14.stratifn* fSCC (Chapter 4), and attendant sebocytes, including the large cluster seen at the right of the image (*Figure 6-11G*; black arrow) and smaller clusters near the top with a distinct absence of normal follicles.

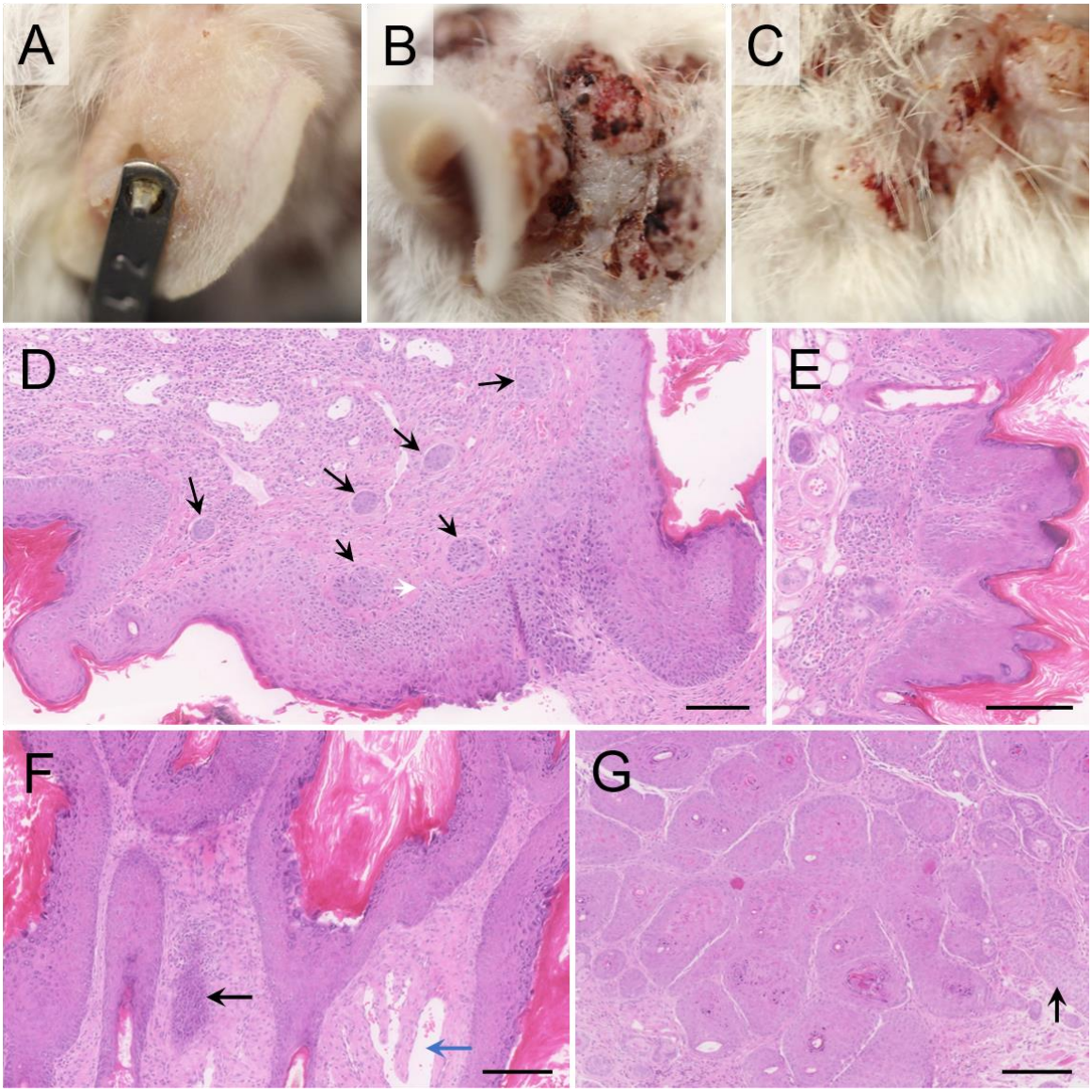

Figure 6-11: *K14.p53$^{flx/flx}$.Pten$^{flx/flx}$.stratifin* mice develop invasive wound-promoted hyperplasia and wound-independent papillomas and carcinomas at an early stage. (**A**) *K14.p53$^{flx/flx}$.Pten$^{flx/flx}$.stratifin* TGE at 11 wks. showing mild hyperplasia with some keratosis. (**B**) Cluster of wound-independent keratotic/scabbed tumours behind the NTE on RU486-treated skin. Skin surrounding these tumours is hairless. (**C**) Cluster of less keratotic wound-independent tumours on the cheek, also lacking hair. (**D**) Histopathology of TGE in **A**, showing disorganised, hyperproliferative epidermis with may hyperchromatic nuclei as in *K14.p53$^{flx/flx}$.stratifin* wound-promoted skin. Multiple invasive tumour nests are apparent (black arrows), and the basal layers of the epidermis appear to be invading into the stroma collectively (white arrow). (**E**) Histology of the tip of the ear, away from the tag site, shows less evidence of invasion but an obviously disorganised hyperkeratotic epidermis lacking clear demarcation of basal, spinous and granular layers. (**F**) Histology of one of the tumours in B, showing hyperplastic and hyperkeratotic epidermis with HF involvement (left and centre bottom of the image). A disorganised mass of invasive cells is present (arrow) and is associated with many immune cells. Neoangiogenesis is apparent in the large branching vessel (blue arrow). (**G**) Poorly differentiated histology of face tumour in **C**, showing intraepidermal keratosis similar. A proliferation of sebocytes is present (black arrow) which, coupled with the hairless nature of the skin here, is indicative of follicular involvement. *Scale bars approx. 100 µm.*

6.6. Discussion

The purpose of this chapter was to assess the effects of elevated Stratifin expression in the context of TSG loss (namely Pten and p53), and thereby to evaluate its potential oncogenic or tumour suppressive role in these contexts.

6.6.1. *K14.p53$^{flx/flx}$.stratifin*

Initial results from examination of the *K14.p53$^{flx/flx}$.stratifin* genotype (*n*=22) suggested little effect, as mice grossly resembled control *K14.p53$^{flx/flx}$*, *K14.p53$^{flx/+}$.stratifin* and *K14.stratifin* mice by 5 months of age (*Figure 6-1*). However, histological analysis of wound-promoted (tagged ear) tissue indicated morphological changes to the skin structure, hyperchromatic nuclei and early signs of invasion, including collective invasion forming tumour buds, despite the lack of overt tumour formation in any of the *K14.p53$^{flx/flx}$.stratifin* cohort.

The presence of large, hyperchromatic nuclei indicates an abnormal accumulation of chromatin due to reduced constraints on cell growth and cell cycle progression; their spread throughout several layers of the epidermis has been shown to correlate with malignancy (Malhotra et al., 2013). Cre-mediated ablation of p53 alone (*K14.p53$^{flx/flx}$*) does not appear to cause notable or widespread hyperchromatism in the epidermis (*Figure 6-2D*), whereas this was found to be common in *K14.p53$^{flx/flx}$.stratifin*. p53 is a master cell cycle regulator, termed the “guardian of the genome” (Lane, 1992), which is able to induce cell cycle arrest at checkpoints during mitosis and following DNA damage, and can induce the intrinsic pathway of apoptosis when excessive DNA damage has occurred (Haupt et al., 2001; Ou et al., 2005). Skin normally exhibits very little p53 staining (Reisman et al., 2012; Chapter 3 *Figure 3-1*)—since few interfollicular cells are actively cycling at any given time—and has been shown to be largely unaffected by targeted p53 knockout, unlike internal tissues (Donehower et al., 2002). This resilience is believed to be due to increased compensatory differentiation to eject mutated cells (Freije et al., 2014), hence the relatively normal gross and histological appearance of *K14.p53$^{flx/flx}$* control mice in this study.

In contrast, nuclear hyperchromatism was a common feature of *K14.p53$^{flx/flx}$.stratifin* TGE skin (*Figure 6-2A-C*) suggesting that the overexpression of *K14.stratifin* in undifferentiated cells is involved in either directly or indirectly driving cell growth and proliferation, causing the accumulation of abnormal chromatin in the absence of functional p53. This likely signals changes in gene expression which could contribute to carcinoma development and progression in synergy with Stratifin overexpression.

While Stratifin is known to have tumour suppressive properties (mostly in relation to cell cycle inhibition) there are several mechanisms by which a high level may result in increased proliferative capacity. For example, although Stratifin can directly antagonise Akt activation (Yang et al., 2006), it can conversely aid in upregulation of mTOR activity (downstream of Akt) by forming a cytoplasmic complex with both mTOR and Keratin 17, resulting in increased cell growth which has been shown to contribute to the pathology of oral SCC (Kim et al., 2006; Mikami et al., 2015). Furthermore, as previously mentioned, Stratifin acts alongside USP-8 in hepatocellular carcinoma to stabilise receptor tyrosine kinases (RTKs), thereby increasing mitogen signalling and driving further uncontrolled cell growth (Kim et al., 2018). Moreover, stimulation of IGF-1R (an RTK) has been found to cause a subsequent upregulation of Stratifin transcription, with Stratifin activity found to positively regulate cell cycle progression after IGF-1 treatment as a result of PI_3K pathway activation in MCF-7 breast cancer cells; an effect which was not impacted by p53 knockdown (Zhang et al., 2004). Taken together, these studies may indicate a positive feedback loop between Stratifin and IGF-1R, similar to that which exists with p53 (Lee & Lozano, 2006). It is also indicative of the extremely contextual nature of Stratifin activity, exemplified by these contradictory roles within the PI_3K/Akt/mTOR pathway.

Other features of this wound-promoted *K14.p53$^{flx/flx}$.stratifin* skin include several which appear to be common to all the models assessed which express *K14.stratifin*, such as stromal hyperplasia and immune infiltration. While further study is needed to assess the specific nature of these features, development of CAFs in the stroma via action of keratinocyte-released Stratifin as well as some yet to be elucidated mechanisms by which this transgene upregulates immune

infiltration are likely to be involved in the development of the invasive phenotype observed. Furthermore, the literature suggests that loss of p53 functionality in skin does not itself cause malignant conversion, however, it does introduce chromosomal instability which may be transformative (Weiss et al., 2010). Thus, the phenotypes of 5–7-month *K14.p53$^{flx/flx}$.stratifin* mice may in truth be generated by commonly acquired mutations of the p53-null background working in synergy with the oncogenic effects of Stratifin overexpression in proliferative cells; a facet which still remains to be assessed via genetic sequencing.

6.6.2. *K14.Pten$^{flx/flx}$.stratifin*

In contrast with the results seen in p53-null mice, expression of *K14.stratifin* on a Pten-null background (*K14.Pten$^{flx/flx}$.stratifin*; *n*=19) exhibited clear exacerbation of the gross *K14.Pten$^{flx/flx}$* phenotype by 15 weeks (*Figure 6-4*). *K14.Pten$^{flx/flx}$.stratifin* mice had prominent hyperplasia and hyperkeratosis on both ears which was more extensive that that seen in either *K14.Pten$^{flx/flx}$* or *K14.Pten$^{flx/+}$.stratifin*, with reddening of the skin indicative of inflammation not observed in controls.

Histological examination of TGE skin of *K14.Pten$^{flx/flx}$.stratifin* (*Figure 6-5A,B*) showed marked hyperplasia and dysplasia, as well as areas of hyperproliferation and invasion, indicating carcinoma development despite the lack of overt tumour formation. This was accompanied by marked immune cell infiltrate (also seen previously in both *HK1.fos*/*K14.stratifin* and *HK1.ras*/*K14.stratifin* tumours) which was not present in *K14.Pten$^{flx/flx}$* and only moderately so in *K14.Pten$^{flx/+}$.stratifin* hyperplasias. Invasion in these lesions may be a combination of the pro-migratory roles of Stratifin, involving both the epidermis and dermis (Ide et al., 2007; Boudreau et al., 2013; Liu et al., 2016) combined with the loss of suppression of cellular migration due to ablation of Pten activity (Tamura et al., 1998). Combined, these changes in cell activity and regulation could explain why invasion appears to be an early event in *K14.Pten$^{flx/flx}$.stratifin* aetiology.

Immunofluorescence analysis of these RU486-treated, wound-promoted *K14.Pten$^{flx/flx}$.stratifin* hyperplasias supported histological data in indicating development of carcinoma, as the early differentiation marker Keratin 1 was found to be lost in hyperproliferative regions, and was reduced in adjacent lower suprabasal layers in pre-malignant hyperplasia. *K14.Pten$^{flx/+}$.stratifin*, by contrast showed no K1 loss, but did exhibit spurious basal layer expression, already described in *K14.stratifin*-only skin (*Chapter 4; Figure 4-15*) and, indeed, in *K14.fos/Pten$^{flx/flx}$* keratoacanthoma where elevated endogenous Stratifin expression has also been detected in basal cells (*Figure 6-7*).

Given the role of Pten in regulation of Akt1 activation, pAkt1^{ser473} was also assessed in *K14.Pten$^{flx/flx}$.stratifin* and control TGEs. As shown previously (Yao et al., 2008), Pten ablation in this model does not initially cause upregulation of Akt activity, likely due to direct inhibition of Akt1 via other phosphatases such as PHLPP1 and 2 (Gao et al., 2005) and possibly also Stratifin (Yang et al., 2006), which seems especially probable given its unusually high basal positivity in *K14.Pten$^{flx/flx}$* wound-promoted skin (*Figure 6-7*).

Mice overexpressing Stratifin on a heterozygous Pten background (*K14.Pten$^{flx/+}$.stratifin*) similarly did not show positivity for pAkt1^{ser473}. However, *K14.Pten$^{flx/flx}$.stratifin* did exhibit positive pAkt1^{ser473} staining, though this was confined to suprabasal cells and seemed to follow the staining pattern of Keratin 1. This may indicate that the abundance of Stratifin in proliferative cells resulting from *K14.stratifin* expression either directly or indirectly inhibits Akt activation; thus, despite oncogenesis, Akt1 does not appear to be a causal factor in this malignancy. Moreover, since pAkt1^{ser473} expression mimics K1 localisation, it would appear to be acting in a pro-differentiation manner, rather than pro-survival, perhaps suppressing p53 activity to limit apoptosis and maintain the skin's barrier properties (Calautti et al., 2005; Lippens et al., 2005). In previous Chapters, the overabundance of p53 in tumours expressing *K14.stratifin* has been documented, therefore, accumulation of activated Akt1 may occur in *K14.Pten$^{flx/flx}$.stratifin* but not in *K14.Pten$^{flx/flx}$* skin in direct response to the abnormally high p53 expression as a counter to apoptosis and the threat to this paramount barrier function of the epidermis (Gottleib et al., 2002).

K14.Pten$^{flx/flx}$.stratifin mice also developed a particularly noticeable disruption to normal hair growth, with the slightly dishevelled appearance of the *K14.Pten$^{flx/flx}$* genotype amplified, including marked thinning of the hair over the crown and a woolly appearance to the ventral hair. Histological observations showed incorrect formation of the hair follicle and shaft in *K14.Pten$^{flx/flx}$.stratifin* RU486-treated skin, which was not observed in *K14.Pten$^{flx/flx}$* counterparts (*Figure 6-6F,G*); indicative of the importance of normal Pten and Stratifin proteins in hair follicle morphogenesis (Suzuki et al., 2003; Herron ret al., 2005; Hammond et al., 2012).

6.6.3. *K14.p53$^{flx/flx}$. Pten$^{flx/flx}$.stratifin*

Subsequently, mice were generated in which *K14.stratifin* was expressed concurrent with both Pten and p53 functional ablation (*K14.p53$^{flx/flx}$.Pten$^{flx/flx}$.stratifin*). Here, unlike in *K14.p53$^{flx/flx}$.stratifin* or *K14.Pten$^{flx/flx}$.stratifin*, RU486-treated mice developed small tumours which were wound-independent and rapidly growing, with the mice requiring biopsy at 13.6 weeks of age on average due to the position of the lesions (frequently around the eyes and face, where mice had spread RU486 after treatment of the ears), or due to persistent scratching which caused bleeding. This latter feature suggested the tumours were itchy, which did not appear to be the case in other *K14.stratifin*-expressing tumour models, but which is a common feature of human cutaneous SCCs (Mills et al., 2012). *K14.p53$^{flx/flx}$.Pten$^{flx/flx}$* controls did exhibit papillomas on the palmar surfaces (again, from touching recently RU486-treated ears) but these were found to be benign and did not appear to cause any discomfort.

Histology of *K14.p53$^{flx/flx}$.Pten$^{flx/flx}$.stratifin* individuals (*Figure 6-11*) showed that the structures were varied, with some exhibiting a mostly benign papilloma appearance with hair follicle enlargement and aberration and small patches of invasive keratinocytes forming nests in the stroma, while others showed widespread dysplasia and carcinoma. The differences in these histopathologies may be the result of a difference in the initiating tumour cell (e.g., interfollicular vs follicular stem cell). Indeed, all tumours which developed in

this genotype were associated with a patch of alopecic skin which, along with the histopathological findings of distorted follicles or loss of discernible follicular structures within the tumours, indicates involvement of hair follicles in the disease aetiology. Alternatively, or perhaps additionally, the varied tumour phenotypes could indicate a different set of further driver mutations has been acquired in each. This appears quite likely, since both p53 and Pten are involved in regulating genomic stability and error checking (Yeo et al., 2016; Hu et al., 2018; Bononi & Pinton, 2015; Hubbard et al., 2016), thus their combined loss likely allows for further mutations to accumulate.

Based on this data and prior *HK1.ras*/*K14.stratifin* results (Chapter 5), it seems that overexpression of Stratifin in the undifferentiated epidermis and hair follicles increases the likelihood of promotion-independent tumour formation compared with controls lacking the *K14.stratifin* construct, suggestive of roles in initiation. Additionally, the changes to the underlying stroma and consistent evidence of invasion in these models indicates a role in tumour progression. Aside from the effects on dermal fibroblasts, Stratifin has been shown to increase migratory potential by forming a complex with keratins 5 and 17 and soluble actin, allowing more rapid changes to cytoskeletal structure and motility.

6.6.4. Future directions

Thus far, *K14.p53$^{flx/flx}$.stratifin* hyperplasias have only been assessed using H&E stained sections to determine features of the wound-associated pathology. In order to better assess whether these are of a dysplastic benign or malignant phenotype, differentiation markers (K1 and K10) will be assessed, along with later differentiation markers loricrin and filaggrin to observe granular layer changes at different time points, since these exhibited a much less keratotic appearance than in other models and histology appears to show patchy granular layer loss. Furthermore, wound-associated Keratin K6 (and its partner, K16) will be investigated, as these are known to provide a less rigid form to the basal cells in order to aid in migration during wound healing (Wong & Coulombe, 2003; Rotty & Coulombe, 2012); a process which has been shown to be co-opted

during cancer cell invasion (Hu et al., 2020), and which was a common finding among *K14.stratifin* models and is again observed in these *K14.p53$^{flx/flx}$.stratifin* despite the lack of tumour formation. The mitotic index will be determined as in *HK1.fos/K14.stratifin* and *HK1.ras/K14.stratifin*, as all mice sacrificed were injected with BrdU prior to biopsy; the hyperchromatism observed suggests a high level of DNA replication though cells may not be undergoing cytokinesis correctly, resulting in the accumulation of chromatin observed.

In both *HK1.fos/K14.stratifin* and *HK1.ras/K14.stratifin* models (Chapters 4 & 5) it was found that p53 was highly expressed even through conversion to SCC; quite unlike models lacking exogenous Stratifin upregulation. It would be interesting, therefore, to see whether p53 is also upregulated in these *K14.Pten$^{flx/flx}$.stratifin* mice. Previous work showed that massive p53 and p21 upregulation was integral to the benign keratoacanthoma aetiology generated via activated Fos expression on a Pten-null background (Yao et al., 2008), which also appeared to show some degree of Stratifin expression in the basal layer, likely transactivated by p53 in those cells (*Figure 6-7C*). However, these novel *K14.Pten$^{flx/flx}$.stratifin* mice did not develop the same KA phenotype, seemingly transitioning directly from dysplastic hyperplasia to invasive carcinoma without a benign tumour stage; this suggests that very high Stratifin expression in basal layer keratinocytes in this background provides a different, more aggressive context to that seen in *HK1.fos-Δ5Pten* KAs. In addition, results in *HK1.ras/K14.stratifin* experiments seem to show a disconnect between p53 and p21 signalling that may be integral to the Type 2 tumour phenotype (which undergoes more rapid conversion than Type 1). Thus, it would also be prudent to test expression and subcellular localisation of p21 in *K14.Pten$^{flx/flx}$.stratifin* TGE skin, as this may indicate whether this may also be a factor in why this genotype produces malignant lesions while the *HK1.fos*-expressing counterparts do not. Indeed, in *HK1.fos-Δ5Pten* KAs, p53 & p21 expression seem to antagonise oncogenic Akt activities, while the pattern of pAkt^{ser473} expression in *K14.Pten$^{flx/flx}$.stratifin* skin suggests the opposite is true in this genetic background, with Akt seemingly driving differentiation, possibly to antagonise p53-mediated apoptosis which is a threat to maintaining the essential barrier function of the epidermis (Naeem et al., 2015; Kermer et al., 2000; Ogawara et al., 2002; Calautti et al., 2005). The differences seen between these genotypes

again exemplifies the highly context-dependent nature of Stratifin activity, requiring more in-depth analysis of the pathways affected to elucidate the mechanisms underlying carcinogenesis in this model.

To begin to explore this, *K14.stratifin* was expressed on a combined p53-null/Pten-null background, thereby removing the effects of Stratifin-induced p53 overexpression believed to be present in *K14.Pten$^{flx/flx}$.stratifin* mice. Here, unlike in the previous bigenic models, small overt tumours were generated. However, these did not appear at the wound-promotion site but on the back of the neck and face; areas most likely to be scratched or bitten and provide a single, initial promotion stimulus (or repeated low-level stimulus if as a result of grooming). These were found to be follicle-related, though clearly exhibited a different histotype to *HK1.fos*/*K14.stratifin* SCCs. Furthermore, histology of tumours from different sites of the same mouse showed differences in their histopathology; this could indicate either a different cell of origin — perhaps from different HF or interfollicular stem cell niches — or differences in the mutations acquired as a result of the ablation of two major TSGs. Genetic sequencing may, therefore, be performed on samples of the various tumours in order to determine whether the latter hypothesis is true. Staining for specific stem cell niche markers (e.g., LGR6 and CD34) may help to determine the niche where each tumour originated and whether different origins produce different pathologies in the context of *K14.Pten$^{flx/flx}$.stratifin* expression.

6.6.5. Conclusions

These data further serve to highlight the oncogenic nature of Stratifin expression, which appears to be separate to the formation of overt tumours and be primarily involved in the conversion to malignancy and invasion. Further study into these models of Stratifin overexpression in the content of TSG ablation may elucidate further roles of Stratifin interaction in known or novel oncogenic pathways and processes, potentially serving to identify further therapeutic targets for the treatment of invasive SCCs.

Chapter 7 Analysis of *HK1.fos/K14.stratifin* keratinocytes *in vitro*

7.1. Introduction

Co-operation between *HK1.fos* and *K14.stratifin* expression *in vivo* resulting in novel carcinogenesis which mimicked human follicular SCC (fSCC) was described in Chapter 4. Both Fos and Stratifin are known to play integral roles in keratinocyte differentiation, with both proteins most abundant in the suprabasal layers of the epidermis, consistent with this activity. Despite its importance in differentiation (Mehic et al., 2005), c-Fos is also a well-described promoter of oncogenesis in skin, with mice overexpressing c-Fos more susceptible to chemical carcinogenesis (Sakai, 1990) and, *in vitro*, its overexpression co-operates with Ras activation to induce malignancy (Greenhalgh & Yuspa, 1988; Greenhalgh et al., 1990). *In vivo*, Fos activation exerts a promotional role in conjunction with H-ras activation, resulting in aggressive papillomatogenesis, but requires further oncogenic events (such as ablation of tumour suppressor Pten and subsequent loss of p53) to progress to wdSCC (MacDonald et al., 2014). Stratifin is normally induced early in the terminal differentiation process and acts to enhance PKC activity (Dellambra et al., 1995). It later binds to and facilitates activity of CALML5, a vital effector of the terminal differentiation programme expressed in the granular layers (Sun et al., 2015).

While this *in vivo* system is useful in assessing the interplay between genes and effects of their downstream targets on carcinogenesis, it does not allow for manipulation of cells to directly assess their responsiveness to differentiation signal or their motility and invasive potential. Thus, to address this, experiments were performed employing primary neonatal keratinocytes cultured *in vitro* using established methods (Hennings et al. 1980; Yuspa et al., 1990) with modifications that prevent spontaneous transformation to then produce cell lines from these primary cultures (Greenhalgh et al., 1989). This allowed for real-time observations and experimental manipulation to study the effects of transgene expression on differentiation signals in normal and transgenic keratinocytes, and to assess the ability of primaries and early passage cell lines (<10) to grow clonally as an indication of transformation and to compare cell motility as an indication of invasive potential.

This chapter primarily aimed to: Identify changes in transgenic keratinocyte growth and differentiation in response to increased calcium concentration using monocultures of primary cells obtained from neonatal pups in the presence of the *HK1.fos* and *K14.stratifin* transgenes. and, subsequently, the cell lines established from these primaries; assess these features as well as relevant protein expression and changes in cellular motility (using a scratch assay) in cell lines derived from primary transgenic keratinocytes.

7.2. Phenotypes of primary keratinocytes cultured from transgenic neonatal epidermis

In Chapter 4, it was established that *HK1.fos/K14.stratifin* mice develop a novel phenotype recapitulating fSCC—unlike classic SCC histotypes seen in *HK1.ras/fos-Δ5Pten* carcinogenesis—which exhibited a highly unusual differentiation programme relative to normal skin. Therefore, to investigate the properties of *HK1.fos/K14.stratifin* keratinocytes further, *in vitro* experiments were performed that assessed their degree of transformation and altered differentiation programme in response to increased calcium concentration, together with migration assays to begin to assess their invasive potential. In skin, keratinocytes are induced to differentiate when they leave the basal layer in response to detachment from the basement membrane (Banno and Blumenberg, 2014) and an increasing calcium gradient (Chapter 1, *Figure 1-1*) (Bikle et al, 2012). *In vitro*, sensitivity to this calcium-mediated differentiation can be utilised as a method of assessing malignant transformation in cultured cells; resistance to increased calcium concentration is indicative of more transformed cells (Kulesz-Martin et al., 1983; Greenhalgh et al., 1989).

Skin was processed as described (Methods Section 2.2.6.) from neonates <36-hours-old, as later skin possesses developed follicular structures which prevent separation of epidermis from dermis and causes significant contamination of keratinocyte cultures with dermal fibroblasts (Hennings et al., 1980; modified in Greenhalgh et al., 1989). Following PCR to confirm genotype, separated epidermis were pooled and plated out at $5x10^6$ cells per T25 flask in order to develop cell lines, and separately plated into 60 mm dishes at approximately 50 cells/mL (around 250 cells total/dish) to perform clonal

growth assays that assess their potential transformation. Keratinocytes were typically cultured in 0.05 mM Ca^{2+} DMEM supplemented with 10% chelexed foetal bovine serum (FBS), 20% keratinocyte growth medium (KGM) (clonal growth medium: CGM). In addition, dermal fibroblasts were extracted to produce fibroblast-conditioned medium (FbCM), such that keratinocytes could be cultured at low plating density using low calcium DMEM supplemented with 10% KGM + 10% FbCM, in place of 20% KGM. This medium was developed to prevent crisis which leads to spontaneous transformation (Greenhalgh et al., 1989) yet establish normal, immortalised keratinocyte cell lines, and was employed in clonal growth assays to assess the colony-forming ability of transgenic keratinocytes compared to wild type (below).

Normal keratinocytes are sensitive to calcium-induced differentiation, changing their cobblestone morphology in proliferative 0.05mM Ca^{2+} medium to a flattened dull morphology indicative of suprabasal cells when switched to an intermediate 0.08mM Ca^{2+} medium for 24 hours, and a stratified morphology after a further 24 hr at 0.12mM Ca^{2+} (*Figure 7-1*). Thus, any resistance to the morphology change or growth in high calcium conditions indicates resistance to differentiation cues and a phenotype consistent with malignant transformation when subsequently grafted onto nude mice (Strickland et al., 1988; Greenhalgh et al., 1989; Greenhalgh et al., 1990).

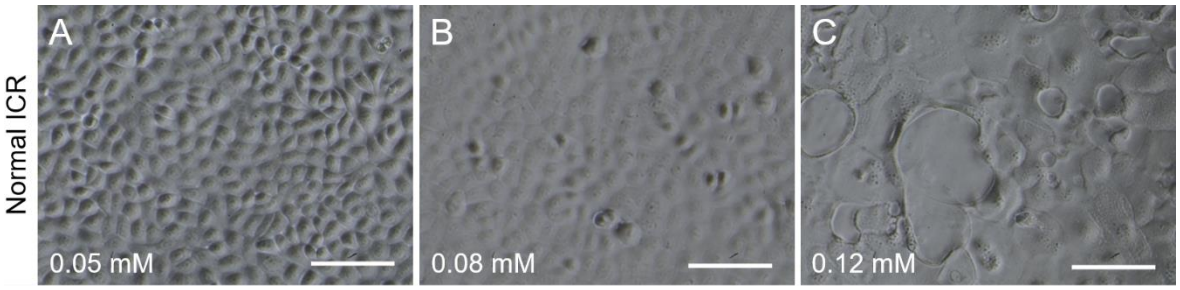

Figure 7-1: Normal (ICR) keratinocytes differentiate in response to increasing Ca^{2+} concentration.
(**A**) ICR cells in low Ca^{2+} (0.05 mM) medium have a cobblestone appearance and regularly sized cells. (**B**) When treated with 0.08 mM Ca^{2+} for 24 hr, the cells develop a dull appearance indicative of suprabasal differentiation. (**C**) These will terminally differentiate into cornified cells (squames) if maintained for 48 hr in 0.08 mM Ca^{2+} or if switched to 0.12 mM for the second 24 hr period, as here.

Typically, normal keratinocytes cultured without FbCM/KGM supplements quickly differentiate in the absence of cell-cell contact. However, in clonal growth media (CGM: low Ca^{2+} DMEM supplemented with 10% FbCM/10% KGM; or low Ca^{2+} DMEM plus 20% KGM) normal keratinocytes develop small, slow growing colonies by 4 weeks that can be cultured over the following months, whereas transformed cells produce more colonies that grow faster and can become confluent within 4 weeks (*Figure 7-2 Panel II*) (Greenhalgh et al., 1989). In addition to clonal growth assays in low Ca^{2+} CGM, a more stringent assessment of transformation involves resistance to calcium-induced differentiation coupled to an ability to grow from clonal density in high Ca^{2+} media (Hennings et al., 1980; Kulesz-Martin et al., 1983; Greenhalgh et al., 1989). Here, this study again found that normal keratinocytes developed several small slow growing colonies in low Ca^{2+} CGM (Greenhalgh et al., 1989) but most cells quickly differentiated, suggesting that these colonies may have derived from original stem cells (*Figure 7-2*).

Unexpectedly, keratinocytes expressing only *K14.stratifin* grew slightly better than *HK1.fos/K14.stratifin* primaries, while both transgenic cultures grew slower than normal keratinocytes in CGM. Wild-type primary keratinocyte morphology in low calcium CGM again showed the expected polygonal cobblestone appearance of proliferative keratinocytes (*Figure 7-2 Panel I*), whereas both *K14.stratifin* and *HK1.fos/K14.stratifin* primary keratinocytes appeared to have fewer cells which were more loosely packed with increased shedding. Furthermore, both these primary *K14.stratifin*-expressing keratinocyte cultures began to adopt a more stretched, somewhat spindle shaped morphology (*Figure 7-2 Panel I)* which became more evident in the derived cell lines, alongside another *HK1.fos/K14.stratifin* line which exhibited a uniquely irregular, flattened appearance and splayed cell morphology (FS1s vs FS3m; *Figure 7-2 Panel III*). In addition, unlike their derived cell lines (below), while *HK1.fos/K14.stratifin* primary cells were found to grow (albeit poorly) from clonal density in low calcium CGM, they were unable to grow at all in high calcium medium (*Figure 7-2 Panel II)*; a surprising finding, given the malignancies generated by this bigenic genotype *in vivo* (Chapter 4).

Another unexpected result was that whilst keratinocytes expressing *K14.stratifin* initially grew better than their *HK1.fos/K14.stratifin* counterparts, they then largely became senescent or terminally differentiated, ultimately producing few colonies, if any, which stained poorly with a specific keratin stain, Rhodamine B (*Figure 7-2 Panel II*). This lack of staining suggests a problem with the intermediate filament network *in vitro* that echoes *in vivo* observations of the disruption that deregulated Stratifin expression brings to the normal differentiation process (Chapter 4 *Figures 4-16—4-20*), which was subsequently pursued further in established cell lines (below). It may be that Stratifin exerts a rapid transition of the initially viable stem cells out of the proliferative niche to one of accelerated differentiation.

These results contrasted starkly with normal primary keratinocytes that grew slowly from clonal density as observed previously (*Figure 7-2 Panel II, row 5*; Hennings et al., 1980; Kulesz-Martin et al., 1983; Greenhalgh et al., 1989), reflecting the seeding behaviour of the stem cells present. Conversely, malignant T52 cells—a line derived from H-Ras-activated SP1 cells transfected with activated v-Fos, which formed pdSCCs when grafted onto nude mice (Strickland et al.,1988; Greenhalgh & Yuspa, 1988)—grew rapidly in either low or high calcium medium, as expected (*Figure 7-2 Panel II row 6*).

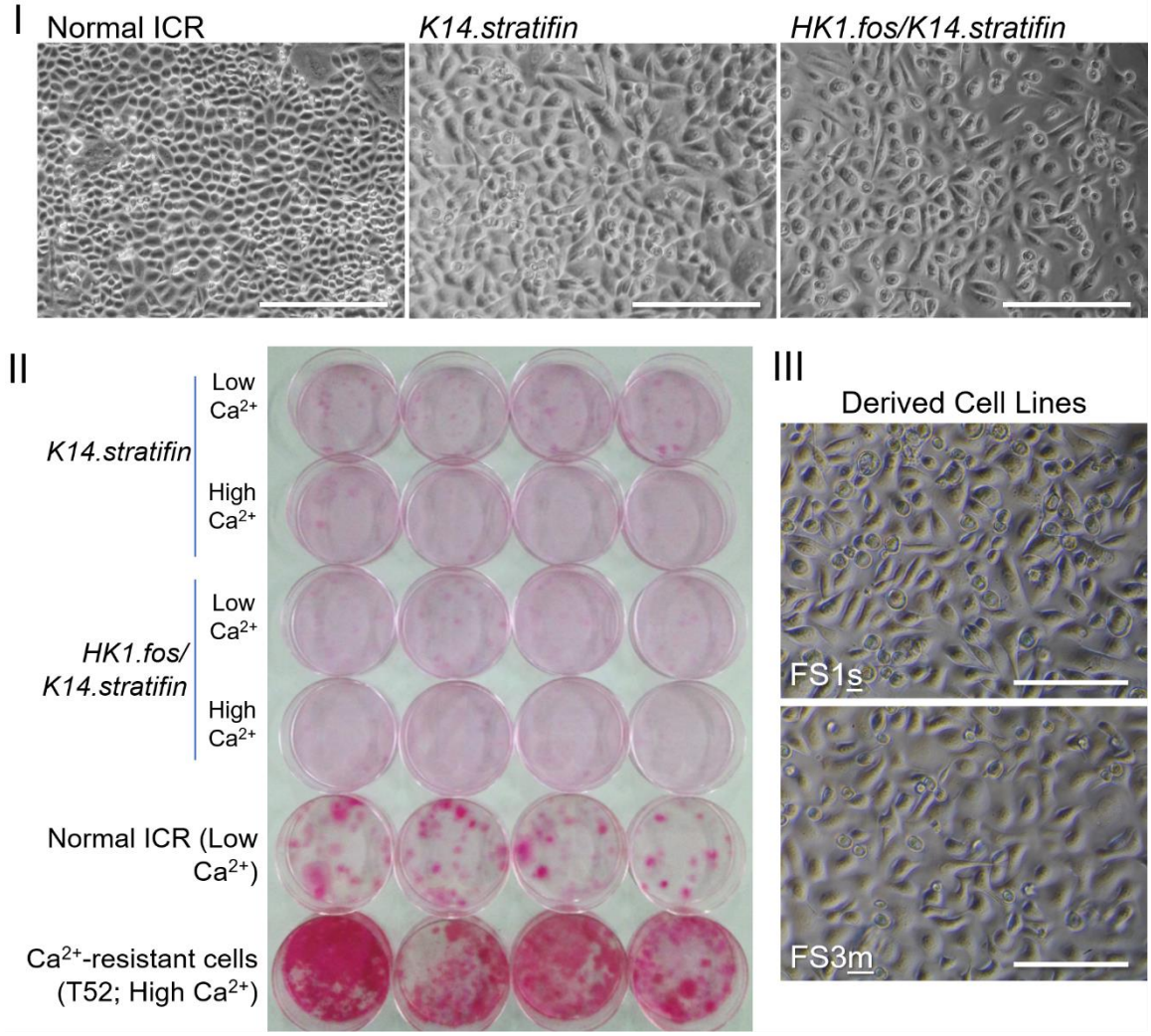

Figure 7-2: *In vitro* analysis of Normal, *K14.stratifin* and *HK1.fos/K14.stratifin* primary keratinocytes.

Panel I: Morphology of Normal primary keratinocytes in low Ca^{2+} medium at 5 days shows cobblestone appearance. Both *K14.stratifin* and *HK1.fos* primary cultures have fewer cells and exhibit more varied and elongated cell shapes ("S" morphology, see below) than Normal.

Panel II: Primary keratinocytes clonal growth assays showed neither *K14.stratifin* (rows 1 & 2) nor *HK1.fos/K14.stratifin* (rows 3 & 4) established viable colonies in low or high calcium that stained with Rhodamine B. In contrast normal keratinocytes developed slow growing colonies, whilst malignant T52 cells (v-H-Ras/v-Fos transformed) grew rapidly even in high calcium media.

Panel III: Elongated cell morphology of *HK1.fos/K14.stratifin*-derived cell line FS1s, retaining features seen in the primary cells above, compared with the more irregular and flattened morphology of the FS3m cell line which appears to mimic the in vivo morphological features of *HK1.fos/14.stratifin* tumours.

7.3. *HK1.fos/K14.stratifin* cell lines exhibit resistance to Ca^{2+}-induced differention correlated with higher Stratifin expression

Cell lines were established from normal ICR mice, *HK1.fos*, *K14.stratifin* and *HK1.fos/K14.stratifin* and, in repeat experiments performed over a total of 2 years, their characteristics at very low passage number (ranging from tertiaries at passage 2 to a max of passage 10 for rapidly growing lines) were compared to T52 SCC keratinocytes and SP1 papilloma cells (Strickland et al., 1988; Greenhalgh & Yuspa, 1988). Thus, two phases of *in vitro* analysis produced phase 1 cell lines: S1A, S2A, FS1s, FS2, FS2s and FS3m; and phase 2 cell lines: ICR^{normal}, WT^{normal}, S4, S5, F1c F5, F6 and FS4 (S = *K14.stratifin*; F = *HK1.fos*; c = derived from clonal density; FS = *HK1.fos/K14.stratifin*). Close examination of their respective morphologies showed that *HK1.fos/K14.stratifin* keratinocytes possessed two distinct subtypes when sub-cloned into lines: "s" referred to more elongated, spindle-shaped morphology (FS1s and FS2s), and "m" to an unusually heterogeneous morphology of splayed cells, reminiscent of *HK1.fos/K14.stratifin* tumour epidermis (FS3m). In addition, it was noted that all *K14.stratifin* lines developed an elongated morphology compared to normal or *HK1.fos* keratinocytes (*Figure 7-2*).

The keratinocyte morphology of selected cell lines and expression of differentiation markers K1/K14 and Stratifin are summarised in *Figure 7-3*, including phenotypes representative of normal (ICR), *HK1.fos* (F1c), *K14.stratifin* (S1A), and both variants of *HK1.fos/K14.stratifin* morphologies (FS2 and FS3m). For each line, keratinocytes were cultured on coated glass chamber slides in low calcium (0.05 mM) CGM medium until near-confluent, then half were switched to high calcium CGM (0.225 mM) medium for 24 hours to assess the level of resistance to calcium in each line before being photographed (*Figure 7-3*, left panel) and fixed in ice cold methanol. Fixed cells were then stained for differentiation markers K1/K14 to assess the levels of altered differentiation, if any (*Figure 7-3*, centre panel), and for Stratifin, to both confirm elevated expression in lines harbouring the *K14.stratifin* transgene (S1A, FS2 and FS3m) and to correlate this with calcium resistance (*Figure 7-3*, right panel).

Of the lines tested, FS2 and FS3m were chosen as exemplars of the different *HK1.fos/K14.stratifin* morphologies identified. FS2 exhibited a generally "cobblestone" appearance but with much greater variation in cell size than in normal keratinocyte cultures, while FS3m exhibited more irregularities in cell morphology (*Figure 7-3 left panel*). Here, *HK1.fos/K14.stratifin* line FS2 possessed the most rapid growth and showed the greatest resistance to Ca^{2+}-induced differentiation, exhibiting very little change to the morphology of the cells other than a slightly flattened appearance, consistent with a malignantly transformed cell line. Conversely, the other *HK1.fos/K14.stratifin* line, FS3m, grew slowly, were difficult to trypsinise, and generally exhibited a flattened shape suggesting a degree of attempted premature differentiation in low calcium; however, it lacked the squames present in normal ICR, F1c or S1A genotypes which would indicate complete terminally differentiation (Figure 7-2, left panel, white arrows).

It may be that this FS3m line represents the stalled stages of spinous differentiation and irregular granular layers observed *in vivo;* however, this awaits analysis of late-stage markers such as filaggrin and loricrin. There is also a possibility that this line may be derived from hair follicle cells as this approach gives cultures believed to be composed of roughly 50% cells from the interfollicular epidermis and 50% from the immature hair follicle buds (Lichti et al., 2008), though this requires confirmation with specific HF markers.

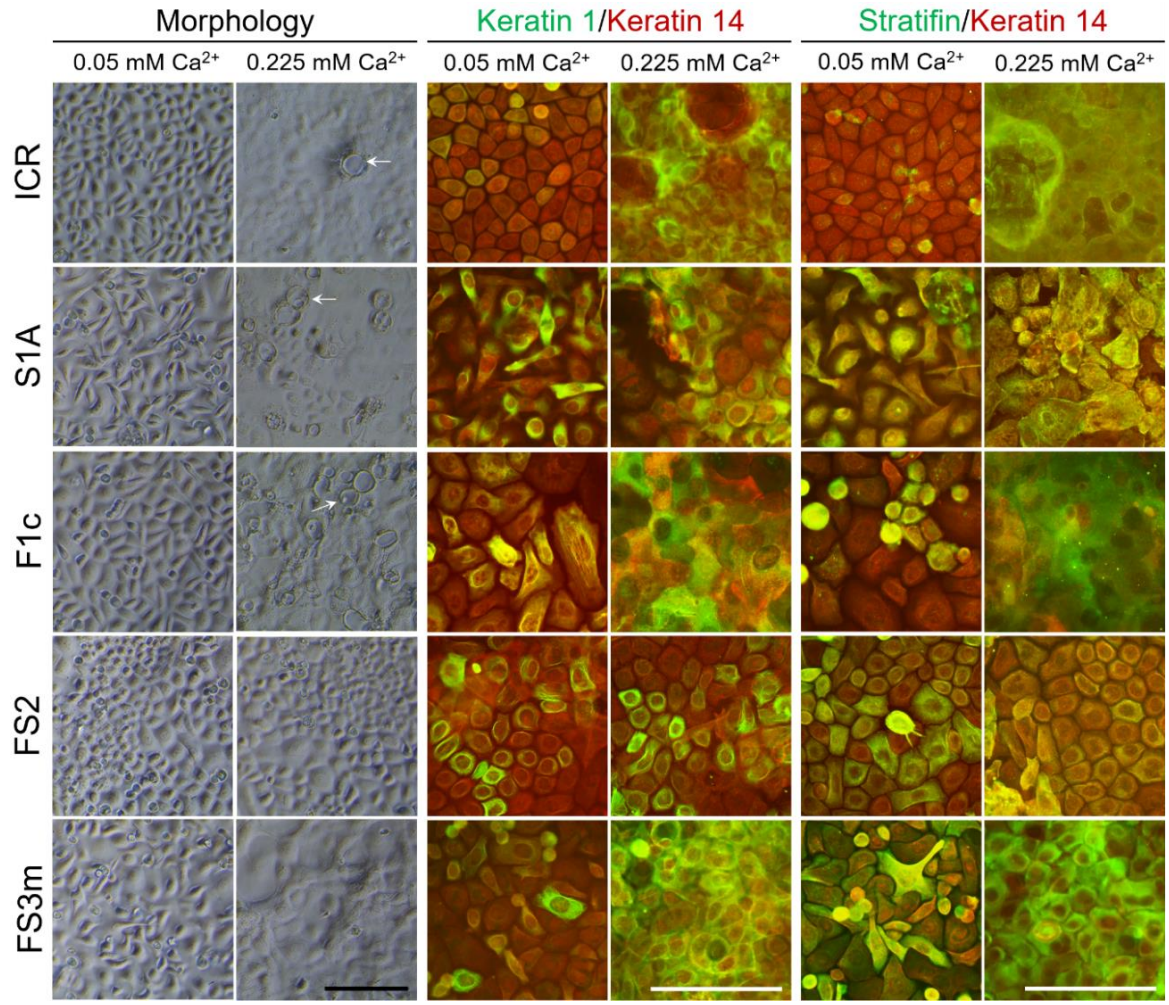

Figure 7-3: All cell lines expressing *K14.stratifin* exhibit spurious K1 expression in low Ca^{2+} medium and some *HK1.fos/K14.stratifin* cells show signs of calcium-resistance.
Left: *Morphology of lines cultured in low (0.05mM) and high (0.225mM) Ca^{2+} CGM.* Normal ICR, *K14.stratifin* (S1A), *HK1.fos* (F1c), show differentiation responses to increased Ca^{2+} with signs of stratification evidenced by presence of squames (white arrows). In low Ca^{2+} CGM, *K14.stratifin* line S1A exhibits elongated keratinocytes while *HK1.fos*-expressing F1c and ICR cells have the normal cobblestone appearance. Conversely, in low Ca^{2+} CGM, *HK1.fos/K14.stratifin* (FS2 and FS3m) cells have a unique morphology and FS2 shows little response to increased Ca2+; while FS3m cells exhibit some resistance but terminal differentiation appears incomplete with no squames developing. **Centre:** *K1/K14 expression analysis*. Normal ICR cells in 0.05mM CGM express little K1 which is induced by the Ca^{2+} switch. In S1A, K1 is expressed early in 0.05mM CGM, particularly in the spindle morphology cells, while not all cells express K1 in high Ca^{2+}, consistent with *in vivo* observations. F1c also exhibit slightly elevated K1 in low Ca^{2+} suggesting premature differentiation due to Fos activity. In FS2 cells, K1 expression is similar in low and high Ca^{2+} whilst in low Ca^{2+}, FS3m exhibit high K1 in oddly flattened cells and virtually uniform K1 expression in high Ca^{2+}; consistent with a stalled, spinous cell morphology. **Right:** *Analysis of Stratifin expression*. ICR cells express few Stratifin positive cells in low Ca^{2+} while staining becomes uniform in high Ca^{2+}. In F1c, small foci of cells strongly express Stratifin suggesting these are differentiating prematurely, while they have a uniform Stratifin profile in differentiated high Ca^{2+} cells. In S1A cells, Stratifin is expressed in most low Ca^{2+} cells, while spindle cells exhibit some polarisation to the sub-cellular localisation in the pseudopodia, while there is more uniform, strong Stratifin expression in high Ca^{2+} cells. Both transformed FS2 cells and FS3m cells exhibit strong Stratifin expression in low Ca^{2+}, which is particularly prominent in the spinous-like cells with pseudopodia. Stratifin expression is not greatly affected in FS2 in high Ca2+ medium due to the resistance to differentiation, but FS3m show strong Stratifin expression in all cells in high Ca^{2+}. *Scale bars approx. 50 µm.*

Interestingly, S1A (expressing only *K14.stratifin*) also showed an elongated cell shape (*Figure 7-3*), as did the other *K14.stratifin* lines: S2A, S4 and S5, usually indicative of transformation, though these cell lines all responded to increased Ca^{2+} by differentiating fully. Conversely, F1c (and F2 (below), F5 and F6 (not shown)) appeared much more similar to ICR tertiary cultures, showing a cobblestone appearance of regularly-sized cells which grew much more slowly than S or FS lines.

In addition to altered morphology, expression of differentiation marker keratins K1 and K14, together with exogenous and endogenous Stratifin were examined in low Ca^{2+} CGM high Ca^{2+} conditions (*Figure 7-3, centre panel*: K1; green/ K14 red). In normal ICR keratinocytes maintained at 0.05 mM Ca^{2+}, expression of K1 was negligible, consistent with a proliferative basal cell phenotype predominantly expressing K5 and K14. These normal cells exhibited greatly increased K1 expression when switched from low (0.05 mM) to high (0.225 mM) calcium medium for 24 hr, indicative of stratification into spinous and granular layer cells. Similarly, in low calcium CGM, Stratifin expression in ICR cells was also low and sporadic (green; right panel) but became abundant in suprabasal high calcium keratinocytes; an expression profile consistent with the differentiation roles for Stratifin observed *in vivo* (Dellambra et al., 1995; Sun et al., 2015).

In contrast, all cell lines expressing *K14.stratifin* exhibited prematurely high K1 expression in low Ca^{2+} CGM medium, and all *HK1.fos/K14.stratifin* cells also showed some signs of calcium-resistance. Both of the *HK1.fos/K14.stratifin* lines expressed high levels of Stratifin in low calcium conditions, yet produced somewhat contrasting results, further highlighting the context-dependent roles of Stratifin. For example, *K14.stratifin* cell line S1A exhibited marked K1 positivity in many keratinocytes grown in low calcium CGM (green, centre panel row 2; as did lines S2A, S4 and S5 not shown), akin to spurious basal layer K1 staining observed in *K14.stratifin* skin (Chapter 4 *Figure 4-15*), *HK1.ras/K14.stratifin* hyperplasia (Supplementary data *Figure S4*), and *K14.Pten*$^{flx/+}$*.stratifin* hyperplasia (Chapter 6 *Figure 6-7*). Additionally, this spurious K1 expression in *K14.stratifin* line S1A was found to be particularly prominent in keratinocytes with a spindle-like morphology, suggesting a

premature commitment to differentiate. Thus, *K14.stratifin* S1A cells were quite responsive to calcium-induced differentiation, and in many cases, differentiation was complete with confluent cultures showing a stratified phenotype complete with squames (*Figure 7-3*, left panel row 2). However, while the majority of *K14.stratifin* and *HK1.fos/K14.stratifin* cells exhibited increased K1 expression when switched to high calcium CGM (*Figure 7-3*, right panel row 2), not all differentiating cells expressed uniform K1, similar to the patchy K1 expression which has been observed *in vivo* in skins overexpressing Stratifin.

Further, S1A cells were confirmed to exhibit widespread Stratifin expression in low calcium CGM due to exogenous *K14.stratifin* expression; however, it was also noted that Stratifin expression was predominantly in the cells with a spindle morphology. Moreover, most Stratifin-positive cells exhibited a polarised sub-cellular localisation, with strongest expression seen in pseudopodia. As proposed above, anomalous Stratifin overexpression may exert a rapid transition of cells out of the proliferative niche to one of accelerated differentiation given the numbers of shedding cells and premature K1 expression (below; *Figure 7-3*); an idea consistent with the fact that primaries at clonal density initially grew but then stalled and either underwent senescence or terminal differentiation.

The *HK1.fos* line assessed, F1c, also exhibited some K1 expression in low calcium medium (*Figure 7-3*, centre panel row 3), though at lower levels than those expressing *K14.stratifin*. K1 expression then greatly increased in response to elevated calcium concentration, consistent with increased Fos expression from the HK1 promoter and the importance of AP-1 in K1 expression induction (Rothnagel et al., 1993). Additionally, F1c cells displayed Stratifin expression in low calcium which appeared to be confined to clusters of cells with slightly different, more compact morphology, possibly indicating early commitment to differentiation despite the low calcium culture medium. This is likely due to Fos activity, given the normal roles of c-Fos in keratinocyte differentiation (Greenhalgh et al., 1993b; Basset-Seguin et al., 1994; Mehic et al., 2005). Stratifin expression in F1c became widespread, similar to ICR and S1A, when exposed to a higher calcium concentration.

Of great interest was the data derived from analysis of the two *HK1.fos/K14.stratifin* lines, FS2 and FS3m, given their contrasting morphologies. Initial analysis of the most rapidly growing *HK1.fos/K14.stratifin* line, FS2, showed little change in morphology when switched to high calcium medium (*Figure 7-3*, left panel row 4) indicating resistance to differentiation and, thus, transformation; a finding supported by their growth from clonal density (below). As observed in S1A cells, many FS2 cells also prematurely expressed K1 in low calcium conditions, although, unlike the other lines assessed, K1 expression did not alter when switched to high calcium medium, again suggestive of malignant transformation (*Figure 7-3*, centre panel row 4) and consistent with the reduced suprabasal K1 expression observed *in vivo* (Chapter 4 *Figure 4-6*). Strong Stratifin expression was detected in most FS2 cells cultured in low Ca^{2+}, while the intense cellular expression observed in many cells in low calcium medium (*Figure 7-3*, right panel row 4) became more diffuse in cell cytoplasm in high calcium, suggesting that the less responsive nature of FS2 cells to differentiation cues were reflected by less endogenous Stratifin expression.

Finally, FS3m cells, which possessed unique morphological changes in low and high Ca^{2+} media (*Figure 7-3*, left panel row 5), were found to express more limited premature K1 in low Ca^{2+} than either FS2 or S1A, though a subset of cells (mainly those with flattened, irregular morphology) did express it strongly (*Figure 7-3*, centre panel row 5). Stratifin expression was seen to be very strong in some undifferentiated cells, while others showed much weaker expression. In high calcium conditions, FS3m expressed a high level of Stratifin, consistent with activation of endogenous Stratifin in suprabasal-like cells in these conditions, yet the cells failed to completely stratify, lacking terminally differentiated squames (*Figure 7-3*, right panel row 5). This result was reminiscent of the failed differentiation *in vivo* that also exhibited large, disordered cells in the suprabasal compartment and lacked a true granular layer (Chapter 4 *Figure 4-2*).

7.4 *HK1.fos/K14.stratifin* cells exhibit transformation and clonal growth correlated with high Stratifin expression

To quantify the difference in Stratifin expression, Western Blot analysis was performed on cells lines grown in low Ca^{2+} CGM (*Figure 7-4*). Band intensity was assessed using ImageJ, and Stratifin expression was normalised to that of the corresponding ß-actin band, then further normalised against WT Stratifin expression value (i.e., WT had a value of 1) with all other values expressed as a fold change.

HK1.fos/K14.stratifin line FS2 exhibited the highest levels of Stratifin expression by far, with a 50-fold increase over WT cells, yet this line possessed the fastest growth and exhibited the most resistance to Ca^{2+}-induced differentiation with little change in morphology. Thus, despite premature Stratifin-associated K1 expression in low Ca^{2+} CGM (*Figure 7-3*), these data again confirm the oncogenic potency of Stratifin in specific contexts. The other *HK1.fos/K14.stratifin* line assessed, FS3m, exhibited the next highest level of expression with an approximately 12-fold increase over normal, again consistent with premature K1 expression and oddly spinous-like morphology in low Ca2+, in addition to incomplete terminal differentiation in high Ca^{2+} CGM. These data indicate that these FS lines have a highly dysregulated response to differentiation signals, suggestive of transformation.

In addition, the average increase in Stratifin expression over normal (WT) was similar in *K14.stratifin*-expressing lines S1A/S2A and *HK1.fos*-expressing lines F1c/F2, at an average of ~6.25 and ~5.25 times the WT value, respectively. These results echo the immunofluorescence analysis which showed where elevated Stratifin expression appeared in many S1A cells (*Figure 7-3*, row 2) whilst in F1c (*Figure 7-3*, row 3) small clusters of cells expressed very high levels of Stratifin expression (which may have been prematurely committing to differentiation due to Fos activity and culture confluence), leading to this perceived similarity in expression via Western Blotting.

These western data confirm elevated Stratifin expression and add further support to the links between elevated Stratifin and *HK1.fos*-associated

expression, in the commitment to (premature, if incomplete) differentiation *in vitro*. Even in the most transformed line *HK1.fos/K14.stratifin* line, FS2, excess of Stratifin appeared to induce K1 in both low and high Ca^{2+} conditions. Nonetheless, when coupled to clonal growth and migration (below) the importance of Stratifin or Fos in terminal differentiation appears to be superseded and their co-operation leads to oncogenic transformation, as observed *in vivo*.

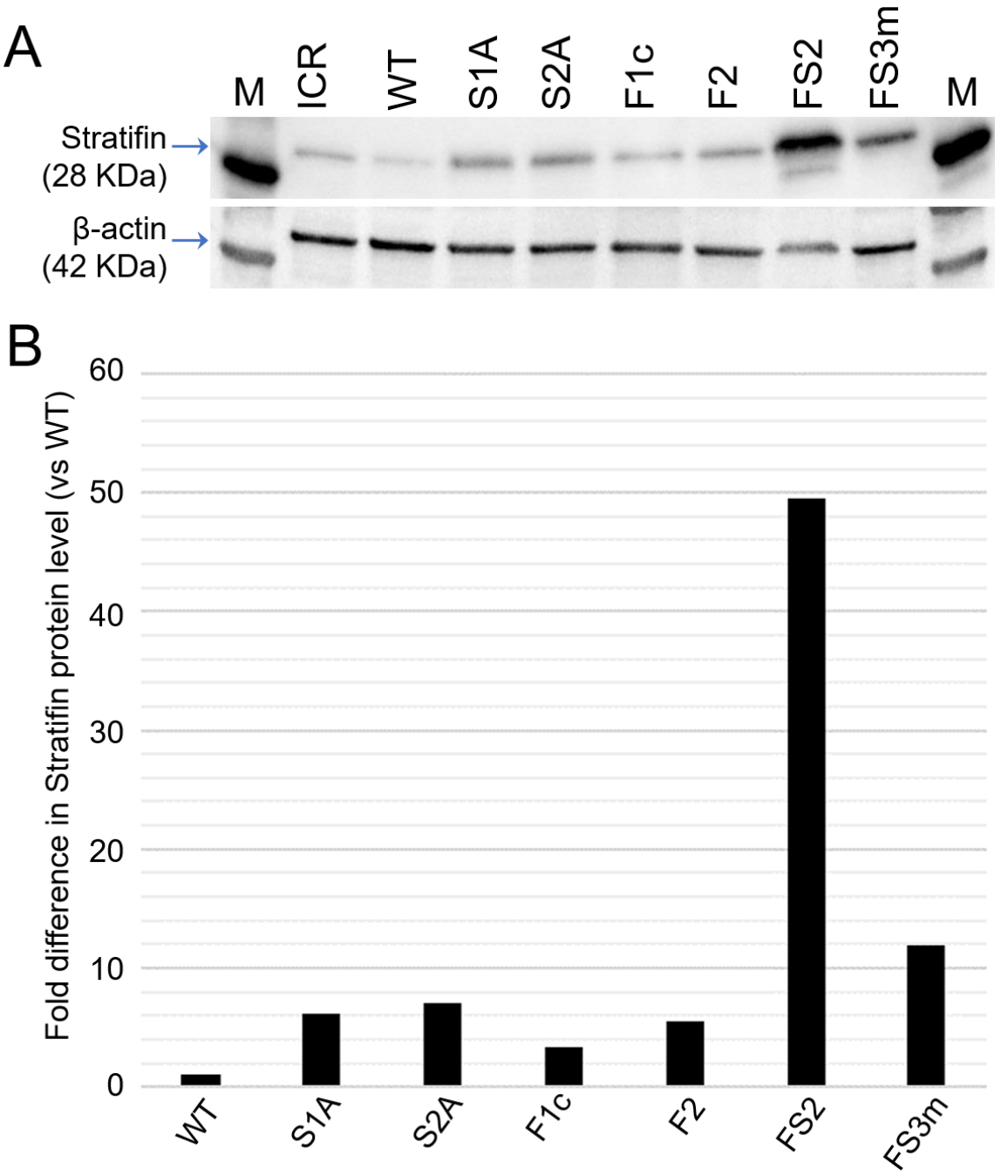

Figure 7-4: Western blot analysis shows that calcium-resistance in *HK1.fos/K14.stratifin* cell lines is correlated with the level of Stratifin expression.
(**A**) Western blot showing Stratifin protein levels normal (ICR and WT), *K14.stratifin* (S1A and S2A), *HK1.fos* (F1c and F2) and *HK1.fos/K14.stratifin* (FS2 and FS3m) cell lines using β-actin as loading control. All cell lysates shown are from cells grown in proliferative Low Ca^{2+} medium. ICR and WT lines showed lowest Stratifin levels, whilst showed F1c and F2 slightly raised levels, consistent with immunofluorescence results. S1A and S2A showed a noticeable increase in Stratifin levels, as expected. FS2 and FS3m showed the highest levels of Stratifin, with FS2 exhibiting a considerably stronger band than any other lysate. 10 µg total protein/well. (**B**) Graph of band intensities normalised to the WT band. *K14.stratifin* lines S1A and S2A show ~6-6.5-fold increase compared to WT. *HK1.fos* lines exhibited ~3.5- and 5.75-fold increase. *HK1.fos/K14.stratifin* lines show greatest levels of expression: FS2 expressed nearly 50-fold more Stratifin than WT, while FS3m expressed approximately 12-fold more than WT.

Also, it should be noted that T52$^{ras/fos}$ SCC cells employed in clonal growth experiments below, had unexpectedly retained Stratifin expression (Appendix 1; McMenemy et al., in preparation, *Figure 7*). This was thought to be due to derivation of parental SP1 cells from DMBA initiated /TPA promoted papillomas (Strickland et al., 1998) and possibility of G-o-F p53 mutations (Wang et al, 1998) giving rise to sustained Stratifin levels. However, *HK1.fos/K14.stratifin* FS2 data suggest an equally valid possibility that Stratifin contributed to Fos-mediated progression of SP1^{ras} papilloma cells into T52 SCC cells.

Given the results regarding morphological and expression differences between cell lines, their ability to grow from clonal density was assessed in low and high Ca^{2+} culture conditions. In repeat experiments, all cells utilised were between sub-culture 3 (SC3; ICR cells) and SC9 (S1A) and 6 dishes were plated out at 250 cells/dish with 3 representative results shown (*Figure 7-4)*. As found for wild-type primary keratinocytes, early passage normal ICR cells formed numerous colonies in low Ca^{2+} CGM (Greenhalgh et al., 1989) which grew very slowly and were thus relatively small when fixed at 4 weeks (*Figure 7-4*, left panel row 1). All *HK1.fos* cell lines including F1c (*Figure 7-4*, left panel row 2) showed almost no propensity for colony formation in low Ca^{2+}, with occasional small clusters of cells visible, possibly linked to the involvement of Fos in suprabasal differentiation, supported by the premature K1 expression seen in IF (*Figure 7-3,* centre panel row 3). *K14.stratifin* lines such as S1A did produce several colonies, all with a larger diameter than equivalent ICR cells, with one especially large colony seen in dish 3 (*Figure 7-4*, left panel row 3). Also, consistent with their transformed phenotype, *HK1.fos/K14.stratifin* FS2 cells formed numerous colonies in low calcium (*Figure 7-4*, left panel row 4), though growth was less extensive than in the malignant T52 cells used as a positive control (*Figure 7-4*, left panel row 6). In addition, and consistent with their odd morphology above, FS3m showed no clonal growth in low Ca^{2+} CGM.

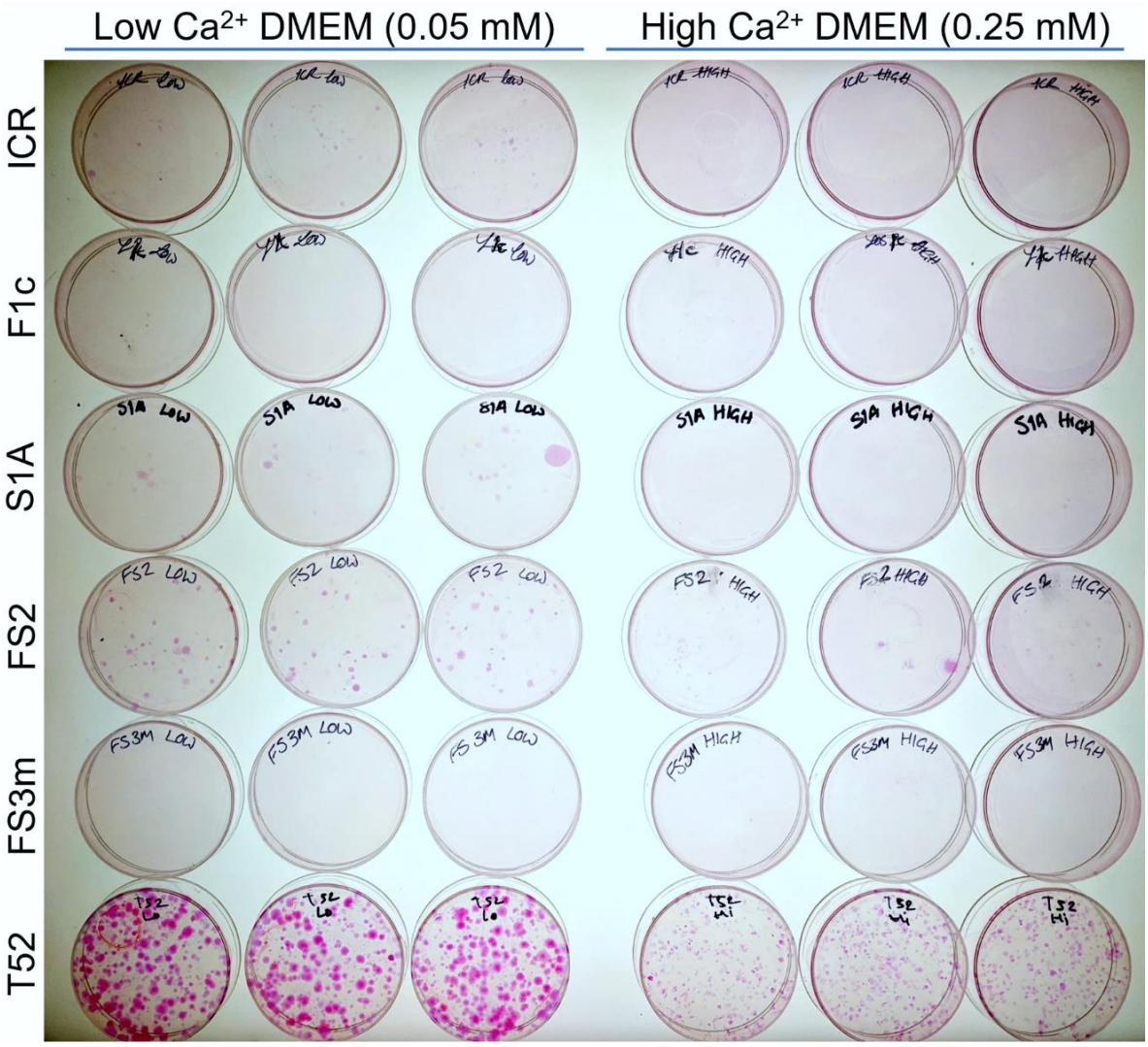

Figure 7-5: Only the highly Stratifin-expressing line, FS2, was able to form colonies from clonal density in high Ca^{2+} culture conditions.

From top: ICR cells plated at ~250 cells/dish (6 dishes; 3 representative shown) formed numerous very small colonies in 21 days in low Ca^{2+} but did not grow at all in high Ca^{2+} medium; One of the three F1c dishes grew a small number of tiny colonies in low Ca^{2+} conditions and did not grow at all in high Ca^{2+}; S1A cell formed numerous small colonies and one large colony in low Ca^{2+} but did not grow in high Ca^{2+}; FS2 produced many small colonies in low Ca^{2+} medium and exhibited some resistance in high Ca^{2+} with the formation of a few small colonies, especially in dish 2; FS3m, interestingly, did not grow from clonal density in either low or high Ca^{2+} conditions; T52 cells, transformed by infection with v-H-Ras and v-Fos constructs, were used as a positive control, showing extensive colony formation in low Ca^{2+} medium and a similar number of smaller colonies in high Ca^{2+}.

After plating out at clonal density (~50 cells/mL; ~250 cells/dish), cells were allowed to attach and settle for 24 hours prior to being switched to high calcium (0.225 mM) medium for the remainder of the assay. In these conditions, only FS2 and the positive control T52 produced any colonies (*Figure 7-4*, right panel rws 4 and 6, respectively), supporting the previous data regarding morphology and differentiation marker expression in high Ca^{2+} (*Figure 7-2*). However, considerably fewer colonies formed in FS2 than in T52, perhaps indicative of a heterogenous population or of a generally less aggressive phenotype.

7.5. Expression of *K14.stratifin* conferred enhanced migration *in vitro*

Stratifin is well-known to influence the extracellular matrix in its normal roles in regulating epidermal homeostasis. Following wounding, studies suggest that Stratifin secretion by keratinocytes targets dermal fibroblasts to upregulate Fos/AP-1 transcription activity, resulting in the production of multiple matrix metalloproteinases that aid in extracellular matrix (ECM) remodelling (Lam et al 2005; Medina et al., 2007; Ghahary et al., 2005; Ghaffari et al., 2006; Ghaffari et al., 2010; Lai et al., 2011) facilitating the necessary changes to the chemical signalling environment. In addition, as outlined in Chapters 5 and 6, these signals cause cancer associated fibroblasts to alter the local ECM via expression of such molecules as Tenascin-C (Räsänen & Vaheri, 2010; Glentis et al., 2017; Ide et al., 2007) that alter collagen type and fibre alignment, that prepare the wound site for re-epithelialisation which in turn, influence basal layer keratinocyte gene expression (Maas-Szabowski et al., 1999; Lai et al., 2011) e.g., wound-associated keratin, K6 (Wojcik et al., 2000; Wong, et al., 2003) and help limit the fibrosis of scarring (Edward et al., 2011; Rahmani-Neishaboor et al., 2012).

Thus, this process is a prime target for subversion in malignant progression, yet despite Stratifin expression being detected at the invasive front in many carcinomas, (Ide et al., 2004; Ide et al., 2007; Neupane & Korc, 2008) the actual migration abilities of keratinocytes that overexpress Stratifin has not been fully investigated. To begin to address this, these cell lines were subjected

to scratch assays (*Figure 7-5A*) to evaluate migratory potential and to see whether cells migrated collectively or individually; both seen *in vivo* (Gaggioli et al., 2007; Krakhmal et al., 2015; Hesse et al., 2016; Glentis et al., 2017; Labernadie et al., 2017). Typically, each cell line was grown to near-confluency then 3 scratches were made per dish. The dishes were photographed at 12-hour intervals over a total period of 120 hours (5 days), with medium changes every two days as standard (low Ca^{2+} CGM).

The results showed that *K14.stratifin*-expressing line (S5) closed all scratches rapidly, within a 36-hour time frame (*Figure 7-5A* row 4 and *B* blue line). The line FS2 was next quickest at 60 hours, which was somewhat unexpected given its proliferative most transformed phenotype (*Figure 7-5A* row 3 and *B* dark green line). Lines which did not overexpress Stratifin, such as F2 (*HK1.fos*) or normal ICR exhibited a markedly slower timeframe for scratch closure; F2 took double the time of FS2 at 120 hours, and ICR cells did not close the scratch within this time frame; indeed, ICR dishes were kept for a total of 10 additional days, though still failed to fully close the scratch gap.

With respect to the modes of invasion or migration in wounds, it was also noticed that in the less migratory *HK1.fos* cells and tertiary ICR cells that the borders of the scratches remained quite straight and rigid; suggesting that these cells migrate as a collective unit rather than as individuals; as observed in re-epithelisation following wounding (Ito et al 2005; Levy et al., 2005). ICR cells, especially, seemed to largely remain at the border of the scratch, suggesting that stark removal of the basement membrane component proteins they had laid down (Pruniéras et al., 1983) may have inhibited their migration across the plastic, which was not observed in any transgenic cells.

Both *K14.stratifin and HK1.fos/K14.stratifin* cells appeared to migrate as individual cells, consistent with the spaces observed between in their primary keratinocyte and cell line cultures (above *Figures 7-2* and *7-3*) and which hint at a less contact-inhibited, more migratory phenotype. Thus, this rapid migration of *K14.stratifin* keratinocytes may reflect a subversion of normal Stratifin roles as keratinocytes migrate out of the follicles during wound re-epithelisation (Ito et al., 2005; Levy et al., 2007; Snippert et al., 2010).

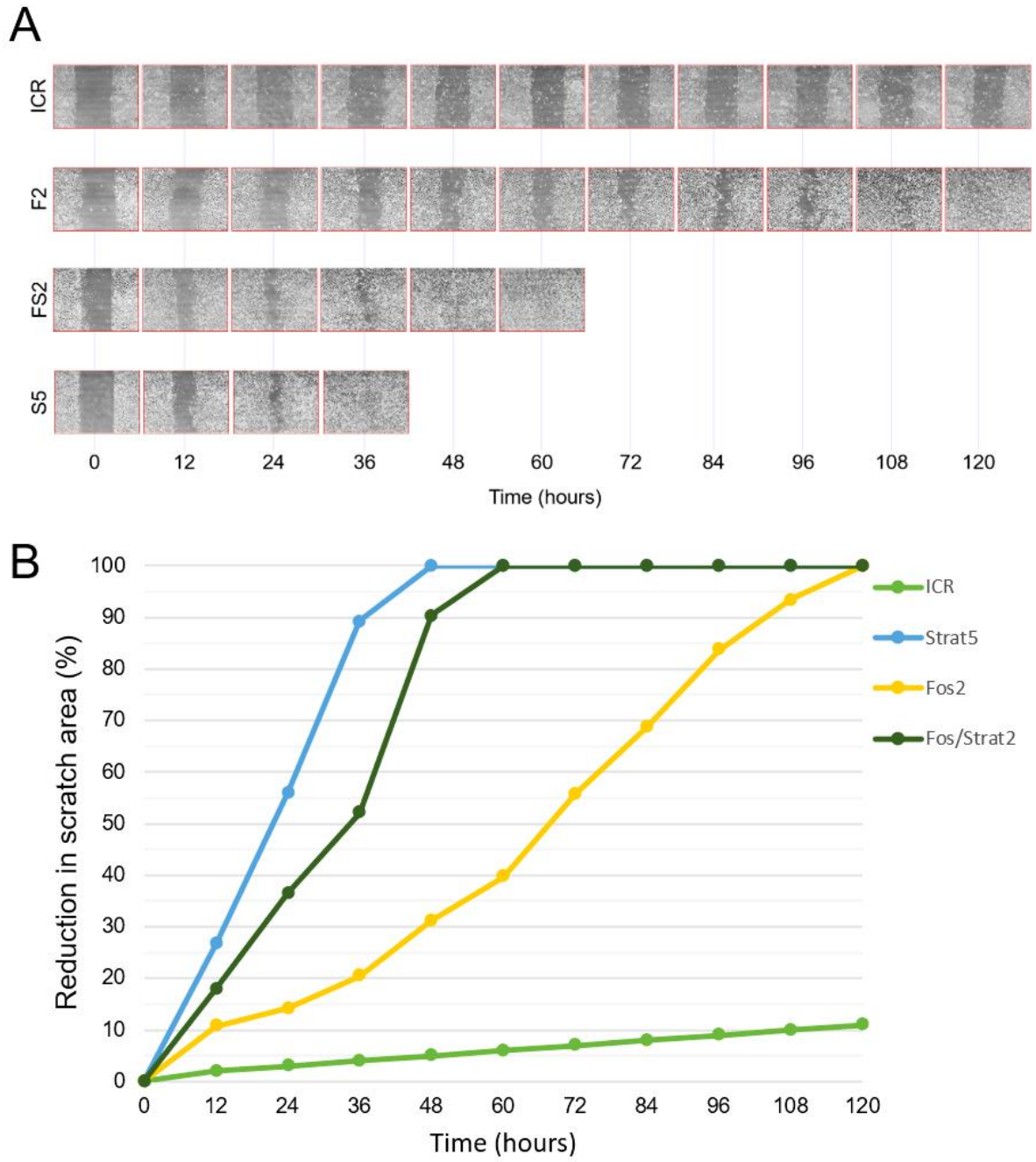

Figure 7-6: Overexpression of Stratifin is correlated with faster scratch closure. (**A**) Examples of scratch assay results in ICR, *HK1.fos* (F2), *HK1.fos/K14.stratifin* (FS2) and *K14.stratifin* (S5) cell lines; 3 scratches were made in 6 dishes per line with one of each removed and fixed at each time point for later analysis. Photos taken at 12 hr time intervals show that normal (ICR) cells did not bridge the gap in the 120-hr duration of the experiment. F2 took 120 hr to close the scratch and was used as the end point. FS2, a line known to express Stratifin at a very high level (*Figure 7-3*), closed the scratch in half that time (60 hr), while S5, expressing only *K14.stratifin*, fully closed all scratches within 36 hr. (**B**) Graphical representation of reduction in the area of all scratches in the experiment, showing the clear difference between cells expressing *K14.stratifin* and those without this transgene. Areas were determined using the area measuring function in ImageJ and averaged per line.

7.6. Discussion

The ability to culture primary transgenic keratinocytes and induce their differentiation via increased calcium levels (Hennings et al., 1980; Greenhalgh et al., 1989) has allowed experiments geared to investigate effects of transgene expression on differentiation markers and assess the degree of transformation via growth from clonal density and resistance to Ca^{2+}-induced differentiation. This classic method of assessing malignant transformation *in vitro* (Kulesz-Martin et al., 1983) was previously employed to study effects of Fos and Ras co-operation (Greenhalgh and Yuspa 1988; Greenhalgh et al., 1990). This resulted in the use of fibroblast condition medium which prevented spontaneous transformation, and also allowed clonal growth of normal primary keratinocytes and development of immortalised cell lines (Greenhalgh et al., 1989).

In terms of differentiation, use of this classic calcium switch identified consequences of Stratifin deregulation consistent with Stratifin induction during the terminal differentiation programme (Dellambra et al., 1995; Sun et al., 2015). It also highlighted the activities of Stratifin in regulating keratinocyte spatial awareness and polarisation (Ling et al., 2010) which are important as basal layer keratinocytes detach from the basement membrane (Bikle et al, 2012; Banno and Blumenberg, 2014). Similarly, effects of Fos activation further strengthened the links between these two proteins in both differentiation (Fisher et al., 1991; Greenhalgh et al 1993b; Basset-Seguin et al., 1994; Mehic et al., 2005) and transformation as seen *in vivo* (Chapter 4).

7.6.1. Primary cell culture

Cells derived from Normal, *K14.stratifin*, *HK1.fos* (not shown) and *HK1.fos*/*K14.stratifin* neonatal mouse skins were cultured in low calcium (0.05 mM) clonal growth medium and assessed for morphological differences and changes in response to high calcium (>0.15 mM). Normal cells exhibited the classic cobblestone pattern of confluent keratinocytes in 5-7 days. Conversely, both *K14.stratifin* and *HK1.fos*/*K14.stratifin* primary cells exhibited varied cell

shape and size, with elongated cells common in both, and lower cell density despite growing more quickly than Normal ICR cells.

These observations suggest effects on both increased proliferation mediated by Stratifin and Fos, followed by or paralleled by alterations in differentiation, e.g., where this subtle shape shift—which was more pronounced in cell lines—would be consistent with spatial awareness/polarisation observed previously *in vitro* (Ling et al., 2010) and may echo the shape shift observed *in vivo* as normal keratinocytes become narrow to leave the basal layer and commit to differentiation (Watt, 1987; Bikle et al., 2012; Banno and Blumenberg, 2014). This idea of rapid growth paralleled by accelerated differentiation was also consistent with premature mK1 expression mediated by excess Stratifin expression in cell lines. Moreover, the intercellular spaces may reflect an increased migratory potential of these cells, as observed in their cell line derivatives that reflect roles for Stratifin in wounding (Rahmani-Neishaboor et al., 2012).

When challenged with an intermediate calcium concentration (0.08 mM) for 24 hours, Normal cells differentiated into a spinous layer phenotype, exhibiting a flattened morphology without the bright cell edges seen in Low Ca^{2+} medium. Either continued exposure to 0.08 mM Ca2+ for a further 24 hr or a single 24 hr challenge in high Ca^{2+} (>0.15 mM) medium resulted in terminal differentiation with granular cells overlain by cornified squames; this progression is shown in *Figure 7-1* as reference for transgenic cell responses.

When plated at clonal density, normal keratinocytes in these conditions formed slowly-growing, stable colonies which stained strongly with Rhodamine B (*Figure 7-2 Panel II*). Interestingly, both primary *K14.stratifin* and *HK1.fos/K14.stratifin* cells grew poorly in low calcium clonal growth medium, forming only small colonies which did not stain strongly with Rhodamine B, which may be indicative of problems with the keratin filament network, as have been observed *in vivo* (Chapter 4). Cells in these colonies were prone to senescence and spontaneous differentiation, which may represent poorer plating efficiency compared with normal cells or a higher sensitivity to low-density culture. This is possibly related to accelerated differentiation, as seen *in vivo* in

several models expressing *K14.stratifin*, where K1 was found to be expressed in some basal cells (Chapter 4 *Figure 4-15*; Chapter 6 *Figure 6-7*; Supplementary data *Figure S4*). T52 cells (v-H-Ras/v-Fos transformed; Greenhalgh et al., 1990) were used as a positive control for malignant cells which grew rapidly in both low and high Ca^{2+} medium, while neither *K14.stratifin* nor *HK1.fos/K14.stratifin* primaries continued to grow after medium was switched to 0.15 mM Ca^{2+}, with morphology showing they had terminally differentiated.

7.6.2. Phenotypes of cell lines derived from primary cultures

Primary keratinocytes were also maintained in low calcium clonal growth medium (to prevent spontaneous malignant transformation) and cell lines were established for further study producing lines designated: Normal: WT, ICR; *K14.stratifin*: S1A, S2A, S4, S5; *HK1.fos*: F1c, F2, F5, F6; *HK1.fos/K14.stratifin*: FS1s, FS2, FS2s, FS3m and FS4. Initial analysis examined morphological changes, hence the suffixes "s" denoted lines with an elongated, spindle-shaped morphology, or "m" with a particularly unusual and irregular morphology, that may reflect establishment of a proliferative line with elements of a spinous layer keratinocyte phenotype. Of note, *K14.stratifin* lines that developed an elongated morphology (typified by the S1A cells shown in *Figure 7-3*) grew fairly quickly, but they also spread throughout flasks/dishes before reaching confluency, suggesting these cells were prone to migrate in monolayer cultures– as confirmed in migration assays (*Figure 7-6*).

In addition, reflecting the complex, context-specific roles Stratifin exerts in the epidermis, all *K14.stratifin* and *HK1.fos/K14.stratifin* lines grew faster than Normal or *HK1.fos* keratinocytes, consistent with studies that show Stratifin aids in cell proliferation, for example, by upregulating mTOR activity by facilitating its interaction with cytokeratin 17 (K17) (Kim et al., 2006; Mikami et al., 2015). However, in all *K14.stratifin* cell lines, Stratifin overexpression gave rise to confluent *K14.stratifin* cultures that exhibited marked shedding of cells in low calcium medium along with notable premature mK1 expression, consistent with a role in the commitment to differentiate (Dellambra et al., 1995; Bikle et al, 2012; Banno and Blumenberg, 2014). These results suggest that

overexpression of Stratifin induced early differentiation in low Ca^{2+} medium consistent with the normal suprabasal differentiation profile for Stratifin observed *in vivo* (Westfall et al., 2003; Trink et al., 2007; Sun et al., 2015).

In contrast, *HK1.fos* cell lines, such as F1c, grew more slowly than the *K14.stratifin* or *HK1.fos/K14.stratifin* lines. The HK1 promoter is largely activated by the same cues as mK1, thus, is more strongly activated in high calcium medium, where it (like endogenous c-Fos) regulates differentiation, as described in Chapter 1 (Fisher et al., 1991; Mehic et al., 2005). However, the modifications to the HK1 promoter allow it to be expressed in a subset of basal-like cells in low calcium conditions (Rosenthal et al., 1991; Rothnagel et al., 1993). Given its roles in differentiation of keratinocytes, this pattern of expression may account for the clusters of mK1 positive cells seen in F1c cultures (*Figure 7-3*), as well as the strong expression of endogenous Stratifin in similar cell clusters in low calcium. These findings suggest that, alone, *HK1.fos* cell lines may be prone to premature differentiation, supported by the fully differentiated phenotype seen in high calcium medium (Greenhalgh et al., 1993b; Basset-Seguin et al 1994; Mehic et al., 2005). This is believed to counter the oncogenic proliferation induced by *HK1.fos* expression in vivo, resulting in only hyperplasia rather than papilloma generation (Chapter 4 *Figure 4-2*) (Greenhalgh et al., 1993b).

HK1.fos/K14.stratifin lines which were assessed for calcium resistance showed varying results. FS2 showed very little change in morphology in response to high calcium medium, while FS3m, which had a markedly different morphology in low calcium to FS2, appeared to differentiate somewhat but did not form cornified cells (squames). This is reminiscent of the different levels of severity in the *HK1.fos/K14.stratifin* phenotype *in vivo*, suggesting that differences in the keratinocytes themselves exist in addition to changes in the microenvironment which drive tumorigenesis. Indeed, differences in cellular expression in keratinocytes form a feedback loop with their microenvironment via paracrine signalling and directly influence the behaviour of stromal and immune cells, which in turn affect tumour development (Goetz et al., 2011).

Morphological changes in response to calcium were supported by the changes in K1 expression in these cell lines. ICR cells did not express Keratin 1 in low calcium medium, which increased greatly due to calcium-induced differentiation. This was also seen in F1c cells, though the cells in low calcium interestingly exhibited some low-level K1 expression, suggesting a subset of cells were primed for differentiation by *HK1.fos* expression, also seen *in vivo*, wherein the wound-promoted hyperplasia is delayed as proliferation is counterbalanced by increased differentiation (Chapter 4 *Figure 4-2*; Greenhalgh et al., 1993b).

7.6.3. Enhanced cell migration was associated with Stratifin overexpression *in vitro*

One consistent feature of Stratifin overexpression *in vitro* was the increase in cell migration which was apparently separate to transformation status. These data are consistent with roles suggested for Stratifin in terms of spatial awareness—indicated here in immunofluorescence (*Figure 7-3*)—and the fact that Stratifin appears in several invasive internal carcinomas (Ide et al., 2004; Neupane & Korc, 2008; Li et al., 2009; Naidoo et al., 2012). The results also indicate that Stratifin-overexpressing keratinocytes can migrate independent of dermal fibroblast interactions that are necessary to provide the ECM remodelling observed in full thickness wounding (Ghahary et al., 2005; Ghaffari et al., 2006; Ghaffari et al., 2010; Lai et al., 2011). This suggests that in wound-healing, paracrine Stratifin secretion from such migratory keratinocytes (Ito et al., 2005) maybe an essential facet that helps reduce fibrosis and scarring thus improving the overall healing process (Edward et al., 2011; Rahmani-Neishaboor et al., 2012).

This increase in motility may be facilitated by the interaction between Stratifin, intermediate filaments (K5 and K17) and soluble actin; a complex which has been shown to potentiate movement of breast cancer cells by mediating a dynamic pool of cytoskeletal components (Boudreau et al., 2013). The reasoning for the lower migratory potential of FS2 cells compared to the *K14.stratifin* lines is unclear; however, this may reflect concurrent activated Fos

expression, as *HK1.fos* lines readily terminally differentiated in response to high calcium medium (*Figure 7-3*), reflecting the importance of Fos in the differentiation program, as described in Chapter 1 (Fisher et al., 1991; Greenhalgh et al 1993b; Mehic et al., 2005). This suggests that expression of *HK1.fos*, while conferring a transformed phenotype in conjunction with high Stratifin expression, actually impeded movement of cells into the scratched area. It may be that Fos transcription factor activity—that regulates expression of many intermediate filaments (Oshima et al., 1990; Ma et al., 1997)—simply creates a different cellular context with reduced migratory potential due to alterations in influence of Stratifin activities.

Nonetheless, once transformed, Western Blot analysis showed clear differences in the level of Stratifin expression between cell lines, with the highly-expressing line FS2 showing both most resistance to Ca^{2+}-induced differentiation and being the only line tested to grow from clonal density in high calcium medium (*Figure 7-5*). This appears to be consistent with the results observed *in vivo* in previous chapters, wherein *K14.stratifin* expression was repeatedly linked to a greater propensity for invasion than in controls not expressing this transgene. Also, whilst the unique phenotype of FS3m remains to be fully elucidated, co-expression of Fos and Stratifin did confer some Ca^{2+} resistance. Here it may be that these cells represent a stalled spinous morphology, with the more moderate 12-fold increase in Stratifin expression over normal seemingly conferring a suprabasal-like phenotype on these cells even in low Ca^{2+} medium. This may account for the weak response to high Ca^{2+} medium which resulted in an incomplete differentiation, denoted by the lack of stratification and cornified cells.

The differences in the characteristics of these *HK1.fos/K14.stratifin* and *K14.stratifin* lines further cements the hypothesis that the effects of Stratifin overexpression vary greatly in different subcellular environmental contexts and appear to indicate that the resulting phenotypes are dose-dependent. This latter point may be an important factor in the different degrees of severity of the *HK1.fos/K14.stratifin* phenotype *in vivo*. The approximately 50-fold excess in Stratifin expression observed in the most transformed FS2 line clearly shows that the synergy between these two proteins is the important factor and combined,

support the hypothesis that increased Stratifin expression confers growth advantages and resistance to differentiation signals in conjunction with Fos activation.

Further, with respect to invasion, whilst the scratched borders of normal keratinocytes remained quite rigid, this was not the case in Stratifin-expressing cells. This suggests that, as observed *in vivo* in the more aggressive *HK1.fos/K14.stratifin* fSCC cells and Type 2 *HK1.ras/K14.stratifin* SCCs, cells appeared to migrate as individuals rather than as a collective unit—an observation also consistent with the spaces between individual *K14.stratifin* and *HK1.fos/K14.stratifin* cells observed in primary and cell line cultures. In contrast the less aggressive Type 1 *HK1.ras/K14.stratifin* SCC cells initially retained some element of the collective cell invasion mode (*Figure 5-7*).

This latter observation suggests that the collective front migration model requires the continued maintenance of cell-cell adhesion, thus E-cadherin—a key component of adherens junctions—would be expected to persist (*Figure 5-7*) (Krakhmal et al., 2015; Hesse et al., 2016), but of necessity in the aggressive cell lines, E-cadherin must be lost to facilitate individual cell invasion.

7.6.4. Limitations

This *in vitro* study utilised keratinocytes derived from neonatal skins to establish primary monocultures from which cell lines were derived for further study. While this produced useful results, there were notable limitations due to resources and time constraints which affected the strength of the study and the robustness of its conclusions. For example, none of the cell lines (with the exception of Fos1c) were clonally derived, thus the populations were heterogeneous and therefore may not have displayed uniform protein expressions and behaviours throughout the cultures. This also means that with each passage, the more transformed cells were likely being selected for, since these trypsinise more readily than normal keratinocytes—though it should be noted that all lines used here were at very early passage numbers (≤ 10). Going forward, clonal colonies will be derived to improve repeatability of the work, and to minimise confounding factors related to uneven transgene expression

within colonies (noted above to be possible with the expression of *HK1.fos* in low Ca^{2+}, proliferative medium).

Additionally, cells grown on chamber slides for immunofluorescence analysis were near confluent when fixed, which is known to change protein expression and behaviour of keratinocytes compared to growing colonies. This issue was later corrected in a repeat experiment, however, time constraints primarily due to work on concomitant *in vivo* studies meant that staining was not completed within the allotted time for research activities and therefore could not be included here. Similarly, logistical problems in performing western blotting meant that, while proteins were isolated and transferred to membranes, the staining and visualisation for a variety of proteins of interest could not be performed as this had to be done at a secondary location and was later postponed indefinitely due to restrictions relating to Covid-19.

While these problems certainly impact the strength of the conclusions which can be drawn, the *in vitro* work nevertheless allowed for better insight into the relationship between *K14.stratifin* expression and keratinocyte morphology and behaviour which was harder to glean from *in vivo* experiments. Importantly, this work also established multiple cell lines for use in future work (detailed below) which could allow for much more insight into the *HK1.fos/K14.stratifin* phenotype and the underlying mechanisms.

7.6.5. Future directions

To further explore potential Stratifin expression role(s) in these models of re-epithelialisation during wound closure and altered migration potential that mimics invasion, experiments are planned to assess the migrating cell fronts for expression of Stratifin and its subcellular localisation; together with E-cadherin, ß-catenin and Keratin K6α, initially employing the fixed dishes and, subsequently, 3D organotypic invasion assays (Edward et al., 2010; Timpson et al., 2011; Appendix 1: McMenemy et al., in preparation). These may also be useful in assessing the effects of Stratifin on normal fibroblasts employed to contract the matrix, as CAFs appeared to play important roles in tumorigenesis

in vivo, and such a setup may allow for easier characterisation of their changes in behaviour and gene expression with time than *in vivo*.

Larger scale protein analysis via Western blotting also remains to be performed on cell lysates obtained from all primary cultures and immortalised cell lines; this includes lysates in both RIPA buffer (for soluble proteins) and SDS/ß-mercaptoethanol buffer (for insoluble components including keratins). Given the notable effects on the keratin filament network observed *in vivo* in *HK1.fos/K14.stratifin* tumours and their apparent follicular origin, expression of various keratins associated with the terminal differentiation programme and with specific compartments of the hair follicles will be examined and quantified relative to normal ICR primary and tertiary cell lysates.

Given the consistently invasive phenotypes seen *in vivo* in previous chapters and the greater migratory potential observed here *in vitro* when Stratifin is overexpressed, further work should also focus on cell components which regulate cell movement, such as the actin cytoskeleton and the proteins with which it associates in pseudopodia (such as that seen in FS3m cells in *Figure 7-3*). This is especially of interest since Stratifin was found to mediate a pool of soluble actin in complex with intermediate filaments in a basal-like breast cancer model (Boudreau et al., 2013), and therefore should be assessed here to see whether the same is true in epidermal cells and whether other components may be involved.

Finally, in the long term, new transgenic mice have been imported to assess effected of E-cadherin loss and ß-catenin overexpression that will allow further investigation of the roles of Stratifin in these *in vitro* and *in vivo* models of keratinocyte differentiation and carcinogenesis.

7.6.6. Conclusions

The cell lines generated in this study have confirmed several observations in vivo, such as premature K1 expression and increased migratory capacity in cells expressing high levels of Stratifin via the *K14.stratifin* transgene. These cultures, along with the proteins which can be analysed from cell lysates of both

primary and cell line cultures, will provide valuable insights into the behaviour of keratinocytes in the fSCC phenotype. This will allow further analysis of the keratinocyte-specific behaviours in this genotype, separate to the effects of immune cells or stromal fibroblasts, allowing insights into fibroblasts-independent migration and invasion mechanisms which appear to be pertinent across all *K14.stratifin*-expressing genotypes studied, here.

Chapter 8 Final Discussion

8.1. Summary of the findings

The main aim of this study was to evaluate the possible tumour suppressive or oncogenic roles of Stratifin in cutaneous squamous cell carcinoma using transgenic mouse models.

In Chapter 3, analysis of endogenous Stratifin expression in a well-characterised multistage model of carcinogenesis (*HK1.ras/fos-Δ5Pten*) showed that its loss occurred subsequent to that of p53, persisting in the well-differentiated carcinoma until p21 loss signalled transition to a poorly-differentiated histotype. This suggested that Stratifin exhibits tumour suppressive roles separate to its positive regulation of p53 levels in the context of this multistage model and may support p21-mediated cell cycle inhibition (Hermeking et al., 1997; Niculescu III et al., 1998; Steiner et al., 2012) until the mutational burden in the absence of p53 and Pten activity tips the balance in favour of progression to pdSCC.

In Chapter 4, experiments progressed to investigate Stratifin activity further in the context of these established models, employing new transgenic mice which overexpresses human Stratifin under the control of a Keratin 14 promoter. This allowed targeting to the undifferentiated epidermis and hair follicle outer root sheath. *K14.stratifin* mice were found to develop epidermal hyperplasia without hyperkeratosis in the epidermis ~6 months after wound promotion (ear tag) was applied; a novel finding which had not been previously reported due to the lack of wound-promotion employed in the original study (Cianfarani et al., 2011).

K14.stratifin expression was then investigated in the context of activated Fos expression (Chapter 4). These mice developed rapidly-growing wound-promoted tumours, and most also developed either hyperplasia/hyperkeratosis or a tumour on the non-tagged ear. Histological analysis, differentiation marker loss and increased BrdU labelling indicated that *HK1.fos/K14.stratifin* tumours converted to malignant carcinoma within weeks and did not require further genetic manipulation to do so; indeed, ablation of p53 in this model had no effect on timing of tumour development or histological appearance. Certain

histological features and the pattern of Keratin 17 staining indicated that the model recapitulated human follicular squamous cell carcinoma (fSCC); described in the literature as an under-recognised neoplasm which is often misdiagnosed and requires further study (Shendrik et al., 2013; Carr et al., 2014). There was also extensive disruption to the keratin filament network, including loss of co-localisation of partner keratins K1 and K10, and perinuclear collapse of K14 — possibly indicating novel activities of Stratifin in regulating intermediate filament stability.

Next, following the unexpected and intriguing *HK1.fos/K14.stratifin* data, Chapter 5 explored the possibility that Stratifin overexpression may also have a tumour promoting, rather than suppressing, role in co-operation with H-Ras activation. Thus, the *K14.stratifin* transgene was co-expressed with *HK1.ras*, which alone results in benign, wound-dependent papillomas. Here, two distinct tumour aetiologies were produced: Type 1 slow growing, wound-dependent tumours which showed signs of malignant conversion after approximately 3-4 months, and Type 2 rapidly-growing, wound-independent tumours which exhibited widespread malignant conversion. These were blatantly of different tumour aetiology to the *HK1.fos/K14.stratifin* fSCCs, with histotypes more closely resembling classic cSCCs than the unusual histotype detailed in Chapter 4. Histological analysis indicated a high stromal content and collective invasion of keratinocytes in Type 1 tumours, while Type 2 featured a more aggressive histotype with both collective and individual cell invasion present. Differences in the co-localisation of K1 and K10 were found, with Type 1 tumours similar to *HK1.ras* controls while Type 2 showed greater divergence, somewhat akin to *HK1.fos/K14.stratifin* results.

In addition, previous studies have shown that ablation of p53 in these *HK1.ras* mice resulted, unexpectedly, in the suppression of tumour development (Greenhalgh et al., 1996); here, this illogical result again appeared in control *HK1.ras/p53*$^{flx/flx}$ genotypes as previously observed. Thus, this provided an opportunity to assess if Stratifin overexpression could by-pass this "p53 paradox". However, unlike *HK1.fos/K14.stratifin* aetiology which appears to be uncoupled from p53 activities, here following p53 ablation, whilst all *K14.ras.p53*$^{flx/flx}$*.stratifin* hyperplasias were found to be sporadically invasive

and have a high level of inflammatory infiltrate, again there was a lack of overt tumour formation.

To further assess the roles of Stratifin overexpression in the context of TSG ablation, preliminary experiments reported in Chapter 6 investigated the consequences of *K14.stratifin* transgene expression in mice lacking either p53 or Pten (*K14.p53$^{flx/flx}$.stratifin* and *K14.Pten$^{flx/flx}$.stratifin*), then subsequently alongside loss of both TSGs (*K14.p53$^{flx/flx}$.Pten$^{flx/flx}$.stratifin*). *K14.p53$^{flx/flx}$.stratifin* mice exhibited signs of malignancy including dysplasia, hyperchromatic nuclei and invasion, which were absent in *K14.p53$^{flx/flx}$* controls. Expression of *K14.stratifin* was then found to greatly exacerbate the Cowden Syndrome phenotype of *K14.Pten$^{flx/flx}$* mice, and histopathology indicated that, while no overt tumours were generated, patches of invasive carcinoma formed on wound-promoted ear skin. This was confirmed by examination of differentiation marker (K1) loss, though Akt upregulation was not determined to be a factor in carcinogenesis. Dual ablation of p53 and Pten concurrent with Stratifin overexpression resulted in wound-independent tumour production with variable histological appearances, though all showed signs of malignant progression. Furthermore, all tumour sites were macroscopically hairless and, as in *K14.Pten$^{flx/flx}$.stratifin* skin, HFs structures appeared to be integral to the pathology, though these, too, did not resemble the fSCCs generated in *HK1.fos*/*K14.stratifin* mice.

Finally, in Chapter 7, primary keratinocytes were obtained from neonatal skins of *HK1.fos*, *HK1.fos*/*K14.stratifin* and *K1.stratifin* transgenic pups, alongside normal controls, to assess effects of these transgenes on Calcium-induced differentiation and cell migration. It was found that despite morphological changes consistent with transformation and their consistent tumorigenic effects *in vivo*, primary transgenic cells did not display resistance to high Ca^{2+} concentrations and terminally differentiated similar to normal ICR cells. They were also unable to grow from clonal density in either low or high Ca^{2+} medium.

Immortalised cell lines derived from the initial primary cultures to facilitate further analysis of their traits *in vitro*. Slight differences in morphology

of the lines were observed compared to normal ICR cells, as well as different levels of resistance to Ca^{2+} and the ability to grow from clonal density; more transformed *HK1.fos/K14.stratifin* cells (line FS2) were found to express the most Stratifin using Western Blot analysis. Lastly, migration potential was assessed using a scratch assay, which showed that higher Stratifin expression was correlated with shortened wound-closure time, though concurrent expression of *HK1.fos* was found to increase closure time over cells expressing *K14.stratifin* alone.

8.2. Contribution of Stratifin to tumour initiation, progression and invasion

The initiation stage of carcinogenesis involves mutations in the sequence of genes or changes to their epigenetic control mechanisms which increase the risk of cancer formation. For example, *HK1.ras*, mimics activating mutations in the *HRAS* gene, with some lines (e.g., 1205) able to form benign papillomas upon wound-promotion, whereas *HK1.fos* give hyperplasia and require further genetic hits over time (often >12 months) to achieve even benign papilloma development. However, these models can universally initiate carcinoma development when subjected to further "hits" (as in *HK1.ras-Δ5Pten* + TPA and *HK1.ras/fos-Δ5Pten*) (Yao et al., 2006; MacDonald et al., 2014). Here, it was found that overexpression of Stratifin alone via the *K14.stratifin* construct produced only mild hyperplasia after several months in wound-promoted skin (Chapter 4), while carcinomas developed in all multigenic models. This indicates that Stratifin, too, is unable to induce carcinogenesis alone, consistent with decades of study indicating the requirement for multiple concurrent genetic aberrations for tumour development (Ashley, 1969; Knudson, 1971, 2001; Renan, 1993).

When *K14.stratifin* was co-expressed with either the *HK1.fos* or *HK1.ras* oncogenes, the skin did progress to carcinogenesis either as an overt tumour (Chapters 4 and 5) or, following additional TSG loss, unusual invasive hyperplasia (Chapters 4 and 6), consistent with roles in cell migration (Chapter 7). Collectively, these data showed that overexpression of Stratifin can act as a

potent tumour promoting agent, as even concurrent expression of *HK1.ras* and *HK1.fos* does not induce progression past the benign papilloma stage without further genetic insult *in vivo* (Greenhalgh et al., 1993c), despite their wide-ranging effects and known oncogenic properties (Milde-Langosch, 2005; Bejjani et al., 2019; Brown et al., 1990; Hancock, 2003).

One aspect which may help to elucidate this is the aberrant expression of Keratin 1 in the basal layer and hair follicles (including stem cell compartments) seen in all skins expressing *K14.stratifin* (Chapter 4 *Figure 4-16*). While this may, at first, seem counterintuitive since early K1 (and K10) expression has been associated with tumour suppression (Kartasova et al., 1992; Santos et al., 2002), the HK1 promoter is sensitive to the same activating cues as the endogenous mK1 (Rosenthal et al., 1991); therefore, it is likely that *HK1.ras* and *HK1.fos* are expressed in the HFs and possibly in a greater number of basal cells when *K14.stratifin* is active.

In all experimental models incorporating *K14.stratifin*, some evidence of keratinocyte invasion was observed, and was extensive in some cases. Instances of both collective and individual cell invasion were found to be present, sometimes in the same tumour, indicating multiple underlying mechanisms at play. Evidence suggests that paracrine signalling to stromal cells and the likely development of cancer-associated fibroblasts (CAFs) is integral to facilitating early invasion (Gaggioli et al., 2007; Glentis et al., 2017), with Stratifin known to be a potent paracrine activator of fibroblasts to facilitate tissue remodelling (Lam et al., 2005; Ghaffari et al., 2010; Liu et al., 2016). This was exemplified in Type 1 *HK1.ras*/*K14.stratifin* tumours, which were largely benign but where patches of carcinoma *in situ* and multiple regions of E-cadherin positive collectively invading cells invasion. This was also supported by the observed marked increase in Tenascin-C expression in all *HK1.ras*/*K14.stratifin* tumour stroma; TEN-C is a matrix glycoprotein which has been proposed as a novel CAF marker (Ni et al., 2017), and has been found to be associated with increased tumour invasion, metastasis, and recurrence (Jahkola et al., 1998; Cai et al., 2017; Sun et al., 2019), in some cases linked to higher Stratifin expression in the associated keratinocytes (Ide et al., 2007). This appears to be consistent with the observations here that invasion precludes overt tumour formation in TSG

ablation models (Chapter 6) and increased migration in vitro (Chapter 7), which echo studies in human carcinomas both in clinical samples and in *in vitro* experiments (Boudreau et al., 2013).

8.3. Significance: potential biomarker and drug target?

8.3.1. Background

Cutaneous SCC (cSCC) is the second most common skin cancer in Caucasians and represents around 20% of skin malignancies (Rogers et al., 2006). It is also the most common cancer overall with the capacity to metastasise (Brougham et al., 2012) and its incidence is increasing, especially in younger and immunocompromised populations (for example, transplant recipients and those being treated for autoimmune conditions) (Christenson et al., 2005; Hunter et al., 2012; Karia et al., 2013; Schmults et al., 2013). True incidence and mortality are difficult to measure, however, with large ranges reported in the registries which do separate SCC data from BCC (Que et al., 2018); indeed, some studies have proposed that the ratio of SCCs to BCCs is actually much closer than the 1:5 often cited (Rogers et al., 2015). Additionally, the incidence of the fSCC subtype believed to be recapitulated by the *HK1.fos/K14.stratifin* mouse model is currently unknown, with reports describing the disease as under-recognised and often mistaken for other entities in the clinic, including BCC (Shendrik et al., 2013), since the histopathology is rather unlike classic cSCC.

In the clinical setting, tumour staging is among the most important aspects when devising treatment options and evaluating prognosis (Que et al., 2018). In superficial or locally invasive cSCC (i.e., contained within the dermis), ablative therapy (e.g., liquid nitrogen) or surgical resection alone may be sufficient, with a 5-year cure rate of >90% (Stratigos et al., 2015). Current European guidelines for treatment of cSCC indicate that surgical margins for resection of low-risk tumours (<2 cm horizontal width) are recommended to be at least 5 mm, while higher risk tumours (>2 cm diameter or >6 mm depth) require larger margins of 10 mm (Stratigos et al., 2015). While this approach is often curative, in sensitive areas of the face, such as the lips and eyelids or skin

overlying the facial nerves, these margins cause disfigurement and loss of functionality which may render them unresectable. In such cases, radiotherapy may be employed as an alternative or as an adjuvant to less radical surgery and provides favourable responses and a similar 5-year survival to surgery in many cases (Al-Othman et al., 2001), especially when combined with platinum-based chemotherapy (Ogata et al., 2020). However, radiotherapy is contraindicated in many situations, including on photodamaged skin, areas which are poorly vascularised areas or prone to trauma (e.g., lower legs), patients who are immunocompromised, or have previously undergone radiotherapy, and those with cancer-predisposition syndromes like *Xeroderma pigmentosum* (Stratigos et al., 2015).

Metastasis to local lymph nodes (LN) is believed to occur in around 4% of cases (Schmults et al., 2013) and has been shown to dramatically reduce the 5-year survival rate to only around 30% (Givi et al., 2011). This is due to its correlation with poorer histological grade and a higher incidence of both local recurrence and distant metastasis than *in situ* or locally invasive disease. While combined surgery and radiotherapy (or radiotherapy with systemic platinum-based chemotherapy in cases which are unresectable) has been shown to provide the best outcomes in the case of LN involvement, many people in the mean age group are ineligible for radiotherapy due to immunodeficiency (Givi et al., 2011; Stratigos et al., 2015; Ogata et al., 2020). In light of this, it is clear that prevention of LN invasion is paramount and new treatment options for those which have already reached this stage are vital if survival is to be improved. Therefore, identification of proteins involved in tumorigenesis and carcinogenesis is necessary for development of targeted therapies which could allow less intensive treatment to be possible, especially those limiting the requirement for repeated hospital treatment as with radiotherapy.

Currently, the only targeted systemic therapies available for advanced SCC are EGFR inhibitors such as Erlotinib and Cetuximab (Gold et al., 2018; Alter et al., 2013; Otaga et al., 2020) and, very recently, Cemiplimab, a monoclonal antibody which targets programmed cell death-1 (PD-1) and has shown promising results (Migden et al., 2018; Guerrero et al., 2019). It should be noted, however, that studies have shown that constitutively active mutant *KRAS* or *HRAS* reduce

efficacy of therapies targeting EGFR (Hah et al., 2014), which occur in 3% and 6% of cSCCs (though *HRAS* may be more prevalent in aggressive SCCs than in general at around 20% (Pickering et al., 2014)).

8.3.2. Biomarker

Biomarkers are signs, including protein expression, which can be used to identify pathological processes with which they are correlated (e.g., PSA glycoprofiling in prostate cancer (Tkac et al., 2019)) or are involved in generating (e.g., BCR-ABL transcripts in chronic myeloid leukaemia (Mishra et al., 2018)). In this study, Stratifin overexpression was consistently shown to have oncogenic effects in a range of transgenic mouse models including those overexpressing the activated oncogenes Fos and H-Ras, and lacking tumour suppressor genes p53 and Pten. The most common features seen across the models were invasion, immune infiltration, and a propensity for wound-independent tumour development.

Stratifin overexpression is correlated with invasion and poor prognosis in multiple carcinoma types, with research showing a link between high Stratifin expression in some internal carcinomas and lymph node metastasis leading to poorer prognosis (Neupane and Korc, 2008; Li et al., 2009; Naidoo et al., 2012; Robin et al., 2020). Even in breast cancer, where Stratifin expression is commonly lost through promoter methylation, studies have shown that in a subset of cases where Stratifin is highly expressed (often triple negative and basal-like subtypes), it is significantly correlated with invasion, and both poorer disease-free survival and disease-specific survival (Simpson et al., 2004; Boudreau et al., 2013; Ko et al., 2014).

While there is some evidence suggesting that Stratifin is retained in many human cutaneous SCCs (Lodygin et al., 2003), there is a paucity of data regarding its expression in these skin cancers. In Chapter 3, it was shown that endogenous Stratifin expression is greatly reduced following malignant conversion in *HK1.ras/fos-Δ5Pten* carcinomas, after the loss of its main activator, p53 (Appendix 1; McMenemy et al., in preparation). However, overexpression of Stratifin in the studies regarding internal carcinomas show

that epigenetic alteration, namely promoter hypomethylation, is the primary mechanism of upregulation, thus, in the context of normal epigenetic regulation and in the absence of p53 (or TAp63) this is perhaps not surprising. Additionally, most cutaneous SCCs possess a mutant G-O-F isoform of p53 which may be able to transactivate Stratifin expression, though this does not appear to have been investigated yet.

All experiments described in this thesis in which Stratifin has been exogenously overexpressed resulted in increased carcinogenesis and invasive potential, thereby supporting the literature describing Stratifin as a "double-edged sword" (Li et al., 2009), as both its loss and overexpression are tumour-promoting but highly context-dependent. This is indicated by the *in vitro* experiments described in Chapter 7, wherein *HK1.fos/K14.stratifin* cell lines which expressed more Stratifin were seen to be more highly transformed and less sensitive to differentiation cues than lines expressing lower levels (FS2 vs FS3m). Similarly, while *HK1.fos*-only lines expressed more Stratifin than normal ICRs, the level was not found to be hugely different to *K14.stratifin* cells by Western Blot quantitation, but as the IF analysis showed, the number of cells expressing the protein above ICR baseline in low calcium medium (discrete clusters in F1c vs all cells in S1A, for instance) created a totally different context which did not promote transformation in these cells.

Furthermore, when *K14.stratifin* was expressed *in vivo* concurrently with p53 ablation (both alone and alongside *HK1.ras* expression), and with Pten ablation, histological analysis indicated the presence of areas of invasive carcinoma; however, no overt tumours were produced (or occasional small ones in *K14.ras.p53flx/flx.stratifin* mice). This suggests that Stratifin has promoting roles in carcinogenesis, but not necessarily in overt tumour development. Indeed, since monogenic *HK1.ras* mice generate benign tumours upon wound-promotion, it may be that, while *K14.stratifin* expression clearly augments the histotype, its main promotion roles are in malignant conversion and invasion rather than early-stage tumour development. Thus, the only model described here in which Stratifin overexpression appears integral to initial tumour development as well as malignant conversion is in the unique

HK1.fos/K14.stratifin fSCC histotype. Hence, Stratifin is likely most use as a biomarker of invasive malignant potential and in prognosis, in specific contexts.

Moreover, since a large proportion of cutaneous SCCs harbour inactivated *TP53* (i.e., loss of p53 function, mainly due to UV-induced pyrimidine dimers) (Giglia-Mari & Sarasin, 2003; Pickering et al., 2014), and do not necessary exhibit overt tumours early in development of SCC, overexpression of Stratifin could be investigated as a potential causative agent in such cases, possibly informing the prognosis in terms of likelihood to convert and become invasive. This is supported by the finding that all SCCs tested in one study exhibited high Stratifin expression, though this data is not conclusive as only 11 SCCs were examined (Lodygin et al., 2003). Stratifin has recently been implicated in resistance to both radiotherapy and several chemotherapeutic drugs in multiple cancer types by preventing senescence in treated cells, and enhancing DNA repair (Han et al., 2006; Han et al., 2009; Chen et al., 2017). This further suggests that high Stratifin expression should be considered as a poor prognostic marker as such tumours may evade therapeutic intervention, while the current study has indicated a high invasive potential, as in several internal carcinomas (Ide et al., 2004; Nakayama et al., 2005; Li et al., 2009; Naidoo et al., 2012; Liu et al., 2016). The results obtained in this study suggest that high levels of Stratifin in basal layer cells should be investigated as a potential biomarker/prognostic marker for invasion in human cutaneous SCCs, and as a specific marker for fSCCs alongside Fos/AP-1 and HF markers (e.g., K17 and CD34) as published previously (Misago et al., 2014).

8.3.3. Drug target

14-3-3 proteins make attractive druggable targets and, as such, drugs targeting 14-3-3 family members have been studied in recent years, including those both stabilising and inhibiting their interactions (Kaplan et al., 2017; Stevers et al., 2018). While generation of small molecule inhibitors of 14-3-3 binding has been successful in several studies, the family members are very similar, meaning that drug targeting of the binding groove with the intention of preventing interactions with a specific 14-3-3 molecule is highly likely to target

most or all family members, creating potentially unacceptable side effects. Recently, secondary binding pockets which are separate to the primary groove have been identified which researchers believe may allow for more specific targeting (Sijbesma et al., 2017); however, they also state that these regions are highly conserved, highlighting their importance but also reducing the capacity for improvement of specificity. In the case of Stratifin (14-3-3σ), this may be less of an issue than with the other 14-3-3s, as this molecule has more unique features than the other members, for example, the salt bridge between Lys^{9} and Glu^{83} and ring-ring interaction between Phe^{25} & Tyr^{84}, both of which only occur in the σ isoform (Wilker et al., 2005). Furthermore, analysis of the crystal structures has shown that a region on the edge of the phosphopeptide binding groove (Ala^{203}-Asp^{215} loop) is most likely responsible for ligand-specific binding, as, despite the highly conserved primary amino acid sequence, 3 AAs are unique to Stratifin (Met^{202}, Asp^{204} and His^{206}) and result in a much more open conformation in this region than in other isoforms (Bezinger et al., 2005). This could, therefore, represent an ideal starting point for drug development to specifically-target Stratifin interactions while sparing the other 14-3-3 functions.

Studies into Stratifin, specifically, have used RNA interference and gene knockouts *in vitro* to reverse the drug and radio-resistance attributed to Stratifin but so far, no drugs have been developed to target this molecule *in vivo* (Han et al., 2006; Han et al., 2009; Chen et al., 2017). Mouse knockout models suggest that systemic targeting of Stratifin is a viable option, as use of a deleting-Cre (CMV-Cre) to constitutively excise the gene in all tissues was found to create a dishevelled fur phenotype in otherwise viable mice (Winter et al., 2016). While this knockout study concluded that these Stratifin-deficient mice were viable, they found that they were more susceptible to DMBA-TPA induced carcinogenesis; a finding which supports the results described here in Chapter 3. However, this would be a consideration for systemic therapy as it suggests depletion of the protein may increase the likelihood of subsequent SCC development.

8.4. Future directions

While some model-specific future experiments have been outlined in the relevant results chapters, there are features common to all the *K14.stratifin* expression models described. These include clear effects on the dermis and tumour stroma, with notable hyperplasia being common. This should be quantified and the reasons for it investigated (Wu et al., 2016), since most information in the literature regarding effects of keratinocyte-releasable Stratifin on the dermis focus on the induction of MMP secretion in wound healing (Medina et al., 2007) and do not describe increased fibroblast proliferation or greater matrix deposition (which, indeed, is a little at odds with the known induction of protease secretion).

Furthermore, marked immune infiltration of both hyperplastic skin and tumours was seen in all *K14.stratifin* models, suggesting a pro-inflammatory role which has not been described previously and which, again, appears to defy the convention that it is anti-inflammatory in wound-healing (Rahmani-Neishaboor et al., 2012). This further underlines the context-dependent nature of Stratifin functions in normal and neoplastic tissues, wherein normally regulated Stratifin appears to largely perform tumour-suppressive functions (which can backfire and introduce resistance to therapies (Han et al., 2006; Han et al., 2009; Chen et al., 2017)) with its loss often allowing cancer growth and progression (Iwata et al., 2000; Umbricht et al., 2001; Cheng et al., 2004; Ling et al., 2012), while unregulated overexpression in cancers seems to invariably have a tumour-promoting effect (Radhakrishnan et al., 2011; Shiba-Ishii et al., 2012; Husni et al., 2019; Robin et al., 2020). This immunological aspect, therefore, should be investigated further to elucidate whether the upregulation in the inflammatory response is direct or indirect, and if this could be targeted to reduce carcinogenicity in these genotypes, as has been shown to be effective in c-Fos-induced pro-tumorigenic inflammation in mice (Briso et al., 2013).

8.5. Conclusions

Initial studies using the *HK1.ras/fos-Δ5Pten* multistage model of carcinogenesis found that normal regulation and loss of Stratifin expression in tumorigenesis supports the literature indicating that Stratifin is a tumour suppressor. However, experiments with mice overexpressing Stratifin in the skin and hair follicles appear to indicate that this upregulation exclusively promotes carcinogenesis and increases the invasive potential of the resultant tumours. This was seen both in the unique follicular SCC histotype generated via co-operation between *HK1.fos* and *K14.stratifin* expression, and in both types of tumour generated in *HK1.ras/K14.stratifin* mice, as well as in the invasive hyperplasias resulting from *K14.stratifin* expression on p53- and Pten-null backgrounds. These findings implicate Stratifin overexpression in oncogenesis, in particular in invasion, as well as seemingly novel role in increasing pro-tumorigenic inflammation. Together, these data suggest Stratifin could be a useful biomarker in cutaneous squamous cell carcinomas, especially in those which are unresectable, in indicating invasive potential; a role which has been alluded to in several internal carcinomas. It provides an attractive new drug target for possible inhibition of lymph node metastasis and, further, in treatment of disseminated disease.

References

Abel EL, Angel, JM & DiGiovanni J. Multi-stage chemical carcinogenesis in mouse skin: fundamentals and applications. *Nat Protoc* 2009; **4**(9): 1350-1362.

Aghazadeh Y & Papadopoulos V. The role of the 14-3-3 family in health, disease, and drug development. *Drug Discov Today* 2016; **21**(2): 278-287.

Aitken A. 14-3-3 proteins: A historic overview. *Semin Cancer Biol* 2006; **16**(3), 162-172.

Alam H, Sehgal L, Kundu ST, Dalal SN & Vaidya MM. Novel function of keratins 5 and 14 in proliferation and differentiation of stratified epithelial cells. *Mol Biol Cell* 2011; **22**(21): 4068–78.

Alter M, Satzger I, Mattern A, Kapp A & Gutzmer R. Treatment of advanced cutaneous squamous cell carcinomas with epidermal growth factor receptor inhibitors. *Dermatology* 2013; **227**: 289-294.

Ardler J & Parmryd I. Quantifying colocalization by correlation: The Pearson correlation coefficient is superior to the Manders overlap coefficient. *Cytometry Part A* 2010; **77A**(8): 733-742.

Arya AK, El-Fert A, Devling T, Eccles RM, Aslam MA, Rubbi CP, Vlatković N, Fenwick J, Lloyd BH, Sibson DR, Jones TM & Boyd MT. Nutlin-3, the small-molecule inhibitor of MDM2, promotes senescence and radiosensitises laryngeal carcinoma cells harbouring wild-type p53. *Br J Cancer* 2010; **103**(2): 186-195.

Ashley DJB. The two “hit” and multiple “hit” theories of carcinogenesis. *Br J Cancer* 1969; **23**(2): 313-328.

Aylon Y & Owen M. The Paradox of p53: What, how, and why? *Cold Spring Harb Perspect Med* 2016; **6**(10): a026328.

Balmain A, Ramsden M, Bowden GT & Smith J. Activation of the mouse cellular Harvey-ras gene in chemically induced benign skin papillomas. *Nature* 1984; **307**(5952): 658-660.

Ballupillai A, Nagarajan RP, Ramasamy K, GovindasamyK & Muthusamy G. Caffeic acid prevents UVB radiation induced photocarcinogenesis through regulation of PTEN signaling in human dermal fibroblasts and mouse skin *Toxicol Appl Pharmacol* 2018; **352**: 87-96.

Bamford S, Dawson E, Forbes S, Clements J, Pettett R, Dogan A, Flanagan A, Teague J, Futreal PA, Stratton MR & Wooster R. The COSMIC (Catalogue of Somatic Mutations in Cancer) database and website. *Br J Cancer* 2004; **91**(2): 355-358.

Banno T & Blumenberg M. Keratinocyte detachment-differentiation connection revisited, *or anoikis-pityrisasi nexus redux*. *PLoS One* 2014; **9**(6): e100279.

Baroni A, Buominno E, De Gregorio V, Ruocco E, Ruocco V & Wolf R. Structure and function of the epidermis related to barrier properties. *Clin Dermatol* 2012; **30**(3): 257-262.

Basset-Seguin N, Demoly P, Moles JP, Tesnieres A, Gauthier-Rouviere C, Richard S, Blanchard JM & Guilhou JJ. Comparative analysis of cellular and tissue

expression of c-fos in human keratinocytes: evidence of its role in cell differentiation. *Oncogene* 1994; **9**: 765-771.

Bejjani F, Evanno E, Zibara K, Piechaczyk M & Jariel-Encontre I. The AP-1 transcriptional complex: Local switch or remote command? *Biochim Biophys Acta Rev Cancer* 2019; **1872**(1): 11-23.

Benzinger A, Muster N, Koch HB, Yates JR 3rd, Hermeking H. Targeted proteomic analysis of 14-3-3σ, a p53 effector commonly silenced in cancer. *Mol Cell Proteomics* 2005a; **4**: 785-795.

Benzinger A, Popowicz GM, Joy JM, Majumdar S, Holak TA & Hermeking H. The crystal structure of the non-liganded 14-3-3σ protein: insights into determinants of isoform specific ligand binding and dimerization. *Cell Res* 2005b; **15**: 219-227.

Berenblum I. The Mechanism of Carcinogenesis. A Study of the Significance of Cocarcinogenic Action and Related Phenomena. *Cancer Res* 1941; **1**(10): 807-814.

Berton TR, Wang XJ, Zhou Z, Kellendonk C, Schütz G, Tsai S & Roop DR. Characterization of an inducible, epidermal-specific knockout system: Differential expression of lacZ in different Cre reporter mouse strains. *Genesis* 2000; **26**(2): 160-161.

Bikle DD, Xie Z & Tu CL. Calcium regulation of keratinocyte differentiation. *Expert Rev Endocrinol Metab* 2012; **7**(4): 461-472.

Blanpain C & Fuchs E. Epidermal stem cells of the skin. *Annu Rev Cell Dev Biol* 2006; **22**: 339-373.

Boniol M, Autier P, Boyle P & Gandini S. Cutaneous melanoma attributable to sunbed use: systematic review and meta-analysis. *BMJ* 2012; **345**:e4757.

Bononi A & Pinton P. Study of PTEN subcellular localization. *Methods* 2015; **77-78**: 92-103.

Bottomley MJ, Thomson J, Harwood C & Leigh I. The role of the immune system in cutaneous squamous cell carcinoma. *Int J Mol Sci* 2019; **20**(8): E2009.

Boudreau A, Tanner K, Wang D, Geyer FC, Reis-Filho JS & Biddell MJ. 14-3-3σ stabilizes a complex of soluble actin and intermediate filament to enable breast tumor invasion. *Proc Natl Acad Sci USA* 2013; **110**(41): E3937-3944.

Boukamp P. Non-melanoma skin cancer: what drives tumor development and progression? *Carcinogenesis* 2005; **26**(10): 1657-1667.

Brabletz T, Jung A, Hermann K, Günther K, Hohenberger W & Kirchner T. Nuclear overexpression of the oncoprotein ß-catenin in colorectal cancer is localized predominantly at the invasion front. *Pathol Res Pract* 1998; **194**(10): 701-704.

Braselmann S & McCormick F. Bcr and Raf form a complex in vivo via 14-3-3 proteins. *EMBO J* 1995; **14**(19): 4839-4848.

Briso EM, Guinea-Viniegra J, Bakiri L, Rogon Z, Petzelbauer P, Eils R, Wolf R, Rincón M, Angel P & Wagner EF. Inflammation-mediated skin tumorigenesis induced by epidermal c-Fos. *Genes Dev* 2013; **27**: 1959-1973.

Brown K, Buchmann A & Balmain A. Carcinogen-induced mutations in the mouse c-Ha-ras gene provide evidence of multiple pathways for tumor progression. *Proc Natl Acad Sci USA* 1990; **87**(2): 538-542.

Brown K, Strathdee D, Bryson S, Lambie W & Balmain A. The malignant capacity of skin tumours induced by expression of a mutant H-ras transgene depends on the cell type targeted. *Curr Biol* 1998; **8**: 516-24.

Brownstein MH, Mehregan AH, Bikowski JB, Lupulescu A & Patterson JC. The Dermatopathology of Cowden's Syndrome. *Br J Dermatol* 1979; **100**(6): 667-73.

Brunet A, Bonni A, Zigmond MJ, Lin MZ, Juo P, Hu LS, Anderson MJ, Arden KC, Blenis J & Greenberg ME. Akt promotes cell survival by phosphorylating and inhibiting a forkhead transcription factor. *Cell* 1999; **96**(6): 857-868.

Cai J, Du S, Wang H, Xin B, Wang J, Shen W, Wei W, Guo Z, & Shen X. Tenascin-C induces migration and invasion through JNK/c-Jun signalling in pancreatic cancer. *Oncotarget* 2017; **8**(43): 74406–74422.

Cain NE & Starr DA. SUN proteins and nuclear envelope spacing. *Nucleus* 2015; **6**(1): 2-7.

Calautti E, Li J, Saoncella S, Brissette JL & Goetinck PF. Phosphoinositide 3-kinase signaling to Akt promotes keratinocyte differentiation versus death. *J Biol Chem* 2005; **280**(38): 32856-32865.

Carr RA, Taibjee SM, Turnbull N & Attili S. Follicular squamous cell carcinoma is an under-recognised common skin tumour. *Diagn Histopathol* 2014; **20**(7): 289-296

Casar B, Arozarena I, Sanz-Moreno V, Pinto A, Agudo-Ibáñez L, Marais R, Lewis RE, Berciano MT & Crespo P. Ras subcellular localization defines extracellular signal-regulated kinase 1 and 2 substrate specificity through distinct utilization of scaffold proteins. *Mol Cell Biol* 2009; **29**(5): 1338-1353.

Caulin C, Nguyen T, Lang GA, Goepfert TM, Brinkley BR, Cai WW, Lozano G & Roop DR. An inducible mouse model for skin cancer reveals distinct roles for gain- and loss-of-function p53 mutants. *J Clin Invest* 2007; **117**(7): 1893-1901.

Chalhoub N & Baker SJ. PTEN and the PI3-kinase pathway in cancer. *Annu Rev Pathol* 2009; **4**: 127-150.

Chang TC, Liu CC, Hsing EW, Liang SM, Chi YH, Sung LY, Lin SP, Shen TL, Ko BS, Yen BL, Yet SF, Wu KK & Liou JY. 14-3-3σ regulates ß-catenin-mediated mouse embryonic stem cell proliferation by sequestering GSK-3ß. *PLoS One* 2012; **7**(6): e40193.

Chen CY, Chen J, He L & Stiles BL. PTEN: Tumor suppressor and metabolic regulator. *Front Endocrinol* 2018; **9**: 338.

Chen Y, Li Z, Dong Z, Beebe J, Yang K, Fu L & Zhang JT. 14-3-3σ contributes to radioresistance by regulating DNA repair and cell cycle via PARP1 and CHK2. *Mol Cancer Res* 2017; **15**(4): 418-428.

Cheng L, Pan C-X, Zhang J-T, Zhang S, Kinch MS, Li L, Baldridge LA, Wade C, Hu Z, Koch MO, Ulbright TM & Eble JN. Loss of 14-3-3σ in prostate cancer and its precursors. *Clin Cancer Res* 2004; **10**(9): 3064-3068

Cheng Q, Cross B, Li B, Chen L, Li Z & Chen J. Regulation of MDM2 E3 ligase activity by phosphorylation after DNA damage. *Mol Cell Biol* 2011; **31**(24): 4951-4963.

Christenson LJ, Borrowman TA, Vachon CM, Tollefson MM, Otley CC, Weaver AL & Roenigk RK. Incidence of basal cell and squamous cell carcinomas in a population younger than 40 years. *JAMA* 2005; **294**(6): 681-690.

Cianfarani F, Bernardini S, De Luca N, Dellambra E, Tatangelo L, Tiveron C, Niessen CM, Zambruno G, Castiglia D & Odorisio T. Impaired keratinocyte proliferative and clonogenic potential in transgenic mice overexpressing 14-3-3σ in the epidermis. *J Invest Dermatol* 2011; **131**(9): 1821-1829.

Clark A, Archibald A, McClenaghan M, Simons J, Wallace R & Whitelaw C. Enhancing the efficiency of transgene expression. *Phil Trans Biol Sci* 1993; **339**(1288): 225-232.

Cockerell CJ. Histopathology of incipient intraepidermal squamous cell carcinoma ("actinic keratosis"). *J Am Acad Dermatol* 2000; **40**(1 Pt 2): 11-17.

Cornell B & Toyo-oka K. 14-3-3 proteins in brain development: neurogenesis, neuronal migration and neuromorphogenesis. *Front Mol Neurosci* 2017; **10**: 318.

Datta S, Dudek H, Tao X, Masters S, Fu H, Gotoh Y, Greenberg ME. Akt phosphorylation of BAD couples survival signals to the cell-intrinsic death machinery. *Cell* 1997; **91**(2): 231-241.

Dellambra E, Patrone M, Sparatore B, Negri A, Ceciliani F, Bondanza S, Molina F, Cancedda FD & De Luca M. Stratifin, a keratinocyte specific 14-3-3 protein, harbors a pleckstrin homology (PH) domain and enhances protein kinase C activity. *J Cell Sci* 1995; **108**(11): 3569-79.

Denning G, Jean-Joseph B, Prince C, Durden DL & Vogt PK. A short N-terminal sequence of PTEN controls cytoplasmic localization and is required for suppression of cell growth. *Oncogene* 2007; **26**(27): 3930-3940.

Depianto D, Kerns ML, Dlugosz AA & Coulombe PA. Keratin 17 promotes epithelial proliferation and tumor growth by polarizing the immune response in skin. *Nat Genet* 2010; **42**(10): 910-914.

DiGiovanni J. Multistage carcinogenesis in mouse skin. *Pharmacol Ther* 1992; **54**(1): 63-128.

Dinehart SM, Nelson-Adesokan P, Cockerell C, Russell S & Brown R. Metastatic cutaneous squamous cell carcinoma derived from actinic keratosis. *Cancer* 1997; **79**(5):920-923.

Donehower L, Harvey M, Slgle BL, McArthur MJ, Montgomery Jr CA, Butel JS & Bradley A. Mice deficient for p53 are developmentally normal but susceptible to spontaneous tumours. *Nature* 1992; **356**: 215-221.

Edward M, Quinn JA & Sands W. Keratinocytes stimulate fibroblast hyaluronan synthesis through the release of stratifin: A possible role in the suppression of scar tissue formation. *Wound Repair Regen* 2011; **19**(3): 379-386.

El-Domyati M, Hosam W, Moftah NH, Raouf HA, & Saad SM. Hair follicle changes following intense pulsed light axillary hair reduction: histometrical, histological and immunohistochemical evaluation. *Arch Dermatol Res* 2017; **309**: 191-202.

Filler RB, Robert SJ & Girardi M. Cutaneous two-stage chemical carcinogenesis. *CSH Protoc* 2007; pdb.prot4837.

Fisher C, Byers MR, Iadarola MJ & Powers EA. Patterns of epithelial expression of Fos protein suggest important role in the transition from viable to cornified cell during keratinization. *Development* 1991; **111**(2): 253-258.

Freije A, Molinuevo, Ceballos L, Cagigas M, Alonso-Lecue P, Rodriguez R, Menendez P, Aberdam D, De Diego E & Gandarillas A. Inactivation of p53 in human keratinocytes leads to squamous differentiation and shedding via replication stress and mitotic slippage. *Cell Rep* 2014; **9**: 1349-1360.

Fuchs E. Epidermal differentiation: the bare essentials. *J Cell Biol* 1990; **111**(6 Pt 2): 2807-14.

Fuchs E & Raghavan S. Getting under the skin of epidermal morphogenesis. *Nat Rev Genet* 2002; **3**(3): 199-209.

Gaggioli C, Hooper S, Hidalgo-Carcedo C, Grosse R, Marshall JF, Harrington K & Sahai E. Fibroblast-led collective invasion of carcinoma cells with differing roles for Rho GTPases in leading and following cells. *Nat Cell Biol* 2007; **9**(12):1392-1400.

Gammon A, Jasperson K & Champine M. Genetic basis of Cowden syndrome and its implications for clinical practice and risk management. *Appl Clin Genet* 2016; **9**: 83-92.

Garrod D & Chidgey M. Desmosome structure, composition and function. *Biochim Biophys Acta* 2008; **1778**(3): 572-587.

Gao T, Furnari F & Newton AC. PHLPP: a phosphatase that directly dephosphorylates Akt, promotes apoptosis, and suppresses tumor growth. *Mol Cell* 2005; **18**(1): 13-24.

Ghaffari A, Li Y, Kilani RT & Ghahary A. 14-3-3 sigma associates with cell surface aminopeptidase N in the regulation of matrix metalloproteinase-1. *J Cell Sci* 2010; **123**(17): 2996-3005.

Ghaffari A, Li Y, Karami A, Tredget EE & Ghahary A. Keratinocyte-releasable stratifin regulates matrix metalloproteinases gene expression in dermal fibroblasts. *J Burn Care Res* 2006; **27**(2): S136.

Ghahary A, Marcoux Y, Karimi-Busheri F, Li Y, Tredget EE, Kilani RT, Lam E & Weinfeld M. Differentiated keratinocyte-releasable stratifin (14-3-3σ) stimulates MMP-1 expression in dermal fibroblasts. *J Invest Dermatol* 2005; **124**(1): 170-177.

Giglia-Mari G & Sarasin A. TP53 mutations in human skin cancers. *Hum Mutat* 2003; **21**(3): 217-228.

Gkantiragas I, Brügger B, Stüven E, Kaloyanova D, Li XY, Löhr K, Lottspeich F, Wieland FT, Helms JB. Sphingomyelin-enriched microdomains at the Golgi complex. *Mol Biol Cell* 2001; **12**(6): 1819-1833.

Glentis A, Oertle P, Mariani P, Chikina A, El Marjou F, Attieh Y, Zaccarini F, Lae M, Loew D, Dingli F, Sirven P, Schoumacher M, Gurchenkov BG, Plodinec M & Vignjevic DM. Cancer-associated fibroblasts induce metalloprotease-independent cancer cell invasion of the basement membrane. *Nature Comm* 2017; **8**: 924.

Goetz JG, Minguet S, Navarro-Lérida I, Lazcano JJ, Samaniego R, Calvo E, Tello M, Osteso-Ibáñez T, Pellinen P, Echarri A, Cerezo A, Klein-Szanto AJP, Garcia R, Keely PJ, Sánchez-Mateos P, Cukierman E & Del Pozo MA. Biomechanical remodeling of the microenvironment by stromal caveolin-1 favors tumor invasion and metastasis. *Cell* 2011; **146**(1): 148-163.

Gold KA, Merrill SK, William Jr WN, Johnson FM, Lee JJ & Glisson BS. Erlotinib in the Treatment of Recurrent or Metastatic Cutaneous Squamous Cell Carcinoma: A Single Arm Phase II Clinical Trial. *Cancer* 2018; **124**(10): 2169-2173.

Gottlieb TM, Leal JF, Seger R, Taya Y & Oren M. Cross-talk between Akt, p53 and Mdm2: possible implications for the regulation of apoptosis. *Oncogene* 2002; **21**:1299-1303.

Greenberg ME & Ziff EB. Stimulation of 3T3 cells induces transcription of the c-fos proto-oncogene. *Nature* 1984; **311**: 433-438.

Greenhalgh DA & Yuspa SH. Malignant conversion of murine squamous papilloma cell lines by transfection with the Fos oncogene. *Mol Carcinog* 1988; **1**: 134-143.

Greenhalgh DA, Welty DJ, Strickland JE & Yuspa SH. Spontaneous rasHa activation in cultured primary murine keratinocytes: consequences of rasHa activation in malignant conversion and malignant progression. *Mol Carcinog* 1989; **3**: 154-161.

Greenhalgh DA, Welty DJ, Player A & Yuspa SH. Two oncogenes Fos and ras co-operate to convert normal keratinocytes to malignancy. *Proc Natl Acad Sci* USA 1990; **87**: 643-647.

Greenhalgh DA, Rothnagel JA, Quintanilla MI, Orengo CC, Gagne TA, Bundman DS, Longley MA & Roop DR. Induction of epidermal hyperplasia, hyperkeratosis, and papillomas in transgenic mice by a targeted v-Ha-ras oncogene. *Mol Carcinog* 1993a; **7**(2): 99-110.

Greenhalgh DA, Rothnagel JA, Wang XJ, Quintanilla MI, Orengo CC, Gagne TA, Bundman DS, Longley MA, Fisher C, Roop DR. Hyperplasia, hyperkeratosis and benign tumor production in transgenic mice by a targeted v-fos oncogene suggest a role for Fos in epidermal differentiation and neoplasia. *Oncogene* 1993b; **8**(8): 2145-2157.

Greenhalgh DA, Quintanilla MI, Orengo CC, Barber JL, Eckhart JN, Rothnagel JA & Roop DR. Cooperation between v-fos and v-rasHA induces autonomous papillomas in transgenic epidermis but not malignant conversion. *Cancer Res* 1993c; **53**(21): 5071-5075.

Greenhalgh DA, Wang WJ, Donehower LA & Roop DR. Paradoxical tumor inhibitory effect of p53 loss in transgenic mice expressing epidermal-targeted v-ras^{ha}, v-fos, or human transforming growth factor α. *Cancer Res* 1996; **56**: 4413-4423.

Habib T, Sadoun A, Nader N, Suzuki S, Liu W, Jithesh PV, Kino T. AKT1 has dual actions on the glucocorticoid receptor by cooperating with 14-3-3. *Mol Cell Endocrinol* 2017; **439**: 431-443.

Hammond NL, Headon DJ & Dixon MJ. The cell cycle regulator protein 14-3-3σ is essential for hair follicle integrity and epidermal homeostasis. *J Invest Dermatol* 2012; **132**(6): 1543-1553.

Hampton T. Skin cancer's ranks rise. *JAMA* 2005; **294**(12): 1476.

Han B, Xie H, Chen Q & Zhang JT. Sensitizing hormone-refractory prostate cancer cells to drug treatment by targeting 14-3-3σ. *Mol Cancer Ther* 2006; **5**(4): 903-912.

Han Z, Dimas K, Tian X, Wang Y, Hemmi H, Yamada K, Kato N, Pantazis P, Ramanujam RJ, Anant S, Wyche JH & Houchen CW. 14-3-3sigma-dependent resistance to cisplatin. *Anticancer Res* 2009; **29**(6): 2009-2014.

Hanahan D & Weinberg RA. The hallmarks of cancer. *Cell* 2000; **100**(1): 57-70.

Hanahan D & Weinberg RA. Hallmarks of cancer: the next generation. *Cell* 2011; **144**(5): 646-674.

Hancock JF. Ras proteins: different signals from different locations. *Nat Rev Mol Cell Biol* 2003; **4**(5): 373-384.

Hanssen AM, Fryns JP. Cowden syndrome. *J Med Genetics* 1995; **32**: 117-119.

Hariharan S, Johnson CP, Bresnahan BA, Taranto SE, McIntosh MJ & Stablein D. Improved graft survival after renal transplantation in the united states, 1988 to 1996. *New Engl J Med* 2000; **342**(9): 605-612.

Harper JR, Reynolds SH, Greenhalgh DA, Strickland JE, Lacal JC & Yuspa SH. Analysis of the ras^{Ha} oncogene and its p21 product in chemically induced skin tumours and tumour derived cell lines. *Carcinogenesis* 1987; **8**: 1821-1825.

Hartsock A & Nelson WJ. Adherens and tight junctions: structure, function and connections to the actin cytoskeleton. *Biochim Biophys Acta* 2008; **1778**(3): 660-669.

Haupt S, Berger M, Goldberg Z & Haupt Y. Apoptosis – the p53 network. *J Cell Sci* 2003; **116**: 4077-4085.

Hemmings BA & Restuccia DF. PI3K-PKB/Akt Pathway. *Cold Spring Harb Perspect Biol* 2012; **4**(9): a011189.

Hennings H, Michael D, Cheng C, Steinert P, Holbrook K & Yuspa SH. Calcium regulation of growth and differentiation of mouse epidermal cells in culture. *Cell* 1980; **19**(1): 245-254.

Hennings H, Shores R, Mitchell P, Spangler EF & Yuspa SH. Induction of papillomas with a high probability of conversion to malignancy. *Carcinogenesis* 1985; **6**(11): 1607-1610.

Hennings H, Glick AB, Greenhalgh DA, Morgan DL, Strickland JE, Tennenbaum T & Yuspa SH. Critical aspects of initiation, promotion, and progression in multistage epidermal carcinogenesis. *Proc Soc Exp Biol Med* 1993; **202**(1): 1-8.

Henrique R, Jerónimo C, Hoque MO, Carvalho AL, Oliveira J, Teixeira MR, Lopes C & Sidransky D. Frequent 14-3-3 sigma promoter methylation in benign and malignant prostate lesions. *DNA Cell Biol* 2005; **24**(4): 264-269.

Hesse K, Satzger I, Chacht V, Köther B, Hillen U ,Klode J, Schaper K & Gutzmer R. Characterisation of prognosis and invasion of cutaneous squamous cell carcinoma by podoplanin and E-cadherin expression. *Dermatology* 2016; **232**: 558-565.

Hermeking H, Lengauer C, Polyak K, He TC, Zhang L, Thiagalingam S, Kinzler KW & Vogelstein B. 14-3-3σ is a p53-regulated inhibitor of G2/M progression. *Mol Cell* 1997; **1**(1): 3-11.

Hermeking H & Benzinger A. 14-3-3 proteins in cell cycle regulation. *Semin Cancer Biol* 2006; **16**(3): 183-192.

Herron BJ, Liddell RA, Parker A, Grant S, Kinne J, Fisher JK & Siracusa LD. A mutation in stratifin is responsible for the repeated epilation (Er) phenotype in mice. *Nat Genet* 2005; **37**(11): 1210-1212.

van der Hoeven PC, van der Wal JC, Ruurs P, van Dijk MC & van Blitterswijk J. 14-3-3 isotypes facilitate coupling of protein kinase C-zeta to Raf-1: negative regulation by 14-3-3 phosphorylation. *Biochem J* 2000; **345**(2): 297-306.

Hossini AM, Quast AS, Plötz M, Grauel K, Exner T, Küchler J, Stachelscheid H, Eberle J, Rabien A, Makrantonaki E & Zouboulis CC. PI3K/AKT signaling pathway is essential for survival of induced pluripotent stem cells. *PLoS One* 2016; **11**(5): e0154770.

Hubbard GK, Mutton LN, Khalili M, McMullin RP, Hicks JL, Bianchi-Frias D, Horn LA, Kulac I, Moubarek MS, Nelson PS, Yegnasubramanian S, De Marzo AM & Bieberich CJ. Combined MYC activation and PTEN loss are sufficient to create genomic instability and lethal metastatic prostate cancer. *Cancer Res* 2016; **76**(2): 283-292.

Hu HB, Yang XP, Zhou PX, Yang XA & Yin B. High expression of keratin 6C is associated with poor prognosis and accelerates cancer proliferation and migration by modulating epithelial–mesenchymal transition in lung adenocarcinoma. *Genes Genomics* 2020; **42**: 179-188.

Hu WL, Jin L, Xu A, Wang YF, Thorne RF, Zhang XD & Wu M. GUARDIN is a p53-responsive long non-coding RNA that is essential for genomic stability. *Nat Cell Biol* 2018; **20**: 492-502.

Husni RE, Shiba-Ishii A, Nakagawa T, Dai T, Kim Y, Hong J, Sakashita S, Sakamoto N, Sato Y & Noguchi M. DNA hypomethylation-related overexpression of SFN, GORASP2 and ZYG11A is a novel prognostic biomarker for early stage lung adenocarcinoma. *Oncotarget* 2019; **10**(17): 1625-1636.

Ide M, Nakajima T, Asao T & Kuwano H. Inactivation of 14-3-3sigma by hypermethylation is a rare event in colorectal cancers and its expression

may correlate with cell cycle maintenance at the invasion front. *Cancer Letters* 2004; **207**: 241-249.

Ide M, Saito K, Tsutsumi S, Tsuboi K, Yamaguchi S, Asao T, Kuwano H & Nakajima T. Over-expression of 14-3-3sigma in budding colorectal cancer cells modulates cell migration in the presence of tenascin-C. *Oncology Rep* 2007; **18**(6): 1451-1456.

Inman GJ, Wang J, Nagano A, Alexandrov LB, Purdie KJ, Taylor RG, Sherwood V, Thomson J, Hogan S, Spender LC, South AP, Stratton M, Chelala C, Harwood CA, Proby CM & Leigh IM. The genomic landscape of cutaneous SCC reveals drivers and a novel azathioprine associated mutational signature. *Nat Commun* 2018; **9**: 3667.

Ito M, Liu Y, Yang Z, Nguyen J, Liang F, Morris RJ, Cotsarelis G. Stem cells in the hair follicle bulge contribute to wound repair but not to homeostasis of the epidermis. *Nat Med* 2005;**11**(12): 1351-1354

Iwata N, Yamamoto H, Sasaki S, Itoh F, Suzuki H, Kikuchi T, Kaneto H, Iku S, Ozeki I, Karino Y, Satoh T, Toyota J, Satoh M, Endo T & Imai K. Frequent hypermethylation of CpG islands and loss of expression of the 14-3-3 sigma gene in human hepatocellular carcinoma. *Oncogene* 2000; **19**(46): 5298-5302

Jamaspishvili T, Berman DM, Ross AE, Scher HI, De Marzo AM, Squire JA & Lotan TL. Clinical implications of PTEN loss in prostate cancer. *Nature Rev Urol* 2018; **15**: 222–234.

Jahkola T, Toivonen T, Virtanen I, von Smitten K, Nordling S, von Boguslawski K, Haglund C, Nevanlinna H & Blomqvist C. Tenascin-C expression in invasion border of early breast cancer: a predictor of local and distant recurrence. *Br J Cancer* 1998; **78**: 1507-1513.

Janus JM, O'Shaughnessy RFL, Harwood CA & Maffucci T. Phosphoinositide 3-kinase-dependent signalling pathways in cutaneous squamous cell carcinomas. *Cancers* 2017; **9**(7): E86.

Jolly LA, Novitskiy S, Owens P, Massoll N, Cheng N, Fang W, Moses HL & Franco AT. Fibroblast-mediated collagen remodeling within the tumor microenvironment facilitates progression of thyroid cancers driven by $BRAF^{v600e}$ and Pten loss. *Cancer Res* 2016; **76**(7): 1804-1813.

Kalluri R & Zeisberg M. Fibroblasts in cancer. *Nat Rev Cancer* 2006; **6**(5): 392-401.

Karia PS, Han J & Schmults CD. Cutaneous squamous cell carcinoma: estimated incidence of disease, nodal metastasis, and deaths from disease in the United States, 2012. *J Am Acad Dermatol* 2013; **68**(6): 957-966.

Kartasova T, Roop DR & Yuspa SH. Relationship between the expression of differentiation-specific keratins 1 and 10 and cell proliferation in epidermal tumors. *Mol Carcinog* 1992; **6**(1): 18-25.

Kermer P, Klöcker N, Labes M & Bähr M. Insulin-like growth factor-I protects axotomized rat retinal ganglion cells from secondary death via PI3-k-

dependent Akt phosphorylation and inhibition of caspase-3 *in vivo*. *J Neurosci* 2000; **20**(2): 722-728.

Kim I-Y & He Y-Y. Ultraviolet radiation-induced non-melanoma skin cancer: Regulation of DNA damage repair and inflammation. *Genes Dis* 2014; **1**(2): 188-198.

Kim S, Wong P & Coulombe P. A keratin cytoskeletal protein regulates protein synthesis and epithelial cell growth. *Nature* 2006; **441**(7091): 362-365.

Kim TD, Choi E, Rhim H, Paik SR & Yang CH. Alpha-synuclein has structural and functional similarities to small heat shock proteins. *Biochem Biophys Res Commun* 2004; **324**(4): 1352-1359.

Kim Y, Shiba-Ishii A, Nakagawa T, Iemura SI, Natsume T, Nakano N, Matsuoka R, Sakashita S, Lee S, Kawaguchi A, Sato Y & Noguchi M. Stratifin regulates stabilization of receptor tyrosine kinases via interaction with ubiquitin-specific protease 8 in lung adenocarcinoma. *Oncogene* 2018; **37**: 5387-5402.

Knudson AG Jr. Mutation and cancer: statistical study of retinoblastoma. *Proc Natl Acad Sci U S A* 1971; **68**(4): 820-823.

Knudson AG Jr. Two genetic hits (more or less) to cancer. *Nat Rev* 2001; **1**: 157-162.

Ko CJ. Keratoacanthoma: Facts and controversies. *Clin Dermatol* 2010; **28**(3): 254-261.

Ko S, Kim JY, Jeong J, Lee JE, Yang WI & Jung WH. The role and regulatory mechanism of 14-3-3 sigma in human breast cancer. *J Breast Cancer* 2014; **17**(3): 207-218.

Krakhmal NV, Zavyalova MV, Denisov EV, Vtorushin SV & Perelmuter VM. Cancer invasion: patterns and mechanisms. *Acta Naturae* 2015; **7**(2): 17-28.

Kruse JP & Gu W. Modes of p53 regulation. *Cell* 2009; **137**(4): 609-22.

Krystel-Whittemore M, Dileepan KN & Wood JG. Mast cell: a multi-functional master cell. *Front Immunol* 2016; **6**: 620.

Kulesz-Martin M, Kilkenny AE, Holbrook KA, Digernes V & Yuspa SH. Properties of carcinogen altered mouse epidermal cells resistant to calcium-induced terminal differentiation. *Carcinogenesis* 1983; **4**(11): 1367-1377.

Laboulaye MA, Duan X, Qiao M, Whitney IE & Sanes JR. Mapping Transgene Insertion Sites Reveals Complex Interactions Between Mouse Transgenes and Neighboring Endogenous Genes *Front Mol Neurosci* 2018; **11**: 385.

Lai A, Ghaffari A, Li Y & Ghahary A. Paracrine regulation of fibroblast Aminopeptidase N/CD13 expression by keratinocyte-releasable stratifin. *J Cell Physiol* 2011; **226**(12): 3114-3120.

Lam E Kilani RT, Li Y, Tredget E & Ghahary A. Stratifin-induced matrix metalloproteinase-1 in fibroblast is mediated by c-fos and p38 mitogen-activated protein kinase activation. *J Invest Dermatol* 2005; **125**: 230-238.

Lane DP. p53, guardian of the genome. *Nature* 1992; **358**: 15-16.

Laronga C, Yang HY, Neal C & Lee MH. Association of the cyclin-dependent kinases and 14-3-3 sigma negatively regulates cell cycle progression. *J Biol Chem* 2000; **275**(30): 23106-23112.

Laude AJ & Prior IA. Palmitoylation and localisation of RAS isoforms are modulated by the hypervariable linker domain. *J Cell Sci* 2008; **121**(4): 421-427.

Lechler T & Fuchs E. Asymmetric cell divisions promote stratification and differentiation of mammalian skin. *Nature* 2005; **437**(7056): 275-280.

Lee JO, Yang H, Georgescu MM, Di Cristofano A, Maehama T, Shi Y, JE Dixon, Pandolfi P & Pavletich NP. Crystal structure of the PTEN tumor suppressor: implications for its phosphoinositide phosphatase activity and membrane association. *Cell* 1999; **99**(3): 323-334.

Lee MH & Lozano G. Regulation of the p53-MDM2 pathway by 14-3-3σ and other proteins. *Semin Cancer Biol* 2006; **16**(3): 225-234.

Le Hir H, Nott A & Moore MJ. How introns influence and enhance eukaryotic gene expression. *Trends Biochem Sci* 2003; **28**(4): s215-220.

Leigh IM, Navsaria H, Purkis PE, McKay IA, Bowden PE & Riddle PN. Keratins (K16 and K17) as markers of keratinocyte hyperproliferation in psoriasis in vivo and in vitro. *Br J Dermatol* 1995; **133**(4): 501-511.

Lesche R, Groszer M, Gao J, Wang Y, Messing A, Sun H, Liu X & Wu H. Cre/loxP-mediated inactivation of the murine Pten tumor suppressor gene. *Genesis* 2001; **32**: 148-149.

Levy V, Lindon C, Harfe BD & Morgan BA. Distinct stem cell populations regenerate the follicle and interfollicular epidermis. *Dev Cell* 2005; **9**: 855-861.

Levy V, Lindon C, Zheng Y, Harfe BD & Morgan BA. Epidermal stem cells arise from the hair follicle after wounding. *FASEB J* 2007; **21**(7): 1358-1366.

Lewis JE, Wahl JK, Sass KM, Jensen PJ, Johnson KR & Wheelock MJ. Cross-talk between adherens junctions and desmosomes depends on plakoglobin. *J Cell Biol* 1997; **136**(4): 919-934.

Li DJ, Deng G, Xiao ZQ, Yao HX, Li C, Peng F, Li MY, Zhang PF, Chen YH & Chen ZC. Identificating 14-3-3 sigma as a lymph node metastasis-related protein in human lung squamous carcinoma. *Cancer Letters* 2009; **279**(1): 65-73

Li Y, Lin X, Kilani RT, Jones JCR & Ghahary A. 14-3-3 Sigma Isoform Interacts with the Cytoplasmic Domain of the Transmembrane BP180 in Keratinocytes. *J Cell Phisiol* 2007; **212**(3): 675-681.

Li Z, Liu J-Y & Zhang J-T. 14-3-3σ, the double-edged sword of human cancers. *Am J Transl Res* 2009; **1**(4): 326-340.

Li Z, Li J, Bi P, Lu Y, Burcham G, Elzey BD, Ratliff T, Konieczny SF, Ahmad N, Kuang S & Liu X. Plk1 phosphorylation of PTEN causes a tumor-promoting metabolic state. *Mol Cell Biol* 2014; **34**(19): 3642-61.

Liaw D, March DJ, Li J, Dahia PL, Wag SI, Zheng Z, Bose S, Call KM, Tsou HC, Peacocke M, Eng C & Parsons R. Germline mutations of the PTEN gene in Cowden disease, an inherited breast and thyroid cancer syndrome. *Nat Genet* 1997; **16**(1): 64-67.

Lichti U, Anders J & Yuspa SH. Isolation and short term culture of primary keratinocytes, hair follicle populations, and dermal cells from newborn mice and keratinocytes from adult mice, for in vitro analysis and for grafting to immunodeficient mice. *Nat Protoc* 2009; **3**(5): 799-810.

Lien WH, Polak L, Lin M, Lay K, Zheng D & Fuchs E. *In vivo* transcriptional governance of hair follicle stem cells by canonical Wnt regulators. *Nature Cell Biol* 2014; **16**: 179-190.

Ling C, Su VM, Zuo D & Muller WJ. Loss of the 14-3-3σ tumor suppressor is a critical event in ErbB2-mediated tumor progression. *Cancer Discov* 2012; **2**(1): 68-81

Ling C, Zuo D, Xue B, Muthuswamy S & Muller WJ. A novel role for 14-3-3sigma in regulating epithelial cell polarity. *Genes Dev* 2010; **24**(9): 947-56.

Liu C, Chang T, Lin Y, Yu Y, Ko B, Sung L & Jun-Yang Liou J. Paracrine regulation of matrix metalloproteinases contributes to cancer cell invasion by hepatocellular carcinoma-secreted 14-3-3σ. *Oncotarget* 2016; **7**: 36988-36999.

Lodygin D, Yazdi AS, Sander CA, Herzinger T, Hermeking H. Analysis of 14-3-3σ expression in hyperproliferative skin diseases reveals selective loss associated with CpG-methylation in basal cell carcinoma. *Oncogene* 2003; **22**(35): 5519-5524.

Lodygin D & Hermeking H. The role of epigenetic inactivation of 14-3-3sigma in human cancer. *Cell Res* 2005; **15**(4): 237-46.

Luscher B, Mitchell PJ, Williams T & Tjian R. Regulation of transcription factor AP-2 by the morphogen retinoic acid and by second messengers. *Genes Dev* 1989; **3**:1507-1517.

Lutzner MA, Guenet JL & Breitburd F. Multiple cutaneous papillomas and carcinomas that develop spontaneously in a mouse mutant, the repeated epilation heterozygote Er/+. *J Natl Cancer Inst* 1985; **75**(1): 161-166.

Ma S, Rao L, Freedberg I & Blumenberg M. Transcriptional Control of K5, K6, K14, and K17 Keratin Genes by AP-1 and NF-κB Family Members. *Gene Exp, J Liver Res* 1997; **6**(6): 361-370.

Maas-Szabowski N, Shimotoyodome A & Fusenig NE. Keratinocyte growth regulation in fibroblast cocultures via a double paracrine mechanism. *J Cell Sci* 1999; **112**(Pt 12): 1843-1853.

Maccario H, Perera NM, Davidson L, Downes CP & Nick R. Leslie. PTEN is destabilized by phosphorylation on Thr366. *Biochem J* 2007; **405**(Pt 3): 439-444.

MacDonald FH, Quinn JA & Greenhalgh DA. Skin carcinogenesis in Ras/fos/PTENnull transgenic mice associates reveals mTOR association with papillomatogenesis/conversion and AKT with malignant progression. *Br J Dermatol* 2011; **164**(4): 934.

Macdonald FH, Yao D, Quinn JA & Greenhalgh DA. PTEN ablation in Ras(Ha)/Fos skin carcinogenesis invokes p53-dependent p21 to delay conversion while p53-independent p21 limits progression via cyclin D1/E2 inhibition. *Oncogene* 2014; **33**(32): 4132-4143.

McGowan KM, Tong X, Colucci-Guyon E, Langa F, Babinet C & Coulombe PA. Keratin 17 null mice exhibit age- and strain-dependent alopecia. *Genes Dev* 2002; **16**: 1412-1422.

Malhotra S, Kazlouskaya V, Andres C, Gui J & Elston D. Diagnostic cellular abnormalities in neoplastic and non-neoplastic lesions of the epidermis: a morphological and statistical study. *J Cutan Pathol* 2013; **40**(4): 10.1111/cup.12090.

Manders EMM, Verbeek FJ & Aten JA. Measurement of co-localization of objects sin dual-colour confocal images. *J Microscopy* 1993; 169(3): 375-382.

Manning BD & Toker A. AKT/PKB signaling: navigating the network. *Cell* 2017; **169**(3): 381-405.

Marino S, Vooijs M, van Der Gulden H, Jonkers J & Berns A. Induction of medulloblastomas in p53-null mutant mice by somatic inactivation of Rb in the external granular layer cells of the cerebellum. *Genes Dev* 2000; **14**(8): 994-1004.

Martelli AM, Tabellini G, Bressanin D, Ognibene A, Goto K, Cocco L & Evangeslisti C. The emerging multiple roles of nuclear Akt. *Biochim Biophys Acta* 2012; **1823**(12): 2168-2178.

Martincorena I, Roshan A, Gerstung M, Ellis P, Van Loo P, McLaren S, Wedge DC, Fullam A, Alexandrov LB, Tubio JM, Stebbings L, Menzies A, Widaa S, Stratton MR, Jones PH & Campbell PJ. Tumor evolution. High burden and pervasive positive selection of somatic mutations in normal human skin. *Science* 2015; **348**(6237): 880-886.

Martincorena I, Raine KM, Gerstung M, Dawson KJ, Haase K, Van Loo P, Davies H, Stratton MR & Campbell PJ. Universal patterns of selection in cancer and somatic tissues. *Cell* 2017; **171**(5): 1029-1041.e21.

Maruthappu T, Chikh A, Fell B, Delaney PJ, Brooke MA, Levet C, Moncada-Pazos A, Ishida-YamamotoA, Blaydon D, Waseem A, Leigh IM, Freeman M & Kelsell DP. Rhomboid family member 2 regulates cytoskeletal stress-associated keratin 16. *Nat Commun* 2017; **8**: 14174.

Masre SF, Rath N, Olson MF & Greenhalgh DA. Epidermal ROCK2 induces AKT1/GSK3β/β-catenin, NFκB and dermal tenascin C; but enhanced differentiation and p53/p21 inhibit papilloma. *Carcinogenesis* 2020; **41**(10): 1409-1420.

Mayo LD & Donner DB. A phosphatidylinositol 3-kinase/Akt pathway promotes translocation of Mdm2 from the cytoplasm to the nucleus. *Proc Natl Acad Sci USA* 2001; **98**(20): 11598-11603.

Maytin EV, Lin JC, Krishnamurthy R, Batchvarova N, Ron D, Mitchell PJ & Habener JF. Keratin 10 gene expression during differentiation of mouse epidermis requires transcription factors C/EBP and AP-2. *Dev Biol* 1999; **216**(1): 164-181.

Medina A, Ghaffari A, Kilani RT & Ghahary A. The role of stratifin in fibroblast-keratinocyte interaction. *Mol Cell Biochem* 2007; **305**(1-2): 255-264.

Mehic D, Bakiri L, Ghannadan M, Wagner EF & Tschachler E. Fos and Jun proteins are specifically expressed during differentiation of human keratinocytes. *J Invest Dermatol* 2005; **124**(1): 212-220.

Mehta KS, Mahajan VK, Chauhan PS, Sharma AL, Sharma V, Abhinav C, Khatri G, Prabha N, Sharma S & Negi M. Metastatic basal cell carcinoma: a biological continuum of basal cell carcinoma? *Case Rep Dermatol Med* 2012: 157187.

Mhawech P. 14-3-3 proteins—an update. *Cell Res* 2005; **15**(4): 228–236.

Micallef L, Belaubre F, Pinon A, Jayat-Vignoles C, Delage C, Charveron M & Simon A. Effects of extracellular calcium on the growth-differentiation switch in immortalized keratinocyte HaCaT cells compared with normal human keratinocytes. *Exp Dermatol* 2009; **18**(2):143151.

Michaelson D, Ali W, Chiu VK, Bergo M, Silletti J, Wright L, Young SG & Philips M. Postprenylation CAAX processing is required for proper localization of Ras but not Rho GTPases. *Mol Biol Cell* 2005; **16**(4): 1606-16.

Migden MR, Rischin D, Schmults CD, Guminski A, Hauschild A, Lewis KD, Chung CH, Hernandez L, Lim AM, Chang ALS, Rabinowits G, Thai AA, Dunn LA, Hughes BGM, Khushalani NI, Modi B, Schadendorf D, Gao B, Seebach F, Li S, Li J, Mathias M, Booth J, Mohan K, Stankevich E, Babiker HM, Brana I, Gil-Martin M, Homsi J, Johnson ML, Moreno V, Niu J, Owonikoko TK, Papadopoulos KP, Yancopoulos GD, Lowy I & Fury MG. PD-1 blockade with Cemiplimab in advanced cutaneous squamous-cell carcinoma. *N Engl J Med* 2018; **379**: 341-351.

Mikami T, Maruyama S, Abé T, Kobayashi T, Yamazaki M, Funayama A, Shingaki S, Kobayaski T, Jun C & Saku T. Keratin 17 is co-expressed with 14-3-3 sigma in oral carcinoma in situ and squamous cell carcinoma and modulates cell proliferation and size but not cell migration. *Virchows Arch* 2015; **466**(5): 559-569.

Milde-Langosch K. The Fos family of transcription factors and their role in tumorigenesis. *Eur J Cancer* 2005; **41**(16): 2449-2461.

Miller S, Wei Z-G, Wilson C, Dzubow L, Sun T-T & Lavker RM. Mouse skin is particularly susceptible to tumor initiation during early anagen of the hair cycle: possible involvement of hair follicle stem cells. *J Invest Dermatol* 1993; **101**(4): 591-594.

Mills KC, Kwatra SG, Feneran AN, Pearce DJ, Williford PM, D'Agostino RB & Yosipovitch G. Itch and pain in nonmelanoma skin cancer: Pain is an important feature of cutaneous squamous cell carcinoma. *Arch Dermatol* 2012; **148**(12): 1422-1423

Mingot JM, Bohnsack MT, Jäkle U & Görlich D. Exportin 7 defines a novel general nuclear export pathway. *EMBO J* 2004; **23**(16): 3227-3236.

Mirmohammadsadegh A, Marini A, Nambiar S, Hassan M, TannapfelA, Ruzicka T & Hangge UR. Epigenetic silencing of the PTEN gene in melanoma. *Cancer Res* 2006; **66**(13): 6546-6552.

Misago N, Toda S & Narisawa Y. Folliculocentric squamous cell carcinoma with tricholemmal differentiation: a reappraisal of tricholemmal carcinoma. *Clin Exp Dermatol* 2012; **37**:484-491.

Mishra S, Lee Y & Park JW. Direct quantification of trace amounts of a chronic myeloid leukemia biomarker using locked nucleic acid capture probes. *Anal Chem* 2018; **90**(21): 12824-12831.

Mittapalli VR, Madi J, Löffek S, Kiritsi D, Kern JS, Römer W, Nyström A & Bruckner-Tuderman L. Injury-driven stiffening of the dermis expedites skin carcinoma progression. *Cancer Res* 2016; **76**(4): 940-951.

Miyazawa K, Iwaya K, Kuroda M, Harada M, Serizawa H, Koyanagi Y, Soto YI, Mizokami Y, Matsuoka T & Mukai K. Nuclear accumulation of beta-catenin in intestinal-type gastric carcinoma: correlation with early tumor invasion. *Virchows Arch* 2000 **437**: 508-513.

Molina JR & Adjei AA. The Ras/Raf/MAPK pathway. *J Thorac Oncol* 2006; **1**(1): 7-9.

Moll R, Divo M & Langbein L. The human keratins: biology and pathology. *Histochem Cell Biol* 2008; **129**: 705.

Mommers JM, van Rossum MM, van Erp PE & van De Kerkhof PC. Changes in keratin 6 and keratin 10 (co-)expression in lesional and symptomless skin of spreading psoriasis. *Dermatology* 2000; **201**(1): 15-20.

Moreira JMA, Gromov P & Celis JE. Expression of the tumour suppressor protein 14-3-3σ is down-regulated in invasive transitional cell carcinomas of the urinary bladder undergoing epithelial-to-mesenchymal transition. *Mol Cell Proteomics* 2004; **3**(4): 410-419.

Morris RJ, Tryson KA & Wu KQ. Evidence that the epidermal targets of carcinogen action are found in the interfollicular epidermis or infundibulum as well as in the hair follicles. *Cancer Res* 2000; **60**(2): 226-229.

Mühlmann G, Ofner D, Zitt M, Müller HM, Maier H, Moser P, Schmid KW, Zitt M & Amberger A. 14-3-3 sigma and p53 expression in gastric cancer and its clinical applications. *Dis markers* 2010; **29**(1): 21-29.

Mullenders LH, Hazekamp-van Dokkum AM, Kalle WH, Vrieling H, Zdzeinicka MZ & Zeeland AA. UV-induced photolesions, their repair and mutations. *Mutat Res* 1993; **299**(3-4): 271-276.

Murthy M & Ram JL. Invertebrates as model organisms for research on aging biology. *Invertebr Reprod Dev* 2015; **59**(sup 1): 1-4.

Myers MP, Stolarov JP, Eng C, Li J, Wang SI, Wigler MH, Parsons R & Tonks NK. P-TEN, the tumor suppressor from human chromosome 10q23, is a dual-specificity phosphatase. *Proc Natl Acad Sci USA* 1997; **94**(17): 9052-9057.

Naidoo K, Jones R, Dmitrovic B, Wijesuriya N, Kocher H, Hart IR & Crnogorac-Jurcevic T. Proteome of formalin-fixed paraffin-embedded pancreatic ductal adenocarcinoma and lymph node metastases. *J Pathol* 2012; **226**(5): 756-763

Naeem AS, Zhu Y, Di WL, Marmiroli S & O'Shaughnessy RFL. AKT1-mediated Lamin A/C degradation is required for nuclear degradation and normal epidermal terminal differentiation. *Cell Death Differ* 2015; **22**: 2123-2132.

Nakayama H, Sano T, Motegi A, Oyama T & Nakajima T. Increasing 14-3-3 sigma expression with declining estrogen receptor alpha and estrogen-responsive finger protein expression defines malignant progression of endometrial carcinoma. *Pathol Int* 2005; **55**(11): 707-715.

Narayanan DL, Saladi RN & Fox JL. Ultraviolet radiation and skin cancer. *Int J Dermatol* 2010; **49**(9): 978-986.

Neupane D & Korc M. 14-3-3σ modulates pancreatic cancer cell survival and invasiveness. *Clin Cancer Res* 2008; **14**(23): 7614-7623.

Neagu M, Caruntu C, Constanin C, Boda D, Zurac S, Spandidos DA & Tsatsakis AM. Chemically induced skin carcinogenesis: Updates in experimental models. *Oncol Rep* 2016; **35**(5): 2516-2528.

Ngeow J, Stanuch K, Mester JL, Barnholtz-Sloan JS & Eng C. Second Malignant Neoplasms in Patients with Cowden Syndrome with Underlying Germline PTEN Mutations. *J Clin Oncol* 2014; **32**(17): 1818-1824.

Ni WD, Yang ZT, Cui CA, Cui Y, Fang LY & Xuan H. Tenascin-C is a potential cancer-associated fibroblasts marker and predicts poor prognosis in prostate cancer. *Biochem Biophys Res Comm* 2017; **486**(3): 607-612.

Niculescu III AB, Chen X, Meets M, Hengst L, Prives C & Reed SI. Effects of p21Cip1/Waf1 at both the G1/S and the G2/M cell cycle transitions: PRB is a critical determinant in blocking DNA replication and in preventing endoreduplication. *Mol Cell Biol* 1998; **18**(1): 629-643.

Nishifuji K & Yoon JS. The stratum corneum: the rampart of the mammalian body. In *Advances in Veterinary Dermatology* 2013. Oxford, UK: John Wiley & Sons, Ltd: 63-77.

Nomura M, Shimizu S, Sugiyama T, Narita M, Ito T, Matsuda H & Tsujimoto Y.14-3-3 interacts directly with and negatively regulates pro-apoptotic Bax. *J Biol Chem* 2015; **290**(11): 6753.

Oberholzer PA, Kee D, Dziunycz P, Sucker A, Kamsukom N, Jones R, Roden C, Chalk CJ, Ardlie K, Palescandolo E, Piris A, MacConaill LE, Robert C, Hofbauer GF, McArthur GA, Schadendorf D & Garraway LA. RAS mutations are associated with the development of cutaneous squamous cell tumors in patients treated with RAF inhibitors. *J Clinical Oncol* 2012; **30**(3): 316-321.

Ogata D & Tsuchida T. Systemic immunotherapy for advanced cutaneous squamous cell carcinoma. *Curr Treat Options Oncol* 2019; **20**(4): 30.

Ogawara Y, Kishishita S, Obata T, Isazawa Y, Suzuki T, Tanaka K, Masuyama N & Gotoh Y. Akt enhances Mdm2-mediated ubiquitination and degradation of p53. *J Biol Chem* 2002; **277**(24): 21843-21850.

Ogrunc M, Di Micco R, Liontos M, Bombardelli L, Mione M, Fumagalli M, Gorgoulis VG & d'Adda di Fagagna F. Oncogene-induced reactive oxygen species fuel hyperproliferation and DNA damage response activation. *Cell Death Differ* 2014; **21**: 998-1012.

Olsen CM & Green AC. More evidence of harms of sunbed use, particularly for young people. *BMJ* 2012; **345**: e6101.

Olumi AF Grossfeld GD, Hayward SW, Carroll PR, Tlsty TD & Cunha GR. Carcinoma-associated fibroblasts direct tumor progression of initiated human prostatic epithelium. *Cancer Res* 1999; **59**(19): 5002-5011.

Oshima RG, Abrams L & Kulesh D. Activation of an intron enhancer within the keratin 18 gene by expression of c-Fos and c-Jun in undifferentiated F9 embryonal carcinoma cells. *Genes Dev* 1990; **4**(5): 835-848.

Ou YH, Chung PH, Sun TP & Shieh SY. p53 C-terminal phosphorylation by CHK1 and CHK2 participates in the regulation of DNA-damage-induced C-terminal acetylation. *Mol Biol Cell* 2005; **16**(4): 1684-1695.

Pakyari M, Farrokhi A, Maharlooei MK & Ghahary A. Critical role of transforming growth factor beta in different phases of wound healing. *Adv Wound Care* (New Rochelle). 2013; **2**(5): 215-224.

Palazzo E, Kellett MD, Cataisson C, Bible PW, Bhattacharya S, Sun HW, Gormley AC, Yuspa SH & Morasso MI. A novel DLX3–PKC integrated signaling network drives keratinocyte differentiation. *Cell Death Differ* 2017; **24**: 717-730.

Papa A, Wan L, Bonora M, Salmena L, Song MS, Hobbs RM, Lunardi A, Webster K, Ng C, Newton RH, Knoblauch N, Guarnerio J, Ito K, Turka LA, Beck AH, Pinton P, Bronson R, Wei W & Pandolfi PP. Cancer-associated PTEN mutants act in a dominant negative manner to suppress PTEN protein function. *Cell* 2014; **157**(3): 595–610.

Paramio JM & Jorcano JL. Beyond structure: do intermediate filaments modulate cell signalling? *Bioessays* 2002; **24**(9): 836-44.

Paramio JM, Segrelles C, Ruiz S & Jorcano JL. Inhibition of protein kinase B (PKB) and PKCzeta mediates keratin K10-induced cell cycle arrest. *Mol Cell Biol* 2001; **21**(21): 7449-59.

Paolino G, Donati M, Didona D, Mercuri SR & Cantisani C. Histology of Non-Melanoma Skin Cancers: An Update. *Biomedicines* 2017; **5**(4): E71.

Perathoner A, Pirkebner D, Brandacher G, Spizzo G, Stadlmann S, Obrist P, Margreiter R & Amberger A. 14-3-3σ expression is an independent prognostic parameter for poor survival in colorectal carcinoma patients. *Clin Cancer Res* 2005; **11**(9): 3274-3279.

Perren A, Komminoth P, Saremaslani P, Matter C, Feurer S, Lees JA, Heitz PU, Eng C. Mutation and expression analyses reveal differential subcellular compartmentalization of PTEN in endocrine pancreatic tumors compared to normal islet cells. *Am J Pathol* 2000; **157**(4): 1097-1103.

Perry ME, Mendrysa SM, Saucedo LJ, Tannous P & Holubar M. $p76^{MDM2}$ Inibits the Ability of $p90^{MDM2}$ to Destabilise p53*. J Biol Chem 2000; 275(8): 5733-5738.

Phan L, Chou PC, Velazquez-Torres G, Samudio I, Parreno K, Huang Y, Tseng C, Vu T, Gully C, Su CH, Wang E, Chen J, Choi HH, Fuentes-Mattei E, Shin JH, Shiang C, Grabiner B, Blonska M, Skerl S, Shao Y, Cody D, Delacerda J, Kingsley C, Webb D, Carlock C, Zhou Z, Hsieh YC, Lee J, Elliott A, Ramirez M, Bankson J, Hazle J, Wang Y, Li L, Weng S, Rizk N, Wen YY, Lin X, Wang H, Wang H, Zhang A, Xia X, Wu Y, Habra M, Yang W, Pusztai L, Yeung SC,

Lee MH. The cell cycle regulator 14-3-3σ opposes and reverses cancer metabolic reprogramming. *Nature Commun* 2015; **6**: 7530.

Pickering CR, Zhou JH, Lee JJ, Drummond JA, Peng SA, Saade RE, Tsai KY5, Curry JL, Tetzlaff MT, Lai SY, Yu J, Muzny DM, Doddapaneni H, Shinbrot E, Covington KR, Zhang J, Seth S, Caulin C1, Clayman GL1, El-Naggar AK, Gibbs RA, Weber RS, Myers JN, Wheeler DA & Frederick MJ. Mutational landscape of aggressive cutaneous squamous cell carcinoma. *Clin Cancer Res* 2014; **20**(24): 6582-6592.

Pierceall WE, Goldberg LH, Tainsky MA, Mukhopadhyay T & Ananthaswamy HN. Ras gene mutation and amplification in human nonmelanoma skin cancers. *Mol Carcinog* 1991; **4**(3): 196-202.

Planchon SM, Waite KA & Eng C. The Nuclear Affairs of PTEN. *J Cell Sci* 2007; **121**: 249-253.

Prior IA, Lewis PD & Mattos C. A comprehensive survey of Ras mutations in cancer. *Cancer Res* 2012; **72**(10): 2457-2467.

Pruniéras M, Regnier M, Fougère S & Woodley D. Keratinocytes synthesize basal-lamina proteins in culture. *J Invest Dermatol* 1983; **81**(1): S74-S81.

Radhakrishnan VM & Martinez JD. 14-3-3gamma induces oncogenic transformation by stimulating MAP kinase and PI3K signaling. *PLoS ONE* 2010; **5**: e11433.

Radhakrishnan VM, Jensen TJ, Cui H, Futscher BW & Martinez JD. Hypomethylation of the 14-3-3σ promoter leads to increased expression in non-small cell lung cancer. *Genes Chromosomes Cancer* 2011; **50**(10): 830-836.

Radhakrishnan VM, Putnam CW & Martinez JD. Activation of phosphatidylinositol 3-kinase (PI3K) and mitogen-activated protein kinase (MAPK) signaling and the consequent induction of transformation by overexpressed 14-3-3gamma protein require specific amino acids within 14-3-3gamma N-terminal variable region II. *J Biol Chem* 2012; **287**(52): 43300-43311.

Rahmani-Neishaboor E, Hartwell R, Jalili R, Jackson J, Brown E & Ghahary A. Localized controlled release of stratifin reduces implantation-induced dermal fibrosis. *Acta Biomater* 2012; **8**(10): 3660-3668.

Rahdar M, Inoue T, Meyer T, Zhang J, Vazquez F & Devreotes PN. A phosphorylation-dependent intramolecular interaction regulates the membrane association and activity of the tumor suppressor PTEN. *Proc Nat Acad Sci* 2009; **106**(2): 480-485.

Räsänen K & Vaheri A. Activation of fibroblasts in cancer stroma. *Exp Cell Res* 2010; **316**(17): 2713-2722.

Ratushny V, Gober MD, Hick R, Ridky TW & Seykora JT. From keratinocyte to cancer: The pathogenesis and modeling of cutaneous squamous cell carcinoma. *J Clin Invest* 2012; **122**(2): 464-472.

Reichelt J, Büssow H, Grund C & Magin T. Formation of a normal epidermis supported by increased stability of Keratins 5 and 14 in Keratin 10 null mice. *Mol Biol Cell* 2001; **12**(6): 1557-1568.

Reis H, Pütter C, Megger DA, Bracht T, Weber F, Hoffmann AC, Bertram S, Wohlschläger J, Hagemann S, Eisenacher M, Scherag A, Schlaak JF, Canbay A, Meyer HE, Sitek B & Baba HA. A structured proteomic approach identifies 14-3-3Sigma as a novel and reliable protein biomarker in panel based

differential diagnostics of liver tumors. *Biochim Biophys Acta* 2015; **1854**: 641-650.

Reisman D, Takahashi P, Polson A & Boggs K. Transcriptional regulation of the p53 tumor suppressor gene in S-phase of the cell cycle and the cellular response to DNA damage. *Biochem Res Int* 2012; **2012**: 808934.

Reitscher K, Keil R, Jordan A & Hatzfeld M. 14-3-3 proteins regulate desmosomal adhesion via plakophilins. *J Cell Sci* 2018; **131**(10): jcs212191.

Ren HZ, Pan GQ, Wang JS, Wen JF, Wang KS, Luo GQ & Shan XZ. Reduced stratifin expression can serve as an independent prognostic factor for poor survival in patients with esophageal squamous cell carcinoma. *Dig Dis Sci* 2010; **55**(9): 2552-2560.

Renan MJ. How many mutations are required for tumorigeneis? Implications from human cancer data. *Mol Carcinog* 1993; **7**: 139-146.

Reuther GW & Der CJ. The Ras branch of small GTPases: Ras family members don't fall far from the tree. *Curr Opin Cell Biol* 2000; **12**(2):157-165.

Ribatti D. The concept of immune surveillance against tumors: The first theories. *Ocotarget* 2017; **8**(4): 7175-7180.

Roberts BJ, Reddy R & Wahl JK 3rd. Stratifin (14-3-3σ) limits plakophilin-3 exchange with the desmosomal plaque. *PLoS ONE* 2013; **8**(10): e77012.

Robin F, Angenard G, Cano L, Courtin-Tanguy L, Gaignard E, Khene ZE, Bergeat D, Clément B, Boujema K, Coulouarn C & Sulpice L. Molecular profiling of stroma highlights stratifin as a novel biomarker of poor prognosis in pancreatic ductal adenocarcinoma. *Br J Cancer* 2020; **123**: 72-80.

Robinson JK & Dahiya M. Basal cell carcinoma with pulmonary and lymph node metastasis causing death. *Arch Dermatol* 2003; **139**(5): 643-648.

Rosenthal DS, Steinert PM, Chung S, Huff CA, Johnson J, Yuspa SH & Roop DR. A human epidermal differentiation-specific keratin gene is regulated by calcium but not negative modulators of differentiation in transgenic mouse keratinocytes. *Cell Growth Differ* 1991; **2**(2):107-13.

Rosenthal N & Brown S. The mouse ascending: perspectives for human-disease models. *Nat Cell Biol* 2007; **9**: 993-999.

Rothnagel JA, Greenhalgh DA, Gagne TA, Longley MA & Roop DR. Identification of a calcium-inducible, epidermal-specific regulatory element in the 3'-flanking region of the human keratin 1 gene. *J Invest Dermatol* 1993; **101**(4): 506-13.

Roth W, Kumar V, Beer HD, Richter M, Wohlenberg C, Reuter U, Thiering S, Staratschek-Jox A, Hofmann A, Kreusch F, Schultze JL, Vogl T, Roth J, Reichelt, Hausser I & Magin T. Keratin 1 maintains skin integrity and participates in an inflammatory network in skin through interleukin-18. *J Cell Sci* 2012; **125**: 5269-5279.

Rotty JD & Coulombe PA. A wound-induced keratin inhibits Src activity during keratinocyte migration and tissue repair. *J Cell Biol* 2012; **197**(3): 381-389.

Rutberg SE, Saez E, Lo S, Jang SI, Markova N, Spiegelman BM & Yuspa SH. Opposing activities of c-Fos and Fra-2 on AP-1 regulated transcriptional activity in mouse keratinocytes induced to differentiate by calcium and phorbol esters. *Oncogene* 1997; **15**: 1337-1346.

Salasche SJ. Epidemiology of actinic keratoses and squamous cell carcinoma. *J Am Acad Dermatol* 2000; **42**(1 Pt 2): 4-7.

Sakai N. Chemical carcinogenesis is accelerated in c-fos transgenic mice. *Kobe J Med Sci* 1990; **36**(1-2): 37-53.

Samuel T, Weber HO, Rauch P, Verdoodt B, Eppel JT, McShea A, Hermeking H & Funk JO. The G2/M Regulator 14-3-3σ prevents apoptosis through sequestration of Bax. *J Biol Chem* 2001; **276**(48): 45201-45206.

Sanchis A, Alba L, Latorre V, Sevilla LM, & Pérez P. Keratinocyte-targeted overexpression of the glucocorticoid receptor delays cutaneous wound healing. *PloS ONE* 2012; **7**(1): e29701.

Santos M, Paramio JM, Bravo A, Ramirez A, Jorcano JL. The expression of keratin K10 in the basal layer of the epidermis inhibits cell proliferation and prevents skin tumorigenesis. *J Biol Chem* 2002; **277**(21): 19122-19130.

Schlingemann J, Hess J, Wrobel G, Breitenbach U, Gebhardt C, Steinlein P, Kramer H, Fürstenberger G, Hahn M, Angel P & Lichter P. Profile of gene expression induced by the tumour promotor TPA in murine epithelial cells. *Int J Cancer* 2003; **104**(6): 699-708.

van der Schroeff JG, Evers LM, Boot AJ & Bos JL. Ras oncogene mutations in basal cell carcinomas and squamous cell carcinomas of human skin. *J Invest Dermatol* 1990 **94**(4): 423-425.

Schütte J, Viallet J, Nau M, Segal S, Fedorko J & Minna J. Jun-B inhibits and c-fos stimulates the transforming and trans-activating activities of c-jun. *Cell* 1989; **59**(6): 987-997.

Segrelles C, Ruiz S, Perez P, Murga C, Santos M, Budunova IV, Martínez J, Larcher F, Slaga TJ, Gutkind JS, Jorcano JL, Paramio JM. Functional roles of Akt signaling in mouse skin tumorigenesis. *Oncogene* 2002; **21**(1): 53-64.

Shao Z, Cai Y, Xu L, Yao X, Shi J, Zhang F, Luo Y, Zheng K, Liu J, Deng F, Li R, Zhang L, Wang H, Li M, Ding Y & Zhao L. Loss of the 14-3-3σ is essential for LASP1-mediated colorectal cancer progression via activating PI3K/AKT signaling pathway. *Sci Rep* 2016; **6**: 25631.

Shendrik I, Crowson AN, Magro CM. Follicular cutaneous squamous cell carcinoma: an under-recognized neoplasm arising from hair appendage structures. *Br J Dermatol* 2013; **169**(2): 384-388.

Shiba-Ishii A, Kano J, Morishita Y, Sato Y, Minami Y & Noguchi M. High expression of stratifin is a universal abnormality during the course of malignant progression of early-stage lung adenocarcinoma. *Int J Cancer* 2011; **129**(10): 2445-2453.

Shiba-Ishii A & Noguchi M. Aberrant stratifin overexpression is regulated by tumor-associated CpG demethylation in lung adenocarcinoma. *Am J Pathol* 2012; **180**(4): 1653-1662.

Shieh SY, Ahn J, Tamai K, Taya Y & Prives C. The human homologs of checkpoint kinases Chk1 and Cds1 (Chk2) phosphorylate p53 at multiple DNA damage-inducible sites. *Genes Dev* 2000; **14**(3): 289-300.

Shin I, Yakes FM, Rojo F, Shin NY, Bakin AV, Baselga J & Arteaga CL. PKB/Akt mediates cell-cycle progression by phosphorylation of p27Kip1 at threonine 157 and modulation of its cellular localization. *Nature Med* 2002; **8**: 1145-1152.

Shultz GS, DavidsonJM, Kirsner RS, Bornstein P & Herman IM. Dynamic reciprocity in the wound microenvironment. *Wound Repair Regen* 2010; **19**: 134-148.

Sijbesma E, Skora L, Leysen S, Brunsveld L, Koch U, Nussbaumer P, Jahnke W & Ottmann C. Identification of two secondary ligand binding sites in 14-3-3 proteins using fragment screening. *Biochemistry* 2017; **56**(30): 3972-3982.

Simons K & Ehehalt R. Cholesterol, lipid rafts, and disease. *J Clin Invest* 2002; **110**(5): 597-603.

Simpson CL, Patel DM & Green KJ. Deconstructing the skin: cytoarchitectural determinants of epidermal morphogenesis. *Nat Rev Mol Cell Biol* 2011; **12**(9): 565-580.

Slaga T. SENCAR mouse skin tumorigenesis model versus other strains and stocks of mice. *Environ Health Perspect* 1986; **68**: 27-32.

Sluchanko NN & Gusev NB. 14-3-3 proteins and regulation of cytoskeleton. *Biochemistry (Mosc)* 2010; **75**(13): 1528-1546.

Starink TM, Meijer CJ & Brownstein MH. The cutaneous pathology of Cowden's disease: new findings. *J Cutan Pathol* 1985; **12**(2): 83-93.

Steiner M, Clark B, Tang JZ, Zhu T & Lobie PE. 14-3-3σ mediates G2–M arrest produced by 5-aza-2′-deoxycytidine and possesses a tumor suppressor role in endometrial carcinoma cells. *Gynecol Oncol* 2012; **127**(1): 231-240.

Steinert PM, Steven AC & Roop DR. The Molecular Biology of Intermediate Filaments. *Cell* 1985; **42**: 411-419.

Stevers LM, Sijbesma E, Botta M, MacKintosh C, Obsil T, Landrieu I, Cau Y, Wilson AJ, Karawajczyk A, Eickhoff J, Davis J, Hann M, O'Mahony G, Doveston RG, Brunsveld L & Ottmann C. Modulators of 14-3-3 protein-protein interactions. *J Med Chem* 2018; **61**(9): 3755-3778.

Stratigos A, Garbe C, Lebbe C, Malvehy J, del Marmol V, Pehamberger H, Peris K, Becker JC, Zalaudek I, Saiag P, Middleton MR, Bastholt L, Testori A & Grob JJ (On behalf of the European Dermatology Forum, European Association of Dermato-Oncology & European Organisation for Research and Treatment of Cancer). Diagnosis and treatment of invasive squamous cell carcinoma of the skin: European consensus-based interdisciplinary guideline. *Eur J Cancer* 2015; **51**(14): 1989-2007.

Strickland JE, Greenhalgh DA, Koceva-Chyla A, Hennings H, Restreppo C, Balaschak M & Yuspa SH. Development of Murine Epidermal Cell Lines Which Contain an Activated ras^{Ha} Oncogene and Form Papillomas in Skin Grafts on Athymic Nude Mouse Hosts. *Cancer Res* 1988; **48**(1): 165-69.

Su F, Viros A, Milagre C, Trunzer K, Bollag G, Spleiss O, Reis-Filho JS, Kong X, Koya RC, Flaherty KT, Chapman PB, Kim MJ, Hayward R, Martin M, Yang H, Wang

Q, Hilton H, Hang JS, Noe J, Lambros M, Geyer F, Dhomen N, Niculescu-Duvaz I, Zambon A, Niculescu-Duvaz D, Preece N, Robert L, Otte NJ, Mok S, Kee D, Ma Y, Zhang C, Habets G, Burton EA, Wong B, Nguyen H, Kockx M, Andries L, Lestini B, Nolop KB, Lee RJ, Joe AK, Troy JL, Gonzalez R, Hutson TE, Puzanov I, Chmielowski B, Springer CJ, McArthur GA, Sosman JA, Lo RS, Ribas A & Marais R. RAS mutations in cutaneous squamous-cell carcinomas in patients treated with BRAF inhibitors. *New Engl J Med* 2012; **366**(3): 207-215.

Su YJ, Chang YW, Lin W-H, Liang CL & Lee JL. An aberrant nuclear localization of E-cadherin is a potent inhibitor of Wnt/ß-catenin-elicited promotion of the cancer stem cell phenotype. *Oncogenesis* 2015; **4**: e157.

Sun BK, Boxer LD, Ransohoff JD, Siprashvili Z, Qu K, Lopez-Pajares V, Hollmig ST & Khavari PA. CALML5 is a ZNF750- and TINCR-induced protein that binds stratifin to regulate epidermal differentiation. *Genes Dev* 2015; **29**: 2225-2230.

Sun Z, Velázquez-Quesada I, Murdamoothoo D, Ahowesso C, Yilmaz A, Spenlé C, Averous G, Erne W, Oberndorfer F, Oszwald A, Kain R, Bourdon C, Mangin P, Deligne C, Midwood K, Abou-FaycalC, Lefebvre O, Klein A, van der Heyden M, Chenard M-P, Christofori G, Mathelin C, Loustau T, Hussenet T & Orend G. Tenascin-C increases lung metastasis by impacting blood vessel invasions. *Matrix Biol* 2019; **83**: 26-47.

Sur I, Ulvmar M & Toftgård R. The Two-Faced NF-κB in the Skin. *Intl Rev Immunol* 2008; **27**(4): 205-223.

Suzuki A, Itami S, Ohishi M, Hamada K, Inoue T, Komazawa N, Senoo H, Sasaki T, Takeda J, Manabe M, Mak TW & Nakano T. Keratinocyte-specific Pten deficiency results in epidermal hyperplasia, accelerated hair follicle morphogenesis and tumor formation. *Cancer Res* 2003; **63**: 674-681.

Tamura M, Gu J, Matsumoto K, Aota S, Parsons R, Yamada KM. Inhibition of cell migration, spreading, and focal adhesions by tumor suppressor PTEN. *Science* 1998; **280**(5369): 1614-1617.

Tan AC, Jimeno A, Lin SH, Wheelhouse J, Chan F, Solomon A, Rajeshkumar NV, Rubio-Viqueira B & Hidalgo M. Characterizing DNA methylation patterns in pancreatic cancer genome. *Mol Oncol* 2009; **3**(5-6): 425-438.

Tan MH, Mester JL, Ngeow J, Rybicki LA, Orloff MS & Eng C. Lifetime cancer risks in individuals with germline PTEN mutations. *Clin Cancer Res* 2012; **18**(2): 400-407.

Tanaka K, Hatada T, Kobayashi M, Mohri Y, Tonouchi H, Miki C, Nobori T & Kusunoki M. The clinical implication of 14-3-3 sigma expression in primary gastrointestinal malignancy. *Int J Oncol* 2004; **25**(6): 1591-1597.

Tautz L, Critton DA & Grotegut S. Protein tyrosine phosphatases: Structure, function, and implication in human disease. *Methods Mol Biol* 2013; **1053**: 179-221.

Thompson AK, Kelley BF, Prokop LJ, Murad MH & Baum CL. Risk Factors for Cutaneous Squamous Cell Carcinoma Recurrence, Metastasis, and Disease-Specific Death: A Systematic Review and Meta-analysis. *JAMA Dermatol* 2016; **152**(4): 419-428.

Timpson P, Mcghee EJ, Erami Z, Nobis M, Quinn JA, Edward M & Anderson KI. Organotypic Collagen I Assay: A Malleable Platform to Assess Cell Behaviour in a 3-Dimensional Context. *J Vis Exp* 2011; **56**: e3089.

Tkac J, Gajdosova V, Hroncekova S, Bertok T, Hires M, Jane E, Lorencova L & Kasak P. Prostate-specific anitigen glycoprofiling as diagnostic and prognostic biomarker of prostate cancer. *Interface Focus* 2019; **9**(2): 20180077.

Tomassi C, Rogerson C, Depledge DP, Jones M, Naeem AS, Venturini C, Frampton D, Tutill HJ, Way B, Breur J, O'Shaughnessy RFL. Kallikrein-mediated Cytokeratin 10 degradation is required for varicella zoster virus propagation in skin. *J Invest Dermatol* 2020; **140**(4): 774-784.

Trink B, Osada M, Ratovitski E & Sidransky D. p63 transcriptional regulation of epithelial integrity and cancer. *Cell Cycle* 2007; **6**(3): 240-245.

Umbricht CB, Evron E, Gabrielson E, Ferguson A, Marks J, Sukumar S. Hypermethylation of 14-3-3 sigma (stratifin) is an early event in breast cancer. *Oncogene* 2001; **20**(26): 3348-3353.

Vassar R, Rosenberg M, Ross S, Tyner A & Fuchs E. Tissue-specific and differentiation-specific expression of a human K14 keratin gene in transgenic mice. *Proc Natl Acad Sci USA* 1989; **86**(5): 1563-1567.

Vassilev LT. Small-molecule antagonists of p53-MDM2 binding: research tools and potential therapeutics. *Cell Cycle* 2004; **3**(4): 417-419.

Vetter IR & Wittinghofer A. The guanine nucleotide-binding switch in three dimensions. *Science* 2001; **294**(5545): 1299-1304.

Vidotto T, Tiezzi DG & Squire JA. Distinct subtypes of genomic PTEN deletion size influence the landscape of aneuploidy and outcome in prostate cancer. *Mol Cytogenet* 2018; **11**(1).

Waite KA & Eng C. Protean PTEN: form and function. *Am J Hum Genet* 2002; **70**: 829-844.

Wajapeyee N, Britto R, Ravishankar HM & Somasundaram K. Apoptosis induction by Activator Protein 2α involves transcriptional repression of Bcl-2. *J Biol Chem* 2006; **281**: 16207-16219.

Wang Q, Oh JW, Lee H-L, Dhar A, Peng T, Ramos R, Guerrero-Juarez CF, Wang X, Zhao R, Cao X, Le J, Fuentes MA, Jocoy SC, Rossi AR, Vu B, Pham K, Xiaoyang Wang, Mali NM, Park JM, Choi J-H, Lee H, Legrand JMD, Kandyba E, Kim JC, Kim M, Foley J, Yu Z, Kobielak K, Andersen B, Khosrotehrani K, Nie Q & Plikus MV. A multi-scale model for hair follicles reveals heterogeneous domains driving rapid spatiotemporal hair growth patterning. *eLife* 2017; **6**: e22772.

Wang W & Shakes DC. Molecular evolution of the 14-3-3 protein family. *J Mol Evol* 1996; **43**(4): 384-98.

Wang X, Trotman LC, Koppie T, Alimonti A, Chen Z, Gao Z, Wang J, Erdjument-Bromage H, Tempst P, Cordon-Cardo C, Pandolfi PP & Jiang X. NEDD4-1 is a proto-oncogenic ubiquitin ligase for PTEN. *Cell* 2007; **128**(1): 129-139.

Wang XJ, Greenhalgh DA**,** Jaing A, He D, Zhong L, Medina D, Brinkly BR & Roop DR. Expression of a p53 mutant in the epidermis of transgenic mice accelerates chemical carcinogenesis. *Oncogene* 1998; **17**: 35-45.

Warren TA, Broit N, Simmons JL, Pierce CJ, Chawla S, Lambie DL, Quagliotto G, Brown IS, Parsons PG, Panizza BJ & Boyle GM. Expression profiling of cutaneous squamous cell carcinoma with perineural invasion implicates the p53 pathway in the process. *Sci Rep* 2016; **6**: 34081.

Watanabe IC, Magalhães RF, de Moraes AM, Stelini RF, Cintra GF, Metze K & Cintra ML. Keratoacanthoma and keratoacanthoma-like squamous cell carcinoma: similar morphology but different pathogenesis. *Medicine (Baltimore)* 2015; **94**(23): e934.

Watt FM. Influence of cell shape and adhesiveness on stratification and terminal differentiation of human keratinocytes in culture. *J Cell Sci Suppl* 1987; **8**: 313-326.

Watt FM & Jensen KB. Epidermal stem cell diversity and quiescence. *EMBO Mol Med* 2009; **1**(5): 260–267.

Weinberg AS, Ogle CA & Shim EK. Metastatic cutaneous squamous cell carcinoma: an update. *Dermatol Surg* 2007; **33**(8): 885-899.

Weiss MB, Vitolo MI, Rosen DM, Denmeade SR, Park BH, Weber DJ & Bachman KE. Deletion of p53 in human mammary epithelial cells causes chomosomal instability and altered therapeutic response. *Oncogene* 2010; **29**: 4715-4724.

Weng LP, Brown JL & Eng C. PTEN coordinates G1 arrest by down-regulating cyclin D1 via its protein phosphatase activity and up-regulating p27 via its lipid phosphatase activity in a breast cancer model. *Hum Mol Genet* 2001; **10**(6): 599-604.

Wennerberg K, Rossman KL & Der CJ. The Ras superfamily at a glance. *J Cell Sci* 2005;**118**(Pt 5): 843-846.

Westfall MD, Mays DJ, Sniezek JC & Pietenpol JA. The Delta Np63 alpha phosphoprotein binds the p21 and 14-3-3 sigma promoters *in vivo* and has transcriptional repressor activity that is reduced by Hay-Wells syndrome-derived mutations. *Mol Cell Biol* 2003; **23**(7): 2264-2276.

White, A.C. & Lowry, W.E. Refining the role for adult stem cells as cancer cells of origin. *Trends Cell Biol* 2015; **25**(1): 11-20.

Wilhelmsen K, Litjens SHM, Kuikman I, Tshimbalanga N, Janssen H, van den Bout I, Raymond K & Sonnenberg A. Nesprin-3, a novel outer nuclear membrane protein, associates with the cytoskeletal linker protein plectin. *J Cell Biol* 2005; **171**(5): 799-810.

Wilker EW, Grant RA, Artim SC & Yaffe MB. A Structural Basis for 14-3-3σ Functional Specificity. *J Biol Chem* 2005; **280**(19): 18891-18898.

Willert K & Nusse R. β-catenin: a key mediator of Wnt signaling. *Curr Opin Genet Dev* 1998; **8**(1): 95-102.

Winter M, Lodygin D, Verdoodt B & Hermeking H. Deletion of 14-3-3σ sensitizes mice to DMBA/TPA-induced papillomatosis. *Oncotarget* 2016; **7**(30): 46862-46870.

Wojcik SM, Bundman DS & Roop DR. Delayed wound healing in keratin 6a knockout mice. *Mol Cell Biol* 2000; **20**(14): 5248-5255.

Wong P & Coulombe PA. Loss of keratin 6 (K6) proteins reveals a function for intermediate filaments during wound repair. *J Cell Biol* 2003; **163**(2): 327-337.

Wu J, Liang C, Chen M & Su W. Association between tumor-stroma ratio and prognosis in solid tumor patients: a systematic review and meta-analysis. *Oncotarget* 2016; **7**(42): 68954-68965.

Wu YJ, Jan YJ, Ko BS, Liang SM & Liou JY. Involvement of 14-3-3 proteins in regulating tumor progression of hepatocellular carcinoma. *Cancers* 2015; **7**: 1022-1036.

Xiao B, Smerdon SJ, Jones DH, Dodson GG, Soneji Y, Aitken A & Gamblin SJ. Structure of a 14-3-3 protein and implications for coordination of multiple signalling pathways. *Nature* 1995; **376**(6536): 188-191.

Yang AY, Lee JH, Shu L, Zhang C, Su ZY, Lu Y, Huang MT, Ramirez C, Pung D, Huang Y, Verzi M, Hart RP & Kong ANT. Genome-wide analysis of DNA methylation in UVB- and DMBA/TPA-induced mouse skin cancer models. *Life Sci* 2014; **113**(1-2): 45-54.

Yang G, Murashige DS, Humphrey SJ & James DE. A Positive Feedback Loop between Akt and mTORC2 via SIN1 Phosphorylation. *Cell Rep* 2015; **12**(6): 937-943.

Yang H, Wen Y, Zhao R, Lin Y, Fournier K, Yang H, Qui Y, Diaz J, Laronga C & Lee M. DNA damage-induced protein 14-3-3sigma inhibits protein kinase B/Akt activation and suppresses Akt-activated cancer. *Cancer Res* 2006; **66**(6): 3096-3105.

Yao D, Alexander CL, Quinn JA, Porter MJ, Wu H & Greenhalgh DA. PTEN loss promoes rasHa-mediated papillomatogenesis via dual up-regulation of AKT activity and cell cycle deregulation but malignant converion proceeds via PTEN-associated pathways. *Cancer Res* 2006; **66**(3): 1302-1312.

Yao D, Alexander CL, Quinn JA, Chan WC, Wu H & Greenhalgh DA. Fos cooperation with PTEN loss elicits keratoacanthoma not carcinoma, owing to p53/p21WAF-induced differentiation triggered by GSK3β inactivation and reduced AKT activity. *J Cell Sci* 2008; **121**(10): 1758-1769.

Yatabi Y, Osda H, Tatematsu Y, Mitsudomi T & Takahashi T. Decreased expression of 14-3-3sigma in neuroendocrine tumours is independent of origin and malignant potential. *Oncogene* 2002; **21**(54): 8310-8319.

Yeo CQX, Alexander I, Lin Z, Lim S, Aning OA, Kumar R, Sangthongpitag K, Pendharkar V, Ho VHB & Cheok CF. p53 maintains genomic stability by preventing interference between transcription and replication. *Cell Rep* 2016; **15**(1): 132-146.

Yohn NL, Bingaman CN, DuMont AL & Yoo LI. Phosphatidylinositol 3'-kinase, mTOR, and Glycogen synthase kinase-3β mediated regulation of p21 in human urothelial carcinoma cells. *BMC Urol* 2011; **11**: 19.

Yoshiki A & Moriwaki K. Mouse phenome research: Implications of genetic background. *ILAR J* 2006; **7**(2): 94-102.

Youssef G, Ono M, Brown SJ, Kinsler VA, Sebire NJ, Harper JI & O'Shaughnessy RFL. Identifying a hyperkeratosis signature in autosomal recessive congenital ichthyosis: mdm2 inhibition prevents hyperkeratosis in a rat ARCI model. *J Invest Dermatol* 2014; **134**: 858-861.

Yu JS & Cui W. Proliferation, survival and metabolism: the role of PI3K/AKT/mTOR signalling in pluripotency and cell fate determination. *Development* 2016; **143**(17) 3050-3060.

Yuspa SH, Kilkenny AE, Steinert PM & Roop DR. Expression of murine epidermal differentiation markers is tightly regulated by restricted extracellular calcium concentrations in vitro. *J Cell Biol* 1989; **109**(3): 1207-1217.

Zagni C, Almeida LO, Balan T, Martins MT, Rosselli-Murai LK, Papagerakis P, Castilho RM & Squarize CH. PTEN mediates activation of core clock protein BMAL I and accumulation of epidermal stem cells. *Stem Cell Reports* 2017; **9**(1): 304-314.

Zhang W & Liu HT. MAPK signal pathways in the regulation of cell proliferation in mammalian cells. *Cell Res* 2002; **12**: 9-18.

Zhang Y, Karas M, Zhao H, Yakar S & LeRoith D. 14-3-3sigma mediation of cell cycle progression is p53-independent in response to insulin-like growth factor-I receptor activation. *J Biol Chem* 2004; **279**(33): 34353–34360.

Zhang M, Qureshi AA, Geller AC, Frazier L, Hunter DJ & Han J. Use of tanning beds and incidence of skin cancer. *J Clin Oncol* 2012 **30**(14): 1588-1593.

Zhang Z, Hou SQ, He J, Gu T, Yin Y & Shena WH. PTEN regulates PLK1 and controls chromosomal stability during cell division. *Cell Cycle* 2016; **15**(18): 2476-2485.

Zhao Y, Yu T, Zhang N, Chen J, Zhang P, Li S, Luo L, Cui Z, Qin Y & Liu F. Nuclear E-Cadherin acetylation promotes colorectal tumorigenesis via enhancing ß-catenin activity. *Mol Cancer Res* 2019; **17**(2): 655-665.

Zhou BP, Liao Y, Xia W, Spohn B, Lee MH & Hung MC. Cytoplasmic localisation of p21Cip1/WAF1 by Akt-induced phosphorylation in HER-2/neu-overexpressing cells. *Nat Cell Biol* 2001; **3**(3): 245-252.

Ziegler A , Jonason AS, Leffell DJ, Simon JA, Sharma HW, Kimmelman J, Remington L, Jacks T & Brash DE. Sunburn and p53 in the onset of skin cancer. *Nature* 1994; **372**(6508): 773-776.

Zomer HD & Trentin AG. Skin wound healing in humans and mice: Challenges in translational research. *J Dermatol Sci* 2018; **90**: 3-12.

Appendix 1: Manuscript in preparation

Persistent 14-3-3σ and p21 limit AKT-related malignant progression following MDM2-associated p53 loss in ras^{Ha}/fos/PTEN skin carcinogenesis

Carol M. McMenemy[1,4], Dajiang Guo[1,2,4], Jean A. Quinn[3] and David A. Greenhalgh[1,5].

[1]Section of Dermatology and Molecular Carcinogenesis, School of Medicine, Dentistry and Nursing, College of Medical, Veterinary and Life Sciences, Glasgow University G31 2ER.

[2] Immune Imaging Program, Centenary Institute, Faculty of Medicine and Health, The University of Sydney, Camperdown, NSW 2050, Australia.

[3] Wolfson Wohl Cancer Research Centre, Institute of Cancer Sciences, College of Medical, Veterinary and Life Sciences, University of Glasgow, Glasgow, Scotland, United Kingdom

[4] These authors contributed equally to this study.

[5]Corresponding Author David A. Greenhalgh, PhD
Section of Dermatology and Molecular Carcinogenesis
david.greenhalgh@glasgow.ac.uk
https://orcid.org/0000-0002-6737-2744

Conflict of interest. The authors declare no conflict of interest.

Running title: 14-3-3σ/Stratifin in transgenic mouse skin cancer

Key words: epidermis; keratoacanthoma; organotypic culture; differentiation, promotion.

Summary: Analysis of *ras^{Ha}/fos/Δ5PTEN^{flx}*-driven skin carcinogenesis reveals that tumour suppressive roles for *14-3-3σ/Stratifin* in papillomatogenesis persist into early, well-differentiated carcinoma, despite p-MDM2^{166}-associated p53 loss; until both 14-3-3σ and p21 loss result in aggressive, p-AKT^{273}-activated carcinoma.

ABSTRACT

To study mechanisms driving/inhibiting skin carcinogenesis, expression of 14-3-3σ [Stratifin] was analysed in stage-specific skin carcinogenesis driven by activated *ras*^{Ha}*/fos* expression [*HK1.ras/fos*] and ablation of *PTEN-mediated AKT regulation* [*K14.creP/Δ5PTEN*^{flx}]. In bi-genic combinations, consistent with 14-3-3σ roles in normal differentiation, epidermal hyperplasia and papillomas displayed elevated expression in supra-basal keratinocytes; associated with supra-basal p-MDM2$^{166/186}$ activation and sporadic p-AKT^{273}. Early *HK1.fos/Δ5PTEN*^{flx} hyperplasia exhibited novel, increased basal-layer14-3-3σ expression, alongside p53/p21 which accelerated epidermal differentiation, highlighted by anomalous basal-layer keratin K1 expression, resulting in keratoacanthoma. Tri-genic *HK1.ras/fos-Δ5PTEN*^{flx} hyperplasia/papillomas also displayed elevated basal-layer 14-3-3σ, possibly geared to maintain the supra-basal p-MDM2^{166} expression and thus increase basal-layer p53 levels via limiting auto-ubiquitination. However, with time, tri-genic basal-layer 14-3-3σ expression decreased alongside supra-basal-to-basal increases in MDM2^{166} which coincided with p53 loss and subsequent malignant conversion. Nonetheless, [p53-independent] 14-3-3σ expression persisted and, together with elevated p21, was associated with downregulated p-AKT1^{273} that limited tumour progression to well-differentiated squamous cell carcinoma; until loss of 14-3-3σ/p21 facilitated progression to aggressive, uniform p-AKT1^{+ve} SCCs. TPA promotion of *HK1.ras-Δ5PTEN*^{flx} mice and rapid transit to poorly-differentiated SCC further highlighted 14-3-3σ tumour suppressive roles, as 14-3-3σ responses in early hyperplasia rapidly diminished; alongside increased p-MDM2^{166}, p53/p21 loss and p-AKT1^{273} activation. In 2D/3D culture contexts, membranous 14-3-3σ expression in normal HaCaT or SP1^{ras61} papilloma keratinocytes remained detectable in malignant T52$^{ras61/v\text{-}fos}$ SCC 2D-cells but not invading 3D-cells. Collectively, 14-3-3σ/Stratifin appears to exert suppressive roles in contexts of *ras/fos/PTEN*^{flx} skin carcinogenesis via MDM2/p53-dependent and p53-independent mechanisms, which alongside p21 inhibit AKT1 activities to limit early-stage malignant progression.

METHODS

Transgenic genotypes and induction of tumours

Transgenic mice expressing activated ras^{Ha} and/or v-fos from a human keratin K1-based vector, modified to express in basal- and supra-basal keratinocytes (*HK1.ras/fos*) have been described previously (Greenhalgh et al., 1993a, 1993b, 1993c; See supplemental data **Fig. S2**). These mice were crossed to mice expressing a keratin K14-driven Cre fusion protein (*K14.creP* (Berton et al., 2000)) and breeding strategies maintained *HK1.ras/fos* and the RU486-inducible *K14.creP* regulator as heterozygous transgenes in mice homozygous for the lox-P-flanked-PTEN exon5 alleles ($\Delta 5PTEN^{flx/flx}$ (Lesche et al., 2001)). Bi-genic and tri-genic combinations of HK1.*ras/fos*-$\Delta 5PTEN^{flx/f/x}$ progeny were genotyped by PCR as described [MacDonald et al., 2014; see Supplemental data Table 1) and PTEN regulation of AKT was inactivated following topical treatment of skin with 2ug RU486 (mifepristone; Sigma, Gillingham, UK) dissolved in 50ul ethanol and 15ul applied to the dorsal surface of each ear and shaved back weekly for 3 weeks; controls received ethanol alone. Papillomas and SCCs were also raised in RU486-treated, bi-genic *HK1.ras*-$\Delta 5PTEN^{flx/flx}$ mice via 3 weekly treatments with 2.5µg/50µL acetone TPA (50µL of 1.6 x 10^{-4}M TPA; Sigma, Gillingham, UK). All experiments adhered to UK Experimental Regulations (Licence: P82170325 to DAG).

Histology, immunofluorescence and immunochemical analysis

Skin biopsies and organotypic rafts were fixed in buffered formalin (24hrs @ 4^{o}C), embedded in paraffin (FFPE) and stained with haematoxylin and eosin. To confirm differentiation status via double-label immunofluorescence, following antigen retrieval (5 mins. boil/10mM sodium citrate), paraffin sections were incubated overnight (4^{o}C) with rabbit anti-mK1 or anti-mK6α (diluted 1:100 (Covance, Richmond, CA) employing guinea-pig anti-K14 antibodies (1:400 (Fitzgerald, Acton, MA) to delineate epidermis; and visualized employing biotinylated-goat anti-guinea pig/Streptavidin-Texas Red (1:100/1:400) (Vector Labs Burlingame, California) or FITC-labeled anti-rabbit IgG (diluted 1:100; Jackson Labs West Grove, PA). FFPE biopsy sections were also analysed for expression status of 14-3-3σ/Stratifin (1:100; rabbit anti-14-3-3σ/stratifin: Invitrogen (ThermoFisher Scientific) cat. # PA5-23507); and p-AKT1 (1:100; abcam #81283 Cambridge, UK; shown) confirming previous data employing Santa Cruz p-$AKT^{1/2/3}$ sc-7985-R (1:50; not shown), counterstained for K14 (as above).

Stage-specific FFPE biopsy sections, rafts and cultured cells were also subjected to immunohistochemical analysis. Following antigen retrieval, FFPE sections were incubated overnight (4°C) with rabbit anti-14-3-3σ/Stratifin (1:100). p53/p21 analysis employed p53 antibodies Abcam cat. # ab31333 or ab #131442 and p21 Proteintech #10355-1-AP) replacing discontinued Santa Cruz p53 (sc#393) and p21 (sc#397). Antibody comparison is shown in Supplementary Fig. S1: where p53 ab#31333 gave a greater nuclear expression;

whilst p53 ab#131442 more closely repeated the nuclear/cytoplasmic expression profile of sc#393 (MacDonald et al., 2014). p-MDM2^{166} analysis employed Abcam anti-MDM2 (phospho-S166) ab131355 1/400). IHC expression was visualised via HRP-conjugated goat anti-rabbit (1:100; 60 mins/RT; Vector Labs Burlingame, California) followed by DAB+ staining (Dako, Amersham Biosciences, Little Chalfont, UK). Photomicrographs employed Axiovision image capture software (Zeiss Microscopes, Cambridge, UK).

Cell culture and organotypic tumour invasion modelling

Normal HaCaT keratinocytes (Boukamp et al., 1988; provided at passage 35/used at passage 49-53), ras^{Ha}-transformed SP1 papilloma and ras^{Ha}/fos transformed T52 carcinoma cells (Greenhalgh & Yuspa, 1988) were cultured in Dulbecco's modified Eagle's medium (w/o Ca^{2+}), supplemented with 10% (chelated) foetal calf serum (FCS) with the calcium concentration adjusted to 0.05 mM (Low Ca^{2+} (Hennings et al., 1980)). C8161 melanoma cells were cultured in standard DMEM/10% FCS (Timpson et al., 2011). All cells were maintained in 5% CO2 at 37°C. For IHC or IF analysis on microscope chamber slides (Millicell EZ SLIDE 8; Millipore), cells were trypsinised, counted and plated at 1000 cells per chamber. Two days later, cells were re-fed with Low Ca^{2+} media, or induced to differentiated by culture in 0.12 mM Ca^{2+} media (Hennings et al., 1980), for 48 hours. Prior to immunofluorescence or immunohistochemical analysis, media was removed, cells washed in PBS and fixed in 10% buffered formalin (5 min; Sigma).

To prepare the organotypic invasion models, primary dermal fibroblasts were prepared as described (Greenhalgh et al., 1989) and cultured in DMEM 10% FCS until confluent. Rat tail collagen solution was prepared via extraction from tendons with 0.5M acetic acid and gels were prepared as described (Timpson et al., 2011). In brief, typically 3 ml 10X DMEM 30% FCS was added to 25ml rat tail collagen (2 mg/ml; 4°C), neutralized with 0.22M sodium hydroxide (pH 7.2). Dermal fibroblasts (7 x 10^4 cells/ml) were seeded in 2.5ml neutralized collagen plated into 35mm dishes and maintained for up to 7 days until fibroblasts contracted the collagen to form a gel raft (~1.5cm diameter). Free-floating collagen rafts were placed into 24-well dishes containing 1 ml media and seeded with 10^4 cells, employing C8161 melanoma cells as a positive invasion control. Each cell-matrix was cultured for 3 days and transferred to 60mm dishes containing a submerged grid for a further 3 days. Subsequently, media was removed to raise cells to the air liquid interface and rafts cultured for 8-10 days with medium changes every two days. Cell-matrixes were fixed in 10% buffered formalin (4°C overnight) and fixed in paraffin for FFPC sections.

RESULTS

14-3-3σ is expressed in differentiating keratinocytes of normal epidermis, *HK1.ras* hyperplasia and papillomas

To investigate the role[s] of *14-3-3σ* in carcinogenesis, expression was assessed initially in normal epidermis together with hyperplasia/papillomas produced by expression of activated ras^{Ha} in transit amplifying keratinocytes [*HK1.ras*] and the expression profile compared to that of p53 and p21 (**Fig. 1A-C**). Consistent with previous studies, normal murine epidermis expressed 14-3-3σ in supra-basal layers with occasional expression detected in proliferative basal-layer keratinocytes (**Fig. 1A)**. This profile is consistent with roles in keratinocyte spatial awareness (Hurd et al., 2003; Ling et al., 2010) and potentially a role in keratinocyte commitment to terminal differentiation as 14-3-3σ expression in occasional basal cells was similar to that of keratin K1 [see **Fig. 1B]**, an early marker of differentiation expressed as basal layer keratinocytes commit to differentiate (Yuspa et al., 1989), alongside normal interactions with p53 (MDM2-see below) and p21 expression as sporadic cells complete a given cell cycle [p53] or exit the proliferative niche (Dotto, 2000).

In pre-neoplastic hyperplasia produced by HK1.ras expression (Greenhalgh et al., 1993), a similar supra-basal *14-3-3σ* expression profile was observed, with occasional positive basal-layer keratinocytes consistent with the relatively normal differentiation pattern in *HK1.ras*-mediated hyperplasia [indicated by keratin1/14 expression] and again sporadic, low-level p53/p21 (**Fig. 1B).** This latter result indicates that at early stages of pre-neoplastic hyperplasia an epidermis appears relatively tolerant of excessive ras^{Ha} signalling in the absence of other neoplastic events (see below ras and ras Fos papers ras p10). However, whilst *HK1.ras* papillomas maintained this profile in terms of supra-basal *14-3*-3σ expression and ordered K1/K14 differentiation; with time more aggressive hyperplasia [not shown] and overt papillomas displayed elevated nuclear p53 and increasing levels of p21 expression (**Fig. 1C**). This apparent independence from *14-3*-3σ protective functions in papilloma basal layers e.g., 14-3-3σ-mediated MDM2 suppression (Lee and Lozano, 2006) may reflects the benign, regression prone nature of these tumours; as at this stage activated p-$MDM2^{166}$ and p-$AKT1^{473}$ expression are also confined to supra-basal layers (see **Figs 5** and **6** below), where presumably 14-3-3σ maintains the relatively normal interactive roles in differentiating keratinocytes.

HK1.fos-Δ5PTEN keratoacanthoma aetiology exhibits basal layer 14-3-3σ expression associated with elevated p53/p21 and accelerated differentiation

In contrast to hyperplasia and papillomas produced by *HK1.ras* expression, bi-genic expression of *HK1.fos* and inducible, inactivation of PTEN-mediated AKT regulation-(*K14.creP-Δ5PTEN*) initially produced a keratotic hyperplasia in RU486-treated *HK1.fos-Δ5PTEN* skin that evolved into keratoacanthomas KA (Yao et al., 2008) rather than malignant conversion. This was due to high expression of compensatory p53/p21, triggered in late-stage hyperplasia/early papilloma by achieving a threshold of AKT-associated GSK3β inactivation (i.e., deregulated,

increased β-catenin), that switched keratinocyte proliferation into an accelerated differentiation, resulting in the classic hyperkeratosis of KA (Ko, 2010) and preventing malignant conversion (Yao et al., 2008; Supplementary Fig. S3).

Analysis of *HK1.fos-Δ5PTEN* hyperplasia (**Fig. 2A** and **B**) showed increasing strands of basal layer keratinocytes exhibiting strong membranous/cytoplasmic 14-3-3σ expression together with increasing expression of p53 (but not p21 which appeared later (MacDonald et al., 2014); **Fig. 2A**); yet at this stage of low p21 activity, K1 expression remained relatively normal (**Fig. 2B**). As disease progressed into overt KA, two distinct histotypes appeared one of massive keratosis interspersed with fronds of keratinocytes that derived from an underlying proliferative form, often confused with wdSCC (Watanabe et al., 2015). Analysis of the frond-histotype found elevated levels of 14-3-3σ expression were retained throughout each epidermal compartment, and this expression was paralleled by strong p53 expression and now p21 also; the latter possibly combining with 14-3-3σ/fos to evoke the anomalous basal layer K1 expression observed in these frond regions (**Fig. 2C**) indicative of an accelerated differentiation.

However, the underlying highly proliferative, wdSCC-like histotypes exhibited reduced 14-3-3σ expression (**Fig. 2C:** green/frond vs yellow/wdSCC-like); with a distinct reduction of 14-3-3σ in basal-layer keratinocytes. Previously, such areas were associated with low levels of both p53 and p21 and were positive for activated AKT expression until the p53/p21 expression induced a basal-to-supra-basal transition of p-AKT^{473} and massive differentiation (Yao et al., 2008). These data now suggest that the trigger for such p53/p21 expression in response to excessive AKT/βcatenin may also involve 14-3-3σ expression to sequester roles in keratinocyte commitment to differentiate and avoid malignant conversion/progression.

HK1.ras/fos-Δ5PTEN **carcinogenesis shows 14-3-3σ expression paralleled by immediate p53/p21 in hyperplasia/papilloma, persists with p21 to limit malignant progression following p53 loss.**

Co-operation between *HK1.ras/fos* and the loss of PTEN-mediated AKT regulation resulted in a rapid papillomatogenesis but malignant conversion required spontaneous p53 loss and further progression initially stalled at a well-differentiated SCC histotype due to persistent p21 (MacDonald et al., 2014). Analysis of late-stage hyperplasia/early papilloma found that *HK1.ras/fos-Δ5PTEN*^{flx} epidermis exhibited high levels of 14-3-3σ in all epidermal layers; with the strongest expression in basal and granular layers, giving an apparent hiatus of protein in the acanthotic layers (**Fig. 3A**). Unlike *HK1.ras* papillomas or *HK1.fos-Δ5PTEN* KAs here the 14-3-3σ expression profile was paralleled by an immediate response of high level p53/p21 expression and strong, supra-basal K1 expression indicating benign papilloma (**Fig. 3A**); with p21 expression mirroring the 14-3-3σ expression profile in acanthotic layers (compare **Fig. 3A** SFN vs p21 IHC). With time, *HK1.ras/fos-Δ5PTEN*^{flx} tumours progressed to wdSCC and as papillomas converted this was associated with p53 loss (**Fig. 3B**). However, analysis of

serial sections as papillomas converted shows that expression of both 14-3-3σ and p21 persisted in areas of p53-negative carcinoma *in situ* (**Fig. 3B**). Higher magnification of these areas suggested that 14-3-3σ expression diminished in the wdSCC basal layers, whereas p21 expression persisted (**Fig. 3B**; MacDonald et al., 2014). This result was confirmed by IF analysis of older, uniform wdSCC (**Fig. 3C**) where persistent 14-3-3σ expression weakened [green to yellow] in basal layers becoming reduced/lost in areas of aggressive, invasive SCC-concomitant with p21 (Macdonald et al., 2014) loss and p-AKT1 activation [see below].

Rapid tumour progression in TPA-treated *HK1.ras-Δ5PTEN* carcinogenesis is associated with early loss of 14-3-3σ, p53 and p21 expression in hyperplasia and papillomas.

The lack of papilloma progression in earlier *HK1.ras-Δ5PTEN* studies (Yao et al., 2006), associated with compensatory p53/p21 (MacDonald et al., 2014) and now consistent with 14-3-3σ expression (**Fig. 1** above) had prompted TPA promotion experiments which resulted in a (very) rapid progression to poorly-differentiated SCC (Yao et al., 2006). Analysis of serial sections from these archival tumours found that all pdSCCs exhibited loss of 14-3-3σ expression (**Fig. 4A**). The lower magnification composite micrograph (**Fig. 4A**) shows this loss in a typical pdSCC (virtually devoid of K1 expression) and fortuitously possessed a strand of untreated hyperplastic skin, where basal-layer 14-3-3σ expression appears quite high; suggesting an initial suppressive response was deployed to loss of PTEN and ras^{Ha} activation – hence, contributing to their lack of progression. If so, this response was short lived, as analysis of serial sections of TPA-promoted *HK1.ras-Δ5PTEN*^{flx} papilloma/SCC shows loss of 14-3-3σ expression parallels loss of p53 and p21; even in areas of K1-positive papilloma (**Fig. 4B**); whilst the earliest biopsies of TPA-promoted *HK1.ras-Δ5PTEN*^{flx} hyperplasia were already devoid of 14-3-3σ, p53 and mostly p21 (**Fig. 4C**). These results collectively highlight the protective nature of these three TSGs where early loss leads to rapid papillomatogenesis, malignant conversion and swift malignant progression to aggressive pdSCC.

Tumour progression/inhibition in *HK1.ras/fos-Δ5PTEN* genotypes shows 14-3-3σ antagonism with activated p-MDM2^{166} expression.

Given the close interactions between *14-3-3σ* and MDM2 expression in the regulation of p53 via ubiquitin removal (Lee and Lozano, 2006), activated p-MDM2^{166} status was compared to 14-3-3σ/p53 expression in stage-specific tumour aetiology (**Fig. 5**). In normal epidermis activated p-MDM2^{166} expression paralleled that of both p53 and 14-3-3σ being mainly supra-basal with occasional positive basal keratinocytes (**Fig. 5A**); a profile consistent with the regulatory loop between *14-3-3σ* and induction of MDM2 to remove p53 whose apoptotic functions are a danger to the paramount barrier function of the epidermis (Haupt et al., 2003; Baroni et al., 2012). Similarly, in overt *HK1.ras* papillomas this regulatory loop is maintained in supra-basal layers (**Fig. 5B** and **C**), but less so in basal layers and is often absent in many strands of basal layer keratinocytes in these benign regression prone papillomas (**Fig. 5C**).

Hence, this lower p-MDM2^{166} activity facilitates the strong compensatory expression of nuclear p53.

However, in *HK1.ras/fos-Δ5PTEN^{flx}* wdSCCs, elevated p-MDM2^{166} expression now appears in basal layer keratinocytes, and this supra-basal-to-basal transition in MDM2 expression was paralleled by a reverse basal-to-supra-basal change in *14-3-3σ* expression levels. Thus, reduced *14-3-3σ* expression in the basal layers and increased p-MDM2^{166} activity would reduce the levels of protective p53 expression (**Fig. 5C**) and once lost a susceptibility to malignant conversion/progression. Oddly in more aggressive *HK1.ras/fos-Δ5PTEN^{flx}* SCC where 14-3-3σ expression is actually lost, resultant p-MDM2^{166} expression in the invasive basal keratinocytes results in only occasional p53-positive cells in residual keratotic areas (**Fig. 5C**).

Tumour progression highlights a cooperative 14-3-3σ/p21 antagonism against activated p-AKT^{473} expression.

A similar situation arose in analysis of p-AKT1^{473} activation and 14-3-3σ expression in *HK1.ras/fos-Δ5PTEN^{flx}* SCC and *HK1.ras-Δ5PTEN^{flx}* pdSCC aetiology **(Fig. 6)**-however this involved p21 rather than p53 and indicated a strong synergism between 14-3-3σ and p21 in this model as suggested by their expression profiles in tri-genic *HK1.ras/fos-Δ5PTEN^{flx}* papillomas (**Fig. 3A**) geared to limit malignant progression. An initial surprising result given the loss of PTEN-mediated AKT regulation came from analysis of p-AKT1^{473} and 14-3-3σ/p21 expression in *HK1.ras/fos-Δ5PTEN^{flx}* hyperplasia/papilloma where activated p-AKT1^{473} expression was virtually absent in the presence of strong 14-3-3σ/p21 co-expression (**Fig. 6A**). However, following malignant conversion, early *HK1.ras/fos-Δ5PTEN^{flx}* wdSCCs exhibited increasing p-AKT1^{473} levels but expression was confined to supra-basal layers; a result consistent with the presence of continued basal-layer 14-3-3σ/p21 co-expression in proliferating cells (**Fig. 6B**), that echoes the basal-to-supra-basal eviction of p-AKT expression in *HK1.fos-Δ5PTEN^{flx}* KAs outlined above (Yao et al., 2008). With time, as aggressive *HK1.ras/fos-Δ5PTEN^{flx}* SCCs exhibited reduced 14-3-3σ expression in basal layers (**Fig. 3C**; above) and this was followed by reduced p21 expression and when both were lost, invasive keratinocytes exhibited uniform p-AKT1^{473} activities throughout the tumour (**Fig. 6C**). Similarly, in TPA-promoted *HK1.ras-Δ5PTEN^{flx}* pdSCC aetiology the early loss of 14-3-3σ/p21 **(Fig. 4**; above) led to very high levels of p-AKT1^{473} expression such that it masked the K14 counterstain (**Fig. 6D**). Indeed, based on these data the specific interactions between AKT/mTOR/MDM2 and p21/p53/Stratifin in malignant conversion/progression are currently under further investigation [manuscript in preparation].

***In vitro* analysis shows 14-3-3σ expression in normal and benign keratinocytes persists in malignant SCC cells grown in 2D-culture but not invading 3D-cells.**

To compare these *in vivo* findings to analysis of cells in culture (**Fig. 7**), 14-3-3σ expression was assessed in normal HaCaT keratinocytes (Boukamp et al., 1988) together with ras^{Ha}-transformed SP1 papilloma cells, established from DMBA/TPA papillomas (Strickland et al., 1988) that give rise to papillomas in nude mouse graft assays; and their derivatives, T52 cells, transformed by introduction of activated Fos (*HVV-fos;* Curran et al., 1982)

which produce carcinomas in graft assays (Greenhalgh & Yuspa, 1988). In each case $SP1^{ras61}$ and $T52^{ras61/HVVfos}$ SCC were selected for resistance to calcium induced differentiation; where SP1 adopts a slow growth phenotype, with a flattened morphology consistent with an apparent stalled attempt to differentiate, whereas $T52^{ras61/HVVfos}$ SCC were completely indifferent to calcium levels.

In 2D cultures, strong membranous/cytoplasmic 14-3-3σ expression appeared in normal immortalised HaCaT and $SP1^{ras61}$ papilloma keratinocytes cultured in Low Calcium (0.05mM Ca^{2+}) media giving a halo appearance to the IF expression analysis (upper panel; **Fig. 7**). Surprisingly 14-3-3σ expression was also observed in malignant $T52^{ras61/v\text{-}fos}$ keratinocytes; again, giving a similar halo appearance to the "cobblestone" cells, but to a lesser extent. When challenged to differentiate in high calcium media (> 0.12mM Ca^{2+}) the more flattened $SP1^{ras61}$ keratinocytes expressed high levels of 14-3-3σ expression but in distinct cellular areas. $T52^{ras61/v\text{-}fos}$ keratinocytes also exhibited a similar, spatially aware 14-3-3σ expression, but to a much lesser extent. In comparison to p53 expression was found to be high and strongly nuclear in HaCaT cells, as reported previously, whereas in Low Cal only sporadic $SP1^{ras61}$ cells expressed low level cytoplasmic p53, although numbers increase in Hi Cal media. Oddly, most malignant $T52^{ras61/v\text{-}fos}$ cells expressed p53 but this was assumed to be a $p53^{175}$ GOF mutant which may explain persistent 14-3-3σ expression given that p53 directly binds the 14-3-3σ promoter to induce expression (Lee & Lozano, 2006).

In 3D organotypic culture HaCaT cells produce a relatively normal skin on organotypic rafts (lower panel; **Fig. 7** H & E) and maintains membranous 14-3-3σ expression in both basal and supra-basal keratinocytes. SP1 cells attempt to create an overt papilloma, which is easily lost in sample processing and where present gave very poor sections susceptible to loss of section in IF/IHC analysis. Indeed, this collagen-based rafting protocol (Timpson et al., 2011) appeared less that optimum for all murine cells assessed compared to human counterparts, e.g., HaCaT or the c8161 human melanoma line employed as a positive invasion control (Welch et al., 1991). Nonetheless the invasive nature of T52 SCC cells essentially nailed the epidermis to the underlying collagen raft to survive processing and exhibited 14-3-3σ expression in only sporadic epidermal cells; with no expression in the migrating invasive cells in either IF or IHC analysis; whilst the invasion control c18161 melanoma cells were completely negative for 14-3-3σ expression. These data again highlight 14-3-3σ roles in spatial awareness and whilst the TSG functions appear to be lost in progression/invasion, in certain malignant contexts, 14-3-3σ expression is still observed and may act to influence tumour outcome.

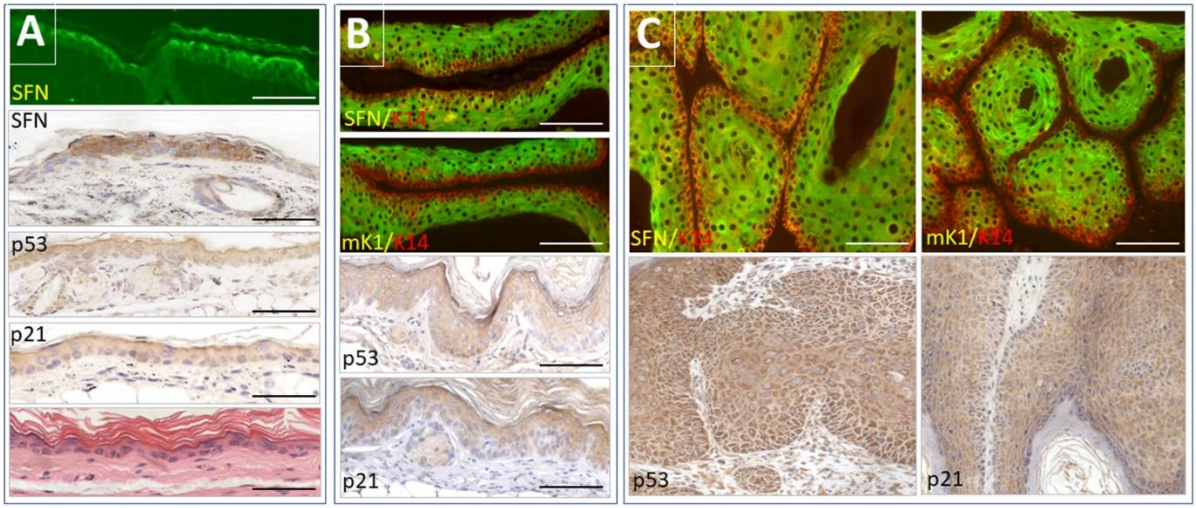

Figure 1. 14-3-3σ, p53 and p21 expression in normal epidermis and pre-malignant phenotypes. **A**, Normal epidermis: single-label immunofluorescence (IF) and immunohistochemical (IHC) analysis show 14-3-3σ expression in supra-basal layers with occasional basal-layer keratinocytes**.** IHC analysis of p53 and p21 show low numbers of sporadic, p53/p21-positive keratinocytes. Bottom panel: histology of normal epidermis. **B**, *HK1.ras* hyperplasia: double-label IF displays supra-basal 14-3-3σ expression (SFN green), with few positive (yellow) basal-layer keratinocytes; K14 counterstain (red) indicates basal layer; serial section stained for keratin K1 (green) and K14 (red) indicates a relatively normal differentiation pattern**.** IHC analysis of p53/p21 shows sporadic, low-level expression. **C,** *HK1.ras* papilloma: 14-3-3σ shows supra-basal expression with occasional positive basal-layer keratinocytes and supra-basal K1 expression indicates benign tumour with expansion of $K14^{+ve}$ basal layers**.** IHC analysis now shows elevated/nuclear p53 and (lesser) p21 expression in basal layer keratinocytes. (Note: p53/p21 analysis employed Abcam ab131442 and Proteintech #10355-1-AP. Discontinued Santa Cruz p53 sc#393 & p21 sc#397 gave identical results; see Supplementary **Figs. S1** and **S2A** and **B** for histological analysis). Bars (**A**) *approx.25-30µm*; (**B**) *approx.75µm*; (**C**). SFN/K14 & K1/K14 *approx.50µm;* p53 *approx.75µm;* p21 *approx. 100µm.*

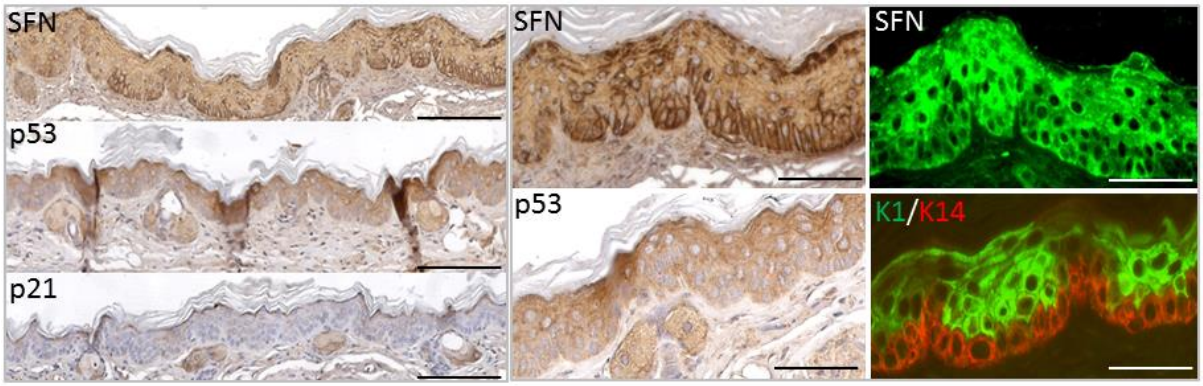

Figure 2. 14-3-3σ, p53 and p21 expression in *HK1.fos-Δ5PTEN*^{flx} keratoacanthoma aetiology. **A,** Composite micrographs of *HK1.fos/*Δ*5PTEN* hyperplasia show strands of elevated basal layer 14-3-3σ expression; whist p53 shows higher (cytoplasmic) expression and p21 is expressed at low/undetectable levels. **B,** At higher magnification, IHC/IF analysis show strong cytoplasmic/membranous 14-3-3σ expression in basal layer strands; yet K1/K14 expression remains relatively normal. p53 analysis shows elevated mainly cytoplasmic expression (Abcam ab 131442). **C**, Overt *HK1.fos/*Δ*5PTEN*^{flx} keratoacanthoma shows that highly differentiated areas (left panel) retain basal-layer 14-3-3σ expression which parallels elevated nuclear p53/p21 expression (p53: Abcam ab 131333) and anomalous basal-layer K1 expression; however less differentiated KA regions (right panel) exhibited weaker, supra-basal 14-3-3σ similar to wdSCC (see Supplementary **Figs. S1** and **S2E** for histological analysis). Bars (**A**) *approx. 120-150µm;* (**B**) *approx.75µm*; K1/K14 *approx.50µm;* (**C**) *approx.75µm;* p21 *approx. 100µm;* K1/K14 *approx.150µm.*

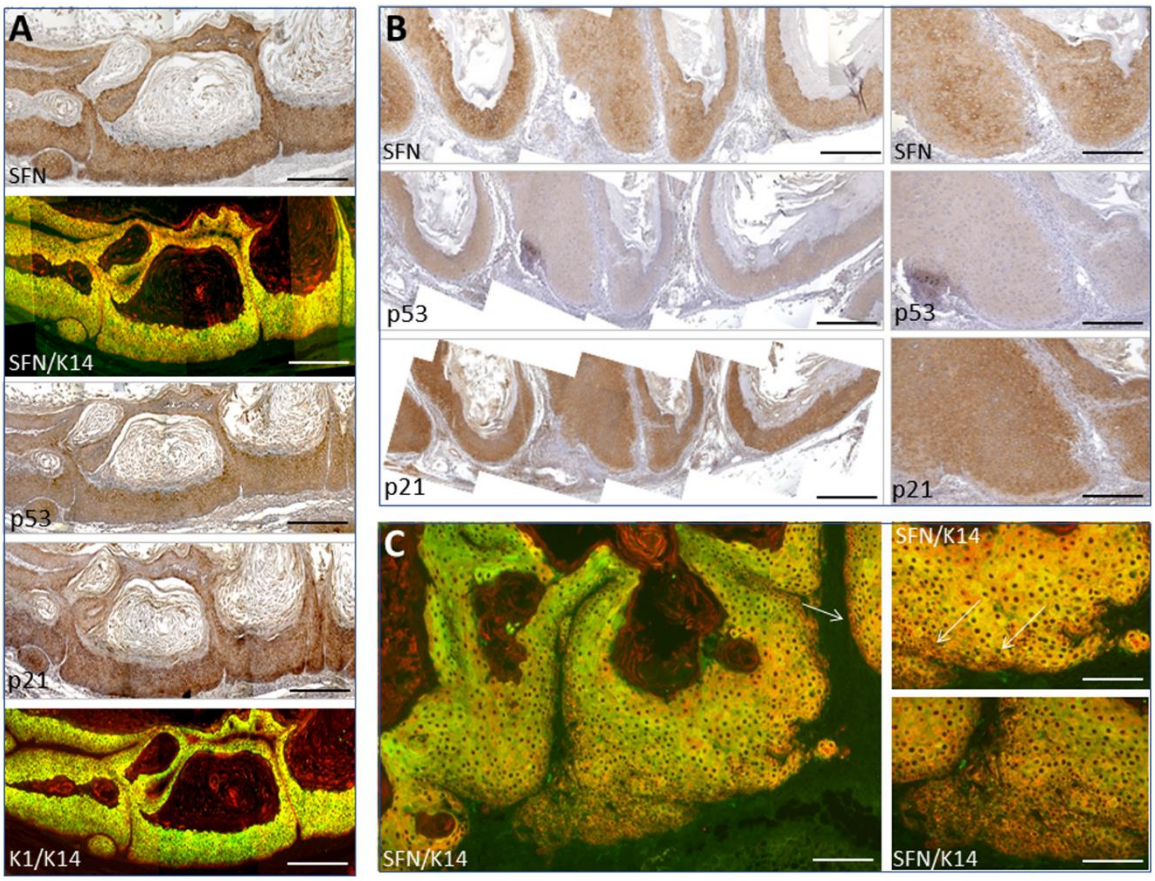

Figure 3. 14-3-3σ, p53 and p21 expression in *HK1.ras/fos-Δ5PTEN^{flx}* SCC aetiology. **A**, IHC/IF analysis of tri-genic *HK1.ras/fos-Δ5PTEN^{flx}* mice show that late-stage hyperplasia/early papilloma exhibits strong basal and upper supra-basal layer 14-3-3σ expression; with a hiatus in the intermediate, acanthotic layers. Strong p53 is also observed in all layers; whilst basal p21 expression paralleled 14-3-3σ with a hiatus in the acanthotic layers. Strong, supra-basal K1 expression indicates benign tumour. **B,** Composite micrographs of *HK1.ras/fos-Δ5PTEN^{flx}* papilloma conversion to wdSCC shows strong 14-3-3σ and p21 co-expression, whereas p53 expression is already lost in the papilloma/wdSCC area. Higher magnification of wdSCC area shows persistent 14-3-3σ expression begins to diminish in basal layers, whereas p21 expression persists. **C**, *HK1.ras/fos-Δ5PTEN^{flx}* wdSCC shows persistent 14-3-3σ expression weakens in basal layers (arrows) becoming reduced/lost in invasive SCC (see Supplementary **Figs. S2C** for histological analysis). Bars (**A**) *approx. 120-150µm;* (**B**) *approx.150µm. & 100µm*; K1/K14 *50µm;* (**C**) *approx.100µm & 75µm.*

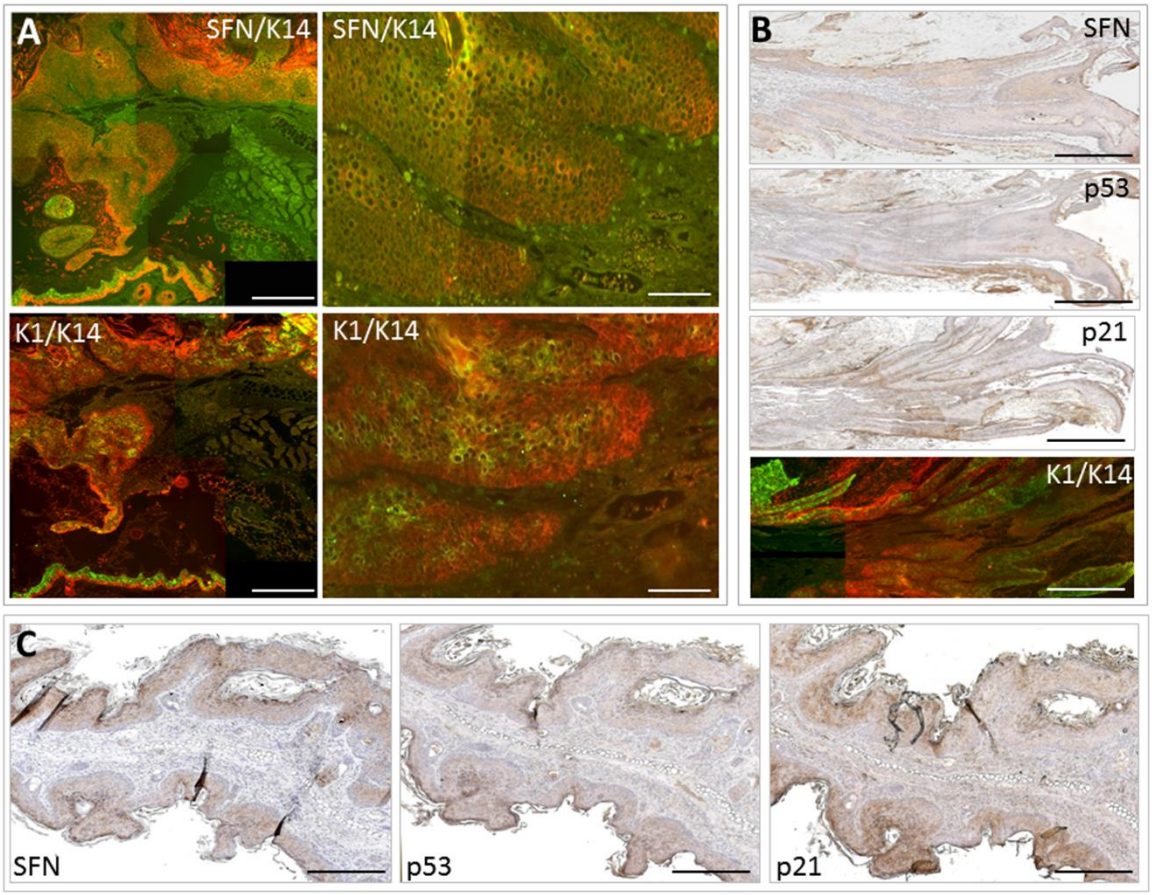

Figure 4. 14-3-3σ, p53 and p21 expression in TPA-promoted poorly-differentiated SCC aetiology. **A**, Serial sections of TPA-promoted *HK1.ras-Δ5PTEN*^{flx} carcinogenesis show loss of 14-3-3σ expression alongside sporadic K1; indicating aggressive, poorly-differentiated SCC compared to epidermal hyperplasia (bottom left). **B,** IHC analysis of TPA-promoted *HK1.ras-Δ5PTEN*^{flx} papilloma/wdSCC shows loss of 14-3-3σ expression parallels loss of both p53 and p21; even in areas of K1-positive papilloma. **C**, TPA-promoted *HK1.ras-Δ5PTEN*^{flx} hyperplasia already shows reduced/lost 14-3-3σ expression paralleled reduced p21 and loss of p53 (see Supplementary **Figs. S2D** for histological analysis. Bars (**A**) *approx. 120-150μm & 50μm;* (**B**) *approx.150μm;* (**C**) *approx.100μm.*

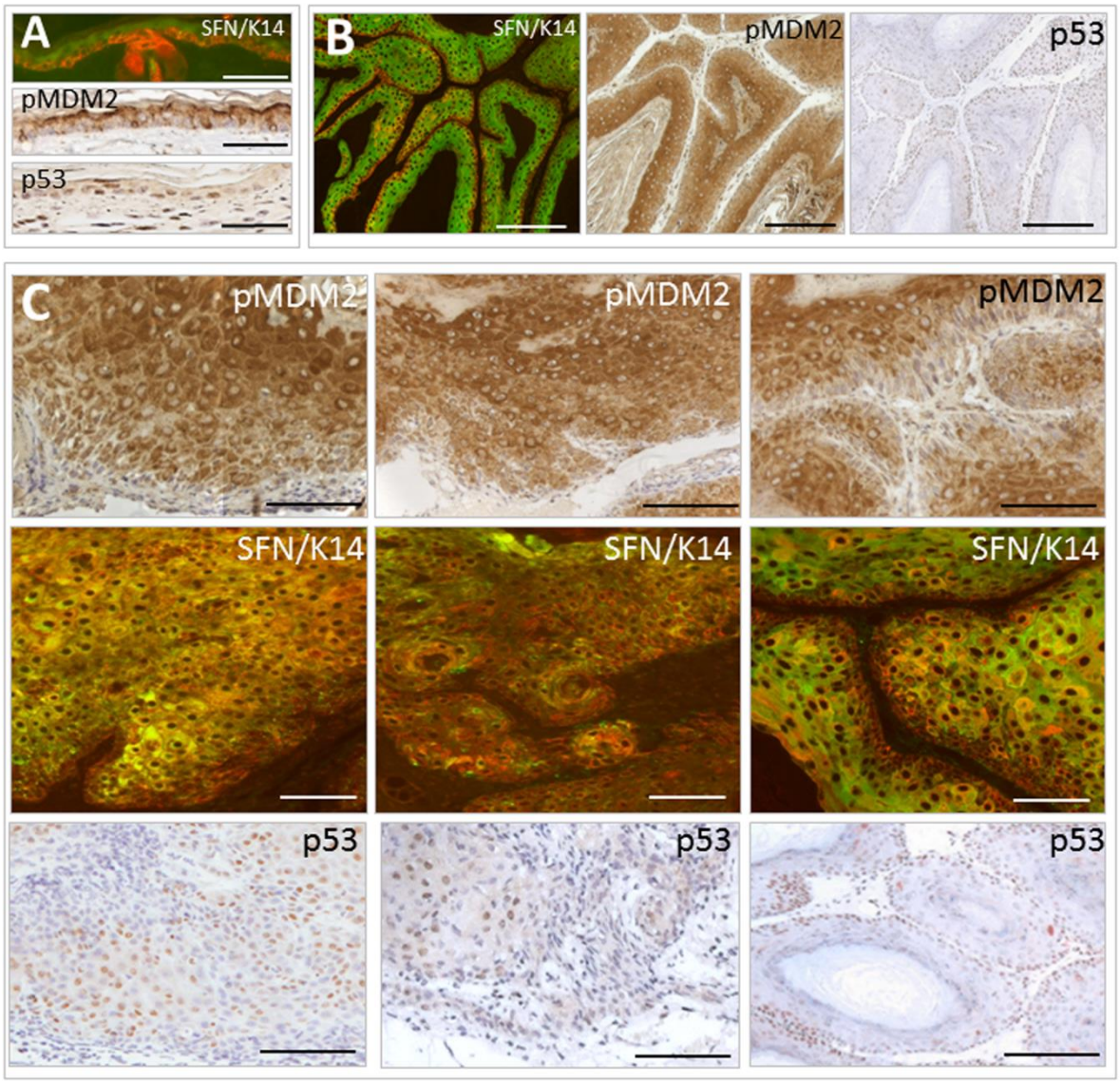

Figure 5. Comparison of p-MDM2[166] and 14-3-3σ/p53 expression in *HK1.ras/fos-Δ5PTEN^{flx}* SCC aetiology. **A**, Normal epidermis shows supra-basal 14-3-3σ parallels activated p-MDM2[166] expression, with occasional sporadic positive basal layer keratinocytes also positive for p53 expression. **B**, Serial sections from *HK1.ras* papillomas show supra-basal 14-3-3σ parallels supra-basal p-MDM2[166] expression; with nuclear p53 appearing in basal layer keratinocytes. **C**, Left: Serial sections from *HK1.ras/fos-Δ5PTEN^{flx}* wdSCCs show elevated basal layer p-MDM2[166] expression, whilst 14-3-3σ remains essentially supra-basal and p53 becomes sporadic/lost; Middle: serial sections from aggressive *HK1.ras/fos-Δ5PTEN^{flx}* SCC/pdSCC shows strong p-MDM2[166] expression in the invasive basal keratinocytes whilst 14-3-3σ reduces further, becoming sporadic alongside occasional p53-positive cells. Right: For comparison *HK1.ras* papilloma exhibits supra-basal 14-3-3σ/p-MDM2[166] expression, with nuclear p53-positive basal-layer keratinocytes. *NB:* p53 analysis employed Abcam ab 131333 (Supplementary **Fig. S1**). Bars (**A**) *approx.25-30µm*; (**B**) *approx.85-100µm*; (**C**) wdSCC and pdSCC *approx.50µm.*

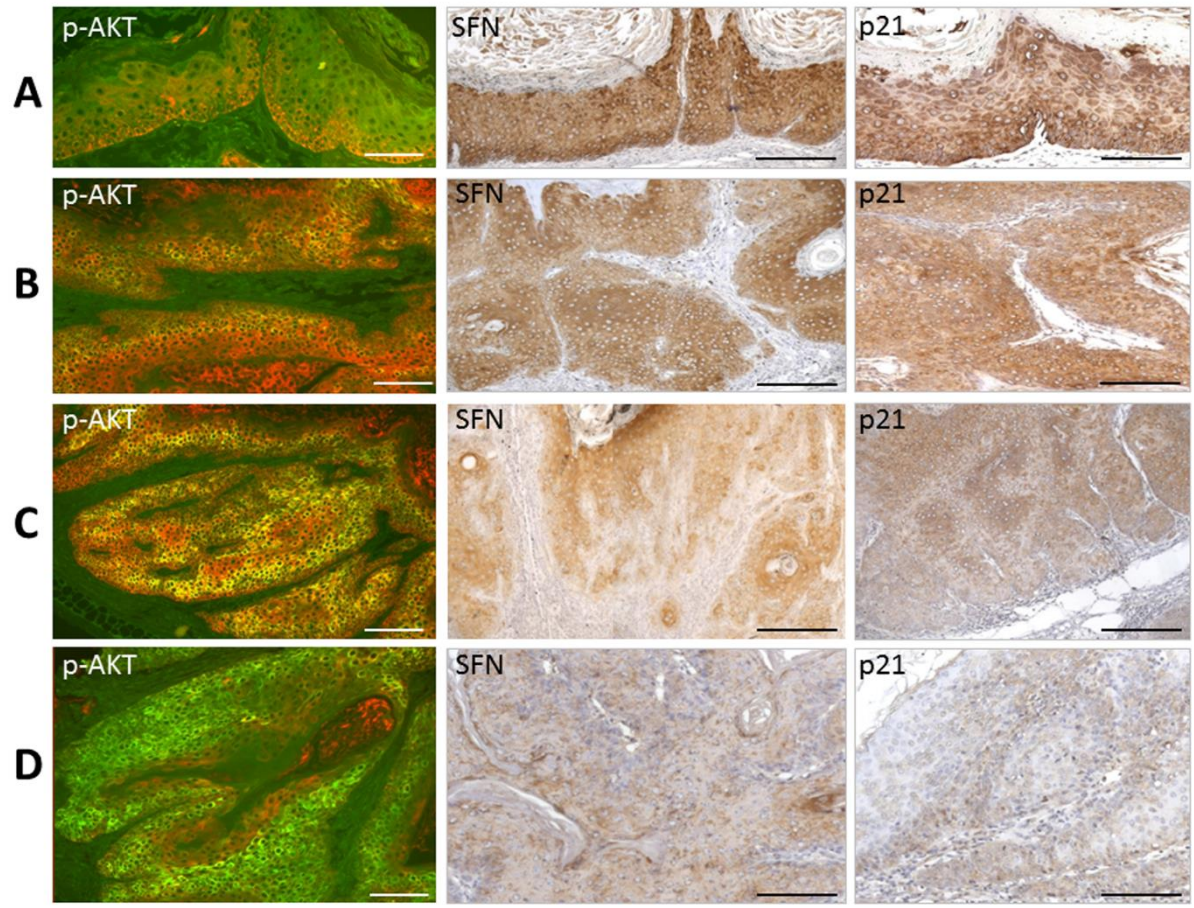

Figure 6. Comparison of p-AKT1^{473} and 14-3-3σ/p21 expression in *HK1.ras/fos-Δ5PTEN^{flx}* and TPA-promoted SCC aetiology. **A,** *HK1.ras/fos-Δ5PTEN^{flx}* hyperplasia (paradoxically) lacks p-AKT1^{473} expression in the presence of strong basal layer 14-3-3σ/p21 co-expression. **B**, Early well-differentiated *HK1.ras/fos-Δ5PTEN^{flx}* SCCs exhibit increasing p-AKT1^{473} expression confined to supra-basal layers in the presence of continued basal-layer 14-3-3σ/p21 co-expression in proliferating cells. **C**, Aggressive *HK1.ras/fos-Δ5PTEN^{flx}* SCC exhibit increasing uniform p-AKT1^{473} expression profile in basal layers paralleled by reduction of 14-3-3σ/p21 expression in the invasive keratinocytes. **D**, TPA-promoted *HK1.ras-Δ5PTEN^{flx}* pdSCC aetiology exhibits very high levels of uniform p-AKT1^{473} expression that masks the K14 counterstain; paralleled by loss of both 14-3-3σ and p21 expression. Bars *approx.85-100µm.*

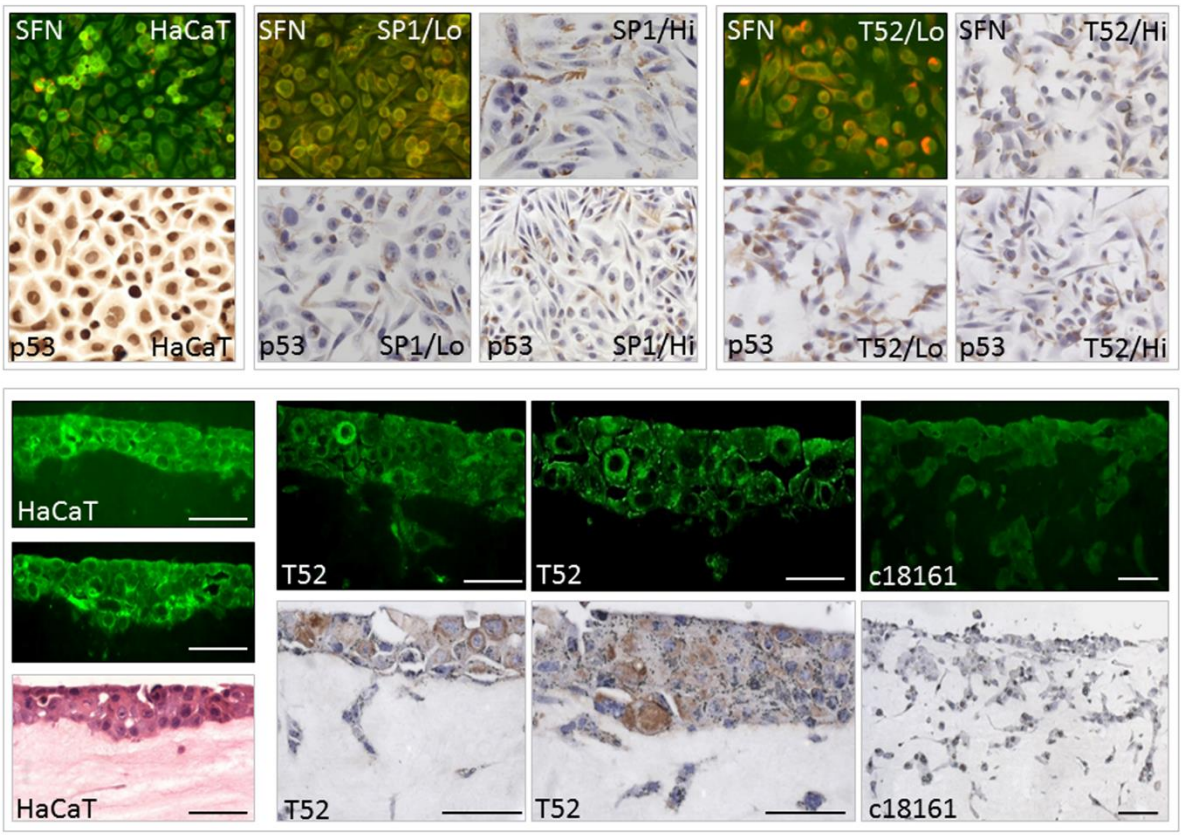

Figure 7: *In vitro* analysis of 14-3-3σ expression in normal, papilloma and malignant cells. *Upper panel*: Normal, immortalised HaCaT keratinocytes express membranous 14-3-3σ/SFN and high levels of nuclear p53 in all cells. Benign SP1 papilloma cells express membranous 14-3-3σ/SFN in proliferative low Ca^{2+} media with a spatially-localised cytoplasmic expression when (partially) differentiating in high Ca^{2+} media. In proliferative and differentiating, media SP1 cells exhibit sporadic, low levels of cytoplasmic p53. Malignant T52 SCC cells express lower levels of membranous 14-3-3σ/SFN in proliferative low Ca^{2+} media; and being resistant to Ca^{2+}-induced differentiation, again exhibit a distinct cytoplasmic localisation in high Ca^{2+} media. In proliferative and differentiating media, T52 cells exhibit cytoplasmic/nuclear levels of (mutant) p53 (Supplementary **S3** for cell morphology).
Lower panel: 14-3-3σ expression in tumour invasion assays. HaCaT cells produce a relatively normal skin on organotypic rafts, with membranous 14-3-3σ expression in both basal and supra-basal keratinocytes. T52 SCC cells exhibit weaker expression overall, except in sporadic cells; however, both IF and IHC analysis show that migrating invasive T52 cells are negative for 14-3-3σ expression. Similarly, c18161 melanoma cells employed as an invasive control are negative for 14-3-3σ expression. Bars *approx.30-40µm*

SUPPLEMENTAL DATA

Table 1 PCR primers and reaction conditions

Transgene	Primer Pair
HK1.ras	5'-GGATCCGATGACAGAATACAAGC-3' 5'-ATCGATCAGGACAGCACACTTGC-3'
HK1.fos	5'-GGATCCATGATGTTCTCGGGTTT-3' 5'-CGATTATTGCCACCCTGCCATG-3'
$PTEN^{WT/FLX}$	5'-ACTCAAGGCAGGGATGAGC-3' 5'-GTCATCTTCACTTAGCCATTGG-3'
Δ5PTEN	5'-ACTCAAGGCAGGGATGAGC-3' 5'-GGTTGATATCGAATTCCTGCAGC-3'
K14.CrePR1	5'-CGGTCGATGCAACGAGTGAT-3' 5'-CCACCGTCAGTACGTGAGAT-3'

Transgene	Initial denaturation	Denaturation	Annealing	Extension	Cycles	Final extension
HK1.ras	5 m; 95°C	30 s; 95°C	60 s; 56°C	60 s; 72°C	35	10 m; 72°C
HK1.fos	2 m; 95°C	30 s; 95°C	30 s; 62°C	60 s; 72°C	35	10 m; 72°C
Pten/Δ5Pten	2 m; 94°C	30 s; 94°C	60 s; 63°C	90 s; 72°C	36	10 m; 72°C
K14.CrePR1	5 m; 94°C	30 s; 94°C	45 s; 58°C	60 s; 72°C	35	10 m; 72°C

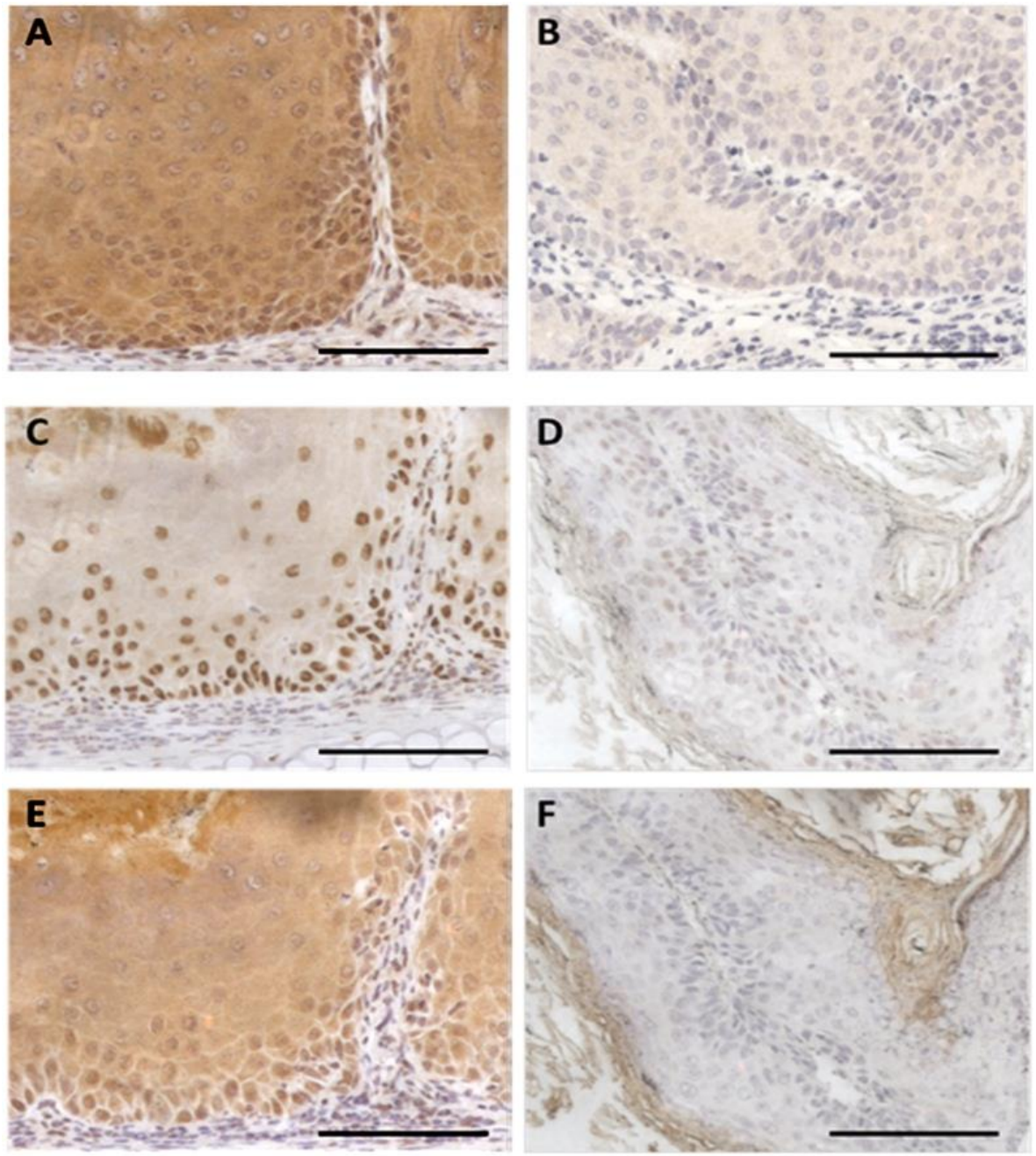

Figure S1: Immunohistochemical analysis of p53 levels: Comparison of Abcam to discontinued Santa Cruz antibodies.

*HK1.fos/*Δ*5PTEN* keratoacanthoma was employed as a p53 positive control: [A] Santa Cruz FL-393; [C] abcam ab31333; [E] abcam ab131442. All three antibodies show positive staining in basal layer nuclei, with ab31333 displaying the strongest nuclear staining and lowest levels of cytoplasmic or background staining. Negative control *HK1.ras/*Δ*5PTEN* TPA-promoted SCC: [B] Santa Cruz FL-393; [D] abcam ab31333; [F] abcam ab131442. No antibody detected p53. *Scale bars approx.50-75 µm.*

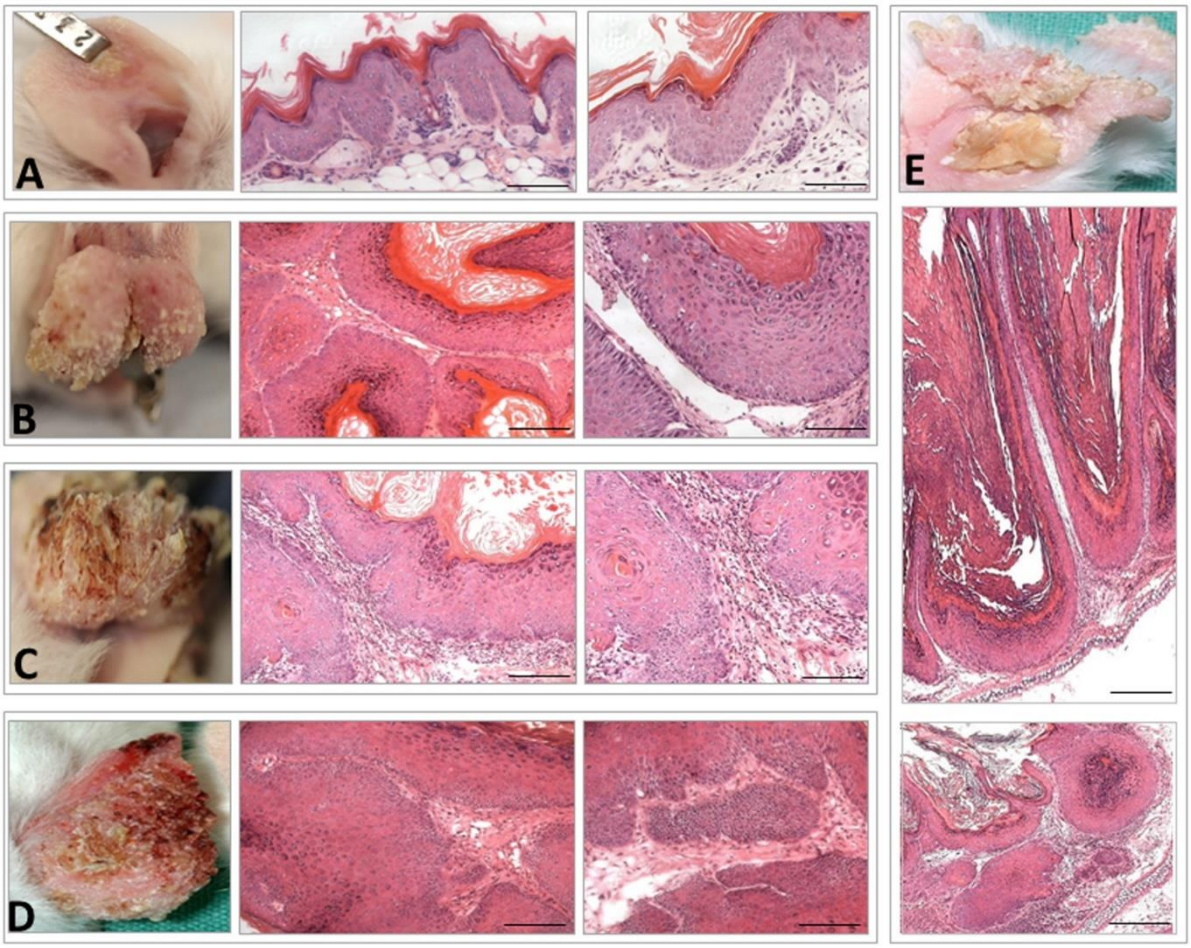

Figure S2: *HK1.ras/fos-Δ5PTEN^{flx}* tumour phenotypes and histotypes. **A,** Typical thickened ear and beginnings of mild, wound promoted keratosis produced in *HK1.fos* mice. Typical hyperplasia shown is exhibited by *HK1.ras/fos* (left) and *HK1.fos.Δ5PTEN^{flx}* (right is serial section from **Fig. 2B**) epidermis. **B,** Typical wound-promoted ear tag papilloma and benign papilloma histotypes exhibited by *HK1.ras* mice. **C,** Typical overt appearance of *HK1.ras/fos-Δ5PTEN^{flx}* wdSCCs with early and later examples of wdSCC histotypes. **D,** Typical overt appearance of aggressive rapid growing TPA-promoted *HK1.rasΔ5PTEN^{flx}* SCCs increased vascularisation and less overt keratosis. Histotypes show examples of an early SCC and later, highly invasive pdSCC**.** **E,** Typical overt appearance of *HK1.fos-Δ5PTEN^{flx}* KA with classic keratotic columns. KA histotypes comprise a convoluted mix of keratosis interspersed with fronds of growing keratinocytes with a very confused differentiation patten; the second histotype often underlying these frond regions resembles wdSCC.

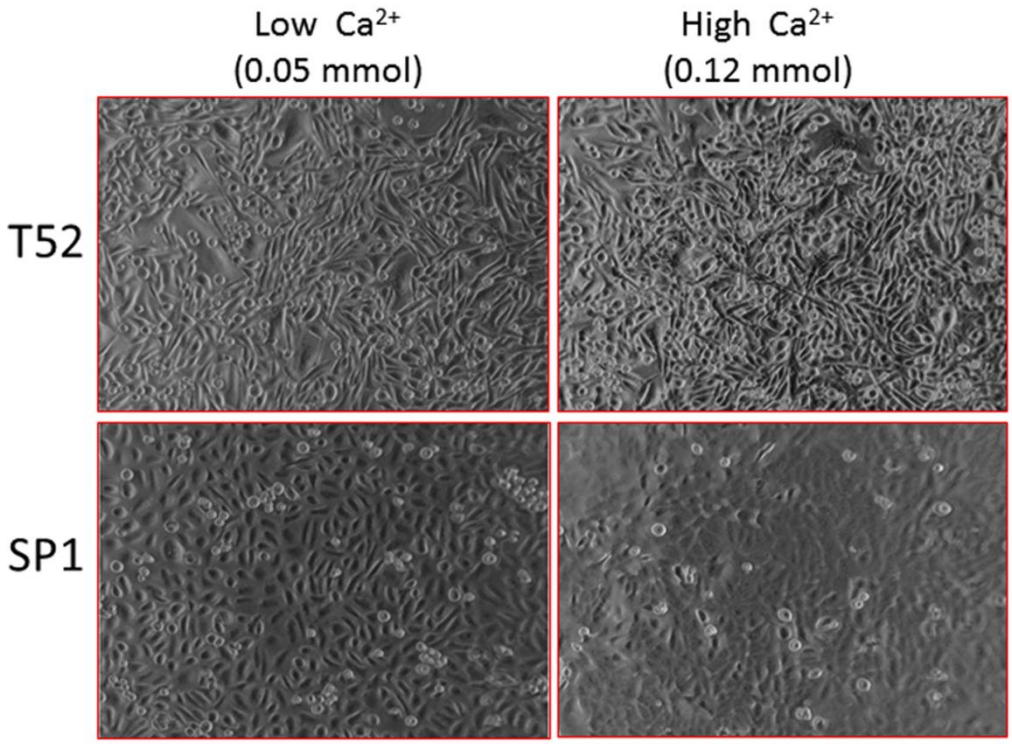

Figure S3: Cell morphology of benign SP1 papilloma and malignant T52 cells cultured in low and High Ca^{2+} media. In proliferative low Ca^{2+} media SP1 papilloma cells have a very similar morphology to that of normal keratinocytes, with an ordered cobblestone morphology. When induced to differentiate by increasing the calcium concentration, SP1 cells partially differentiate, adopting an intermediate morphology similar to that of supra-basal keratinocytes but without progressing to stratified phenotype. In contrast, malignant T52 SCC cells possess a transformed spindle shape and no contact inhibition, becoming overgrown in either Low or Hi Ca^{2+} conditions.

References specific to manuscript:

Boukamp P, Petrussevska RT, Breitkreutz D, Hornung J, Markham A & Fusenig NE. Normal keratinization in a spontaneously immortalised aneuploid human keratinocyte cell line. *J Cell Biol* 1988; **106**: 761-771

Dotto GP. p21(WAF1/Cip1): more than break to the cell cycle? *Biochim Biophys Acta* 2000; **1471**(1): M43-56.

Welch R, Bisi JE, Miller BE, Conaway D, Seftor EA, Yohem KH, Gilmore LB, Seftor RE, Nakajima M & Hendrix MJ. Characterization of a highly invasive and spontaneously metastatic human malignant melanoma cell line. *Int J Cancer* 1991; **47**(2): 227-237.

Appendix 2: Supplementary Figures

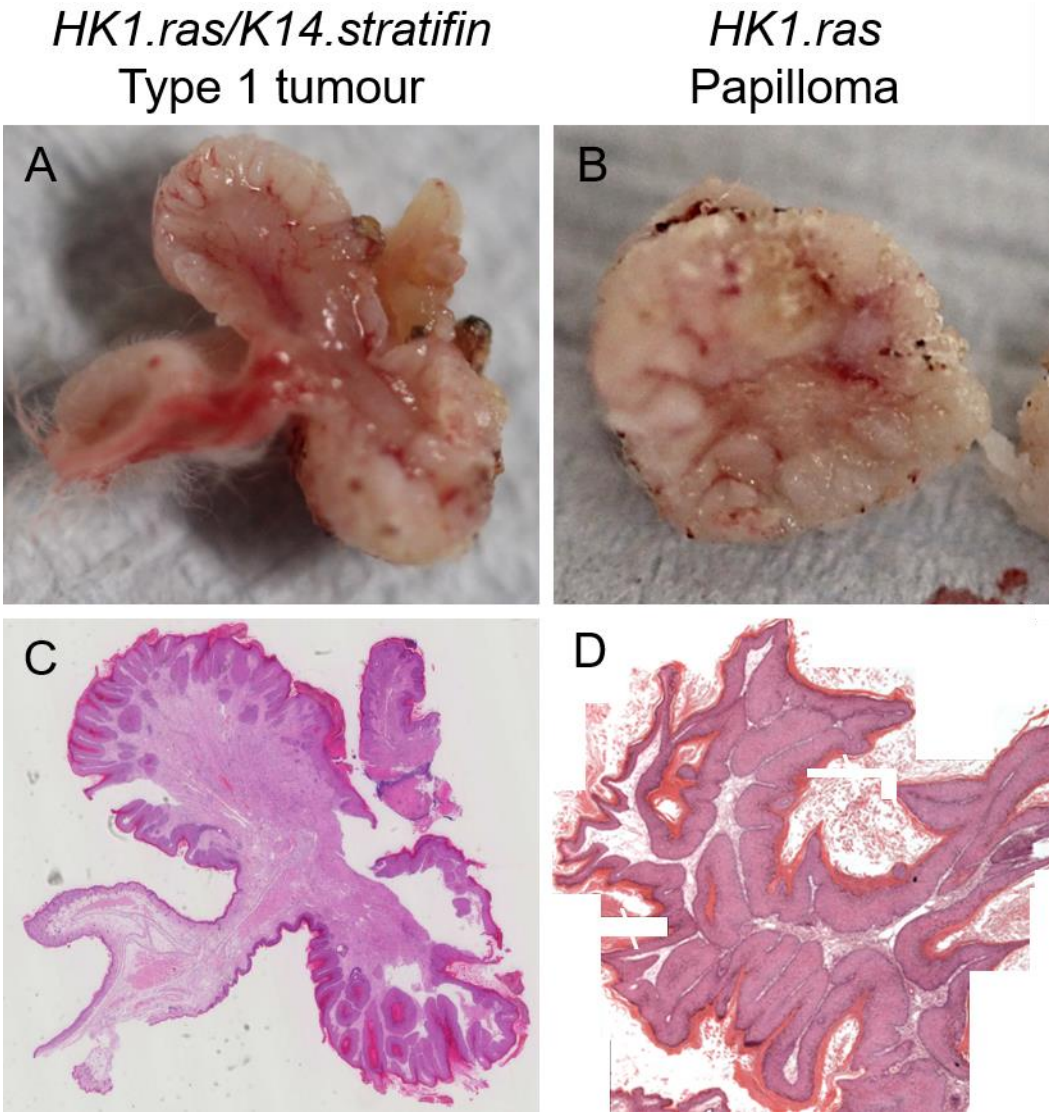

Figure S-1: Gross appearance of *HK1.ras/K14.stratifin* tumour cross-section.
High stromal content of *HK1.ras/K14.stratifin* Type 1 tumours appears grossly as a glassy pink region surrounded by the duller, paler epidermal layer (**A**), confirmed by histology (**C**). *HK1.ras* control papillomas are duller throughout (**B**), reflecting their low stroma/high keratin content (**D**).

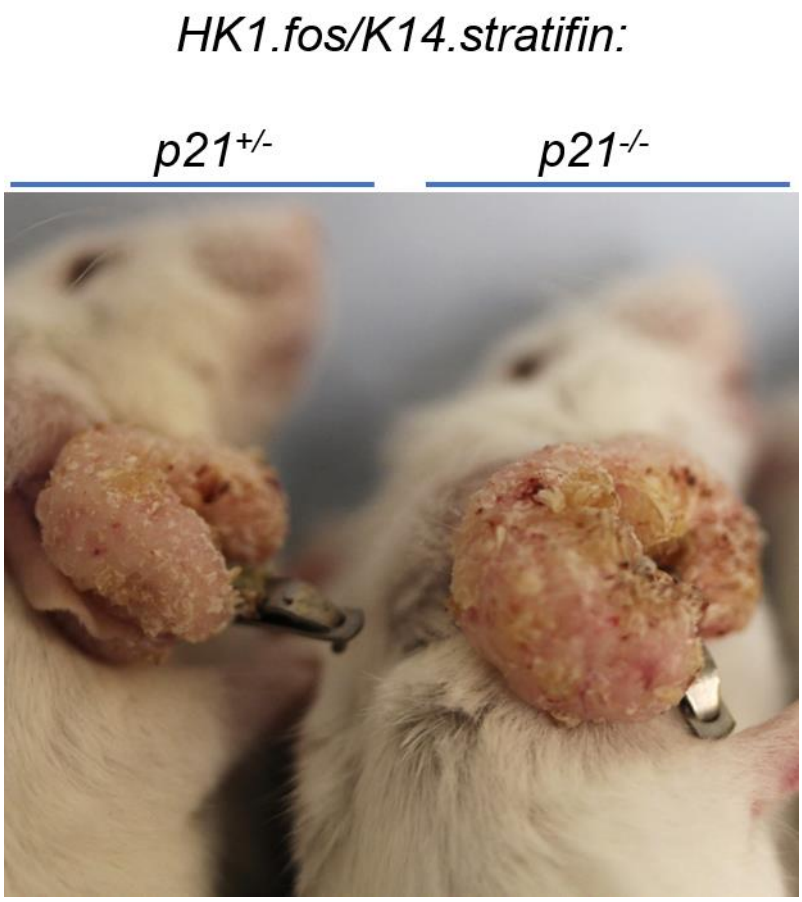

Figure S-2: *HK1.fos/K14.stratifin/p21$^{-/-}$* vs *HK1.fos/K14.stratifin/p21$^{+/-}$* tumours. *HK1.fos/K14.stratifin/p21$^{-/-}$* mice at 9 weeks (5 weeks post-tag) exhibit unusually large tumours at tag (right of image) compared to *HK1.fos/K14.stratifin/p21$^{+/-}$* littermates (left of image) or p21 wild-type mice (see Chapter 4), suggesting p21 loss causes a more aggressive disease, unlike p53 loss which appeared to have no effect.

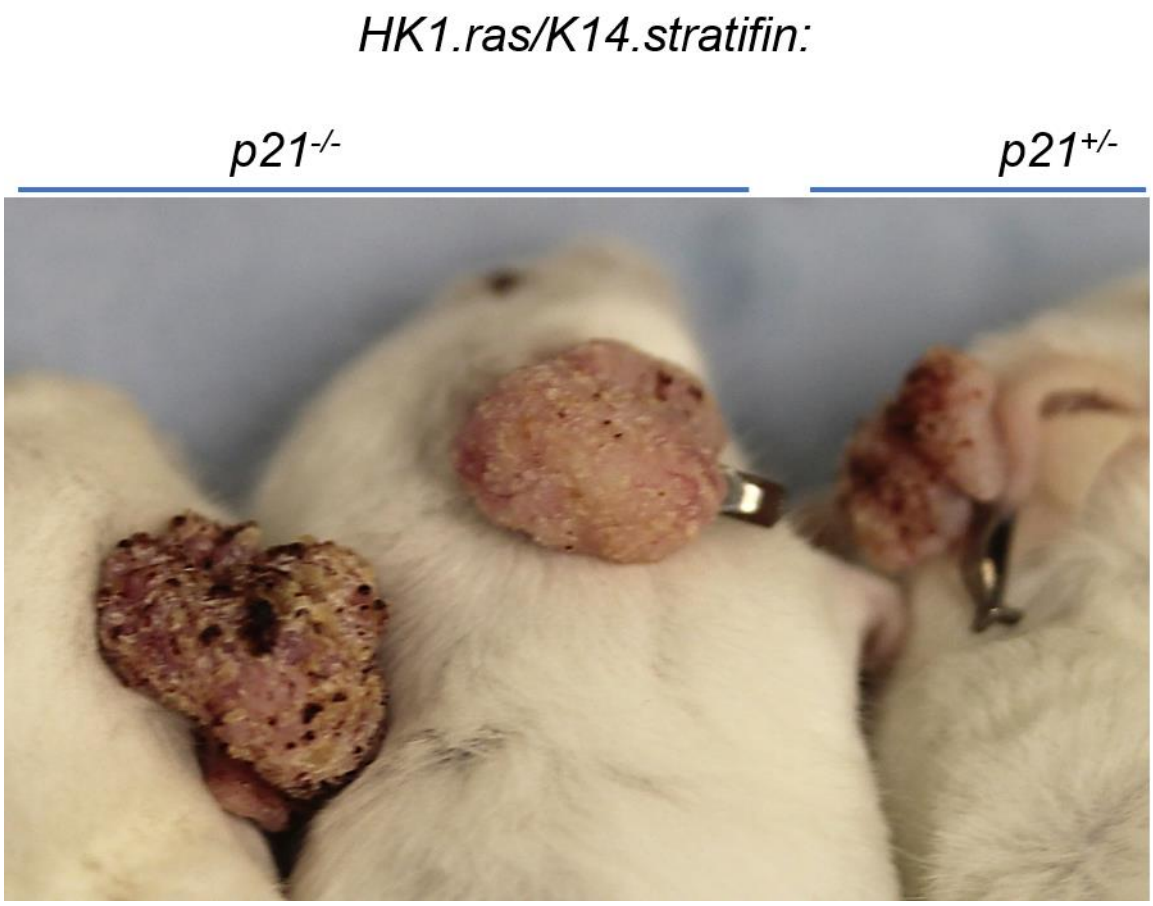

Figure S-3: *HK1.ras/K14.stratifin/p21$^{-/-}$* vs *HK1.ras/K14.stratifin/p21$^{+/-}$* tumours. *HK1.ras/K14.stratifin/p21$^{-/-}$* mice at 9 weeks (5 weeks post-tag) exhibit large tumours at tag (2 mice, left and centre of image) compared to *HK1.ras/K14.stratifin/p21$^{+/-}$* littermates (right of image). These appear to be similar to Type 2 *HK1.ras/K14.stratifin* tumours, as predicted given the lack of p21 nuclear localisation in those samples in p21WT mice. As in HK1.ras mice, p21 ablation does not create the same paradoxical tumour suppressive effect seen with p53 loss on this background.

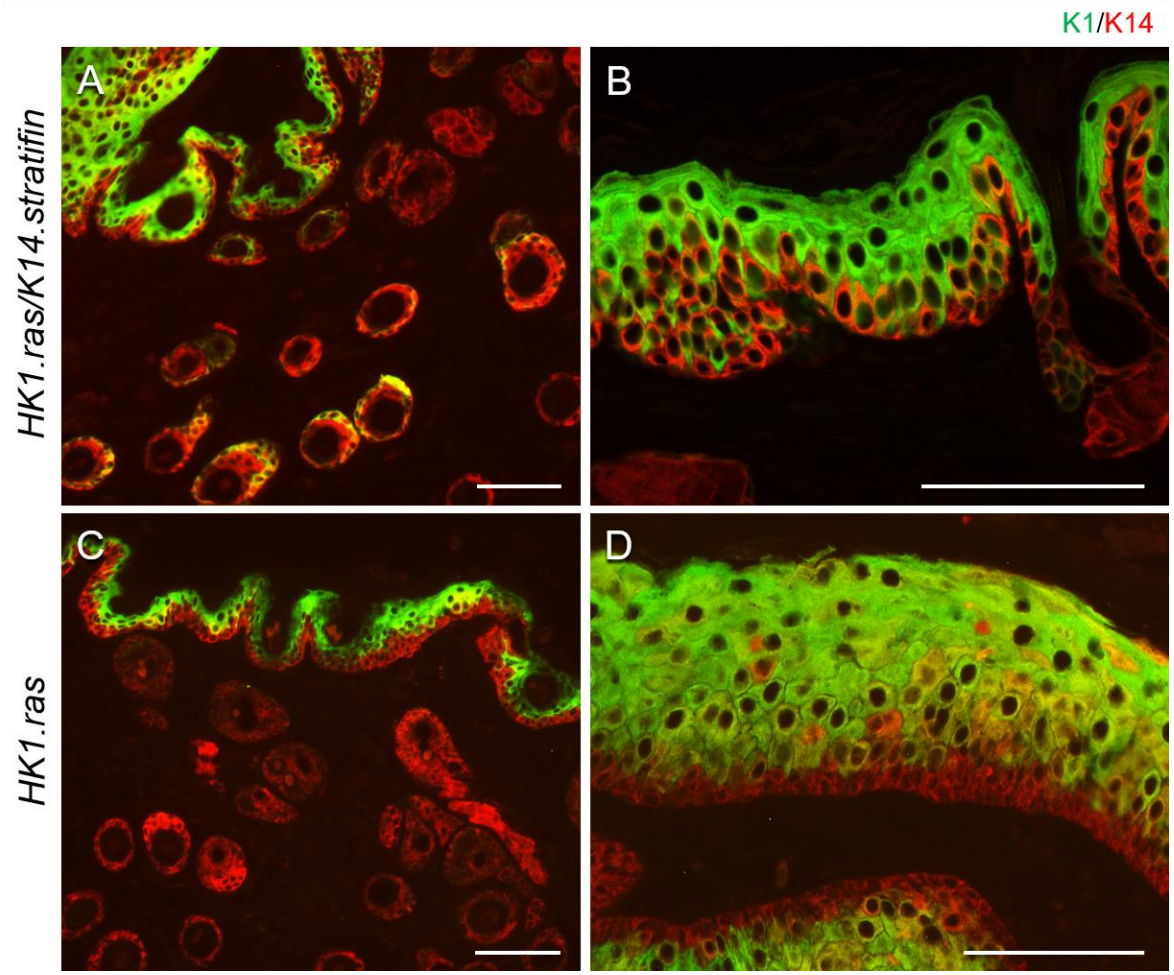

Figure S-4: Spurious expression of Keratin 1 in *HK1.ras/K14.stratifin* skin.
HK1.ras/K14.stratifin skin exhibits spurious Keratin 1 expression in follicles (**A**) and basal layer keratinocytes (**B**) which is not seen in HK1.ras control HFs (**C**) or basal cells (**D**).